Astron Astrophys Rev (2007) 14:217–360
DOI 10.1007/s00159-007-0007-0

REVIEW ARTICLE

Asteroseismology and interferometry

M. S. Cunha · C. Aerts · J. Christensen-Dalsgaard · A. Baglin · L. Bigot · T. M. Brown · C. Catala · O. L. Creevey · A. Domiciano de Souza · P. Eggenberger · P. J. V. Garcia · F. Grundahl · P. Kervella · D. W. Kurtz · P. Mathias · A. Miglio · M. J. P. F. G. Monteiro · G. Perrin · F. P. Pijpers · D. Pourbaix · A. Quirrenbach · K. Rousselet-Perraut · T. C. Teixeira · F. Thévenin · M. J. Thompson

Received: 17 August 2007 / Published online: 1 November 2007

Abstract Asteroseismology provides us with a unique opportunity to improve our understanding of stellar structure and evolution. Recent developments, including the first systematic studies of solar-like pulsators, have boosted the impact of this field of research within astrophysics and have led to a significant increase in the size of the

M. S. Cunha (✉) · T. C. Teixeira · P. J. V. Garcia
Centro de Astrofísica da Universidade do Porto, Rua das Estrelas, 4150-762 Porto, Portugal
e-mail: mcunha@astro.up.pt

C. Aerts
Instituut voor Sterrenkunde, Katholieke Universiteit Leuven, Celestijnenlaan 200 D,
3001 Leuven, Belgium

C. Aerts
Afdeling Sterrenkunde, Radboud University Nijmegen, PO Box 9010,
6500 GL Nijmegen, The Netherlands

J. Christensen-Dalsgaard · F. Grundahl
Institut for Fysik og Astronomi, Aarhus Universitet, Aarhus, Denmark

A. Baglin · C. Catala · P. Kervella · G. Perrin
LESIA, UMR CNRS 8109, Observatoire de Paris, Paris, France

P. Mathias
Observatoire de la Côte d'Azur, UMR 6203, BP 4229, 06304 Nice Cedex 4, France

L. Bigot · F. Thévenin
Observatoire de la Côte d'Azur, UMR 6202, BP 4229, 06304 Nice Cedex 4, France

T. M. Brown
Las Cumbres Observatory Inc., Goleta, CA 93117, USA

O. L. Creevey
High Altitude Observatory, National Center for Atmospheric Research, Boulder, CO 80301, USA

research community. In the present paper we start by reviewing the basic observational and theoretical properties of classical and solar-like pulsators and present results from some of the most recent and outstanding studies of these stars. We centre our review on those classes of pulsators for which interferometric studies are expected to provide a significant input. We discuss current limitations to asteroseismic studies, including difficulties in mode identification and in the accurate determination of global parameters of pulsating stars, and, after a brief review of those aspects of interferometry that are most relevant in this context, anticipate how interferometric observations may contribute to overcome these limitations. Moreover, we present results of recent pilot studies of pulsating stars involving both asteroseismic and interferometric constraints and look into the future, summarizing ongoing efforts concerning the development of

O. L. Creevey
Instituto de Astrofsica de Canarias, Tenerife 38200, Spain

A. Domiciano de Souza
Max-Planck-Institut für Radioastronomie, Auf dem Hügel 69, 53121 Bonn, Germany

P. Eggenberger
Observatoire de Genève, 51 chemin des Maillettes, 1290 Sauverny, Switzerland

P. Eggenberger · A. Miglio
Institut d'Astrophysique et de Géophysique de l'Université de Liège Allée du 6 Août, 17,
4000 Liège, Belgium

P. J. V. Garcia
Departamento de Engenharia Física, Faculdade de Engenharia, Universidade do Porto,
Rua Dr. Roberto Frias, 4200-465 Porto, Portugal

D. W. Kurtz
Centre for Astrophysics, University of Central Lancashire, Preston PR1 2HE, UK

M. J. P. F. G. Monteiro
Centro de Astrofísica e Departamento de Matemática Aplicada da Faculdade de Ciências,
Universidade do Porto, Porto, Portugal

F. P. Pijpers
Space and Atmospheric Physics Group, Imperial College London, Exhibition Road,
London SW7 2AZ, UK

D. Pourbaix
F.R.S-FNRS, Institut d'Astronomie et d'Astrophysique, Université Libre de Bruxelles,
1050 Brussels, Belgium

A. Quirrenbach
Zentrum für Astronomie der Universität Heidelberg, Landessternwarte Königstuhl,
69117 Heidelberg, Germany

K. Rousselet-Perraut
Laboratoire d'Astrophysique de l'Observatoire de Grenoble, BP 53, 38041 Grenoble Cedex 9, France

M. J. Thompson
School of Mathematics and Statistics, University of Sheffield, Hounsfield Road,
Sheffield S3 7RH, UK

future instruments and satellite missions which are expected to have an impact in this field of research.

Keywords Stars: variables: general · Stars: interiors · Techniques: interferometric

Contents

1 Introduction

1.1 Historical perspective

Periodic variable stars have been known to exist since the seventeenth century, when Jan Fokkens Holwarda realized that the magnitude of Mira, a variable star discovered almost a century earlier by David Fabricius, varied periodically with a period of 11 months (Hoffleit 1997). The periodic variability observed by Holwarda is intrinsic to Mira and results from consecutive contractions and expansions of its surface, associated with waves that propagate within its interior. Stars which owe their variability to this phenomenon are known as *pulsating (variable) stars*.

Despite the early discovery by Holwarda, the understanding that some variable stars owe their variability to intrinsic pulsations came almost three centuries later, following a suggestion by Shapley (1914) driven by the difficulties with reconciling the observed variability with the hypothesis of binarity. At about the same time, pulsating stars started being systematically used as tools for astrophysics research following the discovery of the Period-Luminosity relation by Henrietta Leavitt (Leavitt 1908; Pickering 1912). Classical pulsating stars have since been used as “standard candles"

of the Universe and, still today, are of fundamental importance for the determination of astrophysical distances.

During the decades that followed the discovery by Henrietta Leavitt, the theoretical studies of classical pulsating stars were directed towards the mathematical description of the pulsations and the understanding of the mechanism behind their excitation (e.g. Zhevakin 1963, and references therein). In the early 1960s, the discovery and interpretation of solar oscillations (Leighton et al. 1962; Frazier (1968); Ulrich (1970)) opened a new era in the study of pulsating stars. Solar oscillations have been shown to be amazing tools to "look" inside the Sun and image its structure and dynamics. The study of solar oscillations fostered the development of an entire new field of research—known as *Helioseismology* (e.g. Gough 1977a; Duvall 1982; Duvall et al. 1984; Christensen-Dalsgaard et al. 1985)—which has proved extremely successful in probing the physics of the solar interior (see Christensen-Dalsgaard 2002, for a recent review on helioseismology).

Following the success of helioseismology, attempts to use intrinsic oscillations of stars other than the Sun to learn about their internal structure and dynamics have led to the development of *Asteroseismology*. However, the road-map to success of asteroseismology proved much harder, as a result of the limitations brought about by our incapacity to resolve distant stars, and also by the limited number of oscillation frequencies observed in most of them. In fact, even though many different classes of pulsating stars are presently known—most of these are shown in Fig. 1—not all classes of pulsators are suitable for asteroseismic studies (cf. Sect. 1.4).

The twenty-first century has brought important new developments to asteroseismology. With highly precise spectrometers such as CORALIE and HARPS (at ESO-La Silla), UCLES (at AAT), and UVES (at ESO-Paranal) fully operational, it was finally possible to make clear detections of solar-like oscillations in stars other than the Sun (see Bedding and Kjeldsen 2007, for a recent review), thus confirming earlier evidence, found by different authors with different observing techniques and instruments, of excess power in the oscillation spectra of some of these stars (e.g. Brown et al. 1991; Schou and Buzasi 2001). Our understanding of the Sun and solar oscillations, as well as the tools developed in the context of helioseismology, make us confident that the detection of solar-like pulsations in stars other than the Sun will lead to major developments in our understanding of stellar structure, dynamics and evolution.

1.2 Stellar modelling and the ultimate goal of asteroseismology

Broadly speaking, "classical" stellar observables, such as the effective temperature, gravity and metallicity, are insensitive to the details of the internal structure of stars, and do not provide sufficient constraints for the determination of the basic stellar parameters, not to mention the calibration of parameters commonly used in stellar modelling.

Pulsation frequencies, on the other hand, are very sensitive to the details of the internal structure of stars. Each individual frequency probes the stellar interior differently from all other frequencies. Thus, in principle, the accurate measurement of a large number of oscillation frequencies in a given star allows one to study the details of its internal structure. Moreover, such frequencies may provide sufficient constraints to

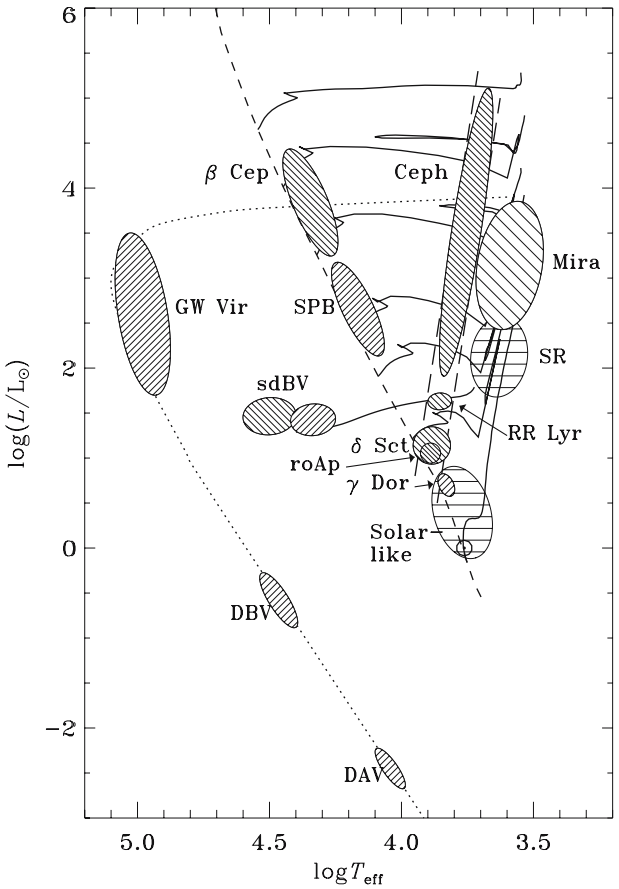

Fig. 1 Hertzsprung-Russell diagram showing different classes of pulsating stars. Some of these are named after a particular member of the class. Others are acronyms, standing, respectively, for: rapidly oscillating Ap (*roAp*); Slowly Pulsating B (*SPB*); subdwarf B variables (*sdBV*). The group labelled GW Vir includes what has formerly been known as the PNNV stars (for Planetary Nebulae Nuclei Variables), and the variable hot DO white dwarfs (DOV); the *DBV* and *DAV* stars are variable DB (helium-rich) and DA (hydrogen-rich) white dwarfs. The parallel *long-dashed lines* indicate the Cepheid instability strip

reduce the allowed space of stellar parameters to the extent that one may be convinced that a star is indeed within a particular error ellipse in the classical HR diagram.

There are many aspects about the physics and dynamics of stellar interiors that are not fully understood and that may be addressed with asteroseismology. To deal with some of the unknown details of the physics of stellar interiors, stellar evolutionary codes include parameters that can be tuned. Most of these relate to the treatment of convection, diffusion and settling of heavy elements, the equation of state and opacities. Among these, the poor treatment of convection and, to some extent, of diffusion, can have important implications in the context of stellar modelling.

Global convective instabilities are present either in the core or envelope of most stars. Nevertheless, the appropriate modelling of convection remains one of the most

difficult tasks in the context of stellar astrophysics. The "standard" recipe for convection in the context of stellar model fitting is the Mixing Length Theory (MLT, Böhm-Vitense (1958); Henyey et al. (1965)). An alternative treatment of convection, developed by Canuto and Mazzitelli (1991, 1992), is also often used. Connected to the treatment of convection is the problem of the extent of overshoot (e.g. Zahn 1991). As observations improve, and, in particular, as more evolved stars are observed, details such as overshoot will become increasingly important in modelling. Strong uncertainties also exist in studies concerning the interplay between convection and other physical phenomena, such as rotation, magnetic fields and radiation. All these limitations, in turn, limit our ability to determine accurate stellar ages and stellar global parameters.

Likewise, element diffusion occurs in most stars. Diffusion plays a key role in a diversity of contexts in stellar astrophysics, including studies of the Sun and of most main-sequence stars and studies of white dwarfs. As a result of diffusion, often the original chemical composition of stars is hidden below the surface and cannot be reached by direct observations. There are indeed several physical mechanisms whose physical description is not yet very well known but whose effect may imply a different mixture at the surface than in the interior. These include gravitational settling, radiative levitation, rotational mixing and mass loss through a stellar wind (Théado et al. 2005a, b). To test deep diffusion models it is necessary to connect them to observations which, in turn, can only be done if accurate models of the atmospheric layers are available. Unfortunately, stars in which the effects of diffusion are most obvious—such as peculiar stars—tend to have complex atmospheres, making the task of directly testing diffusion models hardly possible. Asteroseismology allows us to perform indirect tests to diffusion theories, and make inferences on the competition between diffusion and mixing processes in the interior of pulsating stars. Some attempts to perform such tests have already been carried out using seismic data of roAp stars (Cunha et al. 2004; Vauclair and Théado (2004)).

Except for the case of the Sun, the current understanding of stellar interiors is very limited also concerning the presence of physical agents that may introduce deviations from spherical symmetry. Stellar evolutionary codes assume that stars are spherically symmetric and, thus, aspects such as rotation (let alone differential rotation) and magnetic fields, are commonly ignored when modelling the interior of stars. Until recently, models based on the assumption of spherical symmetry could reproduce reasonably well the observables. That has changed in the past few years, as a result of the development of new instrumentation with capability to resolve (even if, in most cases, indirectly) the surface of stars other than the sun; striking examples are cases where large departures from sphericity have been detected interferometrically (e.g. Domiciano de Souza et al. 2003). This, together with constraints on departures from spherical symmetry also in stellar interiors that may be revealed by stellar oscillations, will continue to motivate the development of a new generation of stellar evolutionary codes that takes into account substantial departures from spherical symmetry, particularly caused by rotation. Encouraging progress has been made in recent years (e.g. Roxburgh 2004, 2006; Jackson et al. 2005; Rieutord 2006a; MacGregor et al. 2007) (see also Rieutord 2006b, for a review).

1.3 Origin and physical nature of the oscillations

The ability to fulfil the ultimate goal of asteroseismology depends critically on the understanding of the physics underlying the observed phenomena. The detailed dependence of the oscillations on the stellar interior, and hence their asteroseismic diagnostic potential, obviously arises from their physical nature. Consequently, in an asteroseismic study it is the nature and origin of the observed pulsations that are considered. In fact, the same star may belong to different pulsating classes (following the traditional classification), if modes of different origin and/or different physical nature are excited.

Stars, including the Sun, display a broad range of pulsations. The large-amplitude pulsators detected initially can generally be understood in terms of spherically symmetric, or *radial*, pulsations. However, in many stars, including the Sun, we observe oscillations with a variety of structure on the stellar surface; in the solar case these extend to modes with a surface wavelength of a few thousand kilometers. In distant stars, which are not resolved, it is only the large scale structure that can be detected, since the small-scale structure is averaged out in the observations. In practice this means that the sensitivity of brightness variations is restricted to modes with less than 3–4 node lines at the surface.

A rough measure of stellar pulsation periods is the *dynamical timescale*

$$t_{\rm dyn} = \left(\frac{R^3}{GM}\right)^{1/2} \propto \bar{\rho}^{\,-1/2}, \tag{1}$$

where R and M are the surface radius and mass of the star, G the gravitational constant, and $\bar{\rho}$ the mean density of the star. Hence, even a simple measurement of a pulsation period gives some indication of the overall properties of a star.

Concerning the physical nature of the oscillations, broadly speaking, the modes are either of the nature of standing acoustic waves (commonly referred to as pressure modes or *p modes*) or internal gravity waves (*g modes*); the latter involve departure from spherical symmetry and hence are nonradial modes. However, particularly in evolved stars, modes of a mixed nature are also found. In addition, the sun shows modes that can be identified as surface gravity waves, of relatively short surface wavelength.

Concerning their origin, the oscillations can be either intrinsically stable, or intrinsically unstable. Intrinsically unstable oscillations result from the amplification of small disturbances, through a heat-engine mechanism, acting in an appropriate region of the star. The original perturbation grows until some amplitude-limiting mechanism sets in, determining the final amplitude. This mechanism may depend on subtle details of the mode, hence the resulting amplitudes can vary strongly over a range of unstable modes. Also, as discussed below, it depends on the precise location of specific features in the opacity within the star, and hence the instability tends to be confined to specific regions in the HR diagram. An example is the *Cepheid instability strip*, indicated in Fig. 1. This type of pulsations, originally observed in stars such as Cepheids, is commonly referred to as *classical pulsations*. In contrast with classical pulsations, intrinsically stable oscillations are stochastically excited by an external forcing—typically near-surface convection. The resulting amplitudes are determined

by the balance between the energy input from the forcing and the damping. Since the damping and forcing typically vary relatively slowly with frequency this tends to lead to the excitation of modes in a substantial frequency range. Pulsations of this type were first found in the Sun, and are commonly referred to as *solar-like pulsations*.

1.4 Selected stellar pulsators

Probably the most successful asteroseismic studies carried out thus far concern white dwarf pulsators. Unfortunately, these stars are not suitable interferometric targets, and, thus, we shall not discuss them in the present review. For recent reviews on asteroseismology of white dwarf pulsators see, e.g. Metcalfe (2005) and Kepler (2007).

From the point of view of asteroseismology a crucial requirement is to have a substantial number of accurately determined frequencies. This is satisfied both for classical, heat-engine-driven pulsators, particularly in stars near the main sequence, and for solar-like pulsators, and indeed both classes are very interesting as asteroseismic targets. However, there are also substantial differences between them. The classical pulsators tend to show much larger amplitudes, and hence they are a priori easier to observe; after all, this is precisely the origin of their "classical" status. However, the distribution of mode amplitudes amongst the modes that are expected to be unstable is highly irregular, and so therefore is the selection of modes observed to a given level of sensitivity. These and other properties of the frequency spectra of classical and solar-like pulsators will be discussed further in Sect. 2.3, where the mechanism driving the oscillations in each of these types of pulsators will be looked at more closely.

Among the classes of pulsating stars along the main sequence that are likely to be most promising when it comes to combined asteroseismic–interferometric studies are the δ *Scuti*, β *Cephei* and the rapidly oscillating Ap or *roAp* stars (shown in Fig. 1).

The δ *Scuti* stars are found at the crossing of the main sequence and the Cepheid instability strip. They have masses between 1.5 and 2.5 $M_\odot$, where $M_\odot$ is the mass of the Sun, and exhibit both radial and non-radial pressure modes and gravity modes. Their observational properties are analysed and reviewed by Rodríguez and Breger (2001). The δ Scuti stars are the main sequence classical pulsators for which the largest number of oscillation modes have been observed. The record holder is FG Vir for which 79 frequencies were detected by Breger et al. (2005) and whose amplitude spectrum is reproduced in Fig. 7. The stars 4 CVn (34 frequencies, Breger (2000)) and XX Pyx (30 frequencies, Handler et al. (2000)) 44 Tau (29 frequencies, Antoci et al. (2007)) are competing for the second place. The observed frequency spectra of these three stars show that the δ Scuti stars have complex oscillation patterns, possibly including variable amplitudes from season to season. As discussed by Breger and Pamyatnykh (2006) such variability is difficult to distinguish from beating between extremely close pairs of modes; in the case of the star FG Vir they identify the observed variability as arising from such beating, although the extremely small frequency separations are difficult to account for on physical grounds.

β *Cephei* stars are the more massive analogues of the δ Scuti stars along the main sequence. They are stars with masses between 8 and 18 $M_\odot$ and also exhibit both radial and non-radial pressure modes and gravity modes. Their observational characteristics

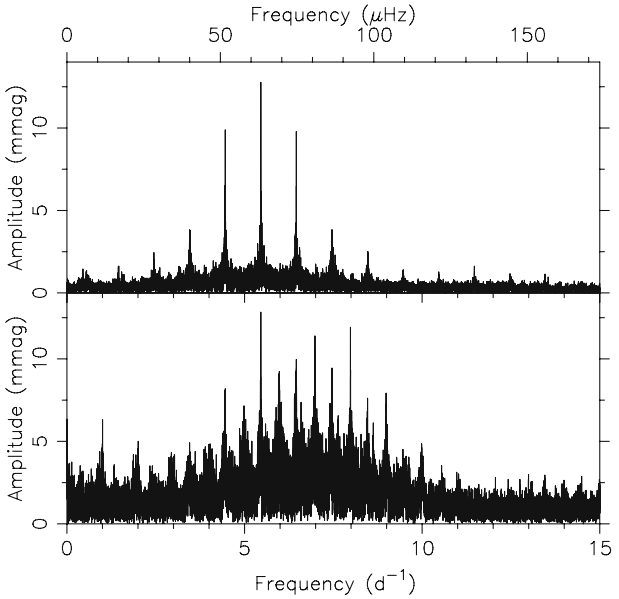

Fig. 2 Amplitude spectrum of the β Cephei star HD 129929 derived from single-site Geneva U data spanning 21 years (*bottom panel*). The *top panel* is the spectral window, resulting from a noiseless sine generated with the observed amplitude of the dominant mode and for the sampling of the data. Data taken from Aerts et al. (2003)

have recently been reviewed by Stankov and Handler (2005). A typical amplitude spectrum resulting from 21 years of single-site photometry is shown in Fig. 2. Recent progress in the seismic interpretation of selected β Cephei stars has raised serious questions about the modelling of these stars, since current standard stellar structure models of B stars are unable to explain the oscillation data for the best-studied stars: HD 129929 (Aerts et al. 2003), ν Eri (Pamyatnykh et al. 2004; Ausseloos et al. 2004), and 12 Lac (Handler et al. 2006; Ausseloos 2005). We return to this issue in Sect. 2.3.1.

Also at the crossing of the main sequence and the Cepheid instability strip, we can find another interesting group of pulsators, namely, the roAp stars (see, e.g. Cunha (2005); Cunha (2007); Kurtz et al. (2004), for recent reviews). While similar in mass and age to main sequence δ Scuti stars, these stars differ from the latter in that they have very peculiar atmospheres, particularly concerning their chemical composition, and are permeated by strong magnetic fields. Moreover, they rotate significantly slower than δ Scuti stars. In principle, the chemical peculiarities observed at the surface of Ap stars provide excellent environments to test diffusion theories. However, the complexity of their atmospheres makes this task rather hard. The pulsating properties of roAp stars are also significantly different from those of δ Scuti stars. Oscillations of roAp stars can be either mono-periodic or multi-periodic and result from acoustic modes generally of significantly higher frequency than those found in δ Scuti stars. The number of frequencies observed in the former is also typically smaller than in the latter.

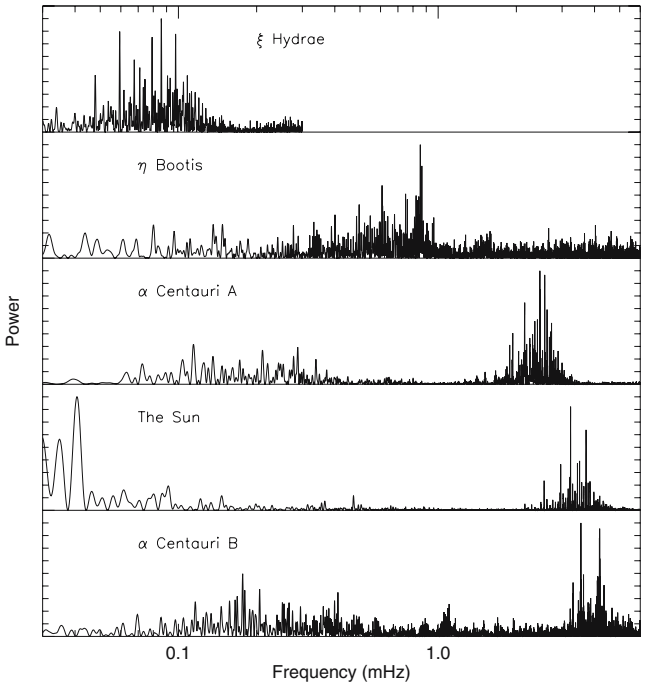

Fig. 3 Power spectra of solar-like oscillations of selected stars, including the Sun, organized in the order of decreasing mean density from bottom to top, and shown on the same frequency scale. The ordinate is arbitrary. The solar data were obtained with GOLF instrument on the SOHO spacecraft, using Doppler observations in light integrated over the disk of the Sun (e.g. García et al. 2001). The α Cen binary system brackets the Sun in mass and has a slightly higher age; data for the A component, with mass around 1.1 $M_{\odot}$, are from Butler et al. (2004), whereas data for the B component, with a mass around 0.9 $M_{\odot}$, are from Kjeldsen et al. (2005). The spectrum for η Boo, a subgiant in the hydrogen shell-burning phase, was obtained by Kjeldsen et al. (1995), whereas the data for ξ Hya, a G7 giant likely in the core helium-burning phase, are from Frandsen et al. (2002)

In addition to the classes mentioned above, other classical pulsators exist along the main sequence such as, e.g. the γ Doradus stars (Kaye et al. 1999, and references therein) and the slowly pulsating B or *SPB* stars (Aerts et al. 1999, and references therein). These two classes consist of stars with multiperiodic gravity modes with periods of order 0.5 to 3 days and thus pose a very serious observational challenge when it comes to detecting numerous modes.

Last, but not least, solar-like pulsators are found among main-sequence core, and post-main-sequence shell, hydrogen-burning stars, on the cool side of the Cepheid instability strip. Figure 3 shows examples of frequency spectra of solar-like pulsators spanning a broad range in stellar properties. The spectra are much denser than those of a typical classical pulsator (cf. Fig. 2). Moreover, the amplitudes are much smaller than those generally found in classical pulsators and they show an "envelope" shape, which is typical of stochastically excited oscillations and is remarkably similar for all the stars illustrated.

1.5 The role of interferometry

Even though the first astronomical applications of interferometry date back to the late nineteenth century and the first measurement of an angular diameter of a star other than the Sun using this technique dates back to the early 1920s (Michelson and Pease 1921), it was mostly during the last decade that optical interferometers became available to a wide astronomical community. During this period, a large window of research opportunities has been opened by a new generation of interferometers, such as CHARA (at Mount Wilson), VLTI (at ESO-Paranal), and Keck (at Mauna Kea).

Interferometry is expected to have a strong impact on studies of pulsating stars and, in that way, on the progress of our understanding of stellar structure and evolution. As we shall see, the success of asteroseismology depends strongly on the availability of accurate global parameters of pulsating stars and on our ability to correctly identify the modes of oscillation observed in each star. The possibility of measuring stellar angular diameters, of determining dynamical parallaxes of binaries, and of mapping stellar surfaces through differential interferometry, is, thus, expected to provide an important contribution to the success of asteroseismic studies.

The review is organized in three main sections. In Sect. 2 we present an extensive review of asteroseismology, with emphasis on those classes of pulsators that are within reach of present interferometric instruments. In particular, in Sect. 2.1 we discuss the observational techniques and instruments currently used to observed stellar pulsations, in Sects. 2.2 and 2.3 we describe the basic properties of the oscillations and their origin, in Sect. 2.4 we present the methods used to infer information about the star from the analysis of asteroseismic data, and, finally, in Sect. 2.5 we highlight the most common difficulties currently faced in asteroseismic studies.

In Sect. 3 we provide a brief review of optical interferometry, focused on aspects that are of relevance to asteroseismic studies. In particular, in Sects. 3.1 and 3.2 we describe some basic principles of optical interferometry, and emphasize particular aspects of stellar physics that can gain from the recourse to this technique. In Sects. 3.3 and 3.4 we discuss the capabilities of the interferometric instruments currently available to the community and emphasize the main limitations faced when using such interferometers to measure stellar angular diameters. Finally, in Sect. 3.5 we discuss the instrumental developments that may be expected in the near future.

Section 4 explores important synergies between asteroseismology and interferometry. Focusing on the main difficulties faced by current asteroseismic studies, described in Sect. 2.5, we discuss ways in which interferometry may help overcome these difficulties, both through direct and indirect contributions to the determination of accurate global parameters of pulsating stars, discussed in Sect. 4.1, and through the contribution to the identification of the modes of oscillation, discussed in Sect. 4.2. Finally, in Sects. 4.3 and 4.4 we briefly describe recent and on-going studies of particular stellar pulsators involving a combination of asteroseismic and interferometric data.

We conclude the review with a brief look into the future, presented in Sect. 5, where we describe relevant ground-based and space projects under study, as well as the impact they are expected to have on the development of this research field.

2 Asteroseismology

2.1 Observations

2.1.1 Photometry, spectroscopy and polarimetry

The mainstay of stellar observations, and therefore also of asteroseismology, are UV, visible and IR light. The flux of neutrinos, gravitational waves, and other more exotic particles is essentially restricted to more extreme states of matter, and can, therefore, be set aside for this discussion.

To observe the oscillations of stars it is necessary to understand the effect the oscillations have on the emergent flux of light. In principle, the emergent flux of light involves an integral over the source function along the line of sight, and hence is influenced by the physical state of the plasma along the latter. In practice this integral is dominated by a particular region, which is wavelength dependent, namely the intersection of the line of sight with a spatially thin shell centred on a surface with an optical depth $\tau = 2/3$. Since stars are normally unresolved, the observed flux is an average over the $\tau = 2/3$ surface, modulated by a function of the angle with the line of sight. By their influence on the location of, and the physical conditions at, the $\tau = 2/3$ surface, stellar oscillations modulate the emergent flux.

There are three types of measurements that may be carried out on light. In particular, one can measure the flux within bands of medium to low spectral resolution the relative flux at high resolution, and the polarization state of the light. These correspond, respectively, to the observational techniques of photometry, spectroscopy and polarimetry. Polarimetry has found very little use in asteroseismology, for a variety of reasons. Normal stars are to a very high degree spherically symmetric and, therefore, the stellar disk on the sky is to a high degree axially symmetric. Hence, in normal stars polarization signatures generally cancel out, when the light is integrated over a stellar disk. Although non-radial pulsations of stars can break the axial symmetry, in particular in the presence of rotation, the integrated effect remains small, also because the intrinsic degree of polarization of most emission mechanisms is itself not usually high. Combined with the difficulty of carrying out polarimetric measurements, polarimetry will probably not make a major impact as an observational technique except perhaps for strongly magnetic stars such as roAp stars. An example of where polarimetry is used in tandem with asteroseismology is Ryabchikova et al. (1997), but there too polarimetry is not used to carry out the asteroseismic observations.

Both photometry and spectroscopy are widely used as asteroseismic techniques. Intensity variations, resulting from the intrinsic pulsation of the star, can be studied from photometric time series. Spectroscopic time series, on the other hand, allow us to measure directly the changes of the surface velocity. It is important to note that observations in intensity and velocity of pulsations in one and the same star sample the same pulsation properties, but not in exactly the same way. In the case of p modes, both the Doppler shift of spectral lines and the intensity variations are weighted averages of the pulsation amplitude over the $\tau = 2/3$ surface (e.g. Dziembowski 1977; Christensen-Dalsgaard and Gough 1982), severely reducing the sensitivity to modes with a high number l of nodal lines on the surface. However, for the Doppler observa-

tions the projection of the velocity onto the line of sight gives rise to one more factor of $\cos\theta$ in the weighting function, where θ is the angle with the line of sight. This difference in weighting generally increases the response of velocity observations to modes of moderate l, compared with intensity observations. An important example, particularly for solar-like oscillations of low-intrinsic amplitudes, are the $l = 3$ modes which have been detected in velocity observations but not in intensity observations. Also, the difference in response can in principle be used to help in identifying the value of l associated with a given period of oscillation, which is one of the major problems in asteroseismology. A similar purpose is served by carrying out photometric observations in various bands (e.g. Stamford and Watson 1981; Watson 1988). Section 4 provides further details on mode identification.

2.1.2 Oscillation frequency spectra

The photometric and spectroscopic time series acquired during observations of pulsating stars can be used to generate frequency spectra. If the signal-to-noise ratio is sufficiently high, the oscillations will generate peaks above the noise, at the corresponding oscillating frequencies. In turn, these frequencies are often used as starting points for asteroseismic studies.

If the time series were "perfect"—i.e. continuous, with no gaps, and lasting forever—one could in principle identify, without ambiguity, the frequencies of all global oscillations of a star, as far as their signal were above the noise. However, the time series acquired are usually far from perfect, and the identification of which peaks correspond to true oscillation frequencies is not always trivial, as described below.

For a known function of time $f(t)$ the amplitude in the frequency domain $F(\omega)$ is obtained by carrying out a Fourier integral:

$$F(\omega) = \int_{-\infty}^{\infty} \mathrm{d}t f(t) \mathrm{e}^{-\mathrm{i}\omega t}. \tag{2}$$

If, for example, the signal were a single-frequency harmonic function, $f(t) = A\cos(\omega_0 t + \delta_0)$, with A the amplitude, δ_0 a phase and ω_0 the *angular frequency,*[1] $F(\omega)$ would have delta-function peaks at $\omega = \omega_0$ and $\omega = -\omega_0$.

In reality, the collection of data, whether it be intensity or velocity, requires a finite amount of time of "integration" during which the detector, normally a CCD, is exposed to radiation; after this there is a dead time during which the CCD is read out and the digitized signal stored on computer or transmitted to a receiving station. The integration time itself is usually short. The time series is therefore not measured continuously but sampled discretely. Normally the detection process is automated to sample the time series equidistantly at a rate that is sufficiently high to resolve the relevant time scales of variation.

In the ideal case the data would therefore be discretely sampled at a constant rate, and one would apply a discrete Fourier transform (DFT) to obtain the signal as a

[1] In addition, particularly when discussing observations, one often also uses the *cyclic frequency* $\nu = \omega/2\pi$.

function of frequency within a band. The highest useful frequency to search for is termed the *Nyquist frequency* $\omega_{\rm Nyq}$. For evenly spaced data, with a sampling interval Δ_t, we have,

$$\omega_{\rm Nyq} = \frac{\pi}{\Delta_t}. \tag{3}$$

In the case of unevenly spaced data, the Nyquist frequency can be quite different from this value, particularly if numerous large gaps or serious undersampling occur.

Since a real data stream has a finite length T, in the Fourier domain there is also a finite frequency resolution, Δ_ω, such that,

$$\Delta_\omega \propto \frac{1}{T}. \tag{4}$$

Generally, if two or more signals present in a time series are more closely spaced than the frequency resolution, these signals will not appear as multiple peaks in the Fourier domain. Instead, single or deformed peaks, or even no peaks will be seen. Moreover, signals with frequencies below this resolution cannot be detected with any confidence.

Besides the limitations associated with the finite length of the time series and with the discrete sampling of the data, in the analysis of real observations there are often difficulties associated also with the problem of "missing data". Because of technical problems, or poor observing conditions, data can be lost either pointwise or in blocks. These missing data are usually distributed randomly within the time series. Moreover, regular gaps in the time series are usually present in observations carried out from ground-based telescopes, due to the incapacity of these telescopes to observe the stars during the day and during the time that the stars are below the horizon. These regular gaps produce additional peaks in the Fourier domain, which can hamper considerably the interpretation of the data, particularly of multiperiodic pulsators. Together these properties of the data sampling are known as the *window function* in the time domain and as the *spectral window* in the Fourier domain. The spectral window has multiple peaks, even for a monochromatic underlying signal, as can be seen in the upper panel of Fig. 2.

A time series containing multiple signals sampled in the same way produces a rather complex Fourier spectrum. In fact, even in the absence of measurement noise, the task of identifying which of the peaks correspond to true oscillation frequencies and which are sidelobes generated by the sampling can be extremely hard. A number of methods have been developed to deal with this problem. A well-known technique is the Lomb-Scargle periodogram (Scargle 1982). A more general discussion of several methods in use in astronomy can be found in Adorf (1995) and Vio et al. (2000). A discussion directed more specifically to asteroseismology can be found in Koen and Lombard (1995), Koen (1999) and Pijpers (2006). Schwarzenberg-Czerny (1997) showed that the Fourier transform is optimal to deduce the frequencies, in the sense that it is equivalent to all methods relying on phase binning and variance estimates, for a given sampling, binning and weighting of the data. While gap-filling techniques and methods to hide aliases have been developed, these cannot extract more frequency information than the Fourier transform (Kurtz 2002).

2.1.3 Ground-based facilities

For the classical pulsators, with relatively high amplitudes, photometry is most commonly used. This is due to the fact that most small and medium-sized telescopes have facilities for doing absolute or relative photometry in a variety of photometric systems (the Johnson, Strömgren and Geneva systems being most common). As mentioned before, asteroseismic studies require long time series of observations. Thus, temporary networks of small and medium size telescopes equipped with photometers are often organized by researchers working in this field.

The Whole Earth Telescope (WET),[2] Delta Scuti Network (DSN)[3] and the STEllar PHotometry International network (STEPHI)[4] are examples of consortia of astronomers who create such temporary networks of telescopes for continuous photometric observations of asteroseismic target stars—networks that for a few weeks or even months mimic the dedicated helioseismic networks such as GONG,[5] BiSON,[6] IRIS, TON[7] and others. Besides these organised networks, also individual scientists have taken the initiative to organise large multisite campaigns on dedicated stars (e.g. Handler et al. 2004; Handler et al. 2006).

These photometric multisite campaigns have been a great success, with many notable discoveries from seismic inferences. PG 1159–035, a DOV pulsating white dwarf star (Winget et al. 1991) and GD 358, a DBV pulsating white dwarf star (Winget et al. 1994), both observed during WET campaigns, are still record holders for the number of independent pulsation modes detected and identified in compact stars. Significant understanding of white dwarf mass, envelope mass, luminosity, differential rotation and other discoveries have come from these studies. More recently the exciting question of crystallisation in the DAV white dwarf BPM 37093 (Kanaan et al. 2005; Brassard and Fontaine 2004; Fontaine and Brassard 2005) has been addressed. The ground-based limit for photometric precision has been pushed to 14 μmag in a WET study of the roAp star HR 1217 (Kurtz et al. 2005) and the amazing eclipsing subdwarf B pulsator PG 1336-018 has been studied (Kilkenny et al. 2003). The simultaneous presence of p and g modes was discovered in the β Cephei stars ν Eri (Handler et al. 2004) and 12 Lac (Handler et al. 2006) and differential rotation was found in the interior of ν Eri (Pamyatnykh et al. 2004), after it had been discovered already for the similar main-sequence B star HD 129929 (Aerts et al. 2003).

Nevertheless, even with the extraordinary efforts of these large teams, duty cycles for the asteroseismic targets do not come close to the 100% that is desired for run lengths of weeks. For that either satellite missions, an asteroseismic telescope in the polar regions, or a permanently dedicated network are needed (see also Sect. 5).

[2] http://wet.physics.iastate.edu.

[3] http://www.univie.ac.at/tops/dsn/intro.html.

[4] http://www.lesia.obspm.fr/~stephi/.

[5] http://gong.nso.edu/.

[6] http://bison.ph.bham.ac.uk/.

[7] http://ton.phys.nthu.edu.tw/index.htm.

As mentioned in Sect. 1.4, the amplitudes of the variations in solar-like pulsators are much smaller than in classical pulsators. To date, all ground-based attempts have failed to detect solar-like intensity variations due to the limitations imposed by the Earth's atmosphere (for a very ambitious attempt, involving most of the then-largest telescopes available, see Gilliland et al. (1993)). Thus, to study solar-like pulsators, one must either acquire photometric data from space, or carry out spectroscopic measurements at large or highly optimised ground-based telescope facilities.

During the past ∼5 years there has been a number of detections of solar-like oscillations in solar-type stars. The technical background behind these detections is the marked increase in the achievable precision of radial–velocity measurements spurred by the detection of extrasolar planets. In order to achieve the high precision needed for the detection of solar-like oscillations ($\sim 5\ \mathrm{m\ s^{-1}}$) highly specialised spectrographs are needed. Consequently, to date only relatively few instruments are available for this.

So far the following spectrographs have produced oscillation spectra with unambiguous excess power and in several cases also detections of individual oscillation frequencies in solar-like pulsators: *HARPS* at the ESO 3.6-m telescope and *UVES* on the VLT,[8] CORALIE at the 1.2-m Euler telescope[9] on La Silla, SARG at the TNG[10] on La Palma and *UCLES* at the AAT[11]. Other telescopes have contributed, but the main results come from the five mentioned above. A summary of recent observations of solar-like pulsations among main-sequence and subgiant stars is provided by Bedding and Kjeldsen (2006).

To date, time at any of these telescopes (except CORALIE) has only been allocated in blocks shorter than 11 nights—and no facility exists for coordinated observations. In the northern hemisphere SARG was, until recently, the only instrument available, but recently SOPHIE at OHP[12] and FIES at the NOT[13] have become operational. In the southern hemisphere, of the remaining four instruments, three are located in Chile and one is located in Australia. A few successful campaigns have been run by coordinating observations from the instruments in Chile and the AAT (e.g. Butler et al. 2004; Bedding et al. 2006; Kjeldsen et al. 2005; Bedding et al. 2007). The lack of a dedicated network of telescopes with capabilities in this field is a major limitation for further progress in ground-based asteroseismic efforts for studying solar-like pulsators. Studies of such a dedicated network are under way. This, and other ground-based projects under study aimed at acquiring continuous spectroscopic time-series of solar-like pulsators are discussed in Sect. 5.

2.1.4 Space missions

Space very early appeared as a preferred place for asteroseismology, using the technique of ultra-high-precision photometry. Observations from space can provide long

[8] http://www.eso.org/public/.

[9] http://obswww.unige.ch/~naef/CORALIE/coralie.html.

[10] http://www.pd.astro.it/sarg/.

[11] http://www.aao.gov.au/about/aat.html.

[12] http://www.obs-hp.fr/www/guide/sophie/sophie-eng.html.

[13] http://www.not.iac.es/instruments/fies/.

and almost continuous datasets on the same objects. Moreover, with very moderate apertures, space photometry can be used to track oscillations with amplitudes around 1 ppm, and with very high sampling rates during extended runs it is, in principle, possible to access characteristic time scales that are out of reach from the ground.

The past two decades have seen a succession of proposals for national and international space projects dedicated to asteroseismology. Moreover, some non-dedicated instruments, such as HST (e.g. Zwintz et al. 2000; Castanheira et al. 1991) and WIRE (Bruntt et al. 2005) have been used (in the former case occasionally, in the latter case regularly) to obtain data for asteroseimic studies.

The Canadian microsat MOST (Walker et al. 2003; Matthews (2005)), launched in June 2003, is able to measure light variations of bright stars for around 40 days continuously and demonstrated the efficiency of the technique. Striking results have been obtained on pulsations of different kinds of pulsators, including a pulsating Oe star (Walker et al. 2005a), pulsating Be stars (Walker et al. 2005b; Saio et al. (2007)), a β Cephei star (Aerts et al. 2006a), a slowly pulsating B stars (Aerts et al. 2006b), a pulsating B supergiant (Saio et al. 2006), a subdwarf B star (Randall et al. 2005a) and Wolf-Rayet stars (Lefévre et al. 2005). In all these examples, ground-based photometry was largely exceeded, both in quality and in duty cycle.

Launched in December 2006, the satellite CoRoT (Baglin 2003) is expected to produce a major step in the domain of space-based asteroseismology. CoRoT is a French CNES-led mission with contributions from seven other entities: Austria, Brazil, Belgium, Germany, Spain, and the RSSD /ESTEC division of ESA. With its 27-cm diameter telescope, CoRoT is expected to detect periodic signals of amplitude as small as a few ppm with lifetimes of a few days, in sixth magnitude stars. Early, so far unpublished, results provide very encouraging indications that this goal will in fact be met.

This mission will observe at least 100 stars (half of them for 150 days, the others for 20 to 40 days), and will produce a dense mapping of the seismic properties (frequencies, amplitudes and life-times) of pulsators all across the HR diagram. Simulations show that, with the frequency resolution and the signal-to-noise ratio that are expected to be reached during the long runs of 150 days, it will be possible to measure the size of the convective cores, the extent of the radiative zones and the angular momentum distribution in intermediate rotators. In addition, the observation of 100,000 faint stars for the CoRoT exoplanet search programme will produce a lot of complementary seismic information. A further advance in space-based asteroseismology will result from the asteroseismic programme on the Kepler mission (e.g. Christensen-Dalsgaard et al. 2007); this will carry out photometric observations, with a precision sufficient to detect solar-like oscillations, for thousands of stars, with the option to observe selected stars continuously or repeatedly over a period of at least 4 years. This and other space-based missions including asteroseismic programmes are discussed further in Sect. 5.

2.2 Basic properties of the oscillations

We restrict the discussion to small-amplitude oscillations of stars that do not rotate very rapidly. In this case the oscillations can be treated as small perturbations about a

static equilibrium structure, and effects of rotation (and some other perturbations to the spherically symmetric structure of the star, such as buried magnetic fields) can also be treated using a perturbation analysis. Thus the basic description of the oscillations is obtained as linearized perturbation equations around a spherical equilibrium structure. It follows that individual modes of oscillation depend on co-latitude θ and longitude ϕ, in spherical polar coordinates (r, θ, ϕ) where r is the distance to the centre of the star, as a spherical harmonic $Y_l^m(\theta, \phi)$. As before, here the *degree* l indicates the number of nodal surface lines and hence describes the overall complexity of the mode and the *azimuthal order* m determines the number of nodes around the equator. In addition, the modes are characterised by their *radial order* n which, roughly speaking, measures the number of nodes in the radial direction (e.g. Scuflaire 1974; Osaki 1975; Takata 2005).

2.2.1 The properties of the modes

The frequencies of oscillation of stellar models can be determined with good precision in the adiabatic approximation, assuming that the perturbations δp and $\delta\rho$ in pressure p and density ρ in a mass element following the motion (the so-called *Lagrangian perturbations*) are related by

$$\frac{\delta p}{p} = \Gamma_1 \frac{\delta\rho}{\rho}, \tag{5}$$

where $\Gamma_1 = (\partial \ln p/\partial \ln \rho)_{\rm ad}$, the derivative corresponding to an adiabatic change. Given this approximation, it is straightforward to compute precise frequencies of a stellar model, and the frequencies therefore provide direct diagnostics of the stellar interior; this is obviously the basis of asteroseismology. However, to understand the diagnostic potential of the frequencies, asymptotic analyses of the oscillation equations are extremely instructive. A convenient approximate equation for this purpose has been derived by Gough (see Deubner and Gough 1984; Gough 1986; Gough 1993), based on an analysis by Lamb (1909):

$$\frac{{\rm d}^2 X}{{\rm d}r^2} + K(r)X = 0, \tag{6}$$

where

$$K(r) = \frac{\omega^2}{c^2}\left[1 - \frac{\omega_{\rm c}^2}{\omega^2} - \frac{S_l^2}{\omega^2}\left(1 - \frac{N^2}{\omega^2}\right)\right]; \tag{7}$$

here $X = c^2\rho^{1/2}{\rm div}\boldsymbol{\delta}\mathbf{r}$, where c is the adiabatic sound speed and $\boldsymbol{\delta}\mathbf{r}$ is the displacement vector. The behaviour of the mode is determined by three characteristic frequencies: the acoustic (or Lamb) frequency S_l, given by

$$S_l^2 = \frac{l(l+1)c^2}{r^2}, \tag{8}$$

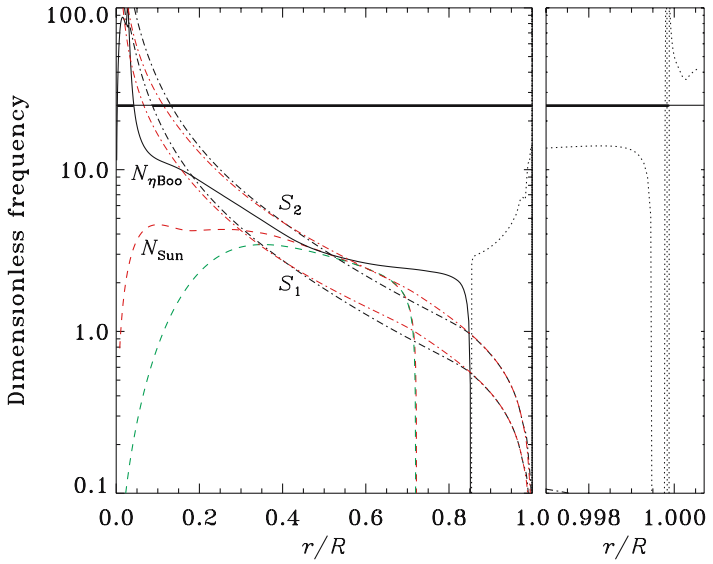

Fig. 4 Dimensionless characteristic frequencies, in units of $(GM/R^3)^{1/2}$, for a 1 $M_\odot$ ZAMS model, a model of the present Sun and of η Boo, a 1.63 $M_\odot$ subgiant. The *dot-dashed curves* show S_l for $l = 1$ and 2, in the solar model (*red*) and the model of η Boo (*black*). The *dashed curves* show N in the ZAMS model (*green*) and the solar model (red), whereas the solid curve shows N in the model of η Boo. Finally, the *dotted curve* shows ω_c in the model of η Boo. For clarity, N is not shown in the atmosphere and ω_c not below the base of the convective envelope. The *horizontal line* marks a typical frequency of stochastically excited modes; it is shown as thicker in regions where such a mode with $l = 1$ propagates in the η Boo model

the buoyancy (or Brunt-Väisälä) frequency N, given by

$$N^2 = g\left(\frac{1}{\Gamma_1}\frac{\mathrm{d}\ln p}{\mathrm{d}r} - \frac{\mathrm{d}\ln\rho}{\mathrm{d}r}\right), \tag{9}$$

and the acoustical cut-off frequency ω_c, given by

$$\omega_c^2 = \frac{c^2}{4H^2}\left(1 - 2\frac{\mathrm{d}H}{\mathrm{d}r}\right), \tag{10}$$

where $H = -(\mathrm{d}\ln\rho/\mathrm{d}r)^{-1}$ is the density scale height. Examples of these frequencies are plotted in Fig. 4 for selected stellar models.

For a fully ionized ideal gas (a good approximation in much of most stars, as long as radiation pressure or degeneracy can be neglected)

$$c^2 \simeq \frac{5}{3}\frac{k_B T}{\mu m_u}, \tag{11}$$

where k_B is Boltzmann's constant, T is temperature, μ is the mean molecular weight and m_u is the atomic mass unit. Also,

$$N^2 \simeq \frac{g^2\rho}{p}(\nabla_{\rm ad} - \nabla + \nabla_\mu), \tag{12}$$

where, following the usual convention,

$$\nabla = \frac{{\rm d}\ln T}{{\rm d}\ln p}, \quad \nabla_{\rm ad} = \left(\frac{\partial \ln T}{\partial \ln p}\right)_{\rm ad}, \quad \nabla_\mu = \frac{{\rm d}\ln \mu}{{\rm d}\ln p}, \tag{13}$$

and g is the local gravitational acceleration. In regions of nuclear burning, μ increases with increasing depth and hence increasing pressure, and therefore the term in ∇_μ makes a positive contribution to N^2.

A mode oscillates as a function of r where $K(r) > 0$ and varies exponentially where $K(r) < 0$; in the former regions the mode is said to be *propagating* and in the latter the mode is *evanescent*. Points where $K(r) = 0$ are *turning points* of the mode.[14] In most cases the mode has large amplitude in just one propagating region which therefore mainly determines its frequency; the mode is said to be *trapped* in such a region. Near the surface typically $S_l \ll \omega$ and the behaviour of the mode is controlled by $\omega_{\rm c}$. Modes with frequency below the atmospheric value of $\omega_{\rm c}$ decay exponentially in the atmosphere and hence are trapped within the star. In the rest of the star $\omega_{\rm c}$ plays a smaller role and the properties of the modes are controlled by S_l and N. In unevolved stars N is relatively low throughout the star. In that case a high-frequency mode is predominantly controlled by the behaviour of S_l; the eigenfunction oscillates as a function of r between the near-surface reflection where $\omega = \omega_{\rm c}$ and a *lower turning point* at $r = r_{\rm t}$, such that $\omega = S_l(r_{\rm t})$ or

$$\frac{c(r_{\rm t})^2}{r_{\rm t}^2} = \frac{\omega^2}{l(l+1)}. \tag{14}$$

This is typical of a p mode. Obviously, at low degree $r_{\rm t}$ is small and the mode samples most of the star, including parts of the core. In particular, radial p modes extend essentially to the centre of the star. The behaviour of these modes can be illustrated in a *ray plot*, such as illustrated in Fig. 5a; as shown, the waves undergo total internal reflection at a surface of radius $r_{\rm t}$, given by Eq. (14).

For low-frequency modes $\omega \ll S_l$ in much of the star, and the mode is oscillatory in a region approximately determined by $\omega < N$; this characterizes g modes. As shown by Fig. 5b such modes can similarly be illustrated by the propagation of rays of internal gravity waves; here, for a model of the present Sun, reflection takes place near the centre and at the base of the convective envelope. However, as is obvious from Fig. 4 and Eq. (12), N may reach very large values in the core of evolved stars. Here K may be positive at relatively high frequency both in the outer parts where ω is greater than both S_l and N, the mode thus behaving as a p mode, and in the core where $\omega < S_l, N$

[14] More precisely, a turning point is a property of the equation that describes the eigenmode, rather than of the mode itself. Hence, the depth $r_{\rm t}$ at which is located the lower turning point of a given mode, for instance, can be slightly different depending on whether the radial displacement or the Lagrangian pressure perturbation is used to describe the mode (e.g. Gough 1993; Schmitz and Fleck 1998).

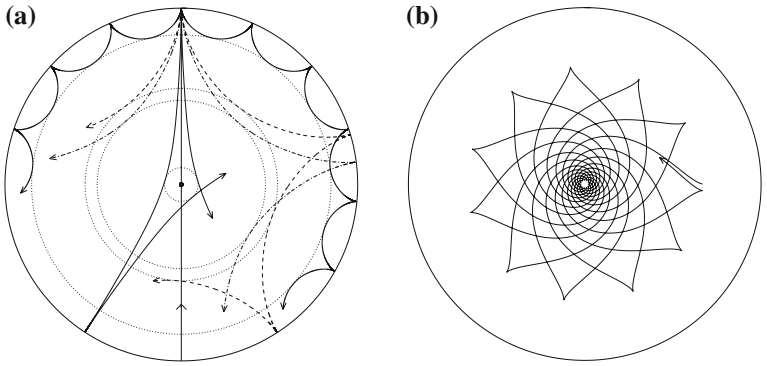

Fig. 5 Propagation of rays of sound or gravity waves in a cross-section of the solar interior. The acoustic ray paths (**a**) are bent by the increase in sound speed with depth until they reach *the inner turning point* (indicated by the *dotted circles*) where they undergo total internal refraction, at the distance r_t determined by Eq. (14). At the surface the acoustic waves are reflected by the rapid decrease in density. Rays are shown corresponding to modes with frequency 3, 000 μHz and degrees (in order of increasing penetration depth) $l = 75$, 25, 20 and 2; the line passing through the centre schematically illustrates the behaviour of a radial mode. The gravity-mode ray path (**b**) corresponds to a mode of frequency 190 μHz and degree 5

and the mode behaves like a g mode. This is illustrated in Fig. 4 in the case of η Boo. Such *mixed modes* have a particularly interesting diagnostic potential (see Sect. 2.4.2).

An important global property of the oscillation modes is their *inertia*

$$E = \frac{\int_V |\boldsymbol{\delta r}|^2 \rho \mathrm{d}V}{M|\boldsymbol{\delta r}|^2_{\mathrm{ph}}} \equiv \frac{M_{\mathrm{mode}}}{M}, \tag{15}$$

also defining the *mode mass* M_{mode}, where M is the mass of the star, $|\boldsymbol{\delta r}|_{\mathrm{ph}}$ is the norm of the photospheric displacement and the integral is over the volume V of the star. Evidently, for modes trapped in the deep interior of the star with an extensive evanescent region between the trapping region and the surface the value of E is expected to be large. With this definition, the kinetic energy of the oscillation is given by

$$\mathcal{E}_{\mathrm{kin}} = \frac{1}{2} M_{\mathrm{mode}} V^2_{\mathrm{rms}} = \frac{1}{2} M E V^2_{\mathrm{rms}}, \tag{16}$$

where V_{rms} is the photospheric rms velocity. On this basis one might expect that it is more difficult to excite a mode to a given amplitude, the higher the value of E; this is certainly the case for stochastically excited modes which tend to be excited to roughly the same energy at a given frequency.

2.2.2 Departures from spherical symmetry

We have so far neglected the dependence of the oscillations on the azimuthal order m. In fact, for a spherically symmetric star the properties of the modes are independent of m: the definition of m depends on the orientation of the coordinate system used to describe the star and this has no physical meaning in the spherically symmetric case.

This frequency degeneracy is lifted by departures from spherical symmetry, of which the most important example is rotation. For a slowly rotating star, with an angular velocity $\Omega(r)$ that depends only on r, the effect of rotation on the frequencies, as observed in an inertial frame, can be expressed as

$$\omega_{nlm} = \omega_{nl0} + m\beta_{nl}\langle\Omega\rangle_{nl}, \tag{17}$$

where $\langle\Omega\rangle_{nl}$ is an average of Ω that depends on the properties of the eigenfunctions in the non-rotating model (e.g. Ledoux 1951; Hansen and Cox 1977; Gough 1981); the constant β_{nl} is sometimes expressed as $1 - C_{nl}$, where C_{nl} is the *Ledoux constant*. For high-order or high-degree acoustic modes $\beta_{nl} \simeq 1$; thus the rotational splitting is given by the average angular velocity. On the other hand, for high-order g modes $\beta_{nl} \simeq 1 - 1/[l(l+1)]$ (e.g. Wolff 1974).

The extent to which the splitting resulting from slow rotation can be detected obviously depends on the rotation rate and the intrinsic frequency width of the observed modes, which in turn depends on the time span of the observation or the mode life time. The inclination of the rotation axis relative to the line of sight to the observer is an additional important factor, for stellar observations where only light integrated over the disk of the star is observed. Gizon and Solanki (2003) studied this effect in the case of stochastically excited modes. In the special case where the rotation axis points towards the observer, only modes with $m = 0$ are visible in integrated light and no rotational splitting is observed. The solar case corresponds to the opposite extreme: here an Earth-bound observer is always close to the equatorial plane and disk-integrated observations are sensitive essentially only to modes where $|l - m|$ is even, including the modes with $m = \pm l$ which display the largest splitting. For intermediate inclinations the sensitivity to the different m is essentially a geometrical effect, affected by the distribution of intensity across the disk as described by the limb-darkening function.[15] Gizon and Solanki (2003) investigated the possibility of determining both the rotation rate and the inclination of the rotation axis from the observed splittings and ratios between the amplitudes of the split modes. Ballot et al. (2006) carried out a similar analysis, but addressing specifically the potential of the CoRoT mission and carrying out Monte Carlo simulations to estimate the errors in the inferred quantities. They concluded that for a rotation rate twice solar it was possible to determine both the inclination and the rotation rate, whereas for rotation at the solar rate the inclination was poorly determined, whereas it was still possible to infer the rotation rate. Gizon and Solanki (2004) extended the analysis to show that with observation of $l = 2$ modes with $m = \pm 1$ and ± 2, which is possible at intermediate inclinations, some information can be obtained about the latitudinal variation of rotation, at least for rotation rates exceeding four times solar. It is worth reminding here that this type of analysis cannot be applied to heat-driven modes, because their intrinsic amplitudes neither follow a regular pattern nor do we understand their selection mechanism.

Equation (17) is valid for sufficiently slow rotations that terms of order Ω^2 and higher can be neglected; in particular, this neglects the effect of rotation on the structure

[15] For radial–velocity observations an additional effect may arise as a result of the rotational shift of the spectral lines across the stellar disk; e.g. (Brookes and Isaak 1978; Christensen-Dalsgaard (1989)).

of the star, through the centrifugal effects. However, many stars rotate too rapidly for this to be valid. Higher order effects cause departures from the uniform splitting given in Eq. (17) and may lead to complex frequency spectra, greatly complicating the analysis of the observed spectra. Second-order effects were considered by, for example, Chlebowski (1978); Saio (1981); Gough and Thompson (1990) and Dziembowski and Goode (1992), whereas third-order effects were treated by Soufi et al. (1998). As a result of the higher order effects, the surface behaviour of a mode is no longer a pure spherical harmonic; this must be taken into account, e.g. in the observational mode identification (Daszyńska-Daszkiewicz et al. 2002). Also, Goupil et al. (2004) showed inter alia that mode coupling caused by rotation can significantly perturb the small frequency separation which is used as a diagnostic of the star's core structure (see Sect. 2.4.1) and they demonstrated how to correct for this at least for stars which are not latitudinally differentially rotating. For even more rapid rotation solutions in terms of expansions in Ω are no longer applicable. Initial results for fully two-dimensional, non-perturbative calculations are becoming available for polytropic models (e.g. Lignières et al. 2006; Reese et al. 2006a, b); interestingly, even at equatorial velocities less than $50\,\mathrm{km\,s^{-1}}$ (in a 1.9 $M_\odot$ model) the precision of the third-order expansion becomes insufficient, compared with the expected observational precision of the CoRoT project (Reese et al. 2006b). The modelling of the equilibrium structure of such rapidly rotating stars is evidently also problematic in the physically realistic case, although some progress is being made (see Sect. 1.2).

Rotation is not the only physical agent that can influence the oscillations in a non-spherically symmetric way. Other symmetry-breaking agents, such as magnetic fields and structural differences associated with stellar spots, can affect both the frequency of the oscillations and the geometry of the pulsations in the surface layers of some pulsating stars. An important difference between the effect on the oscillations of the Lorentz force produced by an axisymmetric magnetic field and the Coriolis force, is that only the latter can detect the sense of the axis of symmetry. Thus, unlike rotation, an axisymmetric magnetic field affects modes with the same absolute value of m in the same way.

Stellar magnetic fields often influence the oscillations in a way that cannot be described in terms of a standard perturbation analysis. If the magnetic field is force free, it will essentially affect the oscillations directly, via the Lorentz force. Since in the outer layers of a star the Lorentz force is comparable to or larger than the pressure forces, even a relatively small magnetic field will influence in a significant manner the dynamics of the oscillations for those modes which have their maximum amplitude in this region, such as, e.g. high-frequency acoustic modes.

The direct effect of strong axisymmetric force-free magnetic fields on stellar oscillations has been studied in the context of roAp stars, which are permeated by magnetic fields with typical magnitudes of a few kG (Dziembowski and Goode 1996; Bigot et al. (2000); Cunha and Gough (2000); Saio and Gautschy (2004); Saio (2005); Cunha (2006)). From these studies it becomes clear that the influence of a magnetic field on acoustic pulsations has three important consequences. Firstly, the frequencies of the oscillations are shifted from their non-magnetic values. This fact is particularly well illustrated by the data and by the results of model calculations for the prototype HR 1217 (Cunha 2001; Kurtz et al. (2002)). Secondly, the oscillations near the surface

are distorted by the magnetic field in such a way that each mode of oscillation is no longer well described by a single spherical harmonic function Y_l^m, but rather by a sum of spherical harmonics with different degrees, l. Thirdly, the coupling of the oscillations with the magnetic field near the surface of the star generates running waves that take away part of the pulsation energy; these include slow Alvénic waves in the interior that are expected to dissipate as they propagate inwardly, towards regions of higher density, and acoustic waves in the atmosphere which will propagate outwardly, along inclined magnetic field lines. Some of these features depend mostly on the magnetic field configuration and on the degree of the modes, while others depend essentially on the magnetic field magnitude and on the structure of the surface layers of the star. A study of the combined effect of rotation and magnetic field in the context of roAp stars has also been carried out by Bigot and Dziembowski (2002). They showed that for the cases of moderate magnetic fields (<1 kG), the quadratic effects of rotation in roAp stars lead to an inclination of the mode axis with respect to the magnetic one. So far, there is no clear evidence of roAp stars for which the rotational and magnetic effects are comparable. Nevertheless, even if weak, the Coriolis effect is essential to interpret the observed multiplets in some roAp stars. In fact, being the only agent that can cause an asymmetry between the $m = \pm 1$ components of a mode, the Coriolis effect must be responsible for the amplitude inequalities found in multiplets observed in some of these stars.

2.3 The causes of stellar oscillations

The characteristics of the frequency spectra, and our ability to interpret them, determine whether or not useful information about the pulsators can be inferred from the seismic data. As mentioned in Sect. 1.4, the frequency spectra of classical pulsators and solar-like pulsators show significant differences, which are associated with the mechanisms that are responsible for driving the pulsations in each case. Understanding the origin of these differences, and acknowledging the limitations that are intrinsic to the frequency spectra for each of these types of pulsators, is an important step towards improving our capability to infer information from them. Also, an understanding of mode excitation is needed for the planning of future observations. Finally, the observed amplitudes and lifetimes of the modes are directly related to the excitation and damping mechanisms; thus, they provide diagnostics of, for example, the properties of convection in solar-like pulsators (e.g. Christensen-Dalsgaard et al. 1989; Samadi et al. 2006).

2.3.1 Heat-engine-driven pulsators

To illustrate the damping and excitation properties we write the time dependence of the oscillations as $\exp(-\mathrm{i}\omega t)$ separating the angular frequency ω into a real and imaginary part as $\omega = \omega_\mathrm{r} + \mathrm{i}\omega_\mathrm{i}$. Obviously the amplitude of the mode grows or decays with time depending on whether $\omega_\mathrm{i} > 0$ or $\omega_\mathrm{i} < 0$. From the equations of stellar oscillations follows the so-called work integral for ω_i,

$$\omega_{\rm i} \simeq -\frac{1}{2\omega_{\rm r}} \frac{{\rm Im}\left[\int_V \frac{\delta\rho^*}{\rho}\delta p\,{\rm d}V\right]}{\int_V \rho|\boldsymbol{\delta}\mathbf{r}|^2{\rm d}V}$$

$$= -\frac{1}{2\omega_{\rm r}} \frac{{\rm Im}\left[\int_V \frac{\delta\rho^*}{\rho}\delta p_{\rm t}{\rm d}V\right]}{\int_V \rho|\boldsymbol{\delta}\mathbf{r}|^2{\rm d}V} + \frac{1}{2\omega_{\rm r}^2} \frac{{\rm Re}\left[\int_V \frac{\delta\rho^*}{\rho}(\Gamma_3-1)\delta(\rho\epsilon-{\rm div}\,\mathbf{F}){\rm d}V\right]}{\int_V \rho|\boldsymbol{\delta}\mathbf{r}|^2{\rm d}V}, \tag{18}$$

where Im and Re indicate the imaginary and real parts, respectively, and $*$ indicates the complex conjugate; also, ϵ is the rate of energy generation per unit mass, $\mathbf{F}$ is the energy flux, and $\Gamma_3-1=(\partial\ln T/\partial\ln\rho)_{\rm ad}$. Finally, $\delta p_{\rm t}$ is the Lagrangian perturbation to the turbulent pressure. We write Eq. (18) as

$$\eta \equiv \frac{\omega_{\rm i}}{\omega_{\rm r}} \simeq \eta_{\rm t}+\eta_{\rm g} = \frac{W_{\rm t}}{I}+\frac{W_{\rm g}}{I}, \tag{19}$$

where

$$W_{\rm t} = -\omega_{\rm r}\,{\rm Im}\left[\int_0^R \frac{\delta\rho^*}{\rho}\delta p_{\rm t} r^2{\rm d}r\right],$$

$$W_{\rm g} = {\rm Re}\left[\int_0^R \frac{\delta\rho^*}{\rho}(\Gamma_3-1)\delta(\rho\epsilon-{\rm div}\,\mathbf{F})r^2{\rm d}r\right], \tag{20}$$

$$I = 2\omega_{\rm r}^3\int_0^R \rho|\boldsymbol{\delta}\mathbf{r}|^2 r^2{\rm d}r.$$

The expression for $W_{\rm g}$ highlights the heat-engine aspect of the excitation: $\delta(\rho\epsilon-{\rm div}\,\mathbf{F})$ is the perturbation to the heating; regions where the heating is positive at compression, i.e. with positive $\delta\rho$, therefore contribute to the excitation of the mode, as expected for a heat engine. Obviously, other regions may have the opposite phasing and excitation of the mode requires that the regions contributing to the excitation dominate in the integral. In this expression the term in $\delta(\rho\epsilon)$ typically contributes to the excitation, since compression leads to an increased temperature and hence increased energy generation rate. However, this contribution to $W_{\rm g}$ is small in most cases. Thus the excitation or damping is dominated by the perturbation to the energy flux.

It should be noticed that it is often convenient to consider the partial integrals for $W_{\rm t}$ and $W_{\rm g}$ as functions of an upper limit r of the integral. In this way the regions of the star dominating the excitation and damping can be identified. Similarly, e.g. $\eta_{\rm g}(r)=W_{\rm g}(r)/I$ can be regarded as a function of the upper limit.

In most cases of relevance here the processes take place near the stellar surface, and the modes can for this purpose be approximated as being radial. Neglecting also $\delta(\rho\epsilon)$ we obtain

$$W_{\rm g} = -{\rm Re}\left[\int_0^R \frac{\delta\rho^*}{\rho}(\Gamma_3 - 1)\frac{{\rm d}\delta L}{{\rm d}r}{\rm d}r\right], \tag{21}$$

where δL is the Lagrangian perturbation of the luminosity L. Assuming also the diffusion approximation for the radiative flux, the contribution of radiation to the luminosity perturbation in Eq. (18) can be written as

$$\delta L_{\rm rad} = \left[4\frac{\delta r}{r} + (4 - \kappa_T)\frac{\delta T}{T} - \kappa_\rho\frac{\delta\rho}{\rho} + ({\rm d}\ln T/{\rm d}r)^{-1}\frac{\rm d}{{\rm d}r}\left(\frac{\delta T}{T}\right)\right]L_{\rm rad}, \tag{22}$$

where $\kappa_\rho = (\partial\ln\kappa/\partial\ln\rho)_T$, $\kappa_T = (\partial\ln\kappa/\partial\ln T)_\rho$ and $L_{\rm rad}$ is the radiative luminosity. In the deep interior, the oscillations are essentially adiabatic and hence the temperature perturbation is related to the density perturbation by

$$\frac{\delta T}{T} \simeq (\Gamma_3 - 1)\frac{\delta\rho}{\rho}. \tag{23}$$

On the other hand, very near the surface the energy content in the stellar matter is too small to affect significantly the perturbation to the flux. The transition takes place approximately at a location $r_{\rm tr}$ such that the thermal timescale $\tau_{\rm th}$ of the layer outside $r_{\rm tr}$, i.e. the time required to radiate the thermal energy of the layer, matches the pulsation period. Thus

$$\Pi \simeq \tau_{\rm th} = \frac{\langle c_V T\rangle\Delta m}{L} = L^{-1}\int_{r_{\rm tr}}^R c_V T 4\pi r^2\rho\ {\rm d}r, \tag{24}$$

where Π is the pulsation period, c_V being the specific heat at constant volume, Δm the mass outside $r_{\rm tr}$, L the luminosity and $\langle\cdots\rangle$ indicates an average over the region outside $r_{\rm tr}$. Inside $r_{\rm tr}$ the oscillations are nearly adiabatic, Eq. (23) being satisfied, whereas outside $r_{\rm tr}$ the flux perturbation is "frozen in" and the contribution to the work integral is negligible.

These considerations form the basis for a simple qualitative understanding of the properties of unstable modes excited by the radiative flux, developed by J. P. Cox (see Cox and Giuli 1968; Cox 1974).[16] In the quasi-adiabatic region we approximate $W_{\rm g}$ by

$$W_{\rm g} \simeq \int_0^R (\Gamma_3 - 1)\frac{\delta\rho}{\rho}\frac{\rm d}{{\rm d}r}\left(\psi_{\rm rad}\frac{\delta\rho}{\rho}\right){\rm d}r, \tag{25}$$

[16] The analysis of stellar instability goes back to Eddington (1926), who pointed out the potentially crucial role of the phasing of the heat leak and hence the opacity for driving the oscillations. The detailed understanding of the Cepheid instability strip was developed in a series of papers by S. A. Zhevakin (e.g. Zhevakin 1953) and J. P. Cox and C. Whitney (e.g. Cox and Whitney 1958). See also the review by Zhevakin (1963).

where the eigenfunctions were taken to be real, energy transport was assumed to be dominated by radiation, and $\delta L_{\rm rad} \simeq -\psi_{\rm rad}\delta\rho/\rho$, with

$$\psi_{\rm rad} = (\kappa_T - 4)(\Gamma_3 - 1) + \kappa_\rho; \tag{26}$$

thus we neglected the terms in $\delta r/r$ and the derivative of $\delta T/T$ in Eq. (22). In the outer parts of the star $\delta\rho/\rho$ typically increases with r; also, except very near the surface, $\psi_{\rm rad}$ is generally negative. Thus if $\psi_{\rm rad}$ does not vary substantially the contributions to the integral in Eq. (25) are negative, giving a negative contribution to $W_{\rm g}$ and hence contributing to damping the mode. The exception are regions where the opacity derivatives (or $\Gamma_3 - 1$) vary rapidly, leading to rapid variations in $\psi_{\rm rad}$. A region where $\psi_{\rm rad}$ increases towards the surface contributes to the driving; however, this would typically be followed by a region where $\psi_{\rm rad}$ decreases and hence, as long as Eq. (25) is valid, the integrated effect of such regions largely cancels. On the other hand, if the transition defined by $r_{\rm tr}$ falls near the region where $\psi_{\rm rad}$ varies rapidly, such that only the lower, driving, part of that region contributes, the net effect may be to make the mode unstable. Thus instability tends to be found in stars and for periods where the transition region coincides with a region of rapid variation in the opacity, e.g. associated with a region of partial ionization of an important opacity source. This is the case for the excitation of the classical Cepheids and other stars in the Cepheid instability strip (cf. Fig. 1); here the dominant effect is associated with the second ionization of helium, except for roAp stars, with much shorter periods, for which the dominant effect is associated with the region of hydrogen ionization (Balmforth et al. 2001; Cunha (2002)).

An extensive overview of the excitation of oscillations through the opacity mechanism was given by Pamyatnykh (1999). Following him, Fig. 6 shows the differential work integral for two modes in a model of a δ Scuti star, as well as the quantity $\psi_{\rm rad}$, which determines the luminosity perturbation in terms of the density perturbation, and the thermal time scale. Evidently, regions where $\mathrm{d}W_{\rm g}/\mathrm{d}\log T$ is positive, contribute to the excitation of the mode. The peak in $\psi_{\rm rad}$ at $\log T \simeq 4.6$ corresponds to the second ionization of helium. As expected, the rising part of this peak causes excitation for both the $n = 1$ and $n = 9$ modes. For the $n = 1$ mode the transition to strongly nonadiabatic oscillations, with $\tau_{\rm th}/\Pi \ll 1$, takes place so close to the region of excitation that the corresponding damping contribution is insignificant; for the $n = 9$ mode, on the other hand, there is strong damping in the outer parts of the helium peak in $\psi_{\rm rad}$. The net effect is that the $n = 1$ mode is unstable while the $n = 9$ mode is stable. (The secondary excitation around $\log T \simeq 4.1$ arises from the first ionization of helium and the ionisation of hydrogen but makes a relatively modest contribution to the overall excitation).

With increasing effective temperature the helium peak in $\psi_{\rm rad}$ moves closer to the surface, in the direction of decreasing $\tau_{\rm th}$. Consequently, higher order modes, with smaller periods, have a tendency to be excited. Thus we may expect to see excitation of higher order modes on the blue (high-temperature) side of the instability strip. This is confirmed by the detailed calculations presented by Pamyatnykh (1999). As discussed by Pamyathykh, a similar effect operates amongst the B stars. These are excited by an opacity feature (visible in Fig. 6b around $\log T \simeq 5.2$) caused by contributions

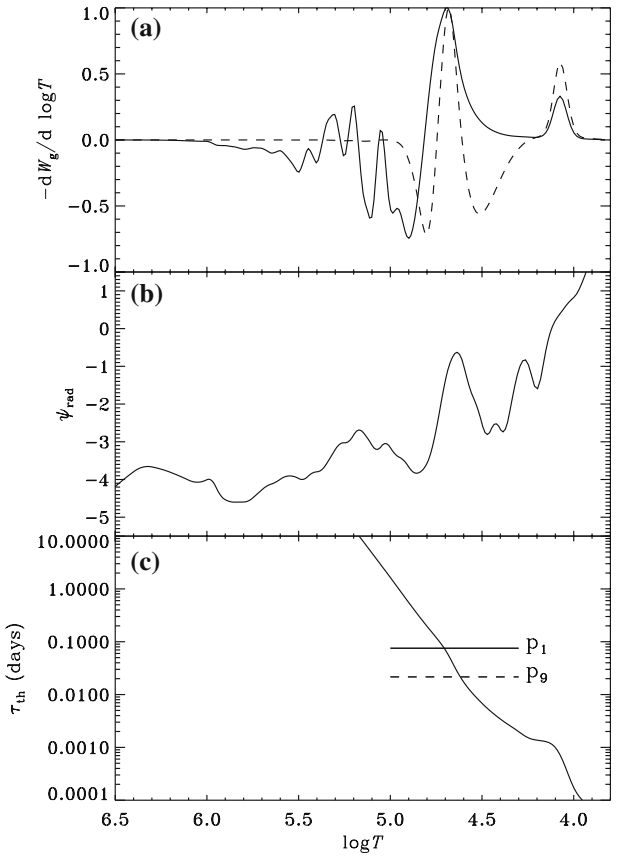

Fig. 6 Differential work integral $-\mathrm{d}W_g/\mathrm{d}\log T$ (cf. Eq. (20); the minus sign is included for consistency with that equation), the function ψ_{rad} (cf. Eq. (26)) determining the response of the opacity and the thermal timescale τ_{th} (cf. Eq. (24)), in a model of a δ Scuti star of mass 1.8 $\mathrm{M}_\odot$, age 0.8 Gyr and effective temperature 7, 500 K. The *solid* and *dashed curves* in **a** and the *solid* and *dashed heavy horizontal lines* in **c** correspond to radial modes of radial order $n = 1$ and 9, respectively (See Pamyatnykh 1999)

from iron-group elements. This causes excitation of low-order acoustic and gravity modes with periods of a few hours in the β Cephei stars, with masses of around 10 $\mathrm{M}_\odot$ and effective temperatures around 25, 000 K. The same mechanism causes excitation of the high-order g-mode oscillations, with periods of a day or more, in the Slowly Pulsating B stars with masses around 4 $\mathrm{M}_\odot$ and effective temperatures around 15, 000 K.[17]

Diffusive processes may play an important role in the excitation of modes in hot stars. In the case of the subdwarf B variables (sdBV stars), Fontaine et al. (2003) found that radiative levitation of iron was required to increase the iron abundance in

[17] The apparently analogous situation regarding the long-period oscillations in the γ Doradus stars on the cool side of the instability strip probably has a different physical origin, since the oscillations in these stars appear to be excited through 'convective blocking'; see below.

the driving region to the point where the observed modes were unstable. Interestingly, Ausseloos et al. (2004) and Pamyatnykh et al. (2004) found that in standard models of the β Cephei star ν Eri, which fitted all the observed frequencies, not all the observed modes were unstable. They inferred that a similar enhancement of the iron abundance in the driving zone might be required to account for the excitation. So far, no consistent evolution calculations of diffusive processes have been carried out in β Cephei models, however. Alternatively, Miglio et al. (2007a) found that the instability of modes in B stars could be enhanced without considering diffusive processes, but using the revised solar mixture by Asplund et al. (2005) (in controversy with helioseismology) and OP opacities (e.g. Seaton 2005); this may contribute to the solution of the issue of mode excitation.

This analysis determines which modes are linearly unstable and hence have a tendency to grow, but it says nothing about the resulting amplitudes. Formally, the amplitude grows exponentially, as $\exp(\omega_{\rm i} t)$, when $\omega_{\rm i} > 0$; clearly, other mechanisms must set in to limit the amplitudes to finite values. For high-amplitude pulsators, such as Cepheids or RR Lyrae stars, a single mode typically dominates and it is reasonable to assume that the driving mechanism is saturated by nonlinear effects in this mode; in fact, early nonlinear calculations of radial oscillations (e.g. Christy 1966) were quite successful in reproducing the observed amplitudes and light- and velocity curves in such stars. For low-amplitude pulsators near the main sequence the situation is far more complex. Here typically a substantial number of modes are excited to observable amplitudes; although the frequency interval covered by the observed modes generally corresponds reasonably well with the interval in which unstable modes are predicted, their amplitudes typically vary greatly and with no obvious pattern. An example is illustrated in Fig. 7. It was suggested by Dziembowski and Królikowska (1985) that in this case the dominant amplitude limiting mechanism could be resonant mode coupling between an unstable mode and a pair of stable lower frequency modes (typically g modes). The resulting amplitudes would therefore depend on the complex spectrum of g modes and the extent to which the resonance conditions were satisfied. The mechanism was examined in detail by Nowakowski (2005). He concluded that, even taking into account rotational splitting, the resonant-coupling mechanism was inadequate to explain the observed amplitudes and proposed that nonlinear saturation of the driving, involving interactions between the unstable modes, must be invoked. It is clear, however, that we still do not have a general understanding of the physical phenomenon that determines the amplitudes in low-amplitude multi-periodic stars, let alone the ability to predict the observed amplitudes in detail. An impressive attempt to remedy the situation are the computations for radial modes by Smolec and Moskalik (2007), who found that collective saturation of the driving mechanism by several acoustic modes can predict amplitudes to the observed level.

We have so far assumed that each mode of oscillation is a simple harmonic function of time. This is true as long as linear theory is adequate; however at larger amplitudes, the behaviour is typically distorted. When only a single frequency is present, the outcome is obviously a set of harmonics of the basic frequency, which together defines the actual light or velocity curve. In multimode pulsators the effect of the non-linearities in the power spectrum is to generate a set of linear combinations of the basic frequencies; this is visible for the δ Scuti star FG Vir in the upper panel of Fig. 7 where the

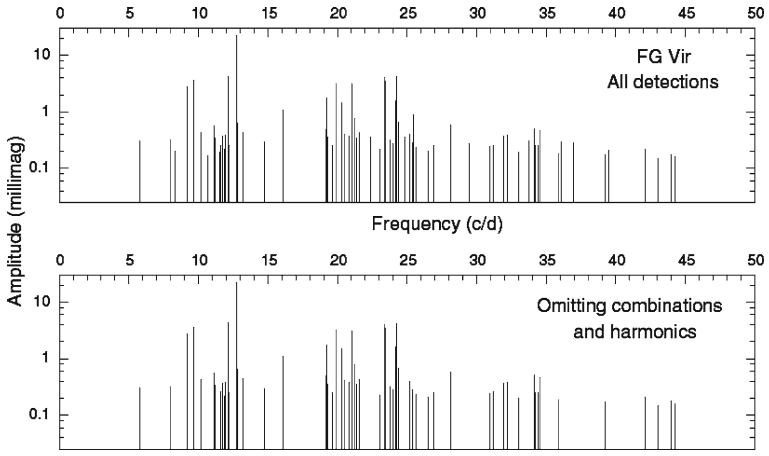

Fig. 7 Observed modes in the δ Scuti star FG Vir, from extensive photometric observations spanning more than a decade. In the *lower panel* combination frequencies, including harmonics, resulting from the non-sinusoidal nature of the oscillations have been removed; this therefore represents the true spectrum of independent oscillations in the star (From Breger et al. (2005), with permission.)

harmonics and combination frequencies are included. This behaviour is particularly striking in observations of white dwarfs (e.g. Winget et al. 1994); it was noted by Wu (2001) and Montgomery (2005) that the amplitudes and phases of the combinations can be used as diagnostics for the convection zone in such stars.

So far we have neglected the convective contributions to the stability of the mode. In addition to the term in the turbulent pressure, shown explicitly in Eq. (18), these include the convective contribution to the flux. The inclusion of these contributions is obviously hampered by the lack of a reliable procedure to compute the effects of convection, even in the static case of the equilibrium model. Various time-dependent convection formulations have been developed to deal with the convection–pulsation interactions, based on differing physical models. The formulation by Unno (1967) was further developed by Gabriel (1974, 1975); Gabriel (1996, 2000), as summarized by Grigahcène et al. (2005). Gough (1977b) developed a somewhat different formulation based on a detailed physical description of the dynamics of convective elements; this was extended to a non-local formulation by Balmforth (1992), based on the non-local description of convection in a static model developed by Gough (1977c) and illustrated in a solar model by Gough (1985a). Alternative formulations were proposed by Stellingwerf (1982) (further developed by, e.g. Kuhfuß (1986); Gehmeyr and Winkler (1992); Feuchtinger (1999)) and Xiong et al. (1997). A review of these different formulations was provided by Baker (1987).

Simple analyses show that convection may contribute to the excitation in the extreme cases of very long and very short convective time scales, compared with the pulsation period. In the former case it is plausible that the convective flux does not react to the pulsations, leading to a negligible convective-flux perturbation $\delta L_{\rm con}$. It was noted by Cox and Giuli (1968) that this might cause excitation if the radiative flux and hence the radiative-flux perturbation become small in the convection zone: since $\psi_{\rm rad}$ is

typically negative, δL is in phase with $\delta\rho/\rho$ just beneath the convection zone; thus the change to very small δL in the convection zone corresponds to a negative $\mathrm{d}\delta L/\mathrm{d}r$ in Eq. (21) and hence to a contribution to the driving. Physically this effect arises from the effective blocking by convection of the luminosity perturbation at the base of the convection zone, leading to heating in phase with compression. Thus the mechanism was dubbed 'convective blocking' by Pesnell (1987). It has been shown that this may account for the driving of the long-period g modes in the γ Doradus stars (e.g. Guzik et al. 2000; Warner et al. 2003); here the convection zones are sufficiently deep that the convective timescale is substantially longer than the pulsation period. More detailed calculations by Dupret et al. (2004, 2005a), using the convection formulation of Gabriel (1996), essentially confirmed that convective blocking dominates the driving of these oscillations.

The opposite extreme, the convective timescale being much shorter than the pulsation period, is relevant to pulsating white dwarfs with significant outer convection zones. The g-mode pulsations in such stars have periods far exceeding the convective timescales in the relatively thin convection zones. It was argued by Brickhill (1983, 1991) for DA white dwarfs that in this case also the convection zone may act to excite the modes; this was confirmed in a more detailed analysis by Goldreich and Wu (1999). In this case the energy input to the convection zone by the flux perturbation at its base is redistributed throughout the convection zone as a result of the short convective timescale, causing heating of the convection zone; since the radiative flux perturbation is in phase with the density perturbation at the top of the radiative region, as argued above, and the density perturbation varies little through the convection zone, heating is in phase with the density perturbation throughout the convection zone, which therefore contributes to the excitation of the mode.

Early detailed calculations of the excitation of modes in the Cepheid instability strip (e.g. Baker and Kippenhahn 1962; Baker and Kippenhahn 1965) found reasonable agreement between the upper limit in effective temperature of instability and the observed blue edge of the instability strip. However, the models remained unstable at much lower effective temperature than observed. In these calculations the interaction between convection and pulsations was ignored. An early demonstration that convective effects can in fact delimit the Cepheid instability strip on the cool side was obtained by Baker and Gough (1979), using the formulation by Gough (1977b), for models of RR Lyrae stars. Gonczi (1981) similarly found stability at the red edge, for Cepheid models, using the formulation of Unno (1967). Stellingwerf (1984) also delimited the RR Lyrae instability strip using the formulation by Stellingwerf (1982). Gehmeyr (1993) studied the suppression of instability by convection at the red edge of the RR Lyrae region, in a fully nonlinear calculation, while Xiong and Deng (2001) used the non-local time-dependent theory of Xiong et al. (1997) to locate the red edge of the δ Scuti instability strip. However, although these calculations generally find that convective effects can account for the stabilization of the cool models, it is striking that the physical description of the effect depends strongly on the detailed convection formulation employed.

To illustrate the effects of convection on the location of the instability strip we consider calculations carried out by Houdek (2000), using a formulation developed by Gough (1977b) and Balmforth (1992). Figure 8 shows the resulting relative growth

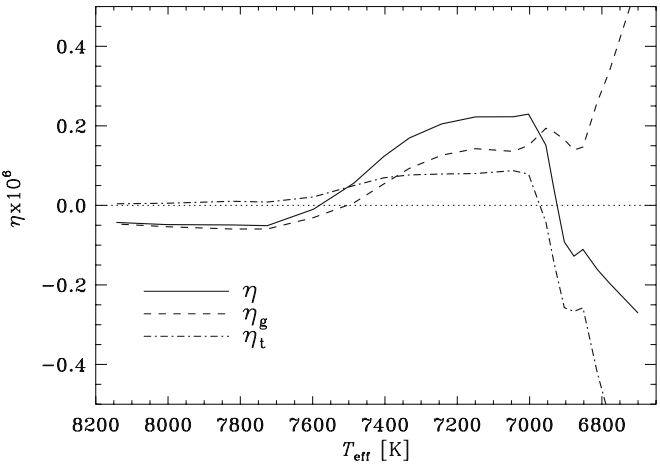

Fig. 8 Stability coefficients $\eta = \omega_i/\omega_r$ for the fundamental radial mode as a function of effective temperature $T_{\rm eff}$, for a 1.7 $M_\odot$ model of a δ Scuti star evolving during the core hydrogen-burning phase. The *dashed* and *dot-dashed curves* show the contributions from the thermal effect and the perturbation to the turbulent pressure, respectively [see Eqs. (19) and (20)], and the solid curve shows their sum (adapted from Houdek 2000)

rates, for an evolution sequence of 1.7 $M_\odot$ models evolving through the Cepheid instability strip during core hydrogen burning and hence corresponding to δ Scuti stars. The onset of instability, at the blue edge of the strip, takes place at $T_{\rm eff} \simeq 7{,}600$ K. Interestingly, the thermal contribution η_g to excitation, which includes the effects of the perturbation to the convective flux, grows strongly as the model $T_{\rm eff}$ decreases; however, this is more than balanced by the large negative values of η_t arising from the perturbation to the turbulent pressure, leading to overall return to stability at a red edge of the instability strip near $T_{\rm eff} = 6{,}900$ K. Further details on the contributions to excitation and damping are illustrated in Fig. 9, for a model just on the cool side of the instability strip. Obviously, the bulk of the HeII ionization zone contributes to the excitation of the mode, essentially as in Fig. 6; but the contribution from the turbulent pressure is damping in most of the convection zone, leading to overall stability.

Extreme cases of interaction between convection and pulsations are probably found in the *Mira variables* on the extreme red-giant branch, with very extensive outer convection zones. Their oscillations are likely excited by the heat-engine mechanism, undoubtedly involving a strong effect of convection, but the details are so far highly uncertain (e.g. Xiong et al. 1998; Munteanu et al. 2005; Olivier and Wood 2005). Owing to their huge radii these stars are excellent targets for interferometry, including early work by Quirrenbach et al. (1992) (see also, for example Ohnaka et al. 2005; Wittkowski et al. 2007), yielding detailed information about their complex atmospheric structure. Since they typically show only one, or at most a few, modes the stars are less interesting from an asteroseismic point of view, although further studies might help elucidate aspects of the convection–pulsation interactions.

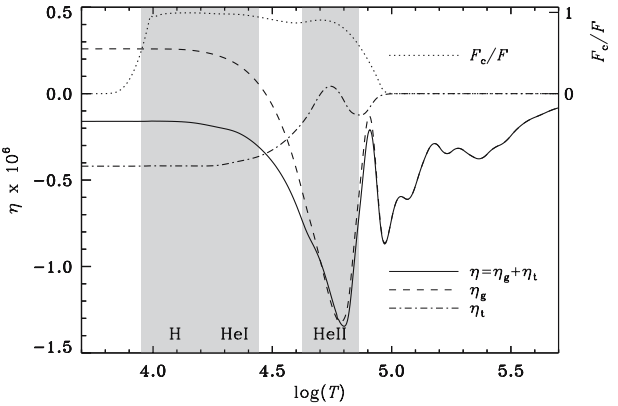

Fig. 9 Relative work integrals, as functions of the upper limit of integration expressed in terms of $\log T$, for the fundamental radial model in a model with $T_{\rm eff} = 6{,}813$ K in the $1.7\,M_\odot$ sequence illustrated in Fig. 8. The *dashed* and *dot-dashed curves* show the contributions from the thermal effect and the perturbation to the turbulent pressure, respectively [see Eqs. (19) and (20)], and the *solid curve* shows their sum. The *shaded areas* indicate the regions of hydrogen ionization (H) and first and second helium ionization (HeI and HeII, respectively). The *dotted curve*, using the right-hand ordinate scale, shows the contribution $F_{\rm c}/F$ of convection to the total flux in the equilibrium model (adapted from Houdek 2000)

2.3.2 Stochastically excited pulsations

It appears that modes in stars on the cool side of the Cepheid instability strip, including the Sun, are generally stable. The excitation of the observed modes is attributed to stochastic forcing by the near-surface convection, a process first discussed in detail in the stellar case by Goldreich and Keeley (1977). Indeed, as pointed out by Lighthill (1952) turbulent flows with speeds approaching the speed of sound generate sound very efficiently, and the near-surface convection is thus a source of strong sound generation in stars with substantial outer convection, exciting the normal modes of the star. Stein (1968) applied Lighthill's theory to the solar convection zone and atmosphere, to estimate the acoustic energy flux generated by convection.

Batchelor (1953) considered the general problem of the stochastic excitation of a damped oscillator. It is straightforward to show that the resulting power spectrum, for a mode of frequency ω_0 and damping rate $\omega_{\rm i}$, is given by

$$P(\omega) \simeq \frac{1}{4\omega_0^2} \frac{P_f(\omega)}{(\omega - \omega_0)^2 + \omega_{\rm i}^2}, \tag{27}$$

where P_f is the power of the forcing function (see also Christensen-Dalsgaard et al. 1989). Thus if the forcing varies slowly with frequency the result is, on average, a Lorentzian profile, with a width determined by $\omega_{\rm i}$. An example of a single realization of such a spectrum, including the fitted Lorentzian profile, is illustrated in Fig. 10, based on 8 years of solar whole-disk observations with the BiSON network. Thus with well-resolved observations the damping rates can be determined from the observed line widths. From the observed surface amplitudes and damping rates in the solar case,

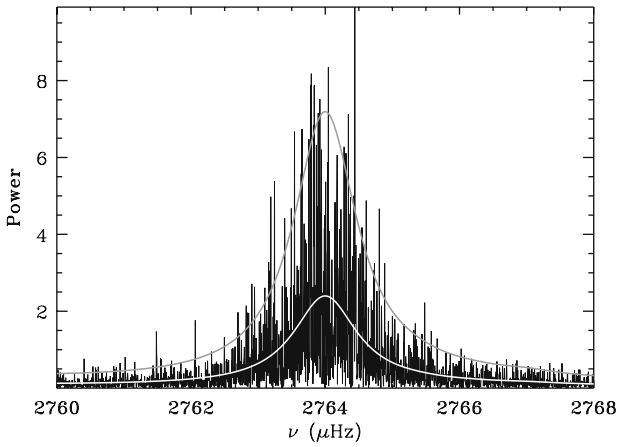

Fig. 10 Observed spectrum, from coherent analysis of 8 years of Doppler observations with the BiSON network, of a single radial mode of solar oscillations (of radial order $n = 19$). The *smooth white curve* shows the fitted Lorentzian profile, while the *grey curve* shows the same profile, multiplied by three (see Chaplin et al. 2002a)

and the mode mass (cf. Eq. (15)), the required rate of energy input can be estimated as

$$\frac{\mathrm{d}\mathcal{E}}{\mathrm{d}t} = |\omega_\mathrm{i}| M_\mathrm{mode} A_V , \tag{28}$$

where A_V is the velocity power, corrected for the geometric effect of averaging over the solar surface (Roca Cortés et al. 1999). In Fig. 11 the result is compared with the stochastic energy input calculated from a detailed hydrodynamical model of near-surface convection (Stein and Nordlund 2001). The agreement between the observations and the computations is evidently quite reasonable. It should be noted, in particular, that in contrast to the heat-engine excitation we obtain a definite theoretical prediction of the mode amplitudes which furthermore tend to vary relatively slowly with frequency. Thus in this case we expect to see the excitation of a fairly complete set of modes over a substantial range of frequencies, obviously easing the problem of mode identification and increasing the asteroseismic information content.

Chaplin et al. (2005) made a detailed analysis of the expected amplitudes of stochastically excited oscillations, summarized by Houdek (2006). The result can be written as

$$\langle V^2 \rangle = \frac{1}{\omega_\mathrm{i} E} \frac{\mathcal{P}_\mathrm{f}}{E}, \tag{29}$$

where $\langle V^2 \rangle$ is the mean square oscillation velocity, E is the mode inertia (cf. Eq. (15)) and $\mathcal{P}_\mathrm{f}$ is a measure of the forcing. From Eqs. (18) and (19), and the fact that the integrals in W_t and W_g are generally dominated by the near-surface layers, it follows that $\omega_\mathrm{i} E$ depends on the behaviour of the eigenfunction near the surface which is largely a function of frequency. The same is true of $\mathcal{P}_\mathrm{f}$. Thus, approximately, we can write Eq. (29) as

$$\langle V^2 \rangle \simeq \frac{\mathcal{F}(\omega)}{E}. \tag{30}$$

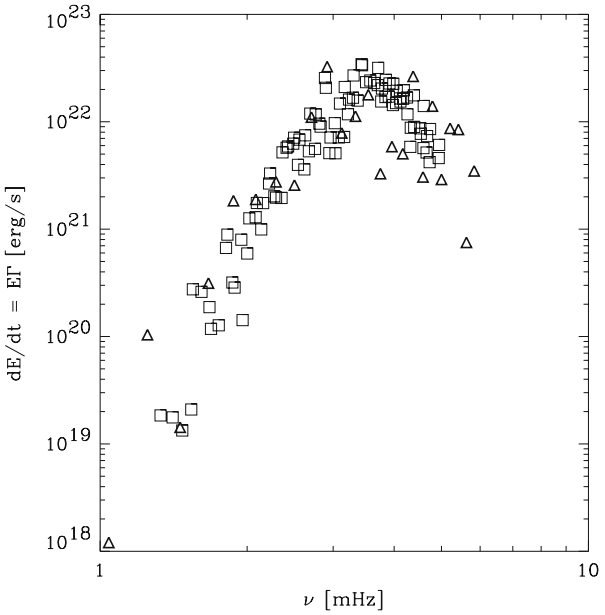

Fig. 11 Comparison of observed and computed energy input to low-degree solar acoustic modes (cf. Eq. (28)). The *squares* are observed values, from Doppler-velocity observations of modes of degree $l = 0$ to 3, with the GOLF instrument on the SOHO spacecraft (Roca Cortés et al. 1999). The *triangles* result from hydrodynamical simulations of solar convection (Stein and Nordlund 2001)

It follows that, at given frequency, the power in the mode scales approximately as E^{-1}; equivalently, given Eq. (16), the mode energy is predominantly a function of frequency.

Based on theoretical estimates of the damping rates and energy input it is evidently possible to predict the expected oscillation amplitudes as functions of stellar parameters (Christensen-Dalsgaard and Frandsen 1983). Kjeldsen and Bedding (1995) showed that the results could be fitted by the simple relation $v_{\rm osc} \propto L/M$, where $v_{\rm osc}$ is the surface velocity. Using Gough's and Balmforth's treatment of convection, Houdek et al. (1999) confirmed that the predicted amplitudes generally increased with increasing luminosity along the main sequence. However, the estimated damping rates and energy input are obviously rather uncertain. In fact it appears that the observed amplitudes of stars hotter than the Sun, including Procyon, are substantially lower than these simple predictions (e.g. Gilliland et al. 1993; Martić et al. 2004). Houdek (2002) found that the predicted amplitudes for α Cen A and β Hyi (both of roughly solar effective temperature) approximately agreed with the observed values, while confirming that the predicted surface velocity for Procyon, which is substantially hotter than the Sun, exceeded the observed value by roughly a factor of two. He speculated that the dominant problem in the calculations might be the computed damping rate, which arises from a combination of several terms of different sign; in particular, he pointed to the neglect of incoherent scattering as a potential deficiency of the damping-rate computation. Hydrodynamical simulations of convection can constrain the parameters

of simpler formulations (Samadi et al. 2003a, b). Stein et al. (2004) made an extensive calculation of the energy input from detailed simulations of a number of stars, concluding, as in the case of the simpler calculations, that the excitation increases with increasing effective temperature and decreasing gravity. An overview of the excitation of solar-like oscillations in pre-main-sequence and main-sequence models was provided by Samadi et al. (2005).

For stars other than the Sun the duration or signal-to-noise ratio of the observations have not allowed resolution of the Lorentzian profile. However, mode lifetimes can be estimated from the statistics of the observed power spectra or inferred frequencies. From such analyses Kjeldsen et al. (2005) found that the mode lifetimes in α Cen A and B were around 3 days at the maximum in power, similar to the Sun; a similar result was obtained by Fletcher et al. (2006). Analysis of amplitude and frequency scatter for the metal-poor subgiant ν Ind by Carrier et al. (2007) indicated a lifetime of at least 9 days, substantially longer than for the Sun. On the other hand, Stello et al. (2006) found that the solar-like oscillations in the red giant ξ Hya (Frandsen et al. 2002) had a lifetime of only a few days, far shorter than the predictions by Houdek and Gough (2002). As noted by Stello et al., this could severely compromise the possibilities of using frequencies of red giants for asteroseismology. Leccia et al. (2007) recently obtained a life time of around 2 days for modes in Procyon, largely consistent with unpublished estimates based on the calculations by Houdek and Gough (2002). This would indicate that the excessive predicted amplitude for Procyon results from problems with the energy input. Interestingly, Houdek (2006) noted, based in part on hydrodynamical simulations by Stein et al. (2004), that there may be partial cancellation between contributions to the forcing from the fluctuating turbulent pressure and the turbulent gas pressure. Further calculations, as well as more precise observations of a broader range of stars, are needed to check whether such effects may account for the observed amplitudes.

The effects of near-surface convection also contribute uncertainties in the calculation of stellar oscillation frequencies. In most cases frequency calculations assume adiabatic oscillations and neglect the dynamical effects of convection, in the form of turbulent pressure, both in the equilibrium model and the pulsations. A full nonadiabatic calculation would require taking into account the effects of the perturbation to the convection flux; this is further complicated by the fact that the convective timescale in the region of substantial nonadiabaticity is generally similar to the oscillation period in the case of solar-like oscillations. Such near-surface effects are characterized by being predominantly functions of frequency, apart from an essentially trivial dependence on the mode inertia E, and by being small at relatively low frequency (Christensen-Dalsgaard and Thompson 1997); modes in the low range of the frequencies of stochastically excited modes are evanescent near the surface and hence are less affected by the near-surface errors in the computations. As illustrated in Fig. 12 these near-surface errors generally dominate the differences between computed and observed frequencies of the Sun (see also Christensen-Dalsgaard 1988). Rosenthal et al. 1999 found that including an averaged hydrodynamical simulation, instead of the normal mixing-length treatment, in models of the solar envelope substantially reduced this near-surface frequency error. Similar results were obtained by Robinson et al. (2003) by including results from simulations in the physics used in the computation of solar models. Earlier, Paternò et al. (1993) found that the differences between the solar

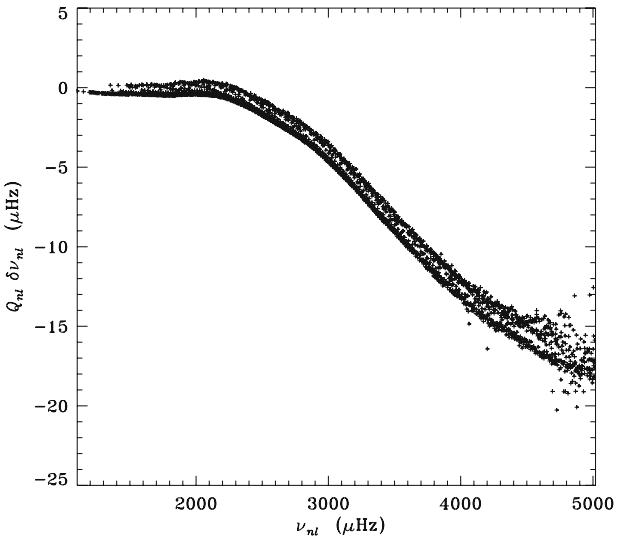

Fig. 12 Frequency differences, in the sense (Sun) – (Model), between observed frequencies from the MDI instrument on the SOHO spacecraft (Kosovichev et al. 1997) and Model S of Christensen-Dalsgaard et al. (1996). Modes with $l \leq 100$ have been included. To compensate for the variation with degree of the mode inertia, the frequencies have been scaled by $Q_{nl} = E_{nl}/\bar{E}_0(\omega_{nl})$ where E_{nl} is the mode inertia (cf. Eq. (15)) and $\bar{E}_0(\omega_{nl})$ is the inertia of a radial mode, interpolated to the frequency ω_{nl} of the mode

and model frequencies were decreased if the Canuto and Mazzitelli (1991) convection treatment was used instead of the Böhm-Vitense (1958) mixing-length treatment used for the model illustrated in Fig. 12 (see also Monteiro et al. 1996); Kosovichev (1995) noted that including turbulent pressure in the calculation of the equilibrium model similarly reduced the differences.

2.4 Seismic inference

The level of information that can be obtained from asteroseismic data evidently depends crucially on the amount and quality of the data. With only a few modes, or the basic structure of the spectrum of solar-like oscillations, we can determine global parameters of the star such as the mass and radius. At the opposite extreme, we may hope to obtain a sufficient number of well-identified modes to be able to carry out inverse analyses to infer details of the structure of at least parts of the star. Regardless of the asteroseismic potential for a given star, it is very important to supplement the asteroseismic data with other types of data, as a test of the consistency of the results or to extend the usefulness of the oscillation frequencies.

The development and testing of procedures for asteroseismic inference are far from trivial. A commonly used, and very effective, procedure is the so-called "hare-and-hounds" exercise. Here artificial data, based, say, on the frequencies of some model, are created by the "hare"; the "hounds" analyse these data with only the information about the underlying model that would be available from real observations. Subsequently

the inferences of the hounds are compared with the truth about the original model. Evidently, the generation of the data should be as realistic as possible, for example taking into account the stochastic nature of the excitation of solar-like oscillations. An example of an application to seismic inferences for solar-type stars has been given by Monteiro et al. (2002). Application to "classical" pulsating stars, within the context of the CoRoT mission, was considered by Thoul et al. (2003), whereas Appourchaux et al. (2006) gave an exhaustive survey of the expected performance of the CoRoT mission based on an extensive series of exercises; Mazumdar (2005) carried out a detailed analysis of asteroseismic inferences for one of these cases. An interesting recent example of this type of exercise, applied to time-series analysis of simulated solar data, is provided by Chaplin et al. (2006).

2.4.1 Basic asymptotic signatures

In many cases observed modes are of high radial order and valuable information can be extracted from the asymptotic properties of the frequency spectrum. This is true both for acoustic modes, particularly as observed in solar-like pulsators, and for the long-period g modes observed in, for example, slowly pulsating B stars, γ Doradus stars and white dwarfs.

The basic asymptotic properties of low-degree high-order acoustic modes were elucidated by Vandakurov (1967) and Tassoul (1980, 1990); they can also be obtained from JWKB analysis of the asymptotic Eq. (6) (e.g. Gough 1986, 1993). The result is that the cyclic frequencies ν_{nl} for acoustic modes of radial order n and degree l are given, in this asymptotic limit, by the expression

$$\nu_{nl} \simeq \left(n + \frac{l}{2} + \frac{1}{4} + \alpha\right) \Delta\nu_0 - [Al(l+1) - \delta]\frac{\Delta\nu_0^2}{\nu_{nl}}, \tag{31}$$

where

$$\Delta\nu_0 = \left(2\int_0^R \frac{\mathrm{d}r}{c}\right)^{-1} \tag{32}$$

is the inverse sound travel time across a stellar diameter, and

$$A = \frac{1}{4\pi^2\Delta\nu_0}\left[\frac{c(R)}{R} - \int_0^R \frac{\mathrm{d}c}{\mathrm{d}r}\frac{\mathrm{d}r}{r}\right]; \tag{33}$$

also, α (which in general is a function of frequency) is determined by the reflection properties near the surface and δ is a small correction term predominantly related to the near-surface region. To leading order, neglecting the last term, Eq. (31) predicts a uniform spacing of modes of the same degree. This difference in frequency of modes of the same degree and consecutive order – ($\Delta\nu_{nl} = \nu_{n+1\,l} - \nu_{nl}$) – is known as the *large frequency separation* and is, to leading order, approximately equal to $\Delta\nu_0$. Also to leading order, Eq. (31) predicts a degeneracy between frequencies of modes with

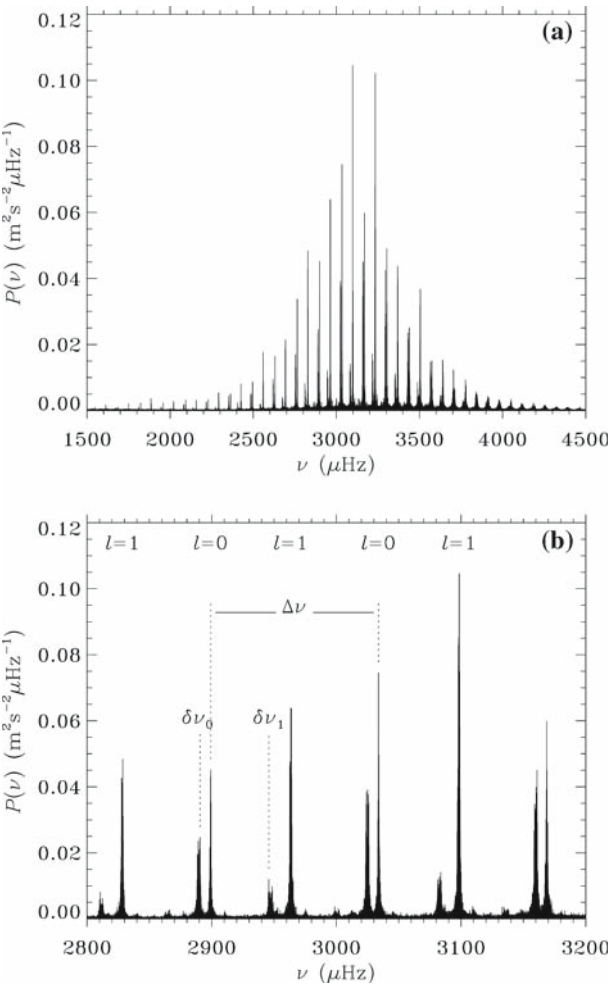

Fig. 13 Power spectrum of solar oscillations, obtained with the six-station BiSON network, using Doppler observations in light integrated over the disk of the Sun; the data span the full 15-year period over which the complete BiSON network has been operating. The ordinate is normalized to show velocity power per frequency bin. **b** An expanded view of the central part of the frequency range. Here some modes have been labelled by their degree l, and the large and small frequency separations $\Delta\nu_{nl}$ and $\delta\nu_{nl}$ [cf. Eqs. (31) and (35)] have been indicated (Note that for simplicity only the relevant indexes were used in the figure) (data kindly provided by the BiSON group. See Chaplin et al. 2007)

degree of the same parity,

$$\nu_{n\,l} \simeq \nu_{n-1\,l+2}. \tag{34}$$

Finally, modes of odd degree fall halfway between modes of even degree. This pattern is clearly observed in solar data (see Fig. 13a) and is one of the clearest indicators for the detection of solar-like oscillations.

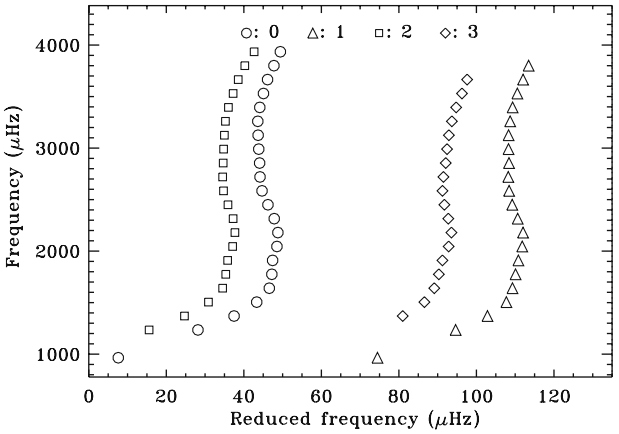

Fig. 14 Echelle diagram for observed solar frequencies obtained with the BiSON network (Chaplin et al. 2002a), plotted with $\nu_0 = 830\,\mu\text{Hz}$ and $\langle\Delta\nu\rangle = 135\,\mu\text{Hz}$ (cf. Eq. (36)). *Circles*, *triangles*, *squares* and *diamonds* are used for modes of degree $l = 0$, 1, 2 and 3, respectively

The departure from the degeneracy in Eq. (34) is reflected in the *small frequency separation*

$$\delta\nu_{nl} = \nu_{n\,l} - \nu_{n-1\,l+2} \simeq -(4l+6)\frac{\Delta\nu_0}{4\pi^2\nu_{nl}}\int_0^R \frac{\mathrm{d}c}{\mathrm{d}r}\frac{\mathrm{d}r}{r}, \tag{35}$$

where we neglected the small term in $c(R)$ in Eq. (33). This frequency structure is also clearly visible in solar data, as shown in Fig. 13b. It is evident that the separation depends on the degree; this can be used to identify the degrees of the observed modes, as was also done in the early phases of helioseismology (e.g. Christensen-Dalsgaard and Gough 1980).

A convenient way to illustrate the details of the frequency spectrum is in terms of an *echelle* diagram. Graphically this corresponds to dividing the spectrum in segments of length $\Delta\nu_0$ and stacking the segments. Thus we express the frequency as

$$\nu_{nl} = \nu_0 + k\langle\Delta\nu\rangle + \tilde{\nu}_{nl}, \tag{36}$$

where ν_0 is a arbitrary reference frequency, k is an integer, $\langle\Delta\nu\rangle$ is a suitable average of $\Delta\nu_{n\,l}$ and the *reduced frequency* $\tilde{\nu}_{nl}$ is between 0 and $\langle\Delta\nu\rangle$. An example, for observed solar frequencies, is illustrated in Fig. 14. Had the asymptotic relation in Eq. (31) been exact, the result would be largely vertical sets of points, separated by the small separation. As shown there are significant departures from this behaviour; in particular, the curvature arises largely from the term in $\alpha = \alpha(\omega)$ in the asymptotic relation; as discussed in Sect. 2.4.3 this behaviour carries information about the helium content in the stellar envelope.

Owing to the factor r^{-1} in the integral in Eq. (35) the small separation is very sensitive to the sound-speed structure of the stellar core. From a physical point of view this is the result of the propagation regions of the modes. The $l = 2$ modes are

reflected at the inner turning point r_t (cf. Eq. (14) and Fig. 5) whereas the radial modes penetrate essentially to the centre. In other parts of the star the modes are very similar; hence the dominant difference in their frequencies arises from the core. This property makes acoustic modes of low degree (so far the only degrees that are observable in distant stars with solar-like oscillations) particularly valuable as diagnostics of stellar cores.

Other frequency combinations which suppress the dominant large-scale structure of the frequency spectrum carry similar information, at least to the extent that the asymptotic description is valid. An example is

$$\delta^{(1)}\nu_{n\,l} = \nu_{n\,l} - \frac{1}{2}(\nu_{n-1\,l+1} + \nu_{n\,l+1}) \simeq -(2l+2)\frac{\Delta\nu_0}{4\pi^2\nu_{nl}}\int_0^R \frac{\mathrm{d}c}{\mathrm{d}r}\frac{\mathrm{d}r}{r}. \qquad (37)$$

The combination of $\delta\nu_{n\,l}$ and $\delta^{(1)}\nu_{n\,l}$ is particularly important in the case of intensity observations where generally only modes of degree $l = 0$, 1 and 2 are detectable.

The usefulness of the large and small frequency separations as asteroseismic diagnostics lies in the fact that they can often be determined with reasonable precision, even when the observed data do not allow reliable determination of individual frequencies. A recent interesting example of this type of analysis was provided by Roxburgh and Vorontsov (2006) who showed that a quantity equivalent to the small separation could be determined from the autocorrelation function of the observed time series, even in cases where the noise level was too high to allow reliable frequency identification.

The dependence of the sound speed on the chemical composition [cf. Eq. (11)] makes the small frequency separations sensitive measures of the evolutionary state of main-sequence stars. This can be illustrated by presenting the effects of stellar evolution in a $(\langle\Delta\nu\rangle, \langle\delta\nu\rangle)$ diagram (e.g. Christensen-Dalsgaard 1984, 1988; Ulrich 1986; Gough 1987), where $\langle\Delta\nu\rangle$ and $\langle\delta\nu\rangle$ are suitable averages of $\Delta\nu_{n\,l}$ and $\delta\nu_{n\,l}$, respectively. An example is shown in Fig. 15. The large separation varies with stellar properties essentially as t_{dyn}^{-1}, whereas the small separation directly reflects the change in the sound speed in the core resulting from the changing compositional structure as the star evolves. The effect of evolution on the sound speed is illustrated in Fig. 16. This is dominated by the increasing mean molecular weight as hydrogen is used in the core, leading to a sound-speed inversion. The effect of the positive sound-speed gradient in the core is evidently to reduce the integral in Eq. (35) and hence the small separation, as shown in Fig. 15.

It should be mentioned that the simple asymptotic expressions have some limitations. The analysis is based on the *Cowling approximation*, neglecting the perturbation to the gravitational potential which in fact has a significant effect on the frequencies of the lowest degree modes (e.g. Robe 1968; Christensen-Dalsgaard 1991). Also, the rapid variation of sound speed in the core of evolved models makes the validity of JWKB analysis questionable. The latter effect is illustrated in Fig. 17, showing $\delta\nu_{n\,l}/(2l+3)$ and $\delta^{(1)}\nu_{n\,l}/(l+1)$ in 1 $\mathrm{M}_\odot$ models on the ZAMS and at an age of 8 Gyr. According to Eqs. (35) and (37) these values should fall on a single function of frequency; while this is approximately the case for the unevolved model, $\delta^{(1)}\nu_{n\,l}/(l+1)$ is far from

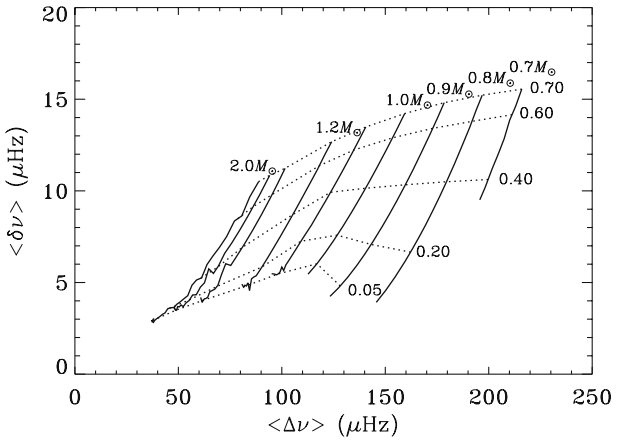

Fig. 15 Stellar evolution in terms of the average large separation $\langle \Delta\nu \rangle$ and small separation $\langle \delta\nu_{n0} \rangle$ [cf. Eqs. (31) and (35)]; the averages were evaluated through least-squares fitting of the asymptotic behaviour [cf. Eq. (31)] to computed frequencies, in the manner of Scherrer et al. (1983). *Solid lines* show evolution tracks at the masses indicated and *dashed lines* show models at constant central hydrogen abundance, also indicated in the figure

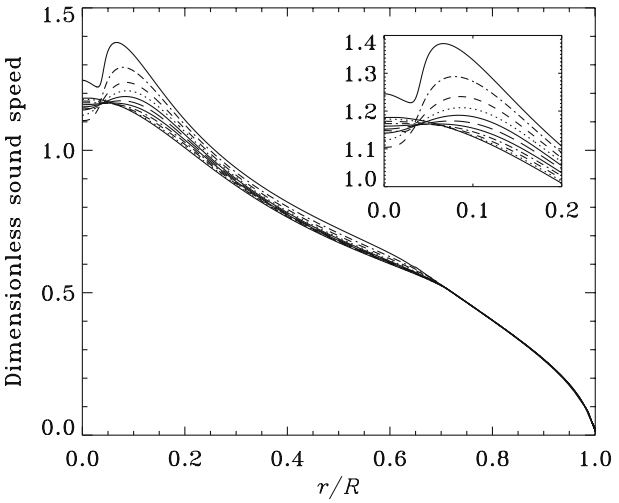

Fig. 16 Dimensionless sound-speed, in units of $(GM/R)^{1/2}$, in a 1 $M_\odot$ sequence, corresponding to Model S of Christensen-Dalsgaard et al. (1996). Results are shown for models of age 0, 1, 2, 3, 4, 5, 6, 7, 8, 9, and 10 Gyr, in the order of increasing sound speed at $r = 0.1\,R$. The *insert* provides a magnified view of the core. The increase in the scaled central sound speed between the last two models arises from the increase in the radius (relevant for the scaling) and the increasing importance of electron degeneracy

this behaviour in the evolved model. This illustrates the encouraging fact that the frequencies contain more information than suggested by the simple asymptotic relation. As discussed in Sect. 2.4.5 this underlies the possibilities for carrying out inverse analyses to infer the structure of stellar cores, even on the basis of just low-degree

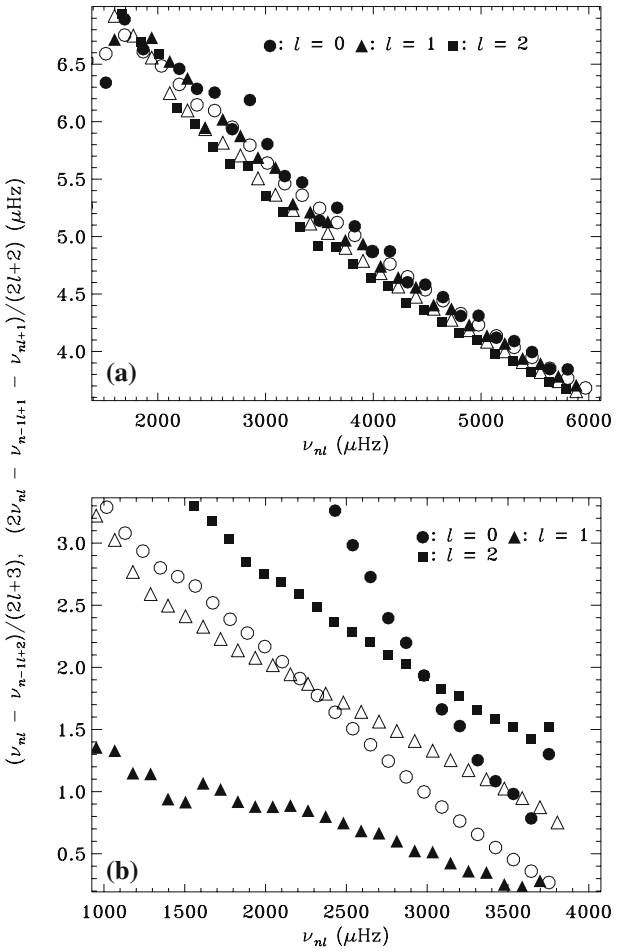

Fig. 17 Scaled small separations for 1 $M_\odot$ models, in a sequence corresponding to Model S of Christensen-Dalsgaard et al. (1996): **a** ZAMS; **b** age 8 Gyr. *Open symbols* show $\delta\nu_{nl}/(2l+3)$ and *closed symbols* show $\delta^{(1)}\nu_{nl}/(l+1)$. Note that according to Eqs. (35) and (37) these scaled values should be independent of l

modes. Asymptotic descriptions that provide a better treatment of the central regions have been developed by Roxburgh and Vorontsov (1994, 2000).

As discussed above (cf. Fig. 12), near-surface problems have a substantial effect on computed frequencies, particularly at high frequency. Since these effects are frequency dependent they also influence the large, and to a lesser extent the small, frequency separations. It was demonstrated by Roxburgh and Vorontsov (2003) that the effect on the small frequency separations could be greatly reduced by considering ratios between small and large frequency separations, such as

$$r_{02}(n) \equiv \frac{\nu_{n\,0} - \nu_{n-1\,2}}{\nu_{n\,1} - \nu_{n-1\,1}}. \tag{38}$$

The analysis was extended to a broader range of stars by Otí Floranes et al. (2005) and Roxburgh (2005), demonstrating that the separation ratios provide a sensitive measure of the properties of stellar cores, even given substantial uncertainties in the treatment of the surface layers.

For high-order, low-degree g modes the *periods* $\Pi_{nl} = 1/\nu_{nl}$ are uniformly spaced; to lowest asymptotic order they satisfy

$$\Pi_{nl} \simeq \frac{\Pi_0}{\sqrt{l(l+1)}} \left(n + \frac{l}{2} + \alpha_g \right), \tag{39}$$

where

$$\Pi_0 = 2\pi^2 \left(\int_0^{r_1} N \frac{\mathrm{d}r}{r} \right)^{-1}, \tag{40}$$

and α_g is a phase constant (e.g. Vandakurov 1967; Smeyers 1968; Tassoul 1980). Thus the period spacing depends on the degree, leading to a more complex structure of the spectrum than in the case of the acoustic modes. Equations (39) and (40) assume a star with a radiative core, and with an outer turning point (where $\omega = N$) at $r = r_1$; in the cases illustrated in Fig. 4 the turning point is typically close to the lower boundary of the convective envelope. If the model has a convective core, the term in $l/2$ is not included in Eq. (39) and the integration limits in Eq. (40) must be suitably modified. Such a situation occurs in the case of the observed high-order g modes in the SPB stars (e.g. Waelkens 1991; De Cat and Aerts 2002; Aerts et al. 2006b) and γ Doradus stars (e.g. Aerts et al. 2004; Moya et al. 2005; Dupret et al. 2005b). Unfortunately, it turned out too difficult so far to disentangle the period spacings due to the rotational splitting effects, because of the lack of identification of l and n. It has thus not yet been possible to exploit the period spacings seismically for these main-sequence stars, as was done for the white dwarfs (Winget et al. 1991, 1994).

Higher order corrections to the expression given by Eq. (39) were discussed by, for example, Tassoul (1980); Ellis (1984, 1986) and Provost and Berthomieu (1986).

2.4.2 Signatures of mixed modes

As mentioned in Sect. 2.2.1 the clean separation between acoustic and gravity modes disappears in evolved stars where the buoyancy frequency in the deep interior reaches values corresponding even to frequencies characteristic of solar-like pulsations. A typical example is the case of η Boo, where solar-like oscillations were first detected by Kjeldsen et al. (1995). Models of this star (e.g. Christensen-Dalsgaard et al. 1995; Guenther and Demarque 1996; Di Mauro et al. 2004) show that it is likely in the subgiant phase, with energy generation in a hydrogen-burning shell. This is also reflected in the large values of N (cf. Fig. 4), arising from the compact core and resulting in very high values of g [cf. Eq. (12)]. Figure 18 shows the evolution with age of selected frequencies in such a model. The radial modes are purely acoustic, with frequencies decreasing as the radius of the star increases, largely in accordance with Eq. (1). The $l = 1$ modes generally follow the same behaviour; also, as expected from Eq. (31),

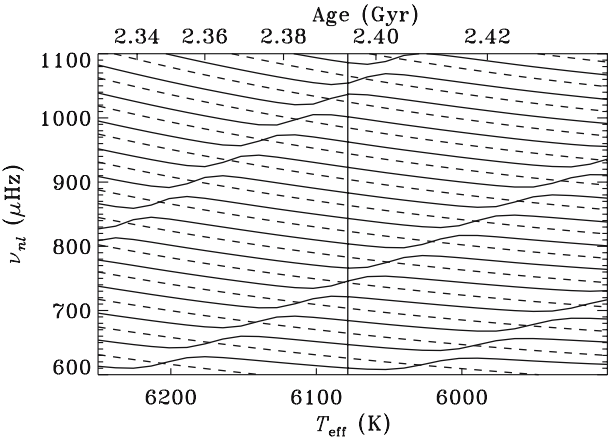

Fig. 18 Evolution of adiabatic frequencies for a model of η Boo. The *lower abscissa* shows the effective temperature $T_{\rm eff}$, the *upper abscissa* the age of the model in Gyr. The *dashed lines* correspond to modes of degree $l = 0$, and the *solid lines* to $l = 1$. The *vertical solid line* indicates the location of the model whose frequencies are illustrated in Fig. 19 (adapted from Christensen-Dalsgaard et al. 1995)

their frequencies are roughly halfway between those of the $l = 0$ modes. However, there is evidently a second class of modes, with frequencies *increasing* with age. These are g modes predominantly trapped under the peak in the buoyancy frequency in the deep interior of the star; with increasing age, the buoyancy frequency increases and so, therefore, do the g-mode frequencies. Where modes of the two classes approach each other, the frequencies undergo an *avoided crossing*, never quite meeting (e.g. Osaki 1975; Aizenman et al. 1977; Christensen-Dalsgaard 1980); indeed, this behaviour is characteristic of eigenvalue problems with several classes of solutions (e.g. von Neuman and Wigner 1929). At the point where the modes are closest they have a mixed character, with substantial amplitudes both in the g-mode and the p-mode propagation regions (see Fig. 4). If such modes can be observed, they would provide information about the core of the star.

For stochastically excited modes it follows from Eq. (30) that the amplitudes are inversely related to the mode inertias defined in Eq. (15), normalized by the surface amplitude. This is typically large for modes partly trapped under the buoyancy frequency in the deep interior. However, as is evident from Fig. 4 the evanescent region between the g-mode and p-mode trapping regions is quite thin for $l = 1$ modes in the η Boo model. Consequently, the mode inertia of the mixed modes only exceeds that of the purely acoustic modes by less than a factor 4 and the modes are likely to be excited stochastically to observable amplitudes. For $l > 1$, on the other hand, the evanescent region is broader; consequently the interaction in the avoided crossing takes place in a smaller interval of age and frequency and the amplitudes of the mixed modes are therefore likely smaller.

It is evident that frequencies of modes undergoing avoided crossing do not satisfy the p-mode asymptotic relation, Eq. (31). Indeed, as shown in Fig. 18 the modes with g-mode behaviour effectively add extra modes between the regular pattern of acoustic mode. This is very visible in the echelle diagram shown in Fig. 19

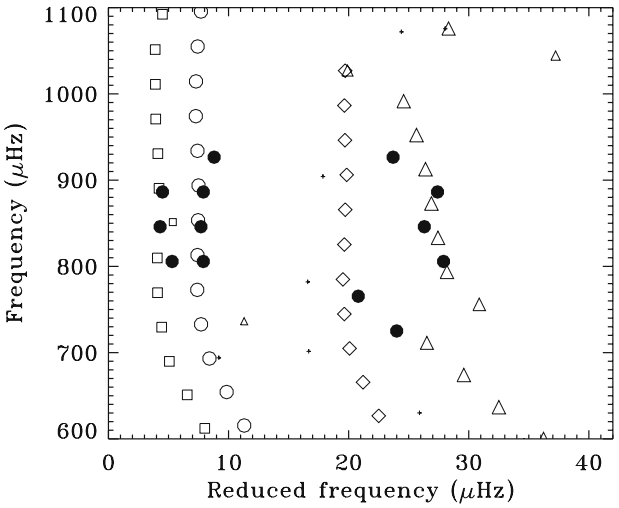

Fig. 19 Echelle diagram for η Boo, with a frequency separation of $\langle \Delta\nu \rangle = 40.3\,\mu$Hz and a reference frequency of $\nu_0 = 846\,\mu$Hz. The *filled circles* show observed frequencies from Kjeldsen et al. (1995). The *open symbols* show computed frequencies for a model of the star (Christensen-Dalsgaard et al. 1995); to compensate for the near-surface effects the computed frequencies have been decreased by 10 μHz, to achieve a reasonable average match to the observations. *Circles* are used for modes with $l = 0$, triangles for $l = 1$, squares for $l = 2$ and diamonds for $l = 3$. The size of the symbols indicates the expected amplitude of the modes, relative to a radial mode of the same frequency, and assuming that all modes are excited to the same energy [cf. Eqs. (16) and (30)]; symbols that would otherwise be too small have been replaced by *crosses*

(Christensen-Dalsgaard et al. 1995). For modes of degree $l = 2$ and 3 the presence of avoided crossings barely affects the behaviour of the frequencies; for $l = 1$, on the other hand, there are obvious departures from the regular behaviour. It is interesting that the observed frequencies of Kjeldsen et al. (1995) show a qualitatively similar behaviour, indicating that the effect of the g-mode propagation region can be observed in this star. This has largely been confirmed by subsequent observations and analyses (Guenther and Demarque 1996; Kjeldsen et al. 2003; Guenther 2004; Carrier et al. 2005). It was noted by Di Mauro et al. (2004) that an alternative would be to model η Boo as being in the phase of central hydrogen burning, but with some convective-core overshoot. Such a model does not show effects of mode mixing in the relevant frequency band and could therefore be excluded if the presence of avoided crossings could be definitely established in the observed frequencies.

Less evolved stars show mode mixing at lower frequencies. Thus such effects are likely in stars pulsating due to the heat-engine mechanism, where the frequency range of the unstable modes typically covers the low-order acoustic and gravity modes. An example may be the β Cephei star ν Eri, where modelling by Pamyatnykh et al. (2004), based on frequencies and mode identification obtained by Handler et al. (2004) and De Ridder et al. (2004), indicated an avoided crossing between the lowest order dipolar p and g modes. Also, the implied effect of an avoided crossing allowed Mazumdar et al. (2006) to place strong constraints on models of the β Cephei star β CMa, based on only frequencies of two identified modes.

With further evolution the buoyancy frequency in the deep interior of the star increases dramatically and the density of g modes becomes extremely large, in the observationally relevant frequency interval. An example of such a star is the G7 giant ξ Hya, where Frandsen et al. (2002) found evidence for solar-like oscillations. The oscillations of a model of this star were discussed in some detail by Christensen-Dalsgaard (2004). For the nonradial modes there are still cases where the frequency resonates with the outer, acoustic, propagation region, resulting in modes of predominantly acoustic nature and hence with a mode inertia similar to that of a radial mode of similar frequency. These modes might in principle be excited to an observable level through stochastic excitation. However, it was noted by Dziembowski et al. (2001) that the very high order of the modes in the g-mode propagating region would lead to strong radiative damping, despite the rather small amplitudes of the modes in this region, possibly to an extent that the non radial modes would be undetectable. In fact, Eq. (18) shows that the integrand in the work integral depends on the divergence of the flux perturbation; assuming radiative transfer the flux perturbation contains the gradient of the temperature perturbation [cf. Eq. (22)], which, relating it to the density perturbation through the approximate adiabatic relation and using the equation of continuity, is itself given by a derivative of the displacement. Thus the integrand of the work integral contains a third derivative of the displacement which, for high-order modes, is obviously potentially large, even for a relatively small displacement in the g-mode propagating region. The interpretation of the observations by Frandsen et al. (2002) is consistent with only radial modes being detected. Nonetheless Hekker et al. (2006) found strong evidence that the dominant modes in ϵ Oph had $l = 2$. This apparent conflict between theory and observations has still to be resolved.

2.4.3 Signatures of sharp features

Abrupt transitions in a star's internal structure cause small departures from the regular p-mode asymptotic spacing discussed earlier. Abrupt changes in stratification (on scales smaller than or comparable with the local wavelength)—e.g. the edge of a convective region or an ionization zone—add to the frequencies (considered say as a function of n) a periodic component

$$\widetilde{\delta\nu} \sim A \cos\left[2(2\pi\nu\tau_d + \phi)\right], \tag{41}$$

where τ_d is the location of the feature in acoustic depth, ϕ is a surface phase, and A is an amplitude. The contribution of the signature from the Sun's second helium ionization zone to the large separation, for instance, is large enough that it should be explicitly taken into account when calibrating the value of the large separation (Monteiro et al. 2002).

A more-studied signature of a sharp feature is that from the base of a convection envelope such as the Sun's. Monteiro et al. (2002) explored the behaviour of this signature as a function of mass and age of the star, using frequencies of stellar models. In particular, they computed the amplitude A of the signal (at a fiducial frequency) and inferred the acoustic depth τ_d of the base of convection zone, as functions of

stellar mass and central hydrogen abundance. If the mass and age are already known, departures from this behaviour can be indicative of, e.g. convective overshooting (see, e.g. Monteiro et al. 2000).

Various authors have looked at the use of the signature of the second helium ionization zone on stellar oscillation frequencies (Monteiro and Thompson 1998, 2005; Pérez Hernández and Christensen-Dalsgaard 1998; Miglio et al. 2003; Basu et al. 2004; Houdek 2004). Basu et al. found that the fractional abundance of helium by mass, Y, can be determined to an accuracy of 0.01–0.02 in most cases with realistic noise estimates. For masses greater than $1.4\,M_{\odot}$, however, they found that the signal fit becomes unreliable. Houdek and Gough (2007) carried out a careful combined analysis of the effect of the helium I and helium II ionization zones on the asteroseismic signatures and obtained a substantially improved fit to the computed behaviour (see also Houdek and Gough 2006). As an example of the application of their technique, Fig. 20 shows the resulting fit to simulated data for a solar-like star.

Mazumdar (2005) proposed a new model calibration tool, using the large separation and the inferred acoustic depth of (say) the convective envelope. Using this with classical constraints, he obtained impressive accuracy in identifying the model properties in a hare-and-hounds exercise aimed at testing data-analysis techniques for the CoRoT mission (see Appourchaux et al. 2006).

The effect of sharp transitions on stellar oscillations has also been studied in the context of roAp stars and white dwarfs. In the former case, Vauclair and Théado (2004) have analysed frequency data for the roAp star HD 60435, and have found evidence for a signature of a steep helium gradient, as expected from results based on models of these stars including helium settling in the stellar envelope. Concerning white dwarfs, the layering resulting from settling in the strong gravitational field has substantial influence on the g-mode spectrum and hence on the asteroseismic diagnostics of white-dwarf properties (e.g. Bradley et al. 1993; Bradley and Winget 1994). An interesting analysis of the effects of sharp features, with application to white dwarfs, was presented by Montgomery et al. (2003).

More recently, the effect on the oscillation frequencies of sharp transitions associated with the edge of convective cores has also been considered theoretically for stars significantly more massive than the Sun (Roxburgh and Vorontsov 2001), and for main-sequence solar-like pulsators (Cunha and Metcalfe 2007). Moreover, attempts to identify the signatures of convective cores in solar-like pulsators from simulated data have been carried out by Mazumdar et al. (2006). In a main-sequence solar-like pulsator the edge of the convective core is located close to the inner turning point of low-degree acoustic modes. Consequently, unlike all other cases discussed above, in this case the signal added by the sharp transition associated with the edge of the core is not periodic. Nevertheless, based on a theoretical analysis of the signal and on simulated data, Cunha and Metcalfe (2007) have shown that such signal should be detected when the data for solar-like pulsators reaches the level of precision expected from space-based dedicated instruments, such as CoRoT, and that the detection of the expected signal in real data of solar-like pulsators will provide unprecedented information about the cores of these stars.

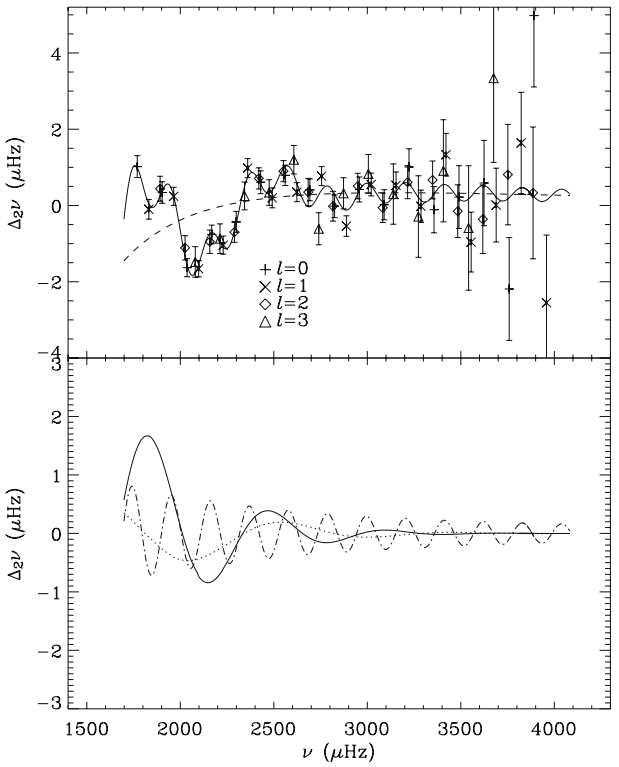

Fig. 20 In the *upper panel* the symbols show second differences $\Delta_2\nu_{nl} = \nu_{n+1\,l} - 2\nu_{n\,l} + \nu_{n-1\,l}$ for the values of l indicated in the figure, in simulated data for a $1\,M_\odot$ model of age 5.54 Gyr. The simulation was based on two periods of 4-months observations, separated by 1 year, with the SONG network (see Grundahl et al. 2007). The *solid curve* shows a fit to $\Delta_2\nu$ (where the subscripts $n\,l$ have been dropped for simplicity) based on the analysis by Houdek and Gough (2007). The *dashed curve* is a smooth contribution, modelled as a third-order polynomial in ν^{-1}, which represents possible near-surface effects (cf. Fig. 12) as well as likely departures at low frequency from the asymptotic expressions underlying the fit. The *lower panel* identifies the remaining individual contributions to the fit. The *dotted* and *solid curves* show contributions from the first and second helium ionization zones and the *dot-dashed curve* is the contribution from the base of the convective envelope

2.4.4 Direct fitting

Clearly, even the most basic seismic signatures, such as the large and small separations discussed above, provide additional constraints to traditional stellar modelling. The first approach to asteroseismic inference is by direct fitting, or forward modelling. Such an approach consists of fitting a set of measured observables for a given star by running forward in time a stellar structure and evolution code which takes as input parameters the (unknown) basic stellar parameters we are trying to determine. Then at each point in time (age) the code produces as output the model observables, which can be compared with the measured ones. Furthermore, the code also produces detailed numerical information on the internal structure of the star.

For a single star, the "classical", non-asteroseismic observables are the effective temperature $T_{\rm eff}$, the logarithm of surface gravity $\log g$, and the surface metallicity $[{\rm M/H}]_{\rm surf}$, which in PopI stars can be identified with the logarithmic surface abundance of iron relative to that in the Sun $[{\rm Fe/H}]_{\rm surf}$.[18] Moreover, whenever the distance is available, also the luminosity L can be derived directly from observations and, so far for only a limited number of stars, also the interferometrically determined radius, R. (Notice that $T_{\rm eff}$, L, and R are interdependent, even if they are three different observables.) The issue of how to include the observed oscillation frequencies as observables into the fits is still under study. Before the advent of spectrographs such as HARPS and UVES, the quantity that could most confidently be determined was the large frequency separation, and perhaps also the small frequency separation. As a result, most of the modelling work done to date used those quantities as the asteroseismic observables for the fits. However, it is now possible to resolve individual oscillation modes, which contain additional information that is lost if only the separations are included in the fits, as pointed out by (2005, and references therein) from his experience in modelling pulsating white dwarfs. A possible way to include the information from the individual modes, suggested by Bedding et al. (2004), is to carry out fits to the frequency ridges for modes with the same degree, l. From the results of such fits one may then define the following set of asteroseismic observables: $\{\nu_0^{\rm (ref)}, \langle\Delta\nu\rangle, r_{02}^{\rm (ref)}\}$, where the superscript 'ref' indicates suitable reference values, e.g. evaluated at peak power. These three (or other similar) parameters may then be used as the asteroseismic observables which, together with the non-asteroseismic observables, must be successfully matched by a stellar model.

In order to obtain a model for the internal structure of a star at a given age, a stellar structure and evolution code will take as input parameters the stellar mass, M, and the initial abundances of hydrogen and helium for the star, X_0 and Y_0, respectively. It starts by calculating the zero-age model for the internal structure of that star, and then evolves it in time in steps until the required age. In addition to those three parameters, such codes also allow some choices regarding details of the physics in the stellar interior. As mentioned earlier, these are mostly related to the treatment of convection, diffusion and settling of heavy elements, the equation of state and opacities, among others. In particular, a parameter is introduced in the formulation of convection. The mixing-length treatment (MLT) describes the characteristic length of turbulence as scaling directly with the local pressure scale height: the scaling factor is known as the mixing length parameter, $\alpha_{\rm ML}$, which is essentially unconstrained and left as a free parameter in the models. When convection is dealt with in the approach of Canuto and Mazzitelli (Canuto et al. 1996) a free parameter is also introduced. The latter formulation has produced only rather small improvements in the results with respect to the MLT, as shown by Miglio and Montalbán (2005). The extent of mixing at the borders of convectively unstable regions is also not fully understood. Overshoot is dealt with in stellar codes by introducing another free parameter describing its extent by scaling with the local pressure scale height. Since the observational data available do not yet allow for testing this parameter in solar-like pulsators, we will not consider

[18] More precisely defined as $\log(N_{\rm Fe}/N_{\rm H}) - \log(N_{\rm Fe}/N_{\rm H})_\odot$, where $N_{\rm Fe}$ and $N_{\rm H}$ are the number densities of iron and hydrogen in the stellar atmosphere.

it in what follows. That will hopefully change in the near future, when better data, particularly of more evolved solar-like pulsators become available.

The problem of direct fitting is thus to fit a set of observables, $\{y_i\} = \{T_{\rm eff}, L, [{\rm Fe/H}]_{\rm surf}, R, \nu_0^{\rm (ref)}, \langle\Delta\nu\rangle, r_{02}^{\rm (ref)}\}$,[19] with associated uncertainties $\{\sigma_i\}$, with a model having as input parameters $\{a_j\} = \{M, X_0, Y_0, \alpha_{\rm ML}, age\}$, where the input parameters are what we are trying to determine; additional parameters may be needed to model the effects of the near-surface problems, particularly in the case of solar-like oscillations (cf. Fig. 12). The best way to approach this problem is to use an objective, automated fitting procedure that is free to search for the best solution within the parameter space defined by physical constraints to the input parameters (for example, the age has to be positive and smaller than the age of the Universe). One such fitting procedure is the Levenberg-Marquardt method (e.g. Bevington and Robinson 2003), which has been successfully used in nonlinear multi-parameter fitting problems in different contexts but with similar needs (e.g. Teixeira et al. 1998; Miglio and Montalbán 2005). This is an iterative least-squares minimization method which locates a χ^2 minimum by combining gradient search when far from the minimum, with expansion of the χ^2 surface near the minimum. The fit is carried out by minimizing

$$\chi^2 = \sum_i [(y_i^{\rm (obs)} - y_i^{\rm (mod)})/\sigma_i]^2 \tag{42}$$

with respect to parameters $\{a_j\}$, where $y_i^{\rm (obs)}$ are the observed values of the observables and $y_i^{\rm (mod)}$ are the corresponding computed model values for the given set of parameters. This procedure produces fast convergence, and is well suited to make use of distributed computing for the calculation of the derivatives for the gradient search. Unfortunately and like most methods, it cannot guarantee convergence to the global minimum, and it may thus be advisable to make several searches with different starting values with respect to the input parameters. This can be carried out in a systematic way by utilizing various forms of non linear optimization techniques, such as genetic algorithms (e.g. Metcalfe et al. 2000; Metcalfe and Charbonneau 2003) or Markov Chain Monte Carlo (MCMC) techniques.[20]

For a binary system the fitting problem is similar to the one described above for a single star, only it involves a larger number of observables and input parameters and some extra constraints. In the case of an "ideal" binary system (cf. α Cen AB, Miglio and Montalbán 2005), the masses of the individual components (A and B) are well determined, which provides us with two more observables. The non-asteroseismic observables involved in the fit are then $\{M_{\rm A}, T_{\rm eff,A}, L_{\rm A}, [{\rm Fe/H}]_{\rm A}, R_{\rm A}, M_{\rm B}, T_{\rm eff,B}, L_{\rm B}, [{\rm Fe/H}]_{\rm B}, R_{\rm B}\}$. If both components have reliably determined individual oscillation frequencies, it is possible to define asteroseismic observables for each component, as explained above for a single star: $\{\nu_{0,{\rm A}}^{\rm (ref)}, \langle\Delta\nu\rangle_{\rm A}, r_{02,{\rm A}}^{\rm (ref)}, \nu_{0,{\rm B}}^{\rm (ref)}, \langle\Delta\nu\rangle_{\rm B}, r_{02,{\rm B}}^{\rm (ref)}\}$. One can

[19] Here we have assumed that the parallax, and hence the luminosity, have been determined. If this is not the case $\log g$ can be included as observable instead.

[20] An application of MCMC to frequency determination for solar-like oscillations was discussed by Brewer et al. (2007).

then include all these observables simultaneously in the fit, or only a subset of them. As for the model, it is assumed that both components of the binary have the same age and initial composition, while the mixing lengths are generally allowed to differ. With these constraints, the input model parameters are then $\{M_{\rm A,mod}, M_{\rm B,mod}, X_0, Y_0, \alpha_{\rm ML,A}, \alpha_{\rm ML,B}, age\}$, where $M_{\rm A,mod}$ and $M_{\rm B,mod}$ are variable model masses and must be distinguished from the observed values, $M_{\rm A}$ and $M_{\rm B}$. Finally, the same fitting procedure as described above performs the least-squares minimization and produces models simultaneously for both components of the binary.

Rather than making a combined fit to the 'classical' observables and the oscillation frequencies, Guenther and Brown (2004) and Metcalfe (2005) recommended fits to the frequencies alone, possibly supplemented by a separate fit to the classical variables $\{T_{\rm eff}, L, [{\rm Fe/H}]_{\rm surf}\}$. Any discrepancy between the results of such separate fits would obviously indicate inconsistencies in the modelling (or the data). This technique was applied by Guenther (2004) to the analysis of observations of η Boo. It should be pointed out, however, that inconsistencies would presumably also be apparent in the residuals from a combined fit, as discussed above. Thus an evaluation of the relative merits of these two different approaches probably requires further investigations, including hare-and-hounds exercises.

Direct fitting is a relatively simple way to find a good first solution to the problem of stellar model fitting. Applications of this method to stars for which both asteroseismic and interferometric data are available are discussed in Sect. 4. Direct fitting is also a crucial step towards providing a close enough starting point for the inverse methods, which will give us access to the actual details of the stellar interior.

2.4.5 Inverse approach

Solving the inverse problem is predicated on solving, at least in some approximation, the forward problem. Here the forward problem is to compute the global resonant frequencies given a stellar model, since the observables to be inverted are global resonant frequencies. The simplest approach to the inverse problem would be to compute frequencies for different models and find which match the observables most closely, in some sense. This is the direct fitting method described in Sect. 2.4.4. At its crudest, this could involve a straightforward match to the frequencies themselves, but this would not distinguish between the myriad possible contributions to any frequency mismatch. Better, as described above, would be a match to certain signatures computable from the frequencies, such as the large and small frequency separations.

More sophisticated inverse methods allow one to "step outside" a given space of models. Most of the inverse techniques are linear, though the forward problem is inherently nonlinear. Thus it is certainly advantageous, and probably necessary, to have a starting model that is "near" the truth. Herein lies one difference between asteroseismology and helioseismology. In helioseismology, we have models of the Sun that are already very close to the truth; whereas the inherent uncertainties in a star's global parameters may mean that even finding a good starting model for a linear inversion becomes part of the inverse process. For some general considerations, see Gough (1985b) and Thompson and Christensen-Dalsgaard (2002).

Linear inversion methods used in helioseismology—and just starting to be used in asteroseismology—fall mainly into two categories: least-squares fitting of the observational data, or optimally localized averages methods. For the sake of illustration, we suppose we have data d_i ($i = 1, \ldots, M$) which are related linearly to some unknown property $\mathcal{Q}(\boldsymbol{r})$ of the interior of the star, where $\boldsymbol{r}$ is in general a 3D position vector, according to

$$d_i = \int_V K_i(\boldsymbol{r})\mathcal{Q}(\boldsymbol{r})\,\mathrm{d}\boldsymbol{r} + \epsilon_i, \tag{43}$$

where the integral is over the whole interior volume V of the star. The *kernels* $K_i(\boldsymbol{r})$ are presumed to be known functions describing the sensitivity of the data to the unknown function $\mathcal{Q}$. The ϵ_i are data noise, whose statistical properties are assumed to be known: for simplicity, we suppose they are independent, normally distributed with zero mean and standard deviation σ_i.

The method of optimally localized averages (OLA), or the Backus-Gilbert method, is based on the work of Backus and Gilbert (1968, 1970). To estimate $\mathcal{Q}$ at some location $\boldsymbol{r}_0$, one seeks coefficients $c_i(\boldsymbol{r}_0)$ so as to construct an *averaging kernel*

$$\mathcal{K}(\boldsymbol{r}_0, \boldsymbol{r}) = \sum_{i=1}^{M} c_i(\boldsymbol{r}_0)K_i(\boldsymbol{r}) \tag{44}$$

that is peaked around $\boldsymbol{r} = \boldsymbol{r}_0$ and is small elsewhere, and has unit integral

$$\int_V \mathcal{K}(\boldsymbol{r}_0, \boldsymbol{r})\mathrm{d}\boldsymbol{r} = 1. \tag{45}$$

Taking the same linear combination both sides of Eq. (43) gives

$$\sum_i c_i(\boldsymbol{r}_0)d_i = \int_V \mathcal{K}(\boldsymbol{r}_0, \boldsymbol{r})\mathcal{Q}(\boldsymbol{r})\mathrm{d}\boldsymbol{r} + \sum_i c_i(\boldsymbol{r}_0)\epsilon_i. \tag{46}$$

If one succeeds in localizing $\mathcal{K}(\boldsymbol{r}_0, \boldsymbol{r})$ about $\boldsymbol{r} = \boldsymbol{r}_0$, then one can regard the left-hand side of Eq. (46) as an estimate $\bar{\mathcal{Q}}(\boldsymbol{r}_0)$ of the unknown function $\mathcal{Q}$ at $\boldsymbol{r} = \boldsymbol{r}_0$. For this estimate to be useful, the choice of coefficients must be moderated so that the error in the estimate propagated from the errors in the data is not too large: thus there is a trade-off between localizing the averaging kernel and reducing the effect of data errors on the solution.

One way of determining the coefficients $c_i(\boldsymbol{r}_0)$ (Gough 1985b) is to choose them to minimize

$$\int_V J(\boldsymbol{r}_0, \boldsymbol{r})\mathcal{K}(\boldsymbol{r}_0, \boldsymbol{r})^2\mathrm{d}\boldsymbol{r} + \mu\sum_i \sigma_i^2 c_i(\boldsymbol{r}_0)^2. \tag{47}$$

Here μ_0 is a parameter whose value is chosen to balance between the conflicting aims of minimizing the first term, and hence localizing the averaging kernel, and minimizing the second term, and hence keeping the effect of data errors on the solution small. The

function J is chosen to penalize the averaging kernel for being non-zero far from the target position $\boldsymbol{r} = \boldsymbol{r}_0$, and should generally increase as $|\boldsymbol{r} - \boldsymbol{r}_0|$ increases. The normalization (45) is imposed as an exact constraint.

An alternative formulation of OLA is Subtractive OLA (SOLA) (Pijpers and Thompson 1992, 1994). In the SOLA method the coefficients $c_i(\boldsymbol{r}_0)$ are chosen to minimize

$$\int_V \big(\mathcal{T}(\boldsymbol{r}_0, \boldsymbol{r}) - \mathcal{K}(\boldsymbol{r}_0, \boldsymbol{r})\big)^2 \mathrm{d}\boldsymbol{r} + \mu \sum_{i,j} E_{ij} c_i(\boldsymbol{r}_0) c_j(\boldsymbol{r}_0), \tag{48}$$

where $\mathcal{T}(\boldsymbol{r}_0, \boldsymbol{r})$ is a chosen target form that the averaging kernel is to resemble and E_{ij} is the error variance–covariance matrix of the observed frequencies. A reasonable choice of target function is a Gaussian in the radial and—if appropriate—the latitudinal directions. In addition to being computationally more efficient, it has been found in a number of helioseismic applications that it is easier to control the localization of the averaging kernel with the SOLA formulation of OLA.

Another widely used class of inversion methods is called Regularized Least Squares (RLS), also known as least squares with Tikhonov regularization (Tikhonov and Arsenin 1977). The unknown function $\Omega(\boldsymbol{r})$ is first approximated by a linear combination of chosen base functions ϕ_j ($j = 1, \ldots, N$):

$$\Omega(\boldsymbol{r}) = \sum_j x_j \phi_j. \tag{49}$$

Often, each ϕ_j is localized to a small region in $\boldsymbol{r}$.

It follows that Eq. (43) becomes a matrix equation,

$$\mathbf{A}\mathbf{x} = \mathbf{b}, \tag{50}$$

where the elements of matrix $\mathbf{A}$ are given by

$$A_{ij} = \int_V K_i(\boldsymbol{r}) \phi_j(\boldsymbol{r}) \, \mathrm{d}\boldsymbol{r}, \tag{51}$$

$\mathbf{x}$ is the vector of the N expansion coefficients x_i, and $\mathbf{b}$ is the vector of the M data d_i. In the RLS method, the expansion coefficients are determined by minimizing

$$\|\mathbf{A}\mathbf{x} - \mathbf{b}\|_2^2 + \lambda^2 \|\mathbf{L}\mathbf{x}\|_2^2, \tag{52}$$

where $\|\cdots\|_2$ denotes the 2-norm of a vector. Typically $\mathbf{L}$ is an approximation to some derivative operator, and λ is a parameter whose value is chosen to determine the relative importance of minimizing the first term (hence fitting the data) and minimizing the second term (and hence keeping the solution "smooth" in some sense). Most commonly, $\mathbf{L}$ has been chosen to be a second-derivative operator in helioseismic applications.

As discussed in Sect. 2.2.2, rotation affects the star's frequencies and hence is amenable to seismic inference. Inversion for the Sun's internal rotation is well established:

see for example Schou et al. (1998) and Thompson et al. (2003). Inversion for stellar rotation is, in principle, also possible. The Sun is a slow rotator and hence rotation can be studied with just first-order perturbation theory [cf. Eq. (17)]. In this case, the relation between the observable rotational splittings and the unknown angular velocity is essentially of the form assumed in Eq. (43) and the techniques discussed above can be directly applied. For more rapidly rotating stars, higher order perturbation theory, or nonperturbative methods, are necessary (see Sect. 2.2.2).

Inversions of artificial data, with observational characteristics as expected for CoRoT targets, indicate that it may be possible successfully to invert for rotation in parts of the star (Lochard et al. 2005). These authors applied a SOLA inversion technique to artificial data computed for a stellar model of 1.55 solar masses, sufficiently evolved to possess some mixed modes in the frequency range expected to be stochastically excited. Their mode set contained 50 $l = 1, 2$ modes including three mixed modes. With this set, and for realistic noise, they were able to obtain sufficient radial resolution to determine the rotational profile in the core with reasonable accuracy between fractional radii 0.1 and 0.3, as well as a rather broad average of the rotation in the outer 40% of the star by radius. Thus for suitable stars one may obtain some indication of rotation both in the core and in the envelope. Suitable stars are those where some mixed modes can be observed as well as p modes, and where the rotation is not so slow that the fractional error on the rotational splitting measurements is too big for the inversion results to be significant.

The above methods can be extended to where there is more than one unknown function. In the case of inferring the radial hydrostatic structure an additional complication is the strongly nonlinear dependence of the observed oscillation frequencies on structure. As proposed by Gough (1978) this is dealt with by linearization around a known reference model, e.g. characterized by sound speed $c_0(x)$ and density $\rho_0(x)$, where x is distance to the centre, in units of the surface radius, and using the variational property of linear adiabatic oscillations (e.g. Chandrasekhar 1964). Assuming that the differences $\delta c/c = (c(x) - c_0(x))/c_0(x)$ and $\delta\rho/\rho = (\rho(x) - \rho_0(x))/\rho_0(x)$ are sufficiently small, the resulting frequency differences $\delta\omega_{nl}/\omega_{nl} = (\omega_{nl} - \omega_{nl,0})/\omega_{nl,0}$, $\omega_{nl,0}$ being the frequencies of the reference model, can be approximated by

$$\frac{\delta\omega_{nl}}{\omega_{nl,0}} = \int_0^R \left(K^{nl}_{c,\rho} \frac{\delta c}{c_0} + K^{nl}_{\rho,c} \frac{\delta\rho}{\rho_0} \right) \mathrm{d}x. \tag{53}$$

(To this expression must be added a term describing the effects of the near-surface errors in the model, cf. the discussion in connection with Fig. 12.) Thus the inverse problem is reduced to a slight generalization of the problem discussed above and can be treated with similar techniques. Instead of (c, ρ) other equivalent pairs of structure variables, involving the adiabatic compressibility Γ_1, can be used; transformations between these different sets of variables are carried out using the constraint of hydrostatic equilibrium. Further transformations are possible if other aspects of the physics of stellar interiors, such as the equation of state, are assumed to be known (e.g. Gough and Kosovichev 1990). A detailed discussion of inversion techniques for this problem, with special emphasis on the helioseismic problem, was provided by Rabello-Soares et al. (1999).

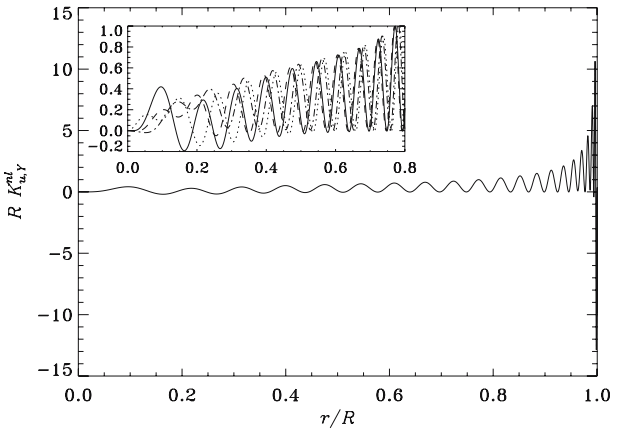

Fig. 21 Structure kernels $K^{nl}_{u,Y}$ relating the change in $u = p/\rho$ to frequency changes, at fixed helium abundance Y, for modes in a model of the present Sun with frequencies near 3,000 μHz; the abscissa is fractional distance to the centre. The main panel shows a radial mode. The insert shows the behaviour in the bulk of the interior for modes with $l = 0$ (*solid curve*), $l = 1$ (*dotted curve*), $l = 2$ (*dashed curve*), and $l = 3$ (*dot-dashed curve*)

Inversions for the radial hydrostatic structure are well established in helioseismology (see for example Gough et al. 1996; Basu et al. 1997). Such inversions have been demonstrated with artificial data for other stars. For example, Basu et al. (2002) considered the quantity $u = p/\rho$, which is a proxy for the (squared) adiabatic sound speed, in combination with the helium abundance Y and assuming the equation of state to be known, so that Γ_1 is known in terms of (p, ρ, Y). Examples of the corresponding kernels $K^{nl}_{u,Y}$, for acoustic modes characteristic of solar-like oscillations, are shown in Fig. 21. In the bulk of the model the kernels have a similar behaviour, essentially reflecting the asymptotic behaviour of the acoustic modes. However, in the core the properties of the kernels depend on degree, in part reflecting the variation of the position of the lower turning point [cf. Eq. (14)]. This richness of behaviour allows inferences to be made beyond the simple asymptotic properties, as was also indicated by the non-asymptotic behaviour of the small frequency separations in Fig. 17. Thus, Basu et al. demonstrated that corrections to u can be well determined in the core of a star like the Sun—though not elsewhere—with only low-degree modes. This is illustrated by the relatively well localized averaging kernels shown in Fig. 22, indicating that some resolution is possible of the correction to u. Further experiments along these lines would evidently be interesting.

2.5 Current limitations to asteroseismic studies

There are a number of observational aspects that may limit the success of asteroseismic studies. While some of these limitations result from intrinsic properties of the pulsations—and would exist even if the data were perfect—others may hopefully be overcome in the future, with the improvement of the seismic and complementary data available for pulsating stars, including data provided by interferometric observations.

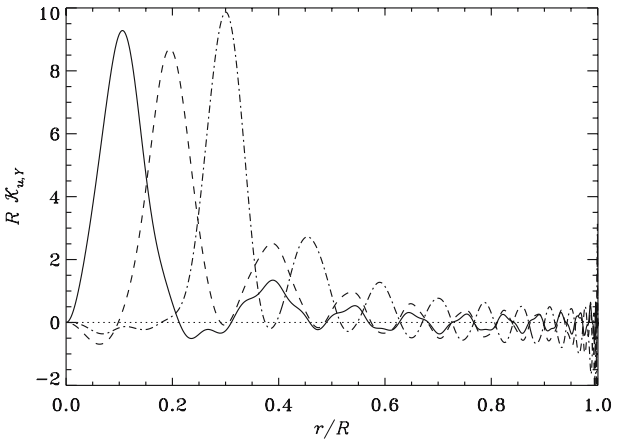

Fig. 22 Averaging kernels for inversion to infer differences in u, defined such that the inferred $\delta u/u$ at $r = r_0$ is approximately given by $\int \mathcal{K}_{u,Y}(r_0, r)(\delta u/u)(r)\mathrm{d}r$. The inversion is based on using a model of the present Sun as reference, and including representative modes with degree l from 0 to 3. The inversions have target locations $r_0 = 0.1R$ (*solid curve*), $0.2R$ (*dashed curve*) and $0.3R$ (*dot-dashed curve*)

2.5.1 Frequency determination

Clearly, our ability to extract information from the frequency spectra depends directly on whether or not the time series from which the spectra are derived allow us to resolve the individual frequencies and to determine each frequency with enough precision. As explained in Sects. 2.1.2 and 2.1.3, to accomplish that we need data sets that are sufficiently long and which have an appropriate coverage, to avoid complicated window functions that may prevent us from identifying which frequencies are real. These can often be obtained for some classical pulsators, traditionally observed photometrically from small or medium-size telescopes, but not for solar-like pulsators, which require either observations from space, or with high-resolution spectrographs available only on very few telescopes.

While the development of means to acquire lengthy and continuous data of pulsating stars is a technical challenge to which the research community can—and is already—responding, there are limitations to the precision with which the individual frequencies may be known in some pulsators, that are related to the excitation mechanism and cannot be avoided. In classical pulsators the modes are typically phase coherent over periods of years or decades, allowing extremely accurate determinations of the frequencies. In the case of white uncorrelated noise with average zero and constant variance σ_N^2 in time, and when no interference occurs between the different true frequencies and the noise peaks, the following error estimates are found, respectively, for the amplitudes, A, frequencies, ν, and phases, δ, of modes with infinite lifetime,

$$\sigma_A = \sqrt{\frac{2}{N}}\,\sigma_{\mathrm{N}}, \quad \sigma_\nu = \frac{\sqrt{6}\,\sigma_N}{\pi\sqrt{N}\,A\,T}, \quad \sigma_\delta = \frac{\sigma_N}{\pi\,\sqrt{2N}\,A}, \tag{54}$$

where, as before, T is the total time span of the data and N is the number of data points (Bloomfield 1976; Montgomery and O'Donoghue 1999). In contrast, for solar-like oscillations the frequency error scales as $T^{-1/2}$, assuming that the observing time is much longer than the mode lifetime, which typically is of the order of a few days for the largest-amplitude modes (e.g. Libbrecht 1992). As an example, the observations of the star FG Vir (Breger et al. 2005), intermittently covering the period 1992–2004, have a relative frequency error as low as around 10^{-8} as estimated from Monte Carlo simulations (M. Breger, private communication); for comparison, the frequency errors of BiSON full-disk solar data obtained with nearly continuous observations over a similar period (Chaplin et al. 2002b), while still impressively small, exceed 10^{-6}.

2.5.2 Mode identification

The observational potential for asteroseismology depends also greatly on our ability to identify the modes of oscillation in the frequency spectra—i.e. the wavenumbers (l, m, n). This is often not an easy task, particularly in classical pulsators. As a result of the mechanism that limits the amplitudes of heat-engine-driven pulsations, in classical pulsators the distribution of mode amplitudes is highly irregular (cf. Sect. 2.3.1). Moreover, the mechanism responsible for exciting the modes does not assure that all modes in a given range of frequency are excited and in most cases the order of the modes excited is such that the asymptotic regime is not applicable and the frequencies in the spectra are not approximately equally spaced. Consequently, it is often difficult or impossible to identify the modes on the basis of the frequency distribution alone; such identification of the observed modes with those of stellar models is evidently required to make use of the information contained in the oscillation frequencies.

By reducing the level of observational noise, more modes may become detectable, improving the chances of identifying the pattern of frequencies; a striking example is the observations of the δ Scuti star FG Vir (e.g. Breger et al. 2005). However, there is a risk that the spectrum becomes impossibly confused by the high density of rotationally split modes of moderate degree, possibly excited to substantial amplitudes and hence visible even in stellar observations with sufficiently high sensitivity (Daszyńska-Daszkiewicz et al. 2006). In fact, for both δ Scuti stars and β Cephei stars the predicted mode spectra are so dense that the splitting due to rotation implies merging of the multiplets whenever the rotation velocity is a significant fraction of the critical velocity (say $>20\%$), a situation quite often encountered in practice for such stars. This explains why the biggest challenge in seismic applications to these stars is the identification of the modes of oscillation. On the other hand, the relatively high amplitudes of the dominant modes make it realistic to observe these stars with long-term multicolour photometry and high-resolution spectroscopy, and hence use amplitude ratios and phase differences as an aid to the mode identification (e.g. Viskum et al. 1998; Garrido 2000; Daszyńska-Daszkiewicz et al. 2005b; Handler et al. 2006). Additional details on mode identification techniques particularly important in the context of classical pulsators will be presented in Sect. 4.

For the γ Doradus stars and the slowly pulsating B stars, the situation is even worse. Besides the difficulties in detecting a large number of modes (cf. Sect. 1.4), brought about by the range of frequencies in which the oscillations are excited, the predicted frequency spectra are so dense (Pamyatnykh 1999; Dupret et al. (2005a)) that we have not yet reached the stage of seismic modelling of individual targets within these classes, although promising attempts were recently made by Moya et al. (2005) and Dupret et al. (2005b) for γ Doradus stars and by Aerts et al. (2006b) for an SPB discovered with MOST.

In solar-like pulsators the oscillation power, given by Eqs. (29) or (30), varies slowly with frequency and generally little with degree at a given frequency (as discussed in Sect. 2.4.2 stars with mixed modes are an exception). For relatively short observing runs the stochastic nature of the excitation may cause a few modes to be excited to exceptionally high or exceptionally low amplitudes; for longer runs, or in average power spectra, one would expect to detect almost all modes in the frequency range where the modes are excited to substantial amplitudes, with the cut-off in degree mentioned in Sect. 1.3, determined by the spatial averaging over the stellar disk ($l \leq 2$ for observations in broadband intensity or $l \leq 3$ for observations in Doppler velocity (e.g. Dziembowski 1977; Christensen-Dalsgaard and Gough 1982). Also, since generally the modes are acoustic modes of fairly high order, they approximately satisfy the simple asymptotic relation given in Eq. (31). This frequency distribution may be used to identify the degrees of the modes, by identifying the small frequency separation as was indeed done in early analyses of helioseismic data (e.g. Christensen-Dalsgaard and Gough 1980). Also, since most modes in a given frequency range at low degree are detected, the number of frequencies available to asteroseismic analysis tends to be large for solar-like pulsators.

2.5.3 Fundamental parameters of pulsating stars

Last, but not least, the success of asteroseismic studies depends greatly on the availability of accurate complementary data for the pulsating stars.

An excellent review of the status of seismic modelling of classical pulsators is available in Michel (2006). In this paper, the author made it clear that, besides hitherto ignored physical effects and lack of mode identification, the unavailability of high-precision basic stellar parameters such as the effective temperature, the gravity and the metallicity, is a serious obstacle to make progress in the modelling. On one hand, the abundances may be available from spectroscopy, but that represents only the surface value and we have rather limited knowledge on how the abundances behave as a function of depth. On the other hand, typical uncertainties for the effective temperatures and gravities of OB field dwarfs are 1,000 K and 0.2 dex, mainly due to the lack of accurate hot calibrators. These numbers decrease to 200 K and 0.1 dex for AF-type main sequence stars, but for those rapid rotation is usually involved adding additional uncertainty. When rotation is slow, these stars become chemically peculiar, and, thus, the determination of their fundamental parameters is subject to large systematic errors. The uncertainty in the fundamental parameters is significantly larger for giant and supergiant stars of OBA spectral type.

The lack of precise fundamental parameters implies that we cannot eliminate a sufficient number of stellar models when we match the sparse number of unambiguously identified oscillation modes. Moreover, it also implies that we might not be able to find a model of the star which is sufficiently close to the truth to guarantee the success of the inverse procedure. The delivery of an accurate independent estimate of either the mass or the radius of the star would therefore imply a major step forward in seismic modelling of classical pulsators, and this is where interferometry will hopefully help a great deal in the near future.

3 Interferometry

3.1 Principles of astronomical interferometry

In the current section, we provide a basic introduction into optical and infrared interferometry. We limit ourselves to the basic principles only and will focus on the quantities that are of relevance for asteroseismic applications. More general basic reviews on interferometry are available in Paresce (1997); Lawson (2000); Quirrenbach (2001a); Bergeron and Monnet (2002), and Monnier (2003).

3.1.1 Imaging

The theoretical framework for astronomical imaging is the theory of diffraction. For an incoherent object, i.e. an object for which individual constituents emit lightwaves that are uncorrelated to each other, the image $\mathcal{I}$ produced at the focus of a telescope is the convolution of the *Object Intensity Distribution* OID by the telescope *Point Source Function* PSF,

$$\mathcal{I}(\alpha, \beta) = (\mathrm{OID} \star \mathrm{PSF})\,(\alpha, \beta), \tag{55}$$

where α and β are angular coordinates. In the presence of the atmosphere, the PSF encompasses the degradation of image quality by turbulence. Transformed to spatial frequency space, this relation becomes,

$$\tilde{\mathcal{I}}(u, v) = \tilde{\mathrm{OID}}(u, v) \times \tilde{\mathrm{PSF}}(u, v), \tag{56}$$

where u and v are spatial frequency coordinates connected to the angular coordinates through the Fourier transform,

$$\mathcal{I}(\alpha, \beta) \overset{\text{Fourier}}{\mapsto} \tilde{\mathcal{I}}(u, v) = \iint \mathcal{I}(\alpha, \beta)\, e^{-2\mathrm{i}\pi(\alpha u + \beta v)}\, \mathrm{d}\alpha\, \mathrm{d}\beta. \tag{57}$$

Here, u and v are linear telescope pupil coordinates normalized by the wavelength. Thus, the larger the pupil, the higher the largest reachable spatial frequency and the larger the resolution in the image. The Fourier transform of the PSF is called the *optical transfer function* (OTF) whose value drops from one at zero spatial frequency to zero at the cut-off frequency of the telescope. The latter is exactly $\mathcal{D}/\lambda$ in the absence of atmospheric turbulence, with $\mathcal{D}$ the diameter of the telescope and λ the

wavelength at which one is observing. The inverse of the cut-off frequency is termed the *angular resolution*. The OTF can also be considered as the autocorrelation of the telescope pupil function. The process of imaging of an object is therefore equivalent to performing a low-pass filtering of the object's spatial spectrum.

3.1.2 Spatial coherence

An interferometer is nothing but a particular case of an imager. For the sake of clarity, let us choose a very simple interferometer with only two telescopes and let us assume the telescope diameter to be zero. Formally, this defines a telescope with a particular pupil function made of two subpupils, the autocorrelation of which has three peaks in spatial frequency space: one centered on zero (the OTF of a single telescope) and two symmetric peaks centered on $\pm\mathcal{B}/\lambda$, with $\mathcal{B}$ the distance between the two telescopes, due to the correlation of the two different pupils. The interferometer performs a band-pass filtering of the object's spatial spectrum at $\mathcal{B}/\lambda$, the reciprocal of which sets the spatial resolution. The PSF associated to the OTF is a fringe pattern with 100% fringe contrast.

The $\pm\mathcal{B}/\lambda$ peaks in the OTF express that the interferometer performs the correlation of the light waves collected by telescopes 1 and 2, denoted as $E_1(\mathbf{x}, t)$ and $E_2(\mathbf{x}, t)$, and measures the spatial coherence of light at the two telescope locations,

$$\gamma_{12}(\boldsymbol{\mathcal{B}}/\lambda) = \mathcal{V}(\boldsymbol{\mathcal{B}}/\lambda) = \frac{\left\langle E_1(\mathbf{x}, t)\,.E_2^{\star}(\mathbf{x}, t)\right\rangle}{\sqrt{\left\langle |E_1(\mathbf{x}, t)|^2\right\rangle\left\langle |E_1(\mathbf{x}, t)|^2\right\rangle}}, \tag{58}$$

with the time average $\langle\cdot\rangle$ taken over $\Delta t \gg \lambda/c$ (Goodman 1985). This correlation can be performed in different ways as beams can be mixed either with a beam splitter or with a focusing optics whose operations are equivalent in the zero telescope diameter case (i.e. when the baseline is large with respect to each individual pupil). The theory of the spatial coherence of light states that the correlation factor, i.e. the mutual degree of coherence or complex visibility, is the Fourier transform of the source normalized spatial intensity distribution,

$$\mathcal{V}(\boldsymbol{\mathcal{B}}/\lambda) = \frac{\iint \mathrm{OID}(\alpha, \beta)\ \mathrm{e}^{-2\mathrm{i}\pi(\alpha\mathcal{B}_\alpha/\lambda+\beta\mathcal{B}_\beta/\lambda)}\ \mathrm{d}\alpha\ \mathrm{d}\beta}{\iint \mathrm{OID}(\alpha, \beta)\ \mathrm{d}\alpha\ \mathrm{d}\beta}, \tag{59}$$

with $\mathcal{B}_\alpha$ and $\mathcal{B}_\beta$ the components of the interferometer baseline $\boldsymbol{\mathcal{B}}$ projected on the sky plane in the direction of the source. This result is known as the *Zernike–Van Cittert theorem*. A multi-telescope interferometer therefore measures the source spatial frequency spectrum at the spatial frequencies defined by its baselines.

3.1.3 The modulus and phase of the visibility function

The interferometric observable is the complex visibility, which is the spatial spectrum of the source. Using Eq. (56) one can understand that the measured fringe pattern can be approximated by the product of the visibility with the fringe pattern obtained on

a point source, which, by definition or using Eq. (59), has $\mathcal{V} = 1$. Information can therefore be derived from the fringe contrast, i.e. from the modulus of $\mathcal{V}$ (denoted as $|\mathcal{V}|$) and from the phase of $\mathcal{V}$. The latter is termed the fringe pattern position δ. It is usually given a value relative to the zero optical path difference translated in phase: $2\pi\delta/\lambda$.

The modulus of the visibility is related to the size of the source. Indeed, the source characteristic angular size is proportional to the reciprocal of the visibility function width. Thus, the larger the source, the smaller the fringe contrast. The phase of the visibility is related to the amount of asymmetry in the object. The visibility of a perfectly point-symmetric source is real and therefore has a phase of $0(\pi)$ whereas the phase of the visibility of an asymmetric source may take any value in the range $[-\pi, +\pi]$.

The simplest and most famous visibility function is that of a uniform disk of angular diameter $\theta_{\rm UD}$ whose modulus is,

$$|\mathcal{V}(\mathcal{B}, \lambda, \theta_{\rm UD})| = \left| \frac{2J_1(\pi \mathcal{B} \theta_{\rm UD}/\lambda)}{\pi \mathcal{B} \theta_{\rm UD}/\lambda} \right|, \tag{60}$$

with a first null at $\lambda/\mathcal{B} = 1.22\ \theta_{\rm UD}$, and where J_1 is the first-order Bessel function of the first kind. This result provided the historical method to measure stellar diameters.

It is now evident from Eq. (60) that long baseline interferometry can, in principle, provide very precise measurements of angular size θ. Combined with a precise measurement of the trigonometric parallax, π, the linear diameter D of stars in the solar neighbourhood can be derived from θ in terms of the solar value $D_\odot$ through the simple relation

$$D[D_\odot] = 107.47\ \theta[\text{mas}]/\pi[\text{mas}]. \tag{61}$$

3.1.4 Aperture synthesis

Traditionally, visibilities are fitted with models that best represent the source spatial intensity distribution to measure parameters that characterize it, such as its diameter, limb-darkening coefficients or star separations and position angles in the case of multiple systems, etc. The ultimate goal of interferometers is to perform imaging with a spatial resolution much higher than that of classical telescopes. An excellent example in the radio domain is the VLA. The primary data provided by the interferometer, the complex visibilities, need to be assembled and inverted through Eq. (59) to reconstruct an image. In order to do so, and ideally, the OTF of a telescope with an equivalent size needs to be sampled with the interferometer baselines. Doing so, the interferometer synthesizes a monolithic telescope OTF (or, more exactly, the support of the OTF) and this process is known as aperture synthesis. The difficulty is to have enough telescopes to achieve this. The Earth rotation helps as the baselines projected in the direction of the source rotate at the pace of the Earth rotation. In practice the sampling is not as perfect as if it were a regular grid and the image cannot be obtained with a simple

inverse Fourier transform. Instead, an image reconstruction algorithm that makes up for missing or irregularly sampled visibilities needs to be used. More and more images are currently produced by optical interferometers (e.g. Kraus et al. 2007).

3.1.5 Interferometers in practice

The specificity of optical radiation is that only intensity can be detected efficiently. As a consequence, lightwaves cannot be directly measured at each telescope and need to be propagated down to the recombination point. This requires a large number of mirrors in practice—at the cost of photometric efficiency—to guide the beams. In addition, atmospheric turbulence has a very short coherence time during which interference fringes have to be measured. This forces individual exposure times to be short. The combination of these two effects leads to a smaller sensitivity than for classical instruments and interferometers need to be operated in wide photometric bands which are in practice limited by the transmission of the atmosphere. Besides spatial coherence of light, interferometers are limited by the temporal coherence of light. In fact, the number of fringes in the fringe pattern is proportional to the reciprocal of the photometric bandwidth. The fringe pattern is therefore very localized and delay lines are required to keep the optical path difference very close to zero to find fringes.

To summarize, an optical interferometer comprises telescopes, an optical train to guide the beams to a delay line system, and subsequently to the beam combiner where lightwaves are mixed to produce fringes. These are the basic sub-systems to which adaptive optics can be added to allow the use of larger apertures. In this case, spatial coherence needs to be restored and a fringe tracking system must be used that allows to stabilize the zero optical path difference, despite the jitter due to turbulence and vibrations.

3.2 Stellar physics with interferometers

This section summarizes astrophysical applications of optical and infrared interferometry, with emphasis on those topics that are relevant for the synergy with asteroseismology. A few attempts have already been made to combine information from both techniques for the modelling of stellar properties (Pijpers et al. 2003; Kervella et al. 2003b, 2004c; Thévenin et al. 2005). Advances in the observing capabilities will increase the potential for combined interferometric and asteroseismic studies in the future.

3.2.1 Stellar diameters

The most straightforward observation with an interferometer is the measurement of a stellar angular diameter: by measuring $\mathcal{V}$ or $\mathcal{V}^2$ with a range of baselines of different lengths, one can determine $\theta_{\rm UD}$ from Eq. (60) through a straightforward χ^2 minimization process. Note that $\theta_{\rm UD}$ is somewhat smaller than the physical diameter of the star, since Eq. (60) assumes that the star is a uniform disk and thus neglects the effect of limb darkening. A correction factor can be computed from a grid of stellar

atmospheres, and applied to $\theta_{\rm UD}$ to calculate the limb-darkened diameter $\theta_{\rm LD}$ (e.g. Quirrenbach 2001a, and references therein). This procedure is frequently better than using a limb-darkened model from the beginning, because interferometric data obtained on baselines $\mathcal{B} \lesssim \lambda/\theta_{\rm UD}$, which resolve the star only partially, cannot distinguish well between uniform and limb darkened disks, or different limb darkening models. It is therefore advantageous to publish model-independent observational results (represented by $\theta_{\rm UD}$) and the adopted model-dependent quantities (represented by the limb darkening correction factor) separately. In general, limb darkening corrections are smaller in the near-infrared than at visible wavelengths; this favours H band or K band observations for precise determinations of stellar diameters, provided that sufficiently long baselines are available.

If the parallax is known, it can be combined with $\theta_{\rm LD}$ to compute the linear radius of the star. At present, i.e. after *Hipparcos* and before *Gaia*, this is most interesting for low-mass main-sequence stars; these are sufficiently close so that good parallaxes are available, and they can be resolved with present interferometers. We discuss such potential targets for asteroseismology in Sect. 4.1 (see also Table 4). It seems that in the mass range $0.5\,{\rm M}_\odot$ to $0.8\,{\rm M}_\odot$ observed radii are systematically larger than predicted by theoretical mass-radius relations (Lane et al. 2001; Ségransan et al. 2003; Berger et al. 2006).

One of the most fundamental applications of interferometry to stellar astrophysics is the calibration of the stellar temperature scale. The effective temperature of a star is defined by

$$T_{\rm eff} \equiv \left(\frac{L}{4\pi\sigma R^2}\right)^{1/4} = \left(\frac{4 f_{\rm bol}}{\sigma \theta_{\rm LD}^2}\right)^{1/4}, \tag{62}$$

where $f_{\rm bol}$ is the bolometric flux and σ the Stefan–Boltzmann constant. The most direct and model-independent way of measuring effective temperatures is thus the combination of bolometric fluxes with angular diameters. More indirect methods such as the infrared flux method described by Blackwell and Shallis (1977), which uses the ratio of the total integrated flux to the flux in the K band as temperature indicator, can be validated by comparison with directly determined effective temperatures (e.g. Hanbury Brown et al. 1974a; van Belle et al. 1999; Mozurkewich et al. 2003; Kervella et al. 2004b).

Diameter measurements of Cepheid variables are of particular interest, as they can contribute to the calibration of their period-luminosity relation, and thus to the distance scale in the local Universe. Several methods have been employed that use different combinations of angular diameters, radial–velocity curves, light curves and trigonometric parallaxes. Most useful, however, are observations that measure not only the average diameter of the Cepheid, but also the diameter variations due to the pulsations (Lane et al. 2000; Armstrong et al. 2001; Kervella et al. 2004a; Mérand et al. 2005). Such data can be combined with radial–velocity curves to determine geometric distances, provided that the *projection factor* $\mathcal{G}$ is known, which is needed to convert observed radial velocities to the radial motion of the stellar atmosphere. The factor $\mathcal{G}$ is usually obtained from theoretical model atmospheres, but it is also possible to use interferometric observations together with the radial–velocity curve and the trigonometric parallax to calibrate $\mathcal{G}$.

3.2.2 Limb darkening and wavelength-dependent diameters

The visibility function of a single star is the Fourier transform of the center-to-limb surface brightness profile $I(\alpha)$:

$$\begin{aligned}\mathcal{V}(k\mathcal{B}) &= \int_0^{\theta/2}\int_0^{2\pi} \cos(k\mathcal{B}\alpha\cos\phi)\, I(\alpha)\,\alpha\,\mathrm{d}\alpha\,\mathrm{d}\phi \\ &= 2\pi\int_0^{\theta/2} J_0(k\mathcal{B}\alpha)\, I(\alpha)\,\alpha\,\mathrm{d}\alpha, \end{aligned} \tag{63}$$

where α is an angular distance coordinate, $k \equiv 2\pi/\lambda$, and J_0 the Bessel function of zeroth order. For stars, the intensity distribution is customarily given as a function of $\mu = \sqrt{1-(2\alpha/\theta)^2}$, rather than α itself. For polynomials

$$I(\mu) = \sum_i a_i \mu^i, \tag{64}$$

Eq. (63) leads to

$$\mathcal{V}(k\mathcal{B}) = \frac{1}{C}\sum_i a_i 2^{i/2}\Gamma\left(\frac{i}{2}+1\right)\frac{J_{i/2+1}(k\mathcal{B}\theta/2)}{(k\mathcal{B}\theta/2)^{i/2+1}}, \tag{65}$$

with

$$C = \sum_i \frac{a_i}{i+2} \tag{66}$$

(Quirrenbach et al. 1996). For a disk of uniform brightness $I \equiv 1$, this formula reduces to the familiar Airy pattern as in Eq. (60).

Since the correct treatment of limb darkening is crucial for precise measurements of effective temperatures, it is important to perform observational checks of theoretical limb darkening curves. This is a fairly difficult task, because data are required around and beyond the first null of the visibility function [as in Eq. (60)], where the signal-to-noise ratio is low. The first such measurement was carried out with the Narrabri Intensity Interferometer; data from a 203-h(!) integration on Sirius showed that the height of the second maximum of the visibility function was consistent with the prediction from a model atmosphere (Hanbury Brown et al. 1974b). Similar observations have been carried out with modern interferometers for Arcturus (Quirrenbach et al. 1996), for α Ari and α Cas (Hajian et al. 1998), for HR 5299, HR 7635 and HR 8621 (Wittkowski et al. 2001), for ψ Phe (Wittkowski et al. 2004), for α Ori and α Her (Perrin et al. 2004), for γ Sge (Wittkowski et al. 2006) and for α Cen B (Bigot et al. 2006). These data are complementary to those obtained with other methods (e.g. transits of extrasolar planets), as many of the targets are giant stars, and all of them are bright and nearby, so that a wealth of additional information is available, including high-resolution spectra.

The wavelength dependence of the limb darkening correction obviously leads to a variation of $\theta_{\rm UD}$ with λ; the ratio $\theta_{\rm UD}(\lambda_1)/\theta_{\rm UD}(\lambda_2)$ can therefore be used as a diagnostic tool for the properties of the stellar atmosphere (Mozurkewich et al. 1991). An even stronger dependence of the diameter on wavelength can be observed in cool evolved stars. At each wavelength, an interferometer measures essentially the diameter of the surface at optical depth value 1. In cool stars with low gravity, the location of this surface can vary by a significant fraction of the stellar radius between wavelengths at which the opacity is high (i.e. at wavelengths corresponding to molecular absorption bands), and those at which it is low (i.e. in the continuum between absorption lines). Strongly wavelength-dependent diameters are therefore measured for Mira stars (e.g. Eisner et al. 2007) and semi-regular variables (e.g. Perrin and Ridgway 2005), but this effect has also been observed in "normal" giants of luminosity class III (Quirrenbach et al. 1993).

3.2.3 Rapidly rotating stars

Rapidly rotating stars deviate from spherical symmetry in two ways: they are noticeably oblate (i.e. flattened), and their surface temperature increases from the equator to the poles (see Fig. 23, top). The latter effect is known as the von Zeipel effect or *gravity darkening* (von Zeipel 1924). The combination of both effects leads to an asymmetric brightness distribution on the sky and thus to visibilities that depend not only on the length, but also on the orientation of the interferometer baseline, and to non-zero closure phases. This has been observed for the bright stars Altair (van Belle et al. 2001; Ohishi et al. 2004; Domiciano de Souza et al. 2005; Peterson et al. 2006b; Monnier et al. 2007), Achernar (Domiciano de Souza et al. 2003), Regulus (McAlister et al. 2005) and Alderamin (van Belle et al. 2006). Interferometric observations also lead to the conclusion that Vega is a rapid rotator seen nearly pole-on (Aufdenberg et al. 2006; Peterson et al. 2006a). In general, reasonable agreement is found between the observations and simple models based on the assumptions of rigid rotation, mass concentration towards the centre of the star and a fully radiative atmosphere. There are some small discrepancies, which may indicate that one or more of the underlying assumptions need to be relaxed; however, at present the data are not sufficient yet to provide strong constraints on more sophisticated models.

Rapid stellar rotation has two important consequences for determination of fundamental properties of stars, and for the comparison of observations with theoretical models: first, the stellar structure and evolution is affected by rotation; second, the star radiates non-isotropically, and thus its observed properties (spectral energy distribution, colours, spectral type, etc.) depend on the inclination of the rotation axis with respect to the line of sight—much more dramatically than one might naively expect, as demonstrated by the example of Vega. Strong differential rotation might further complicate the situation, as stars with different masses and internal structure can appear identical to the observer, while in extreme cases, stars might even have non-convex shapes (MacGregor et al. 2007) (see Fig. 23, bottom right). Direct interferometric observations of the shapes and surface brightness distributions of rapid rotators are thus an indispensable tool for the correct modelling of these stars.

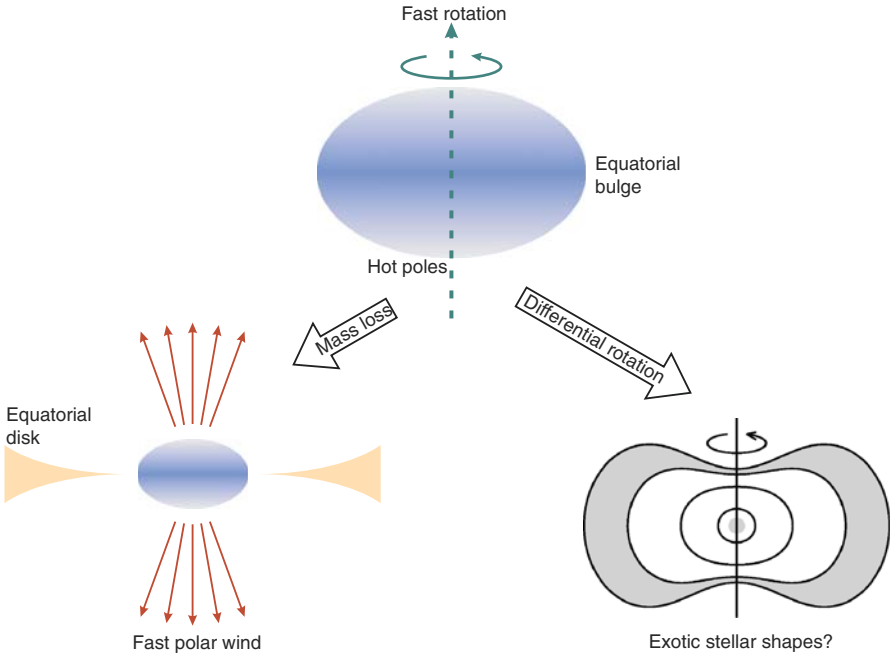

Fig. 23 Rapidly rotating stars develop a pronounced equatorial bulge, which is substantially cooler than the polar regions (*top*). Radiation pressure drives a fast wind from the polar regions if they are sufficiently hot, whereas disks are frequently formed in the equatorial plane (*bottom left*). Stars in which the rotation rate decreases strongly with distance from the axis may assume non-convex shapes, shown here in cross-section with convective shaded regions (*bottom right*, adopted from MacGregor et al. 2007). Future interferometric observations will be needed to determine whether stars with such exotic shapes actually exist

A further consequence of rapid stellar rotation in hot stars is the enhanced radiation pressure near the poles due to the von Zeipel effect, which can drive a polar wind (see Fig. 23, bottom left). This is the most likely explanation of the elongation of η Car (van Boekel et al. 2003) and Achernar (Kervella and Domiciano de Souza 2006) observed interferometrically.

3.2.4 Binary stars

In addition to measurements of stellar diameters, observations of close binary stars is one of the classical applications of optical interferometry. The squared visibility[21] of a binary is given by

$$\mathcal{V}^2 = \frac{1}{(1+\mathcal{R})^2}\left[\mathcal{V}_1 + \mathcal{R}^2\mathcal{V}_2 + 2\mathcal{R}\mathcal{V}_1\mathcal{V}_2\cos\left(\frac{2\pi\mathcal{S}\mathcal{B}\cos\psi}{\lambda}\right)\right], \qquad (67)$$

with $\mathcal{R} \leq 1$ the brightness ratio of the two stars, $\mathcal{V}_1$ and $\mathcal{V}_2$ their individual visibilities, $\mathcal{S}$ their separation and ψ the angle in the (u, v) plane between the interferometer

[21] Single-baseline interferometers normally measure $\mathcal{V}^2$, not $\mathcal{V}$, see Shao and Colavita (1992).

baseline and the line joining the two stars (e.g. Lawson 2000). To determine $\mathcal{S}$, ψ, and the stellar parameters uniquely from measurements of $\mathcal{V}^2$, data have to be obtained for many points in the (u, v) plane. This can be accomplished by observations with multiple baselines, by Earth-rotation synthesis, by taking data at multiple wavelengths (since u and v scale with the wavenumber), or by a combination of these techniques. Repeated observations with good coverage of the orbital phases can then be used to determine a visual orbit (Armstrong et al. 1992a). A better method was developed by Hummel et al. (1993) and applied in most subsequent analyses. Here, the seven orbital elements and the stellar parameters are fitted directly to the observed visibilities. This global approach has the advantage that the fast orbital motion of short-period binaries is taken into account properly.

The goal of binary star observations is normally the determination of fundamental parameters such as the masses, radii and luminosities of the two components. It is usually necessary to combine two or more techniques to achieve this goal, since not all orbital elements can be determined with any single method alone. A particularly useful case are double-lined spectroscopic binaries, for which the visual orbit can also be obtained. However, there is little overlap between the two classes, since spectroscopic binaries tend to have small orbits that are difficult to resolve. Even orbits of double-lined spectroscopic binaries obtained with adaptive optics or speckle techniques are rarely precise enough to give masses better than $\sim 10\%$. This is one of the reasons why interferometric observations of double-lined spectroscopic binaries are of great importance for the determination of fundamental stellar parameters.

Adding the orbital inclination from the interferometric orbit to the spectroscopic elements allows computation of the component masses, and combining the angular diameter of the orbit with the physical scale set by the spectroscopy yields the distance, or *orbital parallax*. Because of the fundamental importance of these data, extensive observations of double-lined spectroscopic binaries have been carried out with almost every interferometer in existence. They are summarized in Table 1, which has been updated from Quirrenbach (2001b). The orbital solutions and error estimates are taken from the references cited and are therefore not uniform. The error bars refer formally to $1\,\sigma$, but some authors may be more conservative than others in assessing systematics in the data or in dealing with discrepancies between different subsets of the data (e.g. different eccentricities from the spectroscopic and interferometric orbits). It should also be pointed out that determining the scale of the orbit (in angular units), and the subsequent computation of the orbital parallax, requires knowledge of the effective central wavelength of the interferometric observations, which depends on the stellar colour (Hummel et al. 1994). Systematic errors in this quantity may easily go unnoticed since they do not affect the χ^2 of the orbital fit. In many cases, however, the precision of the mass determination is limited by the spectroscopic, not by the interferometric orbit.

It is instructive to compare Table 1 with the masses of eclipsing binaries compiled by Andersen (1991). Only a handful of the interferometrically determined masses meet Andersen's accuracy criterion for being useful for critical tests of main-sequence stellar models, which he set at 2%. Furthermore, the baselines used in the observations compiled in the table are generally too short to give good stellar radii (with the exception of Capella). On the other hand, the agreement for the component masses of

Table 1 Interferometrically determined orbits and component masses for double-lined spectroscopic binaries (More details are available in the references listed. The star κ Peg is a triple system; in this case the "wide" (A – Ba/Bb) and "narrow" (Ba – Bb) orbits are listed separately)

System	Spectral Types	a'' [mas]	M_1 [$M_\odot$]	M_2 [$M_\odot$]	Instr.	Ref.
HD 27483	F6V+F6V	1.3	1.38 ± 0.13	1.39 ± 0.13	PTI	K04
α Vir	B1III-IV+B3V:	1.5	10.9 ± 0.9	6.8 ± 0.7	Narrabri	H71
κ Peg B	F5IV+K0V:	2.5	1.662 ± 0.064	0.814 ± 0.046	PTI	M06
V773 Tau A	K2+?	2.8	1.54 ± 0.14	1.332 ± 0.097	KI	B07
θ Aql	B9.5III+B9.5III	3.2	3.6 ± 0.8	2.9 ± 0.6	Mk III	H95
β Aur	A2V+A2V	3.3	2.41 ± 0.03	2.32 ± 0.03	Mk III	H95
12 Boo	F9IV+F9IV	3.4	1.435 ± 0.023	1.408 ± 0.020	PTI	B00
		3.5	1.416 ± 0.005	1.374 ± 0.005	combined	B05b
σ Sco	B1III+B1V	3.6	18.4 ± 5.4	11.9 ± 3.1	SUSI	N07b
γ^2 Vel	O7.5II+WC8	3.6	28.5 ± 1.1	9.0 ± 0.6	SUSI	N07c
BY Dra	K4V+K7.5V	4.4	0.59 ± 0.14	0.52 ± 0.13	PTI	B01
o Leo	F9+A5m	4.5	2.12 ± 0.01	1.87 ± 0.01	combined	H01
HD 9939	K1IV+K0V	4.9	1.072 ± 0.014	0.838 ± 0.008	PTI	B06
σ Psc	B9.5V+B9.5V	5.6	2.65 ± 0.27	2.36 ± 0.24	PTI	K04
64 Psc	F8V+F8V	6.5	1.223 ± 0.021	1.170 ± 0.018	PTI	B99b
93 Leo	G5III+A7V	7.5	2.25 ± 0.29	1.97 ± 0.15	Mk III	H95
ζ^1 UMa	A2V+A2V	9.6	2.51 ± 0.08	2.55 ± 0.07	Mk III	H95
		9.8	2.43 ± 0.07	2.50 ± 0.07	NPOI	H98
ι Peg	F5V+G8V	10.3	1.326 ± 0.016	0.819 ± 0.009	PTI	B99a
η And	G8III+G8III	10.4	2.59 ± 0.30	2.34 ± 0.22	Mk III	H93
α Equ	G2III+A5V	12.0	2.13 ± 0.29	1.86 ± 0.21	Mk III	A92b
27 Tau	B8III+?	13.1	4.74 ± 0.25	3.42 ± 0.25	combined	Z04
HD 195987	G9V+?	15.4	0.844 ± 0.018	0.665 ± 0.008	PTI	T02
ζ Aur	K4Ib+B5V	16.2	5.8 ± 0.2	4.8 ± 0.2	Mk III	B96
θ^2 Tau	A7III+A:	18.6	2.1 ± 0.3	1.6 ± 0.2	Mk III	T95
		18.8	2.15 ± 0.12	1.87 ± 0.11	combined	A06
λ Vir	Am+Am	19.8	1.897 ± 0.016	1.721 ± 0.023	IOTA	Z07
HD 98800 B	K5V+?	23.3	0.699 ± 0.064	0.582 ± 0.051	KI	B05a
ϕ Cyg	K0III+K0III	23.7	2.536 ± 0.086	2.437 ± 0.082	Mk III	A92a
α And	B8IV+A:	25.2	5.5:	2.3:	Mk III	P92,T95
β Cen	B1III+B1III	25.3	11.2 ± 0.7	9.8 ± 0.7	SUSI	D05,Au06
β Ari	A5V+G0V:	36.1	2.34 ± 0.10	1.34 ± 0.07	Mk III	P90
λ Sco	B1.5IV+B2V	49.3	10.4 ± 1.3	8.1 ± 1.0	SUSI	T06
12 Per	F8V+G2V	53.2	1.382 ± 0.019	1.240 ± 0.017	CHARA	Ba06

Table 1 continued

System	Spectral Types	a'' [mas]	M_1 [$M_\odot$]	M_2 [$M_\odot$]	Instr.	Ref.
α Aur	G1III+G8III	55.7	2.56 ± 0.04	2.69 ± 0.06	Mk III	H94
δ Equ	F7V+F7V	231.9	1.193 ± 0.012	1.188 ± 0.012	PTI	M05
κ Peg	F5IV+F5IV	235.0	1.549 ± 0.050	composite	PTI	M06

References: *A92a* Armstrong et al. (1992a), *A92b* Armstrong et al. (1992b), *A06* Armstrong et al. (2006), *Au06* Ausseloos et al. (2006), *Ba06* Bagnuolo et al. (2006), *B96* Bennett et al. (1996), *B99a* Boden et al. (1999a), *B99b* Boden et al. (1999b), *B00* Boden et al. (2000), *B01* Boden and Lane (2001), *B05a* Boden et al. (2005a), *B05b* Boden et al. (2005b), *B06* Boden et al. (2006), *B07* Boden et al. (2007), *D05* Davis et al. (2005), *H71* Herbison-Evans et al. (1971), *H93* Hummel et al. (1993), *H94* Hummel et al. (1994), *H95* Hummel et al. (1995), *H98* Hummel et al. (1998), *H01* Hummel et al. (2001), *K04* Konacki and Lane (2004), *M05* Munterspaugh et al. (2005), *M06* Munterspaugh et al. (2006), *N07b* North et al. (2007b), *N07c* North et al. (2007c), *P90* Pan et al. (1990), *P92* Pan et al. (1992), *T95* Tomkin et al. (1995), *T02* Torres et al. (2002), *T06* Tango et al. (2006), *Z04* Zwahlen et al. (2004), *Z07* Zhao et al. (2007)

β Aur, a system in common between the two samples, is encouraging. Furthermore, analyses of pairs with evolved components such as Capella, ϕ Cyg and α Equ provide useful tests of post-main-sequence evolutionary models (e.g. Armstrong et al. 1992a). The availability of orbital parallaxes giving good luminosities is a clear advantage in this respect.

Comparing Table 1 with the previous version in Quirrenbach (2001b) also shows that quite some progress has been made over the past few years, and that many interferometers have started to cover particularly interesting types of stars, such as β Cephei stars (β Cen and λ Sco) and pre-main-sequence objects (V773 Tau and HD 98800 B). The key to further progress will be observations of stars with well-determined spectroscopic elements and state-of-the-art determination of the metal abundance. Comprehensive tests of stellar models require covering all regions of the HR diagram. Many of the eclipsing systems in Andersen (1991) are also accessible to the new instruments, which could provide improved distances and better luminosity ratios for partially eclipsing systems. The good instantaneous coverage of the (u, v) plane afforded by the multiple baselines and wavelength channels of the new arrays will allow determination of orbits from snapshot observations, making them very efficient instruments for binary programmes.

3.2.5 Circumstellar material

Optical/infrared interferometry has been used extensively to characterize the geometry and physical properties of circumstellar material. Typical examples are measurements of the dust distribution around late-type stars (Danchi et al. 1994), the proof that Be stars are surrounded by geometrically thin disks (Quirrenbach et al. 1997), and the spatially resolved detection and compositional analysis of silicates in the innermost two astronomical units of protoplanetary disks (van Boekel et al. 2004). As mentioned in Sect. 3.2.3, the hot polar regions of rapidly rotating early-type stars may drive bipolar winds; these winds may coexist with equatorial disks (e.g. Malbet et al. 2007).

In the present context, the presence of circumstellar material is relevant mainly because it affects the stellar parameters inferred from photometric, spectroscopic or interferometric observations. It is therefore advisable to perform interferometric observations with a range of baseline lengths and orientations, and to check whether the observed visibilities follow Eq. (65) or, in the case that only short baselines are used, Eq. (60). The presence of circumstellar material will normally manifest itself in a visibility function that does not converge to $\mathcal{V} \rightarrow 1$ for $\mathcal{B} \rightarrow 0$. It is then possible to either correct the derived stellar parameters for the effects of the circumstellar material, or to reject the affected stars from a sample for which high-precision data are sought.

3.3 Present instruments and capabilities

3.3.1 A short overview of current interferometers

As is clear from the discussion in Sect. 3.1, an interferometer (and in particular an optical interferometer) is very different from a focal instrument at a telescope (e.g. a spectrograph). While a few parameters are sufficient to qualify a spectrograph (e.g. spectral resolution and operating wavelength), both the telescopes and recombiners have to be taken into account for an interferometric instrument. Most degrees of freedom are related to the interferometer and not to the focal instrumentation.

Since interferometers measure visibilities and visibilities encode information on the surface brightness distribution of the source at a given angular frequency, the first step in the qualification of an interferometer is to define the angular frequencies made available to constrain the astronomical object brightness distribution. These angular frequencies are the (u, v) space coverage and they depend on

1. the baselines (the physical positions of the telescopes) and on the operating wavelength;
2. the declination of the source, the latitude of the observatory and the hour angle;
3. the number of telescopes;

(e.g. Dyck 2000). Figure 24 illustrates some of these dependencies. More specifically, the baselines and operating wavelength determine the maximum achievable angular frequency ($\mathcal{B}/\lambda$). It limits the minimum angular diameters of the objects that can be resolved to $\theta \sim \lambda/\mathcal{B}$. Small angular sizes can be reached either with large baselines or small operating wavelengths (e.g. observing in the V band, in contrast with the K band, is equivalent in (u, v) space to increase the baselines by a factor of 4). The source declination, observatory latitude and hour angle determine how the baseline vector projects onto the sky as the Earth rotates. Thanks to the Earth rotation, different points in the (u, v) space become accessible.

Finally, the number of telescopes defines the instantaneous number of available baselines and, therefore, the instantaneous number of points where the visibility can be measured. Earth rotation can in some circumstances overcome the limitation of a small number of telescopes. However, the maximum increase in number of (u, v) points due to rotation is a factor of 10. In contrast, the increase of number of telescopes implies that the number of (u, v) points can increase factorially. In order to use all the available telescopes, a focal instrument must be available to combine them.

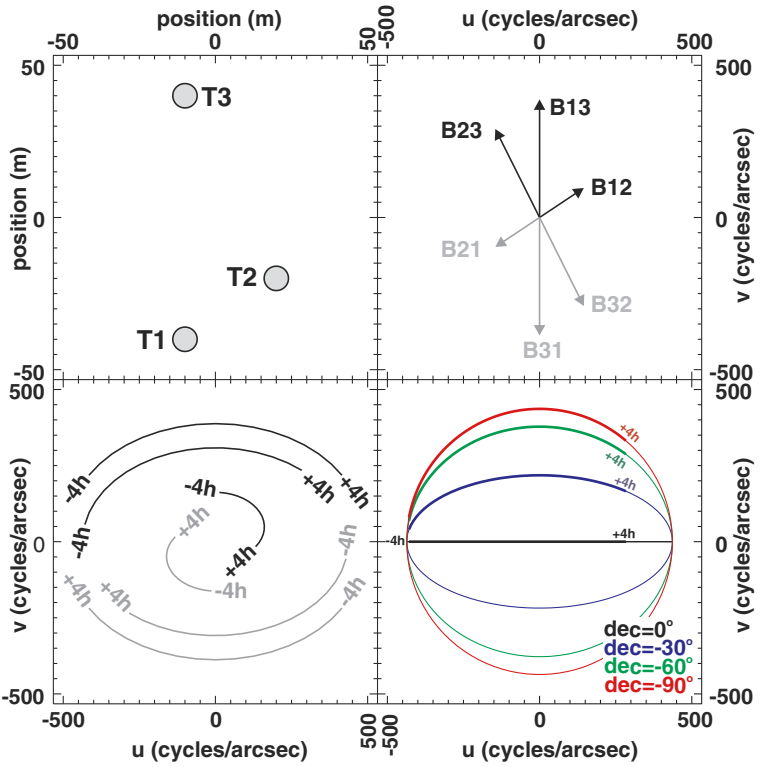

Fig. 24 The (u, v) coverage of an interferometer. *Top left* projection onto the (E, N) plane of the physical positions of the telescopes at the observatory. *Top right* instantaneous (u, v) coverage at a wavelength of 1 μm, assuming the source is at a declination of $-45°$ and passing through the meridian. The telescopes are at a latitude of $-45°$. Although there are two centrosymmetric baselines for each telescope combination, they yield no extra information (the object brightness distribution being a real function, its Fourier transform is centrosymmetric). *Bottom left* dependence of the (u, v) coverage on hour angle (–4h to +4h), for the same parameters as the top right figure. *Bottom right* dependence of the (u, v) coverage on the source declination for the B23 baseline. These curves are ellipse arcs, ranging from a circle arc for a source at a celestial pole, and collapsing to a line segment for a source at the equator

Once the telescopes' positions are defined, an instrument (recombiner) will combine the light and detect the fringes. Two classes of recombiners are available. One class disperses the fringes and detects a visibility spectrum $\mathcal{V}(\lambda)$ at each (u, v) point. This is, in a sense, analog to a spectrograph. The other class detects the visibility in a narrow wavelength range (with one or very few wavelength "pixels") and is, in a sense, analog to a filter-based system.

The performance or limiting magnitude of an interferometer is usually defined for an unresolved source ($\mathcal{V} = 1$). At the detector the fringe contrast is the visibility. The observation of an object with a larger angular diameter implies a decrease of the visibility amplitude and thus also of the fringe contrast at the detector. The limiting magnitude decreases by $-2.5 \log(|\mathcal{V}|)$. In practice, several aspects determine the li-

miting magnitude of an interferometer, the most important one for asteroseismology being fringe tracking[22] and the availability of adaptive optics at the telescopes.[23]

The scientific results discussed in Sect. 3.2 provide an overview of the capabilities of today's interferometers—and, by inference, of their limitations. For the precise determination of fundamental stellar parameters a combination of good spatial and spectral resolution, high sensitivity, broad wavelength coverage (including access to the visible wavelength range), and high operational efficiency (to facilitate the calibration) is vitally important. Unfortunately, none of the present interferometers provides all of these characteristics simultaneously.

At the time of writing this article (mid-2007), seven optical and infrared interferometers are in operation; the main properties of these facilities are summarized in Table 2. The results presented in Sect. 3.2 have been obtained with these instruments and a few additional ones that have already been closed, notably the Mk III Interferometer on Mt Wilson in California and the IOTA on Mt Hopkins in Arizona. We refer the reader to the interferometer web pages for up-to-date information.[24] Table 2 clearly shows that the limiting magnitude of most interferometers does not depend on the aperture diameter and is currently at $m_K = 6 - 7$. Visibilities as small as $\mathcal{V}^2 = 2 \times 10^{-4}$ have been measured (Monnier et al. 2007). It is also evident from Table 2 that there are large differences in the capabilities of the various facilities. In addition to the parameters listed, one has to consider the available spectral resolution, stability of the fringe servo system, speed of acquisition and observing efficiency, site characteristics, calibration procedures and other factors for assessing the suitability of a specific facility for any given scientific question. Particularly interesting for asteroseismology is the combination of a large number of telescopes.

Most technical information on optical/infrared interferometers gets published in the proceedings of the conferences on this topic that are part of the bi-annual SPIE conferences on astronomical instrumentation. The most recent volumes in this series are Léna and Quirrenbach (2000), Traub (2003), Shao (2003), Traub (2004) and Monnier et al. (2006). The reader is referred to these proceedings for more details on existing, planned and historical interferometers. Summary overviews can also be found in the reviews by Quirrenbach (2001a) and Monnier (2003).

3.3.2 Interferometric images in the optical domain

Most of the astrophysical results summarized in Sect. 3.2 have been obtained by fitting model parameters to visibilities observed with interferometers of a single baseline or

[22] The ability to freeze the fringes on the detector and integrate for larger times $\lesssim 100$ s.

[23] The intensity loss is proportional to the strehl ratio at the telescope. Therefore, the capacity to reach lower wavelengths (and therefore higher angular frequencies in (u, v) space) is increased.

[24] Interferometers in the Worldwide web:

- VLTI: http://www.eso.org/projects/vlti/instru/
- CHARA: http://www.chara.gsu.edu/CHARA/
- KI: http://planetquest.jpl.nasa.gov/Keck/keck_index.cfm
- NPOI: http://www.nofs.navy.mil/projects/npoi/
- SUSI: http://www.physics.usyd.edu.au/astron/susi/.

Table 2 Properties of major operational interferometers and associated instrumentation, adapted from McAlister (2000)

Interferometer and Instrument	Number of telescopes	Telescope diameter (m)	Maximum baseline (m)	Operating wavelength (μm)	Limiting magnitude	Spectral resolution	Ref.
VLTI (Paranal, Chile)	4+(4)	8 (1.8)	130 (200)	0.45–20	n.a.	n.a.	G00
VLTI/AMBER	3	n.a.	130 (130)	1.0–2.5	$m_K = 7(5)$	30–12000	
VLTI/MIDI	2	n.a.	130 (130)	8–13	$m_N = 4(0.7)$	30–230	
SUSI (Narrabri, AUS)	11	0.14	640	0.4–0.9	n.a.	n.a.	D99
SUSI/red	2	n.a.	80	0.7	m_V=4	$\Delta\lambda = 80$ nm	
SUSI/blue	2	n.a.	50	0.44	m_B=3	$\Delta\lambda = 1.5$ nm	
KI/K (Mauna Kea, HI)	2	10	85	2.2	m_K=8	$\Delta\lambda = 1.5$ μm	C04
PTI (Mt. Palomar, CA)	2	0.4	110	1.6–2.2	m_K=6	$\Delta\lambda = 0.1$ μm	C99
NPOI (Flagstaff, AZ)	6	0.12	64	0.55–0.85	m_V=6	$\Delta\lambda = 19$ nm	A98
CHARA (Mt. Wilson, CA)	6	1.0	331	0.45–2.4	n.a	n.a.	T05
CHARA/Classic/FLUOR	2	n.a.	331	1.6–2.4	m_K=6	$\Delta\lambda = 350$ nm	
CHARA/MIRC	4	n.a.	331	1.5–2.5	m_K=6	20–300	

The limiting magnitudes quoted are those for the most sensitive instrument configuration, for an unresolved object (published data or available documentation were used to determine the values presented). The limiting magnitudes should be considered with caution, since experimental facilities such as the KI do not have the same stringent requirements as general user facilities, such as the VLTI. For interferometers with hybrid telescope sizes curved brackets are used

References: *A98* Armstrong et al. (1998), *C99* Colavita et al. (1999), *C04* Colavita et al. (2004), *D99* Davis et al. (1999), *G00* Glindemann et al. (2000), *H04* Hale et al. (2004), *T05* ten Brummelaar et al. (2005)

at most a few baselines. This approach works very well if a physical model of the target can be constructed a priori (e.g. a uniform or limb-darkened disk, a von Zeipel model of a rapid rotator or a binary), but it becomes problematic if the brightness distribution is not known beforehand. For example, the thin atmospheres and low gravities of Mira stars result in strong deviations from spherical symmetry, which can be detected with very limited data sets (e.g. Quirrenbach et al. 1992; Ragland et al. 2006). However, for a detailed analysis and an understanding of the causes of these asymmetries one would have to obtain true images that show the shapes and brightness distribution of these "jellyfish-like" objects.

As pointed out in Sect. 3.1.4, interferometric imaging is possible only with arrays that provide good coverage of the (u, v) plane, and sophisticated data analysis algorithms are needed to reconstruct images from visibility data (e.g. Baldwin and Haniff 2002; Quirrenbach 2001a, and references therein). While these theoretical foundations of optical aperture synthesis imaging are well understood, this technique is still in its infancy because of the limited number of telescopes available in present-day arrays (see Table 2), and because of the difficulties inherent in building and operating complex many-telescope beam combiners.

The first images reconstructed from optical interferometers only showed very simple objects such as the binary Capella (Baldwin et al. 1996); the capabilities of the six-telescope beam combiner of NPOI was first demonstrated by imaging the η Vir triple system (Hummel et al. 2003). More recently, the surface of Altair has been imaged with the CHARA Array, directly showing the rotational flattening and von Zeipel effect (Monnier et al. 2007). It is certainly encouraging to see interferometric images that carry truly useful astrophysical information, and with the emergence of more instruments capable of combining four or more telescopes simultaneously; the impact of such images is expected to increase in the near future.

The combination of data taken in multiple spectral channels can further help to increase the (u, v) plane coverage, since the spatial frequency is inversely proportional to the wavelength. This technique obviously works best if the source structure is independent of wavelength as, for example, in binary systems with two components of equal spectral type (Benson et al. 1997). A generalization is possible if the wavelength dependence can be easily parameterized, such as a field of unresolved stars or a spotted stellar surface, which can be described by brightness and colour for each point.

3.4 Limitations of interferometers for the measurement of stellar diameters

We focus now on the fundamental limits of the accuracy of visibility modulus measurements in the context of stellar diameter measurements. Visibility phases are not discussed here as they are not used to constrain diameters. Whenever we speak of an *accurate* visibility modulus measurement, we mean that this measurement is *precise* and *unbiased*. It is important to make this distinction, because an estimate may be based on measurements with a very small statistical dispersion but with a large bias. In this case, it cannot be regarded as accurate. Reaching high accuracies therefore requires to be able to reduce biases to magnitudes smaller than the final error bar.

3.4.1 Sources of visibility errors and biases

Interferometers do not provide a direct measurement of the spatial coherence of a source, because causes of coherence loss can be numerous, the major ones being atmospheric turbulence, polarizations, longitudinal dispersion and vibrations. All these sources of loss will imply that visibilities are observed with a reduced value compared with the case where no losses occur. As a consequence, it is possible to calibrate the losses by normalizing visibilities with the help of the fringe contrast observed for calibrator stars, as long as the coherence losses for the target and for the calibrator are sufficiently similar,

$$\mathcal{V}_{\rm obj} = \frac{C_{\rm obj}}{T} = \frac{C_{\rm obj}}{C_{\rm cal}} \times \mathcal{V}_{\rm cal}^{\rm exp}, \tag{68}$$

where T is the transfer function or the point source response of the interferometer defined in Eq.(2) of Perrin (2003) while $C_{\rm obj}$, $C_{\rm cal}$ and $\mathcal{V}_{\rm cal}^{\rm exp}$ are the fringe contrast measured on the source, the fringe contrast measured on the calibrator and the expected visibility of the calibrator, respectively. For a point-like calibrator, we have $T = C_{\rm cal}$. The two fringe contrast measurements are subject to various noise sources (detector noise, photon noise and background noise) and biases which are discussed below. The expected visibility of the calibrator has an intrinsic error and is estimated from a model with an uncertainty and a potential bias. To reduce sources of errors due to calibrators and instabilities of the interferometer response, the object observations are often bracketed by observations of several calibrators.

3.4.2 Atmospheric turbulence and spatial filtering

The paramount source of error and degradation of the accuracy on the visibility measured by interferometers is atmospheric turbulence. In regular conditions on the ground, only a fraction of the incident photons are coherent. This fraction is given by the coherent energy, which depends on the turbulence strength, the zenith angle and the considered wavelength (see e.g. Quirrenbach 2000, for a definition and discussion). The coherent energy is typically of order 30% but can be increased using adaptive optics. The coherent energy is a fluctuating quantity because the seeing is fluctuating. It is, therefore, difficult to calibrate and this implies a strong limitation on the quality of visibility measurements. Turbulence at the scale of the interferometer, i.e. the average phase over each pupil, also plays a role. These phase differences are called (differential) piston errors. They induce jitter of the fringe pattern, which degrades visibilities. Vibrations have effects similar to turbulence on the stability of interferometers, which is why they are usually merged with turbulence, as we will assume in the following.

The interferometer's response can be written as the product of a slowly varying response $T_{\rm inst}$ with an unstationary atmospheric response. The latter comprises the coherent energy $T_{\rm atm} = E_c$ and the piston effect $T_{\rm piston}$. One way to help solve the issue of fluctuating coherent energy is to benefit from adaptive optics or to reduce the telescope diameter below r_0. In either case, residual phase fluctuations remain. The best procedure consists in spatially filtering almost flat wavefronts with a pinhole,

or, even better, with a single-mode fibre. A single-mode fibre flattens the wavefronts or more exactly selects the fraction of incident lightwaves whose wavefronts are flat. This operation thus trades phase fluctuations against intensity fluctuations that can easily be monitored. The new interferometer response becomes:

$$T = T_{\text{inst}} \times T_{\text{piston}} \times \frac{2\sqrt{P_{\text{A}} P_{\text{B}}}}{P_{\text{A}} + P_{\text{B}}}, \tag{69}$$

with P_{A} and P_{B} the intensities coupled in the fibers at the focus of telescopes A and B, respectively. As these intensities are measured in real time, the response of a single-mode interferometer is $T = T_{\text{inst}} \times T_{\text{piston}}$. This has led to great improvements in the measurements of diameters.The piston term can be further reduced by servoing the fringe position with a fringe tracker or by freezing piston fluctuations with an adequately short exposure time. Under these circumstances and after calibration, the piston effect is more a source of noise than a bias.

3.4.3 Longer time scale sources of errors

The instrumental parts of the coherence losses, apart from vibrations, have long time scales of variation. They are mostly due to polarization and, to a lesser extent, to longitudinal dispersion.

Polarizations with different orientations will neither perfectly interfere nor will they necessarily produce fringes if they are crossed. Differential birefringence will cause interferograms in two orthogonal polarization axes to be shifted and to add up incoherently, the worst case being a shift of half a fringe. Although the effects can be dramatic, recipes are well known to solve the issue, e.g. the use of identical or symmetric optical trains are enough to guarantee very high fringe contrasts.

The nature of longitudinal dispersion is to make the zero optical path difference wavelength dependent. This happens when the index of refraction is different in the two arms of the interferometer or if the two arms have different lengths and if the index of refraction is chromatic. The former case may happen when single-mode fibres are used to propagate the beams. In this case, dispersions need to be matched by adjusting the fibre lengths and using homogeneous fibres. The latter case may happen in the bluest part of the spectrum when propagating beams in unevacuated and unequal interferometer arms. In both cases, solutions are well known and these degradations can be avoided.

As long as the calibrator(s) and the science target are subject to the same coherence losses (which assumes similar reflections on mirrors, e.g. and, therefore, the sources to be nearby and observed with a short time difference if the interferometer properties are temperature dependent) T_{inst} is quite easy to measure. Fig. 25 shows examples of measurements with the single-mode interferometer FLUOR at IOTA.

3.4.4 Calibration and calibrators

As we have discussed, atmospheric errors can be eliminated by going to space, or thanks to single-mode optics. Vibrations can be solved by servoing optical paths.

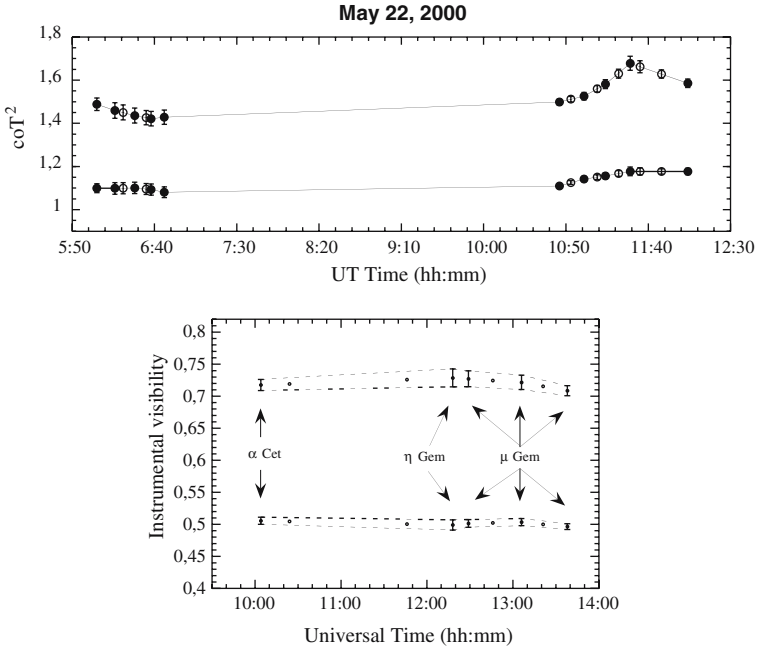

Fig. 25 Examples of transfer functions of the FLUOR instrument at IOTA. *Top panel* squared co-transfer function for the two channels of the interferometer. The calibrator measurements are indicated by *filled circles* the *open circles* represent interpolated values at the time the scientific source was observed (from Perrin 2003, with permission). *Bottom panel* the instrumental visibility, which is the visibility measured for three different calibrators. The *dashed lines* are the 1σ upper and lower limits. The corresponding transfer function is stable to within 1σ on a time scale of 2 h (from Perrin et al. 2004, with permission)

Polarization and dispersion can be tackled by a good design of the interferometer. One remaining difficulty is the computation of the expected visibility of calibrators. As Eq. (68) shows, the ultimate error on the visibility will come from this estimate, even if other sources of errors have been perfectly calibrated. An ideal calibrator is a point-like source as its visibility is exactly 1. However, such a source emits no photons. Realistic sources have a finite diameter. Errors on the expected visibility may come not only from uncertainties on the source angular diameter but also on its geometry. It is necessary to assume spherical symmetry for the source and it is mandatory that this assumption is correct at the resolution of the interferometer, i.e. one must make use of a simple featureless star with a well-known diameter and a very compact atmosphere. Assuming such a star, one difficulty to compute expected visibilities arises from limb-darkening as it changes the apparent angular diameter from one wavelength to another and a correction is required. Theoretical models exist (e.g. Claret 2000) and are tested against interferometric data (e.g. Wittkowski et al. 2004). The effect is lower at infrared than at visual wavelengths because the difference between a uniform and a limb-darkened disk is only of order 2% at red wavelengths.

Angular diameters, and therefore visibilities, can be predicted with two different methods. The first one is a direct method based on a direct measurement of the source

angular diameter and the visibility is extrapolated using a uniform or a limb-darkened disk model. The best demonstrated accuracy on angular diameter measurements is 0.5% in the K band for α Cen A and B (Kervella et al. 2003b). Extrapolating this to the longest baseline of VLTI (200 m) and to the J band leads to the measurements of angular diameters with an accuracy of 0.5% for all stars larger than 1 milliarc seconds (mas). This provides a list of primary calibrators but is not enough to calibrate all VLTI observations, for example, at the highest accuracy of 0.1%, as the required calibrators then are rather 0.1 mas in diameter (see below).

Secondary calibrators whose angular diameters are computed with indirect methods are required. They aim at predicting a zero-magnitude stellar diameter $\theta_{\rm zm}$ as a function of a color index or a spectral type. Stellar diameters for any magnitude then follow from $\theta_m = \theta_{\rm zm} \times 10^{-m/5}$. The typical error is 5% if all stars are taken into account. The prediction error can be reduced to 1.2% for carefully selected A0 to M0 giants using accurate photosphere and atmosphere modelling (Bordé et al. 2002). Kervella et al. (2004c) have shown that this can still be improved using surface brightness relationships for selected dwarfs. These relationships are calibrated with interferometric measurements. The best correlation is found for dereddened $(B - L)$ colours: the residual prediction error is better than 1% and can be smaller than 0.5%. Fortunately, metallicity does not seem to play a role, which eliminates one potential source of bias.

In conclusion, one may consider that the state-of-the-art accuracy for the prediction of diameters for single stars is 0.5%. The accuracy on the derived visibility will then depend on the resolution of the interferometer. Fig. 26 shows the error on the predicted visibility assuming a 0.5% error on the diameter as a function of the calibrator visibility or, equivalently, to the spatial resolution. The error is always smaller than 0.5% and is smaller than 0.1% as long as the visibility is larger than 90%. This sets the minimum level of visibility for calibrators to keep the calibration error of the same magnitude or smaller than other errors.

3.4.5 Fundamental limits on accuracies

Sources of errors are many and only major ones have been discussed here. More thorough discussions would be beyond the scope of this paper. However, the reader has to be made aware that other errors may arise when modelling the visibilities. For example, one must be careful and compute models with the same estimator as the visibility estimator to derive the correct diameter. This is all the more important as the band is wide. Such effects are discussed in Perrin and Ridgway (2005). Also, as discussed in this same paper, the sensitivity to an effect such as piston or chromaticity depends on the choice of the visibility estimator. From Eq. (68) one can establish the following error budget,

$$\frac{\sigma_{\mathcal{V}_{\rm obj}}}{\mathcal{V}_{\rm obj}} = \sqrt{\left[\frac{\sigma_{C_{\rm obj}}}{C_{\rm obj}}\right]^2 + \left[\frac{\sigma_{C_{\rm cal}}}{C_{\rm cal}}\right]^2 + \left[\frac{\sigma_{\mathcal{V}_{\rm cal}^{\rm exp}}}{\mathcal{V}_{\rm cal}^{\rm exp}}\right]^2} \tag{70}$$

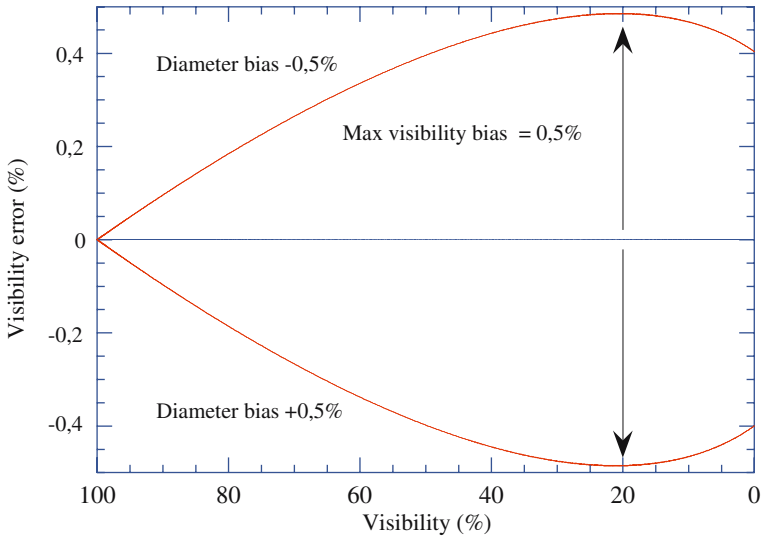

Fig. 26 Error on the predicted visibility of a uniform disk as a function of visibility for a relative error on the diameter of 0.5%. The error remains smaller than 0.1% as long as the visibility value is above 90%

The first two errors can be very small for the brightest sources (photon and detector noise) and are limited by piston noise. At this stage, vibrations can be assimilated along with piston errors. Piston errors can be further reduced with a fringe tracker. The third error term is the dominant one for the brightest sources. In practice it currently is of the order of 0.1%. It is, therefore, the fundamental limitation on visibility accuracies. One way to narrow down or clear its influence and push the limits of accuracy further, is to perform a relative calibration as described in Sect. 3.4.6. With relative calibration one avoids to rely on the exact value of the diameter of the calibrator.

3.4.6 Relative calibration

Relative calibration is an efficient way to search for relative variations of parameters in sources such as those that can be the goal in asteroseismology, where one could attempt to measure the stellar diameter variations due to oscillations. These diameter variations may be small and even below the visibility accuracy imposed by calibrators. The way to get around this difficulty is to use a single stable calibrator. Different visibilities recorded at different baselines and/or different times will share the same calibration fluctuations because the calibration errors are correlated from one measurement to another.

The contributions of correlated and uncorrelated noise for interferometric measurements were already described in Perrin (2003). When fitting a model of the source, absolute parameters (such as the average diameter) will have an accuracy limited by the accuracy on the calibrator diameter, since correlated errors will not average out. Relative parameters, such as those due to the relative amplitude of the oscillations, will, however, only be limited by photon, detector and piston noise. These noise sources

can be reduced by adopting longer exposure times. This can be easily understood with the following simple example. Let us assume that the diameter of a pulsating star with a relative pulsation amplitude of 10^{-3} in diameter is compared with that of quiet stars whose diameters are known to within an accuracy of 10%. If the diameter of the pulsating star is compared with a different calibrator at each observation, then the small pulsation will not be detected because the scatter in diameter measurements will be at least 10% divided by the square root of the number of calibrators. If a single calibrator with poorly known diameter is chosen for each observing period, then the absolute effect of the pulsation on the diameter will still not be detected. However, the oscillation, measured in units of the calibrator diameter, will be detected if the noise permits it. This technique may turn out to be powerful for this kind of application.

3.5 Future projects

Most of the facilities listed in Sect. 3.3 are planning upgrades to their respective infrastructure, and new beam combining instruments. A new imaging interferometer is currently under construction at the Magdalena Ridge Observatory (Buscher et al. 2006). In the following sections we describe possible future developments that could open new vistas for interferometric studies of the structure and surfaces of stars.

3.5.1 The future of the VLTI

The VLTI is unique among all interferometers worldwide in that a large number of institutions are contributing their expertise to its instrumentation programme, and in its ambition to provide an interferometric facility that is accessible to a large number of users and well suited for diverse observing programs. At present, two instruments are operational at the VLTI: AMBER (Petrov et al. 2007) and MIDI (Leinert et al. 2003). AMBER is a near-infrared instrument working in the J, H, and K bands with a spectral resolution up to 10,000. AMBER can combine the beams from three telescopes simultaneously and is thus capable of measuring closure phases. MIDI is a single-baseline instrument that measures correlated spectra with a resolution up to 230 in the N band ($8-13\ \mu$m).

The PRIMA (Phase-Referenced Imaging and Microarcsecond Astrometry) facility (Quirrenbach et al. 1998; Delplancke et al. 2006) will substantially enhance the capabilities of the VLTI by providing real-time fringe tracking and co-phasing. The astrometric mode of PRIMA will be used for an extensive extrasolar planet survey aimed at measuring their masses and orbits (Quirrenbach et al. 2004). The phase-referenced imaging mode of PRIMA will push the sensitivity limit of the VLTI by several magnitudes, because once the interferometer is co-phased, its point-source sensitivity (within the isoplanatic patch) is close to that of a single telescope with equal collecting area. In this observing mode, PRIMA can also serve as a fringe tracker for AMBER and MIDI.

At present, concepts for three second-generation VLTI instruments are being studied by international consortia: GRAVITY (Gillessen et al. 2006), MATISSE (Lopez et al. 2006), and VSI (Malbet et al. 2006). GRAVITY is a dual star instrument

optimized for precision narrow-angle astrometry and interferometric phase referenced imaging of faint objects within a $2''$ field. Its science case is centered on measuring motions in dense stellar clusters, in particular in the cluster surrounding the Galactic Centre. MATISSE will be a successor of MIDI, capable of combining four telescopes simultaneously, and expanding the wavelength range shortward to 2.7 μm, thus including the L and M bands in addition to N. The most important scientific drivers for MATISSE are studies of the formation of stars and planetary systems, and of dust shells around late-type stars. By combining up to six telescopes, VSI, the successor of AMBER, will bring true interferometric imaging and spectro-imaging in the near-infrared to the VLTI, with applications to stellar surface imaging as well as detailed investigations of circumstellar matter around young and evolved stars.

3.5.2 Interferometric high-resolution spectroscopy

Frequently interferometry is regarded as a method that can provide high-resolution *images*; the possibility of obtaining both high *spatial* and *spectral* resolution simultaneously with the same observation is often overlooked. Such observations enable many completely new approaches to fundamental questions in stellar astrophysics. Examples of astrophysical problems that can be addressed by interferometric spectroscopy include:

- *Late-type giant stars:* Measuring the variation of the stellar diameter with wavelength, or even better wavelength-dependent limb darkening profiles, provides a sensitive probe for the structure of strongly extended atmospheres of cool giant stars. Such data can be directly compared with predictions of theoretical models, and provide qualitatively new tests of stellar model atmospheres (Quirrenbach et al. 1993; Quirrenbach and Aufdenberg 2004).
- *Mira stars:* Mira variables possess exceedingly complicated atmospheres, with global asymmetries that change on time scales as short as a few weeks (Quirrenbach et al. 1992). Tracing the propagation of shocks in these atmospheres gives new information on their density structure, and on pulsation mechanisms.
- *Cepheids:* It is possible to perform direct measurements of the projection factors of Cepheid pulsations, which relate the true velocity of the pulsation to the observed radial velocity. Uncertainties in the projection factor $\mathcal{G}$, which presently has to be computed from theoretical models, are a serious limiting factor in current estimates of Cepheid distances with the Baade-Wesselink method (Sabbey et al. 1995; Marengo et al. 2002).
- *Generalized doppler imaging:* The chemical and magnetic properties of stellar photospheres can be mapped with classical Doppler imaging (e.g. Rice 2002; Kochukhov 2004; Kochukhov et al. 2004). However, the reconstruction of stellar surface features from line profile variations alone is plagued with ambiguities. These can largely be resolved by the additional phase information contained in interferometric data (Jankov et al. 2001a). For stars with inhomogeneous surface properties, interferometry enables studies of individual surface regions.
- *Rotational axes:* Determining the rotation axis orientation of the components in binary systems can provide new test for binary formation theories. Stellar rotation

induces a phase difference between the red wings and the blue wings of stellar absorption lines. Measuring the direction of the phase gradient on the sky allows determination of the orientation of the stellar axis (Petrov 1989; Chelli and Petrov 1995). More detailed modelling of the interferometric signal can also provide the inclination of the stellar rotation axis with respect to the line of sight (Domiciano de Souza et al. 2004). One can thus check whether the rotation axes of binaries are aligned with each other, and with the orbital angular momentum.

– *Differential rotation:* Along with the oscillation spectrum, surface differential rotation is a powerful diagnostic of the interior structure of a star. Unfortunately, it is difficult to observe surface differential rotation with classical spectroscopy because of degeneracies between inclination, limb darkening and rotation (e.g. Gray 1977). These degeneracies can be resolved by the additional information from interferometric spectroscopy (Domiciano de Souza et al. 2004). High spectral resolution is essential for this application.
– *Circumstellar disks:* Velocity-resolved interferometric observations in emission lines can be used to determine the geometry and velocity field of outflows from pre-main-sequence stars and of disks around young stars and Be stars.

The required spectral resolution depends on the width of the stellar lines under consideration, of course. For cool stars with narrow lines, the information content increases dramatically with spectral resolution, calling for an interferometric instrument providing a resolution $\gtrsim 50,000$, substantially more than what is available today.

Scanning through the fringe packet can in principle provide the desired spectroscopic information; the envelope of the fringe packet is the Fourier transform of the correlated source spectrum (multiplied by the bandpass of the instrument). This technique is known as double-Fourier interferometry (Mariotti and Ridgway 1988; Mékarnia and Gay 1990); it is appealing because it does not require any special hardware in addition to the scanning delay line. This method should work quite well for observations of strong isolated emission lines, but it is unsuitable for measurements of stellar absorption line spectra. In this case, the spectral resolution and the integrity of the observed spectrum are most certainly limited by calibration problems, because the shape of the whole fringe envelope has to be determined very precisely to allow the extraction of spectral information by Fourier transforming.

It thus appears that standard dispersive spectroscopy is much better suited for most of the applications delineated above. The spectrograph can easily be linked to the interferometer with optical fibers (Quirrenbach 2004a). Full information on the complex visibility $\mathcal{V}$ is contained in the four fringe quadratures, i.e. one has to count the photons at phases 0, $\pi/2$, π and $3\pi/2$ (e.g. Shao and Colavita 1992). A convenient way of generating these four bin counts A, B, C and D, is shifting one polarization by $\pi/2$ with respect to the other, as shown schematically in Fig. 27. An alternative would be a two-stage beam combiner, which sends 50% of the light from each interferometer arm to a "standard" beam combiner, giving the 0 and π outputs and 50% through an achromatic $\pi/2$ phase shifter to a second beam combiner, which thus produces the $\pi/2$ and $3\pi/2$ outputs. The achromatic phase shifter can be realized with adjustable dispersive elements (Mieremet et al. 2000). In either case, for any wavelength λ, the full interferometric information is thus contained in the intensities $A(\lambda)$, $B(\lambda)$, $C(\lambda)$

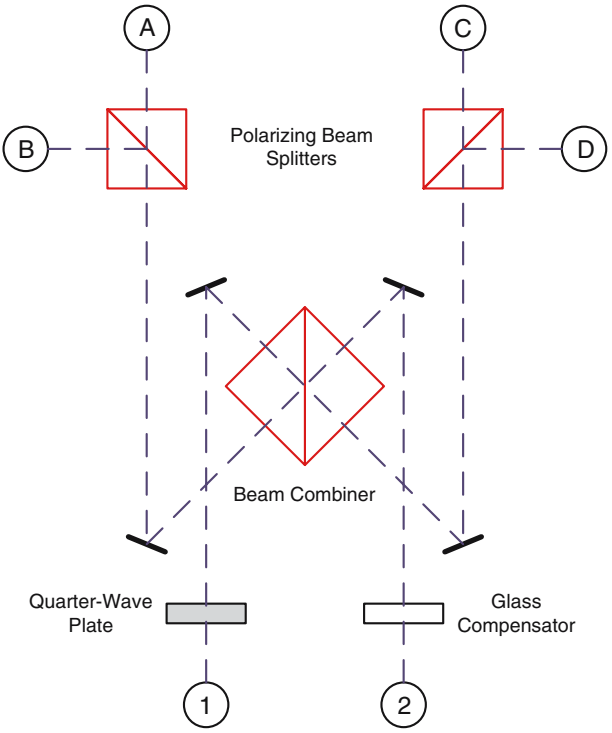

Fig. 27 Sketch of a four-output beam combiner. An external fringe tracker stabilizes the pathlength difference between the beams from two telescopes, which are relayed to the inputs at the bottom of the figure. The quarter-wave plate produces an achromatic $\pi/2$ phase shift between the two polarization states in one beam. The beams from both telescopes are combined at the main beam combiner; light emanating from the right-hand side of the beam combiner is shifted by π with respect to the left side. The two polarizations in each arm are separated by polarizing beam splitters, and the four outputs coupled into fibres for relay to detectors or spectrograph inputs. The phases in the four outputs A, B, C, and D are shifted by 0, $\pi/2$, π, and $3\pi/2$, respectively

and $D(\lambda)$ carried in the four output beams of the beam combiner. These can be routed to a spectrograph with optical fibres.[25]

In the case of the VLTI, one could take advantage of the instrument UVES/FLAMES, which already has a fibre feed for multi-object spectroscopy (Pasquini et al. 2003). This instrument provides a resolution of $\approx 60{,}000$ when a fibre with core diameter of 70 μm is chosen. The required fibre length for coupling UVES to the VLTI is ~ 150 m; fibres of this length and of the type used for the multi-object FLAMES link have a transmission $\geq 80\,\%$ over the wavelength range from 0.6 to 1 μm. The interface between the fibres and the spectrograph could be very similar to that of FLAMES. A similar setup would be possible for the infrared high-resolution spectrograph CRIRES in the

[25] Note that the pathlength of the optical fibre is irrelevant, because it is located after the beam combiner. Consequently, there is no need to use a single-mode fibre; multi-mode fibres will do just as well.

J and H bands, or for other interferometers that are co-located with an observatory at which high-resolution optical or near-infrared spectroscopy is performed.

3.5.3 Kilometric optical interferometer

The present generation of interferometers provide baselines up to ~ 400 m, and thus an angular resolution of a few mas in the near-IR; consisting of two to six telescopes, they provide only limited coverage of the (u, v) plane (see Sect. 3.3). A number of authors (e.g. Ridgway and Roddier 2000; Arnold et al. 2002; Quirrenbach 2004b; Lardière et al. 2007) have discussed concepts for a potential future interferometer array with much better sensitivity, higher angular resolution and much-improved imaging capabilities. A preliminary science case and an assessment of the key enabling technologies for such a kilometric optical interferometer (KOI) have been compiled by Surdej et al. (2005, 2006).

With baselines up to $\mathcal{B} = 10$ km in length and operating at wavelengths down to $\lambda = 0.5\,\mu$m, KOI would deliver images with 10 μas resolution, two orders of magnitude better than any other telescope contemplated at the moment. Combined with a sensitivity (for compact objects) that equals or surpasses present-day large monolithic telescopes, this spectacular angular resolution enables a wealth of completely new observing programmes, including:

- Imaging of Jupiter-size objects (e.g. brown dwarfs) at a distance of ~ 10 pc;
- High-quality imaging of stellar surfaces;
- Asteroseismology based on modes of higher degree;
- Detailed imaging of young stellar objects and pre-main-sequence disks;
- Studies of many types of binary systems;
- Baade-Wesselink distances of pulsating stars, novae and supernovae;
- Dynamics of dense clusters;
- Orbits of stars orbiting the black holes in the centers of nearby galaxies;
- Detailed imaging and imaging spectroscopy of broad-line regions in active galactic nuclei;
- Geometric distances of quasars through reverberation mapping; and
- Resolving the afterglows of gamma-ray bursts.

In the present context it is particularly interesting that observations of solar-like oscillations with degree as high as 60 would allow inversion to infer the structure and rotation of the radiative interior and lower part of the convection zone in a star like the Sun, including the rotational transition layer at the base of the convection zone which is likely crucial for the operation of the solar dynamo (e.g. Thompson et al. 2003). The above are just a few examples of what an interferometer with kilometric baselines could do; many other topics of current interest could be addressed as well.

A specific example of the concepts mentioned is an interferometric array with 27 telescopes and baselines of up to 10 km, as presented by Quirrenbach (2004b) and summarized in Table 3. Such an array could probably be built today with existing technologies, but the cost would be prohibitively high. However, advances in telescope building as needed for the construction of extremely large telescopes with 30–42 m

Table 3 Summary of strawman parameters and characteristics for an interferometer with kilometric baselines. For more details, see Quirrenbach (2004b)

Parameter	Value	Comment
Number of telescopes	27	Needed for snapshot imaging
Telescope phasing	Autonomous	Adaptive optics, laser guide stars
Array co-phasing	External	Dual-star operation
Sky coverage	$\gtrsim 10\%$	At R band, near Galactic pole
Telescope diameter	8–10 m	Needed to get sky coverage
Efficiency	25%	To limit telescope size
Wavelength range	$0.5-20\,\mu$m	Could be reduced to $0.5-2.2\,\mu$m

diameter, and improvements in optical fibre technology, could make a next-generation interferometric facility affordable within the next decade.

4 The interferometry–asteroseismology connection

Some of the major limitations currently faced in asteroseismic studies have been highlighted at the end of Sect. 2. These include the large uncertainties associated with the determination of global parameters of pulsating stars and the difficulties in identifying the modes of oscillation, particularly in classical pulsators. In the present section we address these issues further, emphasizing the unique role that interferometry can play in finding ways to overcome the aforementioned limitations. We review the first attempts ever made to combine asteroseismic and interferometric data in studies of particular pulsators. Moreover, we briefly look at current plans to study additional pulsating stars for which seismic and interferometric data are expected to be available in the near future.

4.1 Improving the determination of global parameters of pulsating stars

There are different ways in which interferometry may help in reducing the uncertainties associated with the determination of global parameters of pulsating stars, hence in helping constrain the models that are to be used in asteroseismic studies. Besides the direct measurement of the angular diameter of bright stars in the solar neighbourhood, for which accurate parallaxes are also available, interferometry can put constraints on the mass and distance of pulsating stars that are members of binary systems. Moreover, the determination of radii of stars in the solar neighbourhood, through the combination of interferometric and astrometric data, will allow us to test for the presence of systematic uncertainties in the determination of global parameters through other methods, such as high-resolution spectroscopy or multicolour photometry. In this way, the interferometric estimates can provide us with new calibrations that may subsequently be used to reduce the uncertainties in the values of global parameters of pulsating stars that are not within reach of current interferometric instruments.

4.1.1 Impact of having an interferometric measurement for the radius

The radius of a star, derived from the combination of its angular diameter and parallax, provides an additional observational constraint that can be used in the fitting procedure described in Sect. 2.4.4. However, it remains to be seen whether adding this interferometric constraint will improve in any significant way the results of the fitting. The question of whether the uncertainties in the fitted model parameters are expected to be reduced by the addition of the interferometric constraint, and, in particular, of which model parameters will benefit most from this addition, was recently addressed by Creevey et al. (2007).

Let us suppose that we have a set of classical and seismic observables, with associated measurement errors, and that we want to determine, through direct fitting, a set of model input parameters with corresponding uncertainties. The impact of including the observable *radius* on the determination of each of the model parameters can be studied through the *Singular Value Decomposition* of the derivative matrix, i.e., the matrix containing the derivatives of the observables with respect to the model input parameters, divided by the measurement errors (Press et al. 1986). As discussed by Brown et al. (1994), and emphasized by Creevey et al. (2007), the role that a given observable plays in the determination of the parameter solution depends crucially on the combination of observables used in the fitting and on the corresponding measurement errors. The *significance* S_i of an observable O_i can be quantified from this analysis as a measure of the extent to which a $1-\sigma$ change in O_i shifts the inferred parameters towards the $1-\sigma$ error ellipsoid in the parameter space (see Brown et al. 1994, for details). We consider the case where the set of observables includes spectroscopic, photometric and various combinations of seismic measurements for a solar-like star. Figure 28 shows the significance of each observable for the determination of the parameter solution in this case. Clearly the radius measurement plays a significant role in the parameter determination, and is partially responsible for the low impact of adding simultaneously, the observables *visual magnitude*, V, and *surface gravity*, g.

According to the results of Creevey et al. (2007), the radius and the large separation play complementary roles in the determination of the model parameters. When the error in the radius increases, the consequent decrease of its significance is accompanied by an increase of the significance of the large separation. Likewise, an increase of the error in the large separation is accompanied by a decrease of its significance, and an increase of the significance of the radius.

Even though Fig. 28 shows that a precise measurement of the stellar radius can have a significant impact on the determination of the model input parameters, it does not tell us which parameters this measurement benefits the most. In this respect, the study mentioned above indicates that a measurement of the radius will have a particularly strong impact on the determination of the model mass. The upper panel of Fig. 29 illustrates how the uncertainty in the mass determination depends on the radius error, for different sets of observables. When the error in the radius drops below 3%, all curves, except for the one with the squares, converge. Since these curves show the results when different sets of seismic observables are included (different symbols), and for different errors in the seismic data (different tones), the fact that they converge

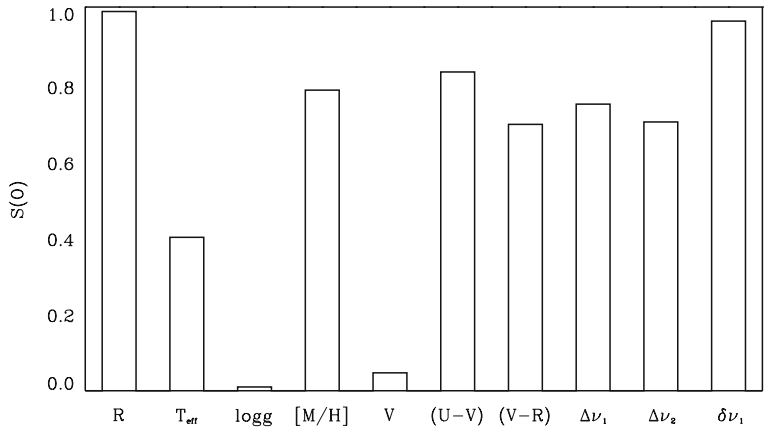

Fig. 28 Relative significance, S, of each of the individual observables, O, for the determination of the model parameters (see Brown et al. 1994, for the mathematical definition of S). A larger value of S implies that the observable has an overall stronger impact on the determination of the parameter solution. The observables are, from left to right, the radius, the effective temperature, the logarithm of surface gravity, the surface metallicity, the visual magnitude, the magnitude difference in the U and V bands and in the V and R bands, the large separations for two pairs of modes, both with degree $l = 0$, and one small separation between modes of $l = 0$ and 2. The analysis assumed errors of $0.01 R_\odot$ in R, 50 K in $T_{\rm eff}$, 0.3 in $\log g$, 0.05 in [M/H] and V, 0.005 in $(U - V)$ and $(V - R)$ and 1.3 μHz in the oscillation frequencies. From Creevey et al. (2007) with permission

when the error in the radius gets sufficiently small indicates that in this case it is mostly the error in the radius that defines the uncertainty in the model mass.

The curve with squares, obtained by including individual frequencies in the set of observables, shows the only case in which the seismic data can impact substantially on the mass determination, even when the error in the radius is below 3%. Unfortunately, as mentioned in Sect. 2, the poor modelling of the outer layers of solar-like stars results in significant systematic errors in the computation of model oscillation frequencies. Thus, using combinations of frequencies that are less subject to the systematic errors may be a better option; full use of the last case considered in Fig. 29 requires procedures for correcting for the near-surface errors. Once the mass is determined with sufficient precision, the individual frequencies can provide a powerful tool to distinguish between different possible solutions and, eventually, provide detailed diagnostics of the properties of stellar interiors.

The lower panel of Fig. 29 illustrates the importance of using a direct measurement of the radius, rather than an observable such as the absolute magnitude, for the mass determination. If the radius is not included in the set of observables, then, even when the errors in the visual magnitude and in the effective temperature are both small, the uncertainty in the mass determination remains large.

To test the results for the theoretical uncertainties discussed above, Creevey et al. (2007) also performed simulations of observations and attempted to recover the true input parameters in an automatic fashion. All the model parameters were recovered to within a $1 - \sigma$ standard deviation. According to their results, reaching 0.1–3.0% error in the radius, allows for the determination of the mass to within 1.0–4.0%. The

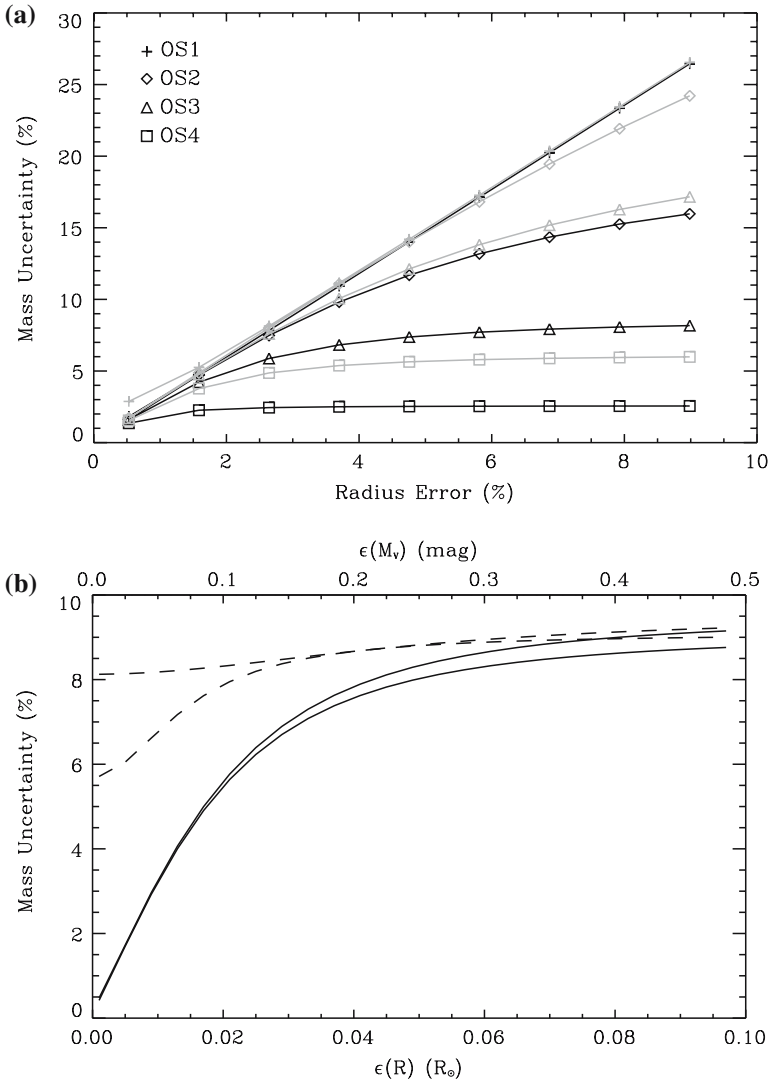

Fig. 29 *Upper panel* Theoretical uncertainty in the mass as a function of the error in the radius, for different combinations of observables. All sets of observables include measurements of the radius, effective temperature and metallicity; apart from radius and frequencies the errors in the observables are as in Fig. 28. Moreover, the set of observables includes: $\langle \Delta\nu \rangle$ and $\langle \delta\nu \rangle$ (*crosses*), a range of $\Delta\nu_{nl}$ (*diamonds*), an additional five small frequency separations (*triangles*) and individual frequencies (*squares*). *Dark lines* show the results when the error in the frequencies is $\epsilon(\nu) = 0.5$ μHz, while the grey are for $\epsilon(\nu) = 1.3$ μHz. *Lower panel* Theoretical uncertainty in the mass as a function of the error in the radius (*full lines*, lower abscissa) as compared with the mass uncertainties as function of the error in the absolute magnitude (*dashed lines*, upper abscissa), when the latter is used as an observable instead of the radius. From Creevey et al. (2007) with permission

simulation results show similar qualitative trends to the theoretical trends, but for errors in the radius larger than 3% all the results were quantitatively better than those shown in Fig. 29.

4.1.2 Asteroseismic targets within reach of interferometric measurements

As discussed in Sect. 3, long baseline interferometry can provide very precise measurements of the angular size θ of stars in the solar neighbourhood. Moreover, the combination of the latter with precise measurements of the trigonometric parallaxes π, through Eq. (61), provides the linear diameters D of the corresponding stars, in terms of the solar value $D_\odot$.

Naturally, the overall impact of interferometric determinations of stellar radii on our understanding of stellar structure and evolution depends on the number of stars for which a high-precision estimate of D can be achieved. To assess that impact, in the following paragraphs we estimate the number of stars for which both precise interferometric angular size *and* trigonometric parallax can be measured.

Following the classical example of requiring a 3% relative accuracy on the radius of a star for it to be useful in constraining stellar structure models (cf. Sect. 4.1.1 see also, e.g. Andersen 1991), we set a 3% relative uncertainty requirement on the linear diameter. This translates into a relative uncertainty of about 2% for both the angular diameter and the parallax, given that they play a symmetrical role in Eq. (61). For peculiar stars with poorly understood physics it may be useful to relax this requirement to several more per cent, but our estimate of the impact is focussed on normal stars.

To adopt a realistic approach, we consider the *proven* capabilities of the infrared single-mode interferometric instruments FLUOR and VINCI (Kervella et al. 2003a). They represent the state of the art in terms of measurement precision, with a typical relative uncertainty on fringe visibility $\mathcal{V}_{\rm obj}$ of $\sigma_{\mathcal{V}^2_{\rm obj}} = \delta\mathcal{V}^2_{\rm obj}/\mathcal{V}^2_{\rm obj} \simeq 1\%$ for less than 10 min of observing time. To relate this uncertainty with the one for the angular diameter, $\sigma_\theta = \delta\theta/\theta$, we define the amplification factor $A_{\rm f}$

$$A_{\rm f} = \left[\delta\mathcal{V}^2_{\rm obj}/\mathcal{V}^2_{\rm obj}\right] / \left[\delta\theta/\theta\right], \tag{71}$$

from which we find

$$\sigma_\theta = \sigma_{\mathcal{V}^2_{\rm obj}}/|A_{\rm f}|. \tag{72}$$

We recall that the visibility $\mathcal{V}_{\rm obj}$ is a function of the interferometric baseline length, $\mathcal{B}$, and of the wavelength, λ, at which the observations are carried out.

In order to determine the smallest angular diameter that can still be measured with low enough relative uncertainty, we consider the longest possible baseline of the VLTI (Glindemann et al. 2004), that is, $\mathcal{B} = 202\,$m. For the wavelength, we consider the H band ($\langle\lambda\rangle = 1.64\,\mu$m) which is accessible by using the AMBER (Petrov et al. 2003) instrument on the VLTI. This setup ($\mathcal{B} = 202\,$m, $\lambda = 1.64\,\mu$m) is almost equivalent to the usage of the maximum baseline of $\mathcal{B} = 330\,$m at which the CHARA Array can operate equipped with the FLUOR instrument working in the K band at $\lambda = 2.2\,\mu$m (ten Brummelaar et al. 2003). For the VLTI-AMBER H band configuration and the 1% visibility relative uncertainty adopted here, the amplification

factor criterion $|A_f| > 0.5$ gives a minimum requirement on the angular diameter of $\theta > 0.52$ mas.

For the parallax, we have considered the values listed in the *Hipparcos* catalogue (Perryman et al. 1997). While this catalogue generally gives the best estimate for nearby moderately cool to moderately hot stars, this is not always the case for the very late-type red dwarfs beyond M2V and for the hottest OB stars. However, we choose not to consider them in the present discussion. Dwarfs beyond M2V are in most cases too small to be within reach of accurate angular diameter measurements while there are hardly any massive OB stars within the close solar vicinity. Typically, the *Hipparcos* parallaxes of the considered stellar sample, excluding the coolest and hottest dwarfs, have errors $\simeq 0.9$ mas. This sets a limit of $\pi > 45$ mas, i.e., $d < 22$ pc to fulfill the uncertainty requirements. We selected all the stars in the *Hipparcos* catalogue fulfilling this criterion and found a total of 1,196.

To determine the number of stars that satisfy both criteria derived above, i.e. $\theta > 0.52$ mas and $\pi > 45$ mas, we have to estimate the angular diameter of all *Hipparcos* stars within a distance of 22 pc. To accomplish this, we used broadband photometry and the surface brightness relations calibrated by Kervella et al. (2004c). In particular, we used their relation

$$\log \theta_{\rm LD} = 0.2752\,(V - K) + 0.5178 - 0.2V, \tag{73}$$

where $\theta_{\rm LD}$ is the limb-darkened angular diameter (in mas), V is the visual magnitude (V band) and K the infrared one (K band). We extracted the visual and infrared photometry from the *Hipparcos* and 2MASS (Cutri et al. 2003) catalogues, respectively. Interstellar reddening can be neglected for such nearby stars, so the result of our computation is a list of angular diameters for all 1,196 stars in our sample. These angular diameters are then used to compute the relative uncertainties σ_θ using the amplification factor A_f defined above. The relative uncertainty of the *Hipparcos* parallax σ_π is subsequently used to estimate the total relative uncertainty on the linear radius through the relation $\sigma_R \approx \sqrt{\sigma_\theta^2 + \sigma_\pi^2}$. In some cases, the interferometer can fully resolve the star and measure its limb darkening. In those cases, the angular diameters can in principle be measured with very high accuracy and we set $\sigma_\theta = 0$.

The result of this selection is that the radii of $\simeq 450$ stars can be derived with a relative uncertainty smaller than 3%. Their positions in the Hertzsprung-Russell (M_V, $V - K$) diagram are presented in Fig. 30. Decreasing the radius relative uncertainty to 1% results in a sample of 77 stars, well spread over the main sequence. The 19 stars whose radius can in principle be obtained within 0.5% relative uncertainty are listed in Table 4. As a remark, the best radius estimates to date ($\simeq 0.2\%$) have been obtained on α Cen A and B by Kervella et al. (2003b) and by Bigot et al. (2006) on α Cen B.

Overall, it appears that the linear radii of a broad variety of dwarfs can be derived with good to excellent precision using a combination of interferometry and trigonometric parallaxes. These stars cover the main sequence from A0V down to M4V (with the addition of *Proxima Centauri*, M5.5V). A few tens of giants and subgiants are also within reach, mostly in the G-K spectral range. Among the measurable hot dwarfs,

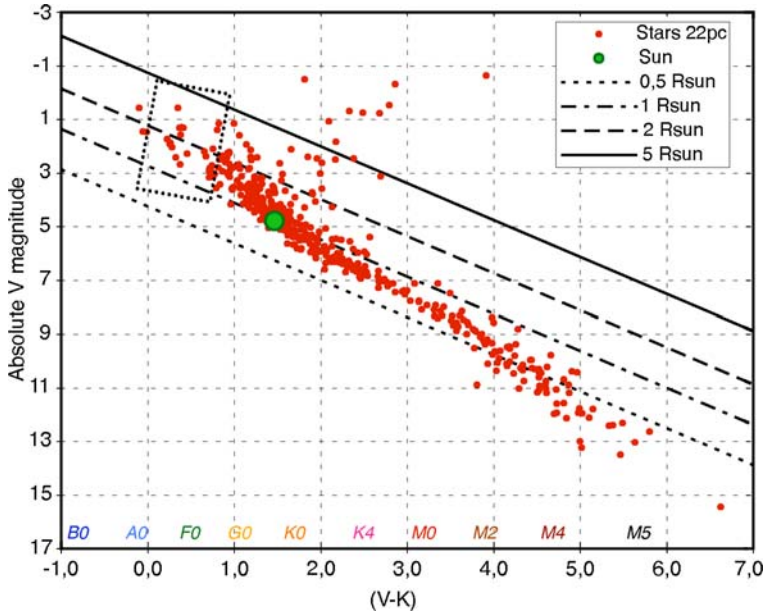

Fig. 30 Positions in the HR diagram of the stars within 22 pc accessible to a linear radius measurement with a total relative uncertainty below 3% through a combination of interferometric angular diameter and *Hipparcos* parallax. The *diagonal lines* are radius isocontours, and the *shaded box* on the *left* is the lower part of the classical instability strip

many are known to be fast rotators (e.g. Altair and Vega), and the geometrical deformation of their photospheres can be measured using different baseline orientations and/or closure phase measurements (Domiciano de Souza et al. 2003).

Currently, the main factor preventing a higher number of stars from being resolved by interferometry is the interferometric baseline length. However, even with an infinitely long baseline, only $\simeq$ 800 stellar radii would be measurable with a relative uncertainty smaller than 3%, due to the uncertainty in the *Hipparcos* parallaxes. In many cases, the parallax is by far the limiting factor in the radius estimation. In particular, the CoRoT targets are currently outside the 3% accessible domain as defined above, due to large uncertainties associated with their parallax determinations. Measuring accurate parallaxes of bright and nearby stars thus appears to be the key to increasing the precision of stellar radius estimates. One of the central goals of *Gaia*, an ESA mission with expected launch in 2011, is the determination of accurate positions of a large number of stars in our galaxy. As a consequence, major improvements are expected in this context in a not too distant future.

4.1.3 Interferometry of binary stars

Even though a number of stars in the classical instability strip are found to be within reach of interferometric measurements, hardly any of the well-established classical pulsators with precise parallax determinations satisfy that condition. Naturally, new

Table 4 List of the nearby stars whose linear radius is measurable with a relative uncertainty σ_R below 0.5%

Name	Sp. type	$\sigma_\pi(\%)$	$\sigma_\theta(\%)$	$\sigma_R(\%)$
α Cen A	G2V	0.19	LD	0.19
α Cen B	K1V	0.19	LD	0.19
ϵ Ind	K5V	0.25	LD	0.25
61 Cyg B	K7V	0.25	0.08	0.27
GJ 411	M2V	0.23	0.13	0.26
ϵ Eri	K2V	0.27	LD	0.27
τ Cet	G8V	0.29	LD	0.29
Procyon A	F5IV-V	0.31	LD	0.31
GJ 887	M2/M3V	0.29	0.18	0.34
η Cas A	G0V SB	0.37	LD	0.37
δ Pav	G5IV-Vvar	0.40	LD	0.40
82 Eri	G8V	0.33	0.23	0.40
GJ 380	K5V	0.39	0.11	0.41
σ Dra	K0V	0.27	0.30	0.40
χ Dra A	F7Vvar	0.39	0.14	0.41
Sirius	A0m	0.42	LD	0.42
Vega	A0Vvar	0.43	LD	0.43
AX Mic	M1/M2V	0.45	0.15	0.47
Altair	A7IV-V	0.48	LD	0.48

"LD" in the σ_θ (relative error on the angular diameter) column designates the stars that are fully resolved by the AMBER-VLTI instrument in the H band, and that are therefore accessible to limb darkening measurements

bright classical pulsators might be discovered from space photometry assembled by missions such as WIRE and MOST. A nice such example is the bright star Altair which was found to be a δ Scuti star from the analysis of WIRE white-light photometry (Buzasi et al. 2005). Unfortunately, despite the small relative uncertainty in its parallax, which is below 0.5%, rapid rotation, between 70 and 90% of its critical velocity, and the lack of mode identification, limit considerably the seismic modelling of this star (Suárez et al. 2005).

Given the small number of known classical pulsators within reach of interferometric measurements, the major contribution of interferometry to asteroseismic studies of this type of pulsators will most likely come from the observation of binaries with a pulsating component. As mentioned in Sect. 2 the binarity can be an asset for asteroseismology because it in principle allows for a reduction of the observational error box associated with the fundamental parameters of the components. Quite a number of bright classical pulsators are found among spectroscopic binaries see, e.g. Pigulski 2006, for a recent review). This is particularly the case for the pulsating B stars (for overviews, see De Cat et al. 2000; Aerts and De Cat 2003), but also for δ Scuti stars, as, e.g. θ^2 Tau (Kennelly et al. 1996b) and γ Doradus stars (De Cat et al. 2006).

Historically, *visual binaries* were first recognized, due to their proximity on the sky and their relative orbital motion. Even though Kepler's third law ties the size and period of the orbit with the sum of the masses of the two components, the angular

nature of the observations prevents that sum from being accessible unless the distance to the system is known.

As a consequence of the improvement of the observation techniques, the two stars are no longer required to be seen for an orbit to be derived. For instance, astrometric binaries are double stars where one component is often too faint to be detected but its mass disturbs the space trajectory of the primary, causing a periodic astrometric wobble around the trajectory of a genuine single star. Although the distance is known in such cases, only the absolute size of the primary orbit is accessible, thus limiting again the use of Kepler's third law.

Switching to interferometry does not really help for the cases of visual or astrometric binaries. While an interferometer greatly improves the resolving power, the relative angular positions suffer the same limitations as the old micrometric visual data. They yield the angular size of the relative orbit which can only be changed into the mass sum if the distance to the system is known.

Spectroscopy, especially radial velocities, offers a valuable alternative to positional astronomy. Unlike visual binaries, *spectroscopic* ones are not distance limited in the sense that the binary signature does not deteriorate with the distance to the system. Another advantage is that, in case of double-lined systems, the mass ratio is directly available. Unfortunately, the size of the orbit is entangled with the orbital inclination which prevents derivation of the sum of masses and, therefore, the individual masses.

Even though an adjective—visual or spectroscopic—often describes how a binary was detected, the observation methods often overlap after the discovery. Thanks to the improvement of both spectroscopy towards small radial velocity amplitudes and interferometry towards close binaries, the overlap has expanded substantially over the past 20 years. Whereas none of the above types of binaries makes the distance or individual masses available, resolving spectroscopically and visually the components of a binary yields both the individual masses and the distance to the system, the latter through the computation of the so-called *dynamical parallax*. This leads to hypothesis-free stellar masses and distances and provides the desired constraints on the error box. A catalogue of spectroscopic binary orbits is available in, e.g. Pourbaix et al. (2004) and provides a list of candidates for further interferometric observations (McAlister 1976).

In order for the binarity to be of help in asteroseismology, we need to be able to determine the stellar masses with a relative uncertainty of at most a few percent. In order to achieve that, interferometric data must be accompanied by accurate spectroscopy. Many meanwhile interferometrically resolved binaries still have only 50+ years old spectroscopic orbits. It is also worth realizing that recent precise radial velocities do not per se lead to accurate spectroscopic orbit determination. As shown for α Cen (Dravins and Nordlund 1990a, b; Pourbaix et al. 2002), the systematic shift in radial velocities caused by, for instance, the gravitational redshift and the convective blueshift, can largely exceed the quoted precision of the measurements. Such systematic effects can only be quantified well from a full coverage of the orbit. It is therefore wise to select binaries whose period is sufficiently short for the orbit to be covered at least once with one and the same instrument. Although this condition on the period decreases the likelihood of being able to resolve the binary interferometrically, it does not make

the task impossible, as seen from the studies of, e.g. Capella (Bagnuolo and Hartkopf 1989) and Atlas (Zwahlen et al. 2004). However, it does require long-term monitoring.

For massive binaries with classical pulsators, the requirement of a few percent precision on the masses is very stringent. Improvements in the component masses, through the determination of the dynamical parallax from the combination of high-precision spectroscopy covering the orbit and interferometric data, were achieved for the δ Scuti star θ^2 Tau (Tomkin et al. 1995), and for the β Cephei stars β Cen (Ausseloos et al. 2006) and λ Sco (Tango et al. 2006). The hypothesis-free masses of these stars are, however, not yet precise enough to be of sufficient help in the seismic modelling (see also Sect. 5).

4.1.4 Indirect impact on global parameter determination

In the absence of a direct measurement of the stellar radius, a combination of the star's luminosity and effective temperature is often used to derive a value for the radius. However, classical methods used to derive the effective temperature, such as multi-band photometry and spectroscopy, either rely on calibrations or on atmospheric models. Consequently, the effective temperatures commonly used to place the stars in the HR diagram, and thus to constrain their seismic analysis, are often subject to systematic errors which can only be tested for, and hopefully corrected, when independent measurements of the same quantities are available.

Interferometry is expected to play an important role in this context. The determination of the angular radii allows new determinations of the effective temperature of these stars that can be used to test for the presence of systematic errors in the values derived when using other techniques. Even though to some degree the new effective temperature determinations may also depend on atmospheric models, since a bolometric correction has to be applied to determine the bolometric flux of the star, one might expect that the extra information gained by the direct measurement of the angular diameter of the star will make the two measurements largely independent of each other, hence allowing us to test for systematic errors.

The new, interferometric based, determinations of the effective temperatures of nearby stars will also allow us to test and improve the calibrations that are commonly used in the photometric determination of effective temperatures of stars for which no spectroscopic data are available. The improvement of these calibrations is of particular importance when studying pulsators among peculiar stars and low-metalicity stars. The uncertainty in the effective temperature determinations for these stars can easily exceed 200 K. However, their study is tremendously important, as they provide different environments in which models of stellar interiors and of stellar atmospheres can be tested.

In roAp stars, for instance, the emission is so anomalous, with heavy line blanketing in the ultraviolet and consequent redistribution of the flux over larger wavelengths (Leckrone 1973), that the photometric calibrations used for normal stars cannot be relied upon when studying them. Often, the values for the effective temperature of these stars derived from different methods do not agree within their formal errors, which is a clear indication that some form of systematic or calibration error is present. A convincing indication that systematic errors are likely to be present in the values

available for the effective temperatures of roAp stars is given by Matthews et al. (1999). In their work, the authors found that the parallaxes predicted from asteroseismic data of roAp stars are systematically larger than the parallaxes determined by *Hipparcos* for the same stars. This result was corroborated by the work of Cunha et al. (2003) in which the authors have tried, without success, to bring the seismic and astrometric data for one of the roAp stars in the sample into agreement, by exploring a grid of models with different physics and chemical composition. Unfortunately, the number of potential roAp stars that may be resolved by current interferometric instruments is very small. Nevertheless, new values for the effective temperature of only a few of these stars, derived from their angular diameters, could have a strong impact on the seismic study of the whole class.

The potential of interferometry to improve indirectly global parameter determination of stellar pulsators goes even beyond the detection of systematic errors in classical methods or the possibility of deriving new, more adequate calibrations. In fact, the stellar limb darkening measured by the modern interferometric instruments is sufficiently accurate to be used as diagnostics on the stellar outer layers, in particular on the temperature profiles. These, in turn, put direct constraints on atmospheric models. To take advantage of the instrumental performance of the interferometers, a similar effort in numerical modelling of stellar atmospheres has to be done. In particular, the standard 1D hydrostatic models of atmospheres such as ATLAS (Kurucz 1992) or Phoenix (Hauschildt et al. 1999) have to be improved. Indeed, these models are based on very limiting assumptions. Even if the temperature structure in the 1D codes can always be calibrated by a judicious choice in the free parameters (e.g. mixing length), it can never reproduce the temperature profile in the transition (surface) region since the coupling between radiation and gas dynamics is essential there. On the contrary, 3D radiative hydrodynamical models initiated two decades ago by Å. Nordlund, R. Stein and co-workers to model the solar convective surface (Nordlund 1982; Stein and Nordlund 1989, 1998) do not suffer from these unrealistic physical hypotheses. They solve the complete set of hydrodynamical equations coupled with radiative transfer with realistic equations-of-state and opacities to obtain 3D, time-dependent, inhomogeneous models of stellar atmospheres. The realism of these simulations is now such that they can reproduce almost perfectly solar and stellar line profiles (for both shifts and asymmetries, e.g. Asplund et al. 2000, for FeI lines) and provide reasonable modelling of aspects of solar envelope structure and acoustic oscillations (e.g. Rosenthal et al. 1999) and granulation (e.g. Stein and Nordlund 1989; Nordlund and Stein 1991; Trampedach et al. 1998; Svensson and Ludwig 2005).

The use of these 3D radiative hydrodynamical codes in the context of interferometry has been proposed recently by Aufdenberg et al. (2005) for Procyon, and by Bigot et al. (2006) for the K-dwarf α Cen B for which new visibility measurements were obtained with VINCI/VLTI. There are significant differences between the structures of the atmosphere obtained by 1D and 3D radiative hydrodynamical approaches, especially for stars with not-so-late spectral type (such as F stars) and for metal poor stars. The amplitude and position of the second and higher order lobes of visibility are very sensitive to the limb darkening and therefore to the temperature structure of the atmosphere, which provides then strong constraints on the models. The importance of such accurate limb darkening measurements forces us to prepare a grid of stellar

3D limb darkening model descriptions, similar to the limb darkening laws produced by Claret (2000) using Kurucz's grid of 1D atmospheres, covering the whole HR diagram with solar and low metallicities. Such a grid is necessary to prepare and exploit future interferometric angular diameter measurements. Moreover, these 3D radiative hydrodynamical approaches have to be used for deriving other fundamental parameters of the stars as well, such as the surface gravity and the abundances combined with a non-local thermodynamic equilibrium treatment of the line transfer (Thévenin and Idiart 1999). An interesting, if controversial, aspect of the 3D modelling is its application to the determination of solar abundances, yielding abundances of carbon, nitrogen and particularly oxygen well below the previously assumed values (for a review, see Asplund 2005). Models computed with these abundances are in stark disagreement with the results of helioseismology (e.g. Turck-Chièze et al. 2004; Antia and Basu 2005; Bahcall et al. 2006; Basu et al. 2007), and no obvious solution to this difficulty has yet been found (Guzik 2006).

A promising recent development has been the modelling of rather larger parts of the solar convection zone (Stein et al. 2006), covering supergranular scales and a somewhat deeper region and hence potentially more realistic models of solar oscillations. Similar results can be expected for other stars in the foreseeable future. When combined with asteroseismic diagnostics from mode excitation and frequency shifts (cf. Sect. 2.3.2) we can finally expect a reliable treatment of the near-surface regions.

4.2 Mode identification

As mentioned earlier, for asteroseismology to reach its full potential, it is not only necessary to measure the oscillation frequencies. It is also necessary to identify the modes in terms of the number of radial nodes n, and the number and position of nodal lines over the surface, which is characterized by the spherical wavenumbers (l, m).

With sufficiently accurate measurements of the stellar effective temperature, luminosity and/or radius, and a mass inferred from fitting an evolutionary track, it is possible, in principle, to deduce expected oscillation frequency patterns. The large frequency separation is a special case of such a pattern for p-mode oscillations in the asymptotic frequency regime of slowly rotating stars. Similarly, period spacings can be used for g-mode oscillations in the asymptotic regime. Direct observational constraints on the separations may also become available whenever numerous oscillation modes are observed. According to Eq. (31), the ratio of a p-mode oscillation frequency, corrected for surface effects and for rotational splitting, and half of the large separation, should be an integer number approximately equal to $2n + l$. Hence, knowledge of the theoretically expected *or* observationally determined large separation reduces the likely range of appropriate values of l and n, for any measured oscillation frequency, to the combination $2n + l$. However, this still leaves considerable ambiguity in the mode identification and it assumes that rotation does not prohibit the selection of the central frequency peak of the rotationally split multiplets. This comfortable situation is seldom encountered, except perhaps in solar-like stars (see Sect. 4.3 for examples).

When only a limited number of modes is excited to observable amplitude, or when the modes do not follow particular frequency separations, or whenever a very dense

frequency spectrum is predicted, the frequency values alone are insufficient to derive the wavenumbers. In this case, one could in principle proceed with seismic modelling considering *all* values for (l, m, n) for any of the detected frequencies. In order to limit the computation time of such forward modelling, the values of the degree l are usually limited from the geometric arguments mentioned in Sect. 1.3. It is then customary to consider modes with $l \leq 3$ and to assume $m = 0$, when no obvious evidence for rotational splitting is found in the Fourier transform of the time series.

This procedure is not very satisfactory though, because rotation can easily result in non-equidistant splitting and imply merging of frequency multiplets in such a way that they cannot be unravelled. Moreover, quite a number of classical pulsators show evidence for modes with degree $l \geq 4$, while not showing evidence for modes of lower degree, which presumably are not excited to observable amplitudes. In these cases, the assumption of $m = 0$ is unjustified. The quest for *empirical mode identification* has therefore become an extended topic by itself in asteroseismology. With this term we mean the assignment of l and m values to each of the observed frequencies from the data themselves, without relying on the (unknown) details of the model properties of the star. It is usually impossible to obtain a correct mode identification for each detected oscillation frequency. However, even only one correct (l, m) identification, e.g. the one for the dominant mode, can imply a serious reduction of the free parameter space in the modelling and is therefore worthwhile to attempt.

Empirical mode identification is a tedious and sophisticated task. It requires a detailed confrontation between oscillation theory applied to the outer stellar atmosphere and observational characteristics, such the observed amplitudes and phases of light-curves, of radial–velocity curves or of line–profile variations. Essentially two types of diagnostics are in use to identify the modes. One of them is based on time series of multicolour photometry and the other one relies on time series of line–profile variations detectable from high-resolution spectroscopy.

4.2.1 Mode identification from multicolour photometry

The amplitude and phase behaviour of an oscillation mode can be markedly different when measured in different filters of a photometric system. These differences depend on the degree l of the mode and form the basis of a photometric mode identification method. Only the oscillation frequencies observed in all the filters are considered for mode identification. The idea is that the degree l of a given oscillation mode, whose frequency is detected in all the filters of the photometric system, may be derived from the comparison of the amplitude and phase values measured with different filters.

Different versions of this mode identification method are present in the literature. It was originally proposed by Stamford and Watson (1981), relying on the work by Dziembowski (1977) and Balona and Stobie (1979). Subsequently, Watson (1988) improved the method by bringing it into applicable form, while Heynderickx et al. (1994) included the perturbation of the limb darkening into it. For an extensive review of the method, we refer to Garrido (2000). All these versions are based on adiabatic oscillation theory, and treat the non-adiabaticity of the oscillatory behaviour in the outer atmosphere by means of an unknown ad-hoc parameter $R_{\rm nad}$ (usually denoted as $R \in$

[0, 1], although this is very confusing as it is the standard symbol for the stellar radius, hence our notation of $R_{\rm nad}$). The theoretical expressions for the amplitude and phase of the light curve in the different filters (i.e. as a function of wavelength) depend, among other things, on the geometrical configuration of the nodal lines with respect to the observer, i.e. on the values of (l, m, i), where i is the inclination angle between the axis of symmetry of the oscillation and the line-of-sight. The axis of symmetry of the oscillation is usually taken to be the rotation axis, except for the roAp stars where the magnetic axis is a more natural and hence better choice.

It was already realized by Stamford and Watson (1981) that the functional dependence of the amplitude and phase on the mode geometry allows one to group the m and i parameters into one single factor which is independent of wavelength. It is therefore possible to eliminate this factor, and with it the very disturbing and unknown inclination angle, by considering amplitude ratios and phase differences among the different filters. This is the procedure that is always adopted nowadays. The disadvantage is that the information on the m-value is lost and, consequently, only the degree l of the mode can be identified. The theoretical expressions for amplitude ratios and phase differences require the computation of the perturbed version of the adopted limb darkening law and of the perturbed stellar flux as a function of effective temperature and gravity. This brings us back to the need of good atmospheric models (see Sect. 4.1.4). In particular, it turns out that this identification method is rather sensitive to the adopted treatment of convection for stars with outer convection zones, such as δ Scuti and γ Doradus stars (Garrido 2000).

A big step forward was achieved with the new versions of the method developed by Brassard et al. (1995) for white dwarfs, by Balona and Evers (1999) for δ Scuti stars, and by Dupret et al. (2003) for all main-sequence oscillators. In these works, a non-adiabatic treatment of the oscillations in the outer atmosphere was included, with different levels of sophistication, through which the unknown ad-hoc factor $R_{\rm nad}$ was eliminated. Dupret et al. (2003) illustrated their method for β Cephei stars, slowly pulsating B stars, δ Scuti stars, and γ Doradus stars. The dependence on the adopted theory of convection remains for the latter two classes of pulsators. A non-adiabatic treatment similar to that of Dupret et al. (2003) was presented by Randall et al. (2005b) in the context of pulsating subdwarf B stars. However, the latter does not contain an equally detailed treatment of the oscillations in the outer atmosphere.

The theoretical amplitude ratios and phase differences are dependent on the stellar fluxes, which are determined by the radius, effective temperature and mass (or equivalently, the gravity) of the star. As discussed above, these parameters are often not known with high precision. Their uncertainties must be propagated into the final selection of the best value for l from the observed amplitude ratios. This was often ignored in the past, but is taken care of in modern applications of this method following Balona and Evers (1999). Examples of such applications are available in Handler et al. (2003, 2005, 2006); De Ridder et al. (2004) and Shobbrook et al. (2006) for β Cephei stars, in De Cat et al. (2005, 2007) for slowly pulsating B stars, in Dupret et al. (2005b, 2005c) for δ Scuti and γ Doradus stars, and, finally, in Jeffery et al. (2004, 2005) and Tremblay et al. (2006) for subdwarf B stars. We refer the reader to these papers for more detailed information.

4.2.2 Mode identification from line–profile variations

The introduction of high-resolution spectrographs with sensitive detectors in the 1980s, had a large impact on the field of empirical mode identification. Spectroscopic data indeed offer a very detailed picture of the pulsational velocity field. It remains a challenge to obtain spectra covering the overall beat period of the multiperiodic oscillations, with a high resolving power (typically above 40,000) and with a high signal-to-noise ratio (typically above 200 and preferably much higher than that), for a good temporal resolution (typically below a few percent) in the sense of the ratio of the integration time to the oscillation period. The latter condition is necessary in order to avoid smearing out of the oscillations during the cycle.

Methodology to derive the full details of the pulsational velocity field (at least six unknowns, see below) tends to be complex. For this reason, multicolour photometric observations, which can only lead to an estimate of the wavenumber l but which can be obtained from small telescopes, are still of utmost importance for mode identification. Such data are especially suitable for the study of long-period pulsations because small telescopes are available on longer time scales.

Each spectral line is subject to different broadening mechanisms, among which atomic broadening which is usually negligible, pressure broadening giving rise to a Lorentz profile and thermal broadening characterized by a Gaussian profile. These three mechanisms act on a microscopic scale and lead to a global time-independent broadening of the spectral line. This is why they are usually treated together by means of the so-called *intrinsic line–profile*, whose shape is the convolution of two Lorentz profiles and a Gaussian profile. This convolution results in a *Voigt profile*. In practice one tries to avoid having to use spectral lines that are sensitive to pressure broadening (such as the hydrogen lines) for mode identification because the oscillatory signal is much less visible in their wings compared with lines that are mainly thermally broadened. In the latter case, it is justified to assume a Gaussian for the intrinsic line broadening function. This is particularly justified for hot stars with low to moderate density.

Rotational broadening of the spectral lines is observed as being time independent as long as no surface inhomogeneities occur. Stellar oscillations, on the other hand, give rise to periodic broadening of the line–profiles. The shape of the line–profile is completely determined by the parameters occurring in the expression for the pulsation velocity which can be obtained from Eq. (6). In particular it is dependent on the wavenumbers (l, m) of all the oscillation modes.

The *Doppler effect* determines how much a spectral line centred at the wavelength λ_0 is broadened, according to:

$$\frac{\Delta\lambda}{\lambda_0} = \frac{v}{\tilde{c}}, \tag{74}$$

in which v is the component of the total velocity field $\mathbf{v}$ at the stellar surface in the line of sight and $\tilde{c}$ is the speed of light. The velocity vector $\mathbf{v}$ consists of a component due to the surface rotation and a component due to the oscillations. In the case of a constant rotation over the stellar surface, the rotational component $\mathbf{v}_{\rm rot}$ is easy to

derive and can be written in terms of the rotational frequency Ω, giving rise to the *equatorial rotational velocity* ΩR, and the inclination angle.

In the case of spheroidal modes in the approximation of a non-rotating star, the pulsation velocity expressed in a system of spherical coordinates (r, θ, φ) centred at the centre of the star and with polar axis along the axis of symmetry of pulsation, is given by:

$$\mathbf{v}_{\rm puls} = \left(v_r, v_\theta, v_\varphi\right) = N_l^m v_{\rm p} \left(1, K\frac{\partial}{\partial\theta}, \frac{K}{\sin\theta}\frac{\partial}{\partial\varphi}\right) Y_l^m(\theta,\varphi) \exp\left(-{\rm i}\omega t\right). \quad (75)$$

In this expression, N_l^m is a normalization factor for the $Y_l^m(\theta, \varphi)$, $v_{\rm p}$ is proportional to the pulsation amplitude, and K is the ratio of the horizontal to the vertical velocity amplitude. The latter can be found from the boundary conditions and turns out to be $K \simeq GM/(\omega^2 R^3)$ in the approximation of a non-rotating star (e.g. Unno et al. 1989).

In order to compute the line–profile shape, we have to determine the normalized flux at a particular wavelength (or velocity). Consider a system of spherical coordinates (r', θ', φ') with the polar axis coinciding with the direction to the observer. In order to compute the theoretical line profile, one subdivides the visible stellar surface into infinitesimal elements $({\theta'}_i, {\varphi'}_j)$, $i = 1, \ldots, N$; $j = 1, \ldots, M$ where N and M are typically 180 and 360, respectively, thanks to the present-day computational power. The velocity field due to the rotation and the pulsation leads to a Doppler shift at a point (R, θ', φ') on the visible equilibrium surface of the star. The local contribution of a point (R, θ', φ') to the line profile is proportional to the flux at that point. We assume that the intensity $I_\lambda(\theta', \varphi')$ is the same for all points of the considered surface element. The flux through the surface element surrounding the point (R, θ', φ') thus is the product of the intensity $I_\lambda(\theta', \varphi')$ and the projection on the line of sight of the surface element around the considered point:

$$I_\lambda(\theta', \varphi')\ R^2\ \sin\theta'\ \cos\theta'\ {\rm d}\theta'\ {\rm d}\varphi'. \quad (76)$$

An important effect that changes the flux over the visible surface is the limb darkening. For line–profile variation calculations, the linear approximation of the limb darkening law largely suffices, because the profile variations are dominated by the Doppler shifts due to the surface velocity. The flux of a surface element centred around the point $P(R, \theta', \varphi')$ of the equilibrium surface with size $R^2 \sin\theta'\, d\theta'\, d\varphi'$ then is

$$I_0\ h_\lambda(\theta')\ R^2\ \sin\theta'\ \cos\theta'\ {\rm d}\theta'\ {\rm d}\varphi', \quad (77)$$

where h_λ is the adopted limb darkening law and I_0 the intensity at $\theta = 0$. As discussed earlier, interferometry may play a role in improving our knowledge of h_λ and thus in the interpretation of line-profile variations.

Perturbations of the intensity and of the surface due to the oscillations change the line profile. Usually, however, these effects are far less important than the velocity effect for slowly rotating classical pulsators without surface inhomogeneities, and one therefore often assumes $\delta I_\lambda(\theta', \varphi') = 0$ during the oscillation cycle. However, one can easily generalize any line profile generation code to include the non-adiabatic

perturbation of the intensity, $\delta[I_0\, h_\lambda(\theta')]$, as well as the perturbed surface size of the elements due to the oscillation.

In order to take into account intrinsic broadening effects, the local line profile is convolved with an intrinsic profile, which, in the simplest approximation, is taken to be Gaussian with variance $\sigma_{\rm th}^2$, where $\sigma_{\rm th}^2$ depends on the spectral line considered. Generalizations to an intrinsic Voigt profile or a profile derived from a stellar atmosphere model are easily performed, but imply much longer computation times.

The time dependence of the temperature eigenfunction may be important for the computation of the intrinsic line profile when the spectral line is sensitive to small temperature variations. For this reason, one carefully selects the best spectral line for mode identification. It is advantageous to use an unblended, deep, thermally broadened line which is insensitive to small temperature changes in the line-forming region in the atmosphere (e.g. De Ridder et al. 2002). This choice thus depends on the spectral type of the star. For β Cephei stars, e.g. the best line is the Si III 4560 Å triplet (Aerts and De Cat 2003) while for slowly pulsating B stars the Si II 4130 Å doublet is ideally suited (Aerts et al. 1999). For very fast B-type rotators, these multiplet lines are unfortunately blended and one has little choice but to consider the isolated He I 6678Å line (e.g. Balona et al. 1999) or other helium lines (e.g. Rivinius et al. 2003). Temperature effects on line profile variations of δ Scuti and γ Doradus stars have not been studied carefully.

We represent by $p(\lambda)$ the line profile and by λ_{ij} the Doppler-corrected wavelength for a point on the star with coordinates (θ_i', φ_j'), i.e.

$$\frac{\lambda_{ij}-\lambda_0}{\lambda_0}=\frac{\lambda(\theta_i',\varphi_j')-\lambda_0}{\lambda_0}=\frac{\Delta\lambda(\theta_i',\varphi_j')}{\lambda_0}=\frac{v(\theta_i',\varphi_j')}{\tilde{c}}, \tag{78}$$

with $v(\theta_i', \varphi_j')$ the component of the sum of the pulsation and rotation velocity of the considered point in the line of sight. An explicit expression for $v(\theta_i', \varphi_j')$ can be found in, e.g. Aerts et al. (1992). The line profile is then given by

$$p(\lambda)=\sum_{i,j}\frac{I_0 h_\lambda(\theta_i')}{\sqrt{2\pi}\sigma}\exp\left(-\frac{(\lambda_{ij}-\lambda)^2}{2\sigma^2}\right)R^2\sin\theta_i'\cos\theta_i'\Delta\theta_i'\Delta\varphi_j', \tag{79}$$

where the sum is taken over the visible stellar surface ($\theta' \in [0°, 90°]$, $\varphi' \in [0°, 360°[$) and where we have assumed a constant Gaussian intrinsic profile and a non-variable surface normal for simplicity. As discussed above, this formula for the computation of line–profile variations should be generalized in order to take into account the following additional time-dependent effects: a variable surface normal, a variable flux through non-adiabatic temperature and gravity variations, a time-dependent intrinsic profile, Coriolis and centrifugal correction terms to the pulsation velocity expression. The most up-to-date line–profile generation codes take into account most of these effects, except for those due to the centrifugal force (e.g. Townsend 1997; Schrijvers et al. 1997; De Ridder et al. 2002; Zima 2006).

The principle of line–profile fitting as a mode identification method is obvious: one generates theoretical line–profiles (λ, $p(\lambda)$) over the oscillation cycle from Eqs. (78)

and (79), or their more sophisticated version including temperature and Coriolis effects, and one compares them with the observed ones to select the set of parameters that results in the closest resemblance to the data. In order to do this objectively, one must construct an atlas of theoretical profiles for different values of (l, m) and for realistic ranges of the the other line–profile parameters (velocity amplitude of each of the modes, rotation velocity, inclination angle and intrinsic profile width). This method is relatively easy and straightforward to apply to a monoperiodic oscillator. Whenever more than one mode is present, however, the method becomes unrealistic in computation time because one cannot scan a large enough parameter space. The latter has six dimensions for one mode and increases with three for any additional mode, in the approximation where one neglects temperature and Coriolis effects.

To overcome the computational obstacle of line–profile fitting, and to make the identification more objective, quantitative mode identification methods have been developed since the late 1980s. With each of these, one replaces the observed line–profile variations with carefully studied diagnostics derived from the data. One such method is based on the moment variations of the spectral lines and was first introduced Balona (1986a, b; 1987) and further developed by Aerts et al. (1992), Aerts (1996) and Briquet and Aerts (2003). This method relies on the mathematical property that the line profile is fully characterized by its first three velocity moments. The latest version of the moment method has been applied to many different types of classical pulsators. This method is very powerful for low-degree modes ($l \leq 4$) in slow rotators ($v \sin i \leq 50\,\mathrm{km\,s^{-1}}$).

A second method, which will be shown below to be more relevant in terms of the interplay with interferometry, was first introduced by Gies and Kullavanijaya (1988), and further developed by Kennelly et al. (1996a); Schrijvers et al. (1997); Mantegazza (2000) and Zima (2006). Its use is illustrated and explained in Fig. 31. It is based on the properties of the amplitude and phase distribution across the line profiles for each oscillation frequency and its harmonic. These properties are linked to the (l, m)-value of the mode, and to the inclination angle, as can be seen from Fig. 31.

The computation of the amplitude and phase behaviour across the profile is particularly suited to analyse line–profile variations due to high-degree ($l \geq 4$) modes in rapid rotators ($v \sin i \geq 50\,\mathrm{km\,s^{-1}}$), because we need a high resolving power within the lines to interpret small moving subfeatures. The method can also be applied to slow rotators with low-degree modes, however, when combined with the moment method (e.g. Telting et al. 1997). In contrast to the moment method, no rigorous mathematical derivation for the amplitude and phase variations across the profile as a function of l and m is available, despite efforts (e.g. Hao 1998). For this reason, Telting and Schrijvers (1998) performed an extensive Monte Carlo simulation study to exploit the method visualized in Fig. 31 in terms of mode identification for p modes, including effects of the Coriolis force in the velocity eigenfunction. From these simulations, they reached the following conclusions:

– There exists a strong correlation between the phase difference $\Delta\psi_0$ at the blue and red edge of the profile for the oscillation frequency ω and the degree of the mode. A good estimate of l is

$$l \approx (0.10 + 1.09\,|\Delta\psi_0|/\pi) \pm 1. \tag{80}$$

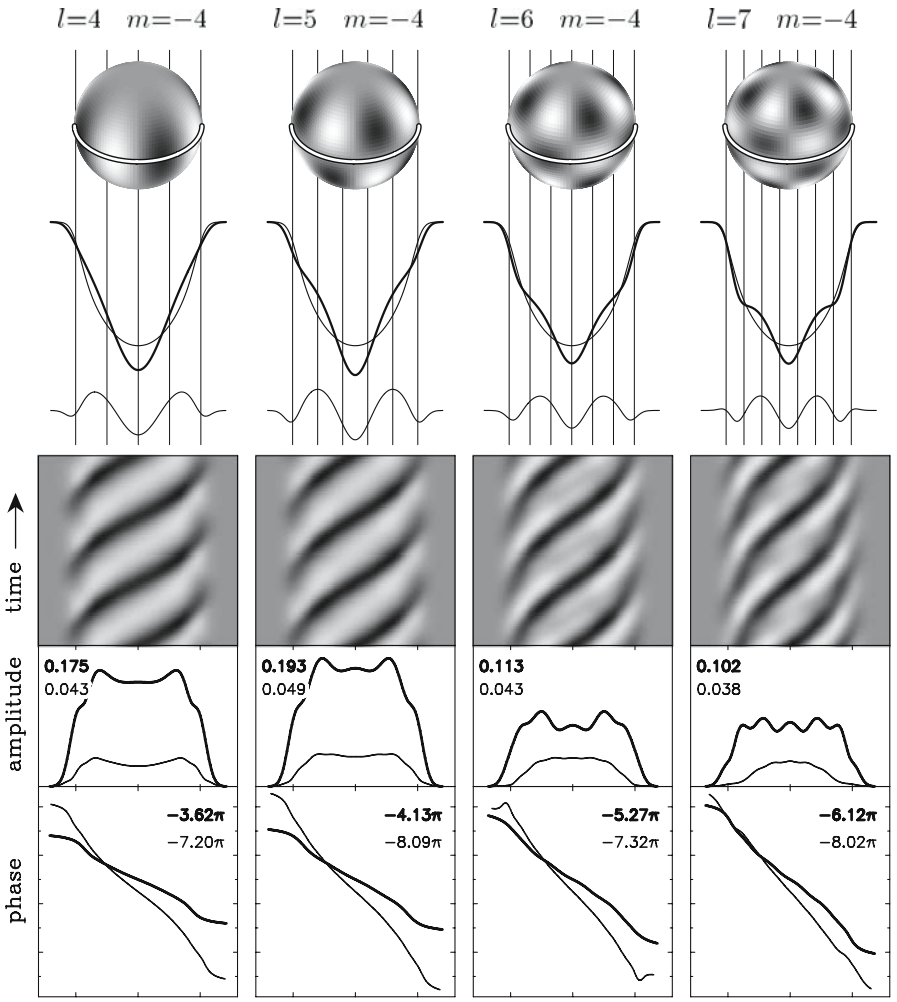

Fig. 31 Simulated line–profile variations due to non-radial oscillations of different (l, m). From *top* to *bottom* we show: a representation of the radial part of the eigenfunction, the line–profile due to the mode at a particular phase in the cycle in comparison with the profile without an oscillation, the difference between the two profiles, a grey-scale representation of the profiles with respect to the mean during three cycles, the distribution of the amplitude across the pulsation-induced line-profile variations (*thick line*) and its first harmonic (*thin line*) with the maximum values indicated, the distribution of the phase across the pulsation-induced line–profile variations (*thick line*) and its first harmonic (*thin line*) in units of π radians with the blue-to-red phase differences $\Delta\psi_0$ and $\Delta\psi_1$ used in Eqs. (80) and (81) indicated. The projected equatorial rotation velocity is indicated by the *outer vertical lines* in the *top panel*. Figure reproduced from Telting and Schrijvers (1997) with permission

– There exists a clear but less strong correlation between the phase difference $\Delta\psi_1$ from blue to red for the first harmonic of the oscillation frequency 2ω and the azimuthal number of the mode. A good estimate of m is

$$m \approx (-1.33 + 0.54\,|\Delta\psi_1|/\pi) \pm 2. \tag{81}$$

The simulations of Telting and Schrijvers (1998) clearly showed that the original suggestion by Gies and Kullavanijaya (1988) to associate the phase differences of the oscillation frequency with a measure of its m-value, is not appropriate. A similar simulation study for g modes is not available.

The fitting formulae (80) and (81) are easy to apply once the oscillation frequencies are determined. However, they provide only a crude estimate of the degree and azimuthal order with a large uncertainty, particularly for low-degree modes. It is therefore necessary to model the amplitude and phase across the profile in full detail to achieve a reliable identification. In order to do that, one computes theoretical line profile variations from Eqs. (74) and (79), derives their amplitude and phase across the profile as in Fig. 31 and compares them with those derived from the observations. The earliest such application was made for the star β Cephei by Telting et al. (1997) and is depicted in Fig. 32 for the dominant radial mode and for the three best solutions found for the identification of the second, low-amplitude mode.

Zima (2006) introduced a statistical significance test into the Telting and Schrijvers (1998) method. In this way, he was able to discriminate more easily between different mode identification solutions. He tuned and applied his method, which he termed *pixel-by-pixel method*, to observed line–profile variations of the δ Scuti star FG Vir (Zima et al. 2006).

4.2.3 Improvements through interferometric data

The pixel-by-pixel method described above exploits the amplitude and phase across the profile as mode identification diagnostic by relying, through Eqs. (74) and (79), on the expression for the pulsational velocity in terms of l and m. The Doppler effect is considered to be the dominant source of information in interpreting the variations in Eq. (79) in terms of l and m. A new interesting idea was put forward by Berdyugina et al. (2003a). They inverted a time series of line–profile variations, turning in this way the data into a stellar surface brightness distribution. This comes down to an image reconstruction method, also termed Doppler imaging in the context of spotted stars. They applied this inversion without assuming any pre-knowledge of the physical cause of the variations of the line profiles. After having performed the inversion, the authors assumed that the most important cause of the line–profile variations in Eq. (79) are surface brightness variations superposed onto a time-independent broadened Doppler profile. Rather than focusing on $v(\theta'_i, \varphi'_j)$ in the interpretation of Eq. (79), they thus considered $\delta[I_\lambda(\theta', \varphi')]$ to be the dominant information for the mode identification. Such a situation may occur for rapidly rotating stars, whose velocity perturbation due to the oscillations is very small compared with its rotational broadening. In such a case, the pulsation-induced intensity perturbations gain importance with respect to the velocity perturbations. Berdyugina et al. (2003b) applied their method to the rapidly rotating β Cephei star ω^1 Sco and found it to be capable of recovering l and m of the oscillation, which had been derived before from the pixel-by-pixel method by Telting and Schrijvers (1998). This brings us to the capability of combining surface brightness distributions and variations derived from interferometry, with surface velocity variations derived from high-resolution spectroscopy. We first describe how such brightness distributions can be measured interferometrically.

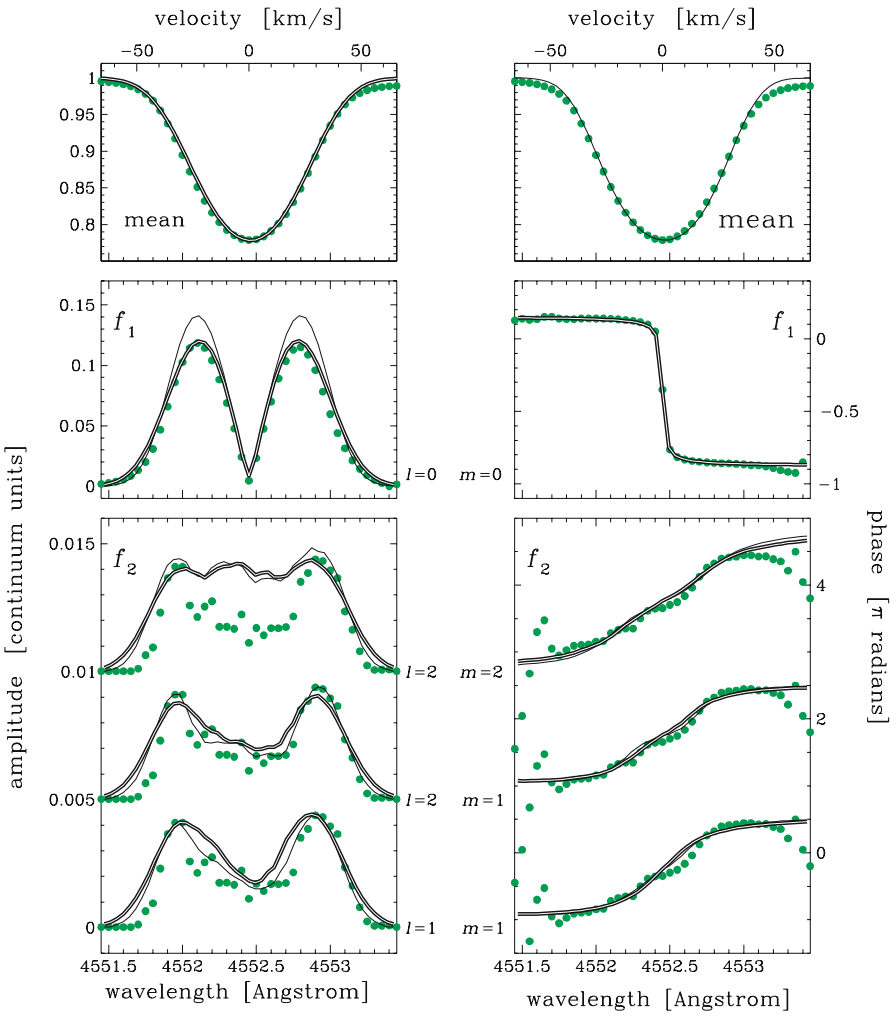

Fig. 32 Line–profile computations (*full lines*) are compared with data (*dots*) for the star β Cephei. The *top panel* shows the average profile, the *middle panels* the amplitude and phase across the profile for the dominant radial mode and the *lower panels* the amplitude and phase of the three most likely identifications of the small-amplitude non-radial mode (f_2). Figure reproduced from Telting et al. (1997) with permission

Long before the availability of appropriate instrumentation, Vakili and Percheron (1991) suggested to study surface variations due to non-radial oscillations of rapidly rotating stars from long-baseline interferometry. When the baseline is long enough, images of stellar surfaces can be obtained without a priori information on the targets. This is possible with the CHARA array (ten Brummelaar et al. 2005) and an instrument operating in the visible, or with the OHANA project (Perrin et al. 2006). As an example, the installation of the instrument GI2T/REGAIN (Mourard et al. 2003) at the combined focus of CHARA could give access to the location of abundance spots

in chemically peculiar stars via direct visibility measurements in the second and third lobes of the visibility function. However, with the baseline lengths and numbers of baselines currently available from interferometers, there are still quite severe limitations to the number of resolution elements over stellar surfaces. To overcome these limitations, a combination of interferometric information coming from existing instruments with lower angular resolution (such as the VLTI (Rantakyro et al. 2004) and classical observables may be used to map submilliarcsecond (sub-mas) structures in stellar surfaces. This technique, known as differential interferometry (Beckers 1982; Aime et al. (1984)) couples spatial and spectral information by measuring fringe phases throughout a spectral range (around an absorption/emission line for instance). The "fringe phase" observable being proportional to the stellar photocenter, photocenter displacements throughout absorption/emission lines can be measured (at a sub-mas level) and local features generating such lines can be located. By itself, this technique may be used, for instance, to map the surface spots in chemically peculiar pulsators, such as roAp stars, and, thus, provide additional non-seismic constraints about the atmospheric structure and magnetic fields, that are extremely valuable when studying these pulsators.

From the point of view of mode identification, the combination of the two techniques mentioned above, namely time-resolved spectroscopy and differential interferometry, seems to be a promising approach. As already anticipated by Jankov et al. (2001a), this combined technique can be successful in identifying oscillation modes with $l > 2$ in rapid rotators, providing information on the modes that can perhaps not be obtained from each of the two methods separately. The flux variations due to the non-radial modes introduce a complex pattern in the uv plane. This can be disentangled by comparing the associated photocenter displacements due to the oscillations with predicted monochromatic intensity maps of a non-pulsating star. In practice, one simulates photocenter displacements as a function of (l, m, i). Such a simulation defines a particular "spatial filter" for each (l, m, i). Applying one-by-one all these spatial filters to the data allows one to identify the true nature of the mode. This is illustrated in Fig. 33, in which the original signal in panel (a) is compared with a map (b) recovered from spectra alone with a method similar to the one of Berdyugina et al. (2003a), as well as to the map based on the photocenter shifts alone (panel c), or a combination of both (panel d). The limitations of panels (b) and (c) are particularly apparent in the reconstruction of the features below the equator, where a loss of contrast occurs. A significant improvement with respect to these separate reconstructions is obtained using both spectra and photocenter shifts simultaneously as in panel (d).

Domiciano de Souza et al. (2002, 2003) and Jankov et al. (2004) showed that measurements of the displacement of the photocenter across the stellar disk using closure phase allows mapping of the surface brightness, but requires a minimum of three telescopes in an interferometric array in such a way that fringes are collected for all three baselines. The simulation study by Jankov et al. (2004) anticipates that the closure phase measurements are sufficiently sensitive to detect a mode of low (l, m). In general, however, numerous modes are simultaneously excited. In such more realistic cases, the photocenter displacements are "washed out" by the averaging effect of the many (l, m)-values. In that case, one can perform *stroboscopic interferometry*. The aim of this is to pursue an identification for a fixed number of oscillation frequencies

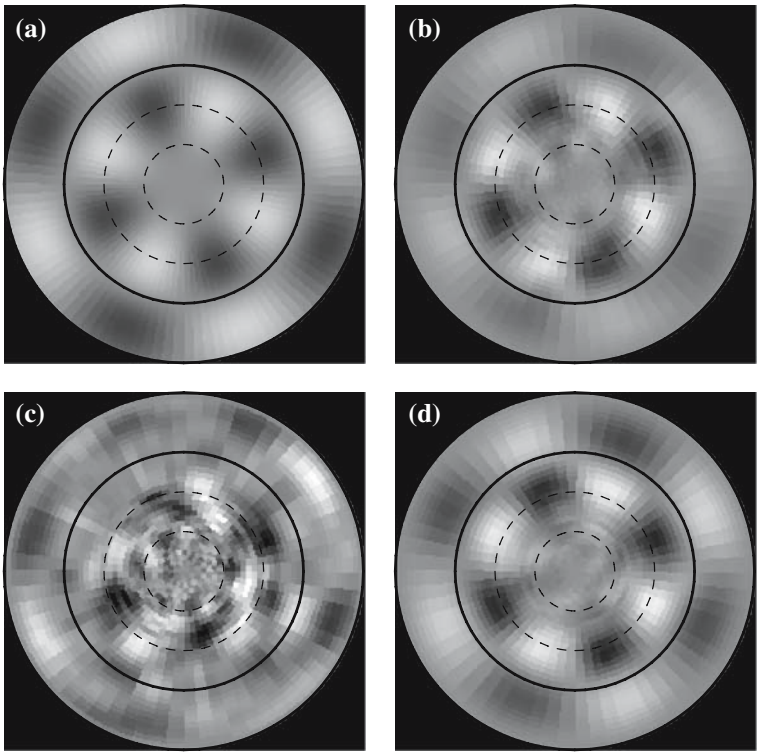

Fig. 33 **a** Simulation of the pole-on projection of the stellar surface brightness perturbations due to an $l = 5, m = 4$ mode on a star with an inclination angle of $i = 45°$. The equator and the latitudes 30° and 60° are represented by full and dashed circles, respectively. Reconstruction based on **b** simulated flux spectra, **c** photocenter shifts, and **d** combined flux spectra and photocenter shifts. Figure reproduced from Jankov et al. (2001b) with permission

which have been derived from time series analysis of observables of any kind. When carrying out the interferometric measurements, a selected oscillation frequency is used to phase-lock the data to this frequency. In this way, all surface structure that is not associated with this frequency is assumed to be removed. This would greatly improve the phase closure signal strength.

It is important to note that the phase-locking does not need to be carried out during the observations, which would create insurmountable problems in its practical implementation. Rather, the interferometric fringes may be collected at the normal cadence which needs to be sufficiently high compared with the oscillation frequencies. The frequency filtering can be done as a post-processing step by an appropriate weighting procedure. The design of such weights is a standard time-series analysis/inverse problem. A further advantage of doing the latter is that it would be possible to design the appropriate weights for each of the measured oscillation frequencies separately, and use the same set of interferometric observations to constrain the identification of all the oscillation modes whose frequencies are known from other diagnostics.

4.3 Current studies of pulsating stars including interferometric constraints

Sections 4.1 and 4.2 give a clear indication that results from observations obtained with current interferometric instruments are likely to have a very significant impact in asteroseismic studies in the very near future. At present, however, the number of pulsating stars for which sufficiently accurate interferometric and asteroseismic data are available is still limited. In this section we review the results of a few case studies of stellar pulsators involving a combination of interferometric and asteroseismic constraints.

4.3.1 α Cen

As emphasized earlier, the study of binary systems with combined interferometric and asteroseismic constraints is of particular interest. The visual binary α Cen is amongst the most promising systems in this context. Besides the availability of precise luminosities, masses and chemical composition for both components, interferometric and seismic constraints have recently been obtained for this system. The linear radii of α Cen A and B are known with high precision, thanks to the combination of precise parallaxes (Söderhjelm 1999) and angular diameters measured with VINCI, at VLTI (Kervella et al. 2003b; Bigot et al. (2006)). Moreover, solar-like oscillations have been detected, first in α Cen A by Bouchy and Carrier (2002), and then in component B by Carrier and Bourban (2003). The oscillations of both components were meanwhile studied in more detail by Bedding et al. (2004) and Kjeldsen et al. (2005).

The numerous and precise observational constraints available make the binary system α Cen a suitable target to test stellar structure and evolution models in conditions that are slightly different from those in the Sun. This is the reason why α Cen has been the subject of many theoretical studies, in particular since the detection of solar-like oscillations in α Cen A (see, e.g. Thévenin et al. 2002; Thoul et al. (2003); Eggenberger et al. (2004); Miglio and Montalbán (2005); Yildiz (2007)).

Miglio and Montalbán (2005) modelled α Cen by means of the Levenberg-Marquardt non-linear fitting algorithm (e.g. Bevington and Robinson 2003) that performs a simultaneous least-squares adjustment of the model parameters ($M_{\rm A}$, $M_{\rm B}$, Y_0, Z_0, $\alpha_{\rm A}$, $\alpha_{\rm B}$, age) to all the observational constraints. A goal was to study how the results of the fit depend on the "physics" included in the stellar models, and on the choice of classical, interferometric, and seismic observables considered in the fitting procedure. Here, the subscripts A and B refer, respectively, to the components A and B of the system. The addition of a precise linear radii to the observational constraints resulted in a reduction of the size of the error box associated with the position of the star in the HR diagram, and, in turn, in a reduction of the uncertainties in the parameters derived from the fitting. This reduction in the uncertainties associated with the derived parameters is particularly important when evaluating the significance of adding an extra free parameter in the modelling, as, for instance, when considering two distinct mixing-length parameters for components A and B of the system. However, the authors also found that when using the linear radii, instead of $T_{\rm eff}$, as the observable, the agreement between the observed and the model average large separations becomes worse. As discussed in Fig. 12, this is likely a consequence of the

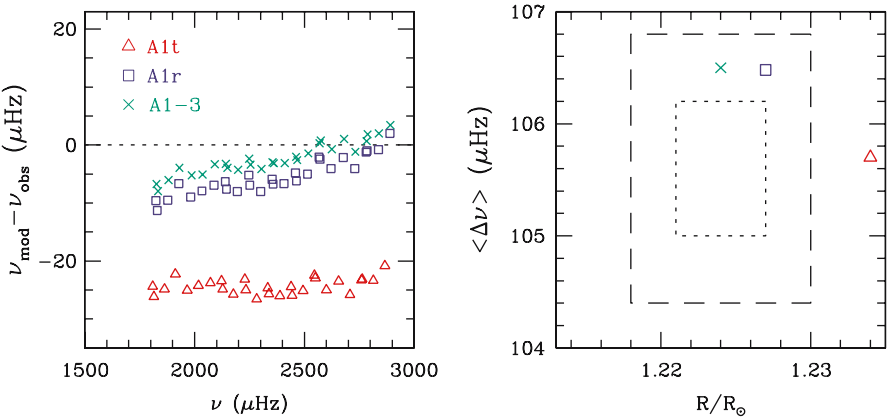

Fig. 34 Difference between theoretical and observed frequencies for models of α Cen A (*left*), and a radius $\langle\Delta\nu\rangle$ diagram (*right*) comparing the values predicted by the models (see Miglio and Montalbán 2005) to the 1- and 2-σ error boxes in R and $\langle\Delta\nu\rangle$. The models are calibrated considering among the constraints: $T_{\rm eff}$ and $\langle\Delta\nu\rangle$ (A1t), the radius and $\langle\Delta\nu\rangle$ (A1r) and, in the case of model A1-3, including in the fit the radius and the combination of frequencies suggested by Roxburgh and Vorontsov (2003). Though the observed $\langle\Delta\nu\rangle$ is well reproduced, model A1t predicts a radius which is inconsistent with the observed value and is responsible for a large shift between observed and theoretical frequencies. When the interferometric radius is included in the fit (A1r, A1-3), the predicted $\langle\Delta\nu\rangle$ is larger than the observed: this discrepancy (which is well known in the solar case) is likely to be related to surface effects

inaccurate modelling of the surface layers of the star, which directly influences the value of the large separation at high frequency. In order to avoid this problem, when deriving global parameters of α Cen through the fitting procedure, the authors followed the suggestion of Roxburgh and Vorontsov (2003), and considered as seismic observables, combinations of frequencies that are largely independent of near-surface layers [cf. Eq. (38)].

Figure 34 compares the results for α Cen A obtained when different observables are included in the fitting. When $T_{\rm eff}$ and the average observed large separation, $\langle\Delta\nu\rangle$, are used (model A1t) a large discrepancy is found between model and observed frequencies. Moreover, in this case the radius of the model is inconsistent with the interferometric one. On the other hand, when the interferometric radius is used instead of $T_{\rm eff}$ (models A1r and A1-3), the difference between model and observed frequencies is significantly reduced. However, the average large separations derived from the models are found to be larger than the observed one. Model A1-3, obtained when using the interferometric radius and the combination of seismic observables suggested by Roxburgh and Vorontsov (2003), shows the best agreement with the observations both in what concerns the predicted frequencies and radius.

4.3.2 τ Cet

τ Cet is a G8 V star. It was one of the first asteroseismic candidates to have its radius measured by VINCI at the VLTI (Pijpers et al. 2003; Di Folco et al. 2004). Having an accurate measurement of the stellar radius allowed Teixeira et al. (in preparation) to

construct preliminary models for τ Cet, and to predict both the average large separation, and the location, in frequency, of the expected envelope for solar-like oscillations. As a logical follow-up of that work, an asteroseismic campaign with the HARPS instrument at the 3.6-m telescope in Chile was carried out. Despite adverse weather and unexpected technical problems at the telescope, 32 oscillation frequencies were measured, corresponding to mode degrees of $l = 0, 1, 2, 3$. The asteroseismic data provided further independent constraints for the modelling, in addition to the four "classical", non-asteroseismic observables ($T_{\rm eff}$, L, [Fe/H], R).

A large range in values of τ Cet's metallicity and effective temperature is reported in the recent literature. Estimates of [Fe/H] published over the last four years range from -0.57 to -0.4, while those of $T_{\rm eff}$ range from 5,270 to 5,420 K. In these (not unusual) circumstances, a precise determination of the stellar radius, through the combination of interferometric data and the parallax, is particularly important.

To model τ Cet, the authors used the Aarhus STellar Evolution code (Christensen-Dalsgaard 1982, 2007), and the Aarhus Adiabatic Pulsation code (Christensen-Dalsgaard and Berthomieu 1991), coupled to an automated fitting procedure based on the Levenberg–Marquardt optimization method running on a cluster with eight processors. The procedure searches the parameter space for the combination of stellar parameters (M, X_0, Y_0, α, age) that best reproduces the non-asteroseismic and asteroseismic observables for the star. Whilst it is relatively straightforward to include the "classical" observables in the fit, the asteroseismic observables present a bigger challenge.

In the asymptotic regime, the theory of stellar oscillations predicts the frequencies to exhibit regular spacings with characteristic large and small separations [cf. Eqs. (31) and (35)]. However, for τ Cet the oscillation frequencies around peak power for low l values are not yet in the asymptotic regime. Nonetheless, the authors first attempted a fit to the observations based on an asymptotic relation, to match the large and small separations. This resulted in finding a best solution with predicted individual frequencies significantly shifted from the observed ones, as shown in Fig. 35.

In order to include the absolute values of the observed frequencies in the fit, the authors used functions to fit the frequency ridges in the échelle diagram, as suggested by Bedding et al. (2004). From those, an absolute frequency, a large separation and a small separation were derived, and these quantities were used as asteroseismic observables in the optimization procedure. The resulting solution was encouraging, as can be seen in Fig. 36a. However, the model did not appear to match particularly well the observations for the higher frequency modes. Moreover, the mixing-length parameter resulting from the fit of the seismic data was significantly larger than in the solar case. Once again, this was interpreted as a consequence of the deficient modelling of the outer layers of the star (cf. discussion in Fig. 12). Consequently the authors decided to include a surface correction in the fit, by scaling the empirical solar surface frequency correction to the case of τ Cet. That resulted in a very satisfactory fit, as shown in Fig. 36b, now with a mixing-length parameter close to that for the Sun.

4.3.3 β Hyi

β Hyi is a bright G2 subgiant. Despite early attempts to detect solar-like oscillations in this star (Frandsen 1987; Edmonds and Cram 1995), such oscillations were confirmed

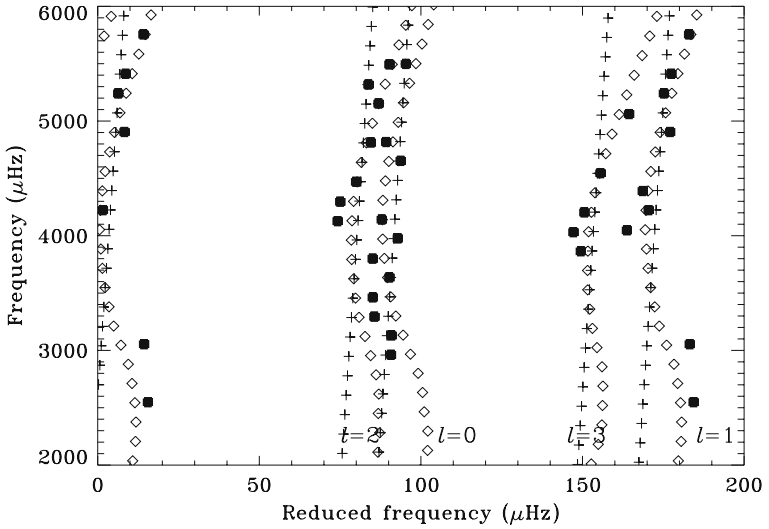

Fig. 35 Echelle diagram showing the observed frequencies for τ Cet (*thick crosses*; Teixeira et al., in preparation) and the model frequencies (*diamonds*), with an average large separation $\langle \Delta\nu \rangle = 168.83\,\mu$Hz; the *thin crosses* indicate the asymptotic relation. The model and asymptotic relation frequencies have been increased by 35 μHz to coincide with the observed frequencies

only with the works of Bedding et al. (2001) and Carrier et al. (2001), using UCLES and CORALIE, respectively. Recently, a dual-site campaign, involving HARPS and UCLES (Bedding et al. 2007), allowed for the identification of 28 oscillation modes, some of which showing a clear indication of avoided crossings, as expected from theoretical studies of this star (Fernandes and Monteiro 2003; Di Mauro et al. 2003) (see also Sect. 2.4.2). From these results, the authors derived the mean density of β Hyi to be $\bar{\rho} = 0.2538 \pm 0.0015\,\mathrm{g\,cm^{-3}}$.

Recently (North et al. 2007a) have measured the angular diameter of β Hyi using Sydney University Stellar Interferometer, having found a limb-darkened angular diameter of 2.257 ± 0.019 mas. Combining the latter with the Hipparcos parallax for the star, the authors found a linear radius $R = 1.814 \pm 0.017\,\mathrm{R_\odot}$, which combined with the mean density derived from asteroseismic data, allowed them to derive a mass $M = 1.07 \pm 0.03\,\mathrm{M_\odot}$. This value of the mass is in agreement with previous determinations based on model fitting of the observables, but is significantly better in precision. With these recent asteroseismic and interferometric constraints, it should be possible in the near future to produce improved models of β Hyi and investigate on physical aspects of its interior.

4.3.4 θ^2 Tau

As mentioned above, Tomkin et al. (1995) have combined spectroscopically and interferometrically measured orbits to deduce the fundamental parameters of the δ Scuti star θ^2 Tau. They achieved the following ranges for the masses of the components: $M_\mathrm{A} = 2.1 \pm 0.3\,\mathrm{M_\odot}$, $M_\mathrm{B} = 1.6 \pm 0.2\,\mathrm{M_\odot}$ and a distance of 44.1 ± 2.2 pc. While

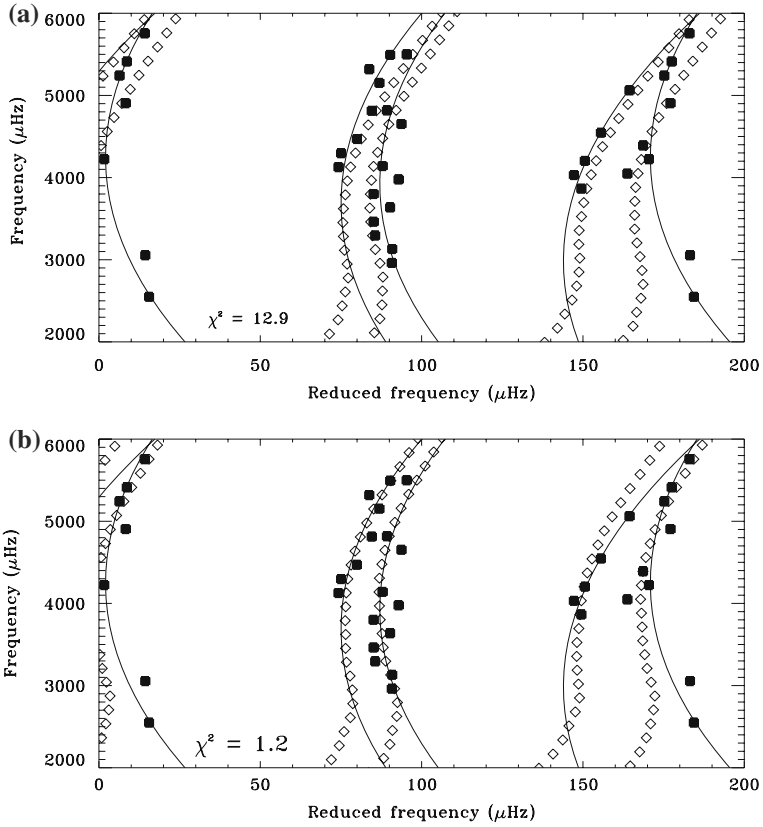

Fig. 36 Echelle diagrams showing the observed frequencies (*thick crosses*; Teixeira et al. in preparation), the best-matching Bedding et al. functions (*curves*), and the model frequencies (diamonds) for two cases: **a** without surface correction, and **b** with surface correction (100% relative correction). An average large separation $\langle \Delta\nu \rangle = 168.83\,\mu$Hz was used

these are valuable mass determinations for a system including a classical pulsator, they remain largely above 10% relative precision.

The star was the subject of a large multisite campaign resulting in multicolour ground-based photometry (Breger et al. 2002), as well as of a WIRE space photometric campaign (Poretti et al. 2002). This resulted in 11 established frequencies in the range 10.8 to 14.6 $\mathrm{c\,d^{-1}}$, which corresponds to the region of radial p_5 to p_6 modes for appropriate stellar models. The largest stumbling block in the seismic modelling, is the lack of good mode identification for this star, despite the accurate measurements of its line–profile variations (Kennelly et al. 1996b). This prevented Breger et al. (2002) from reaching a conclusion on the evolutionary status of the pulsating primary. In particular, it was impossible to deduce if the δ Scuti star is in a post-main-sequence phase (in agreement with models with or without core overshooting) or is still on the main sequence (compatible with computed models including core overshooting). The main uncertainties in the modelling, besides the mode identification, are due to the simple treatment of the convective flux in the hydrogen ionization zone.

4.4 Future studies of pulsating stars including interferometric constraints

Besides the studies presented above, a number of additional ones of pulsating stars combining interferometric and asteroseismic constraints have been proposed and are awaiting the acquisition of seismic or interferometric data. Among these are the binary system 12 Boo, in which both components are expected to show solar-like oscillations, and the classical pulsators α Vir (Spica), λ Sco and β Cen (three β Cephei stars). Moreover, future interferometric observations with AMBER at VLTI are planned for the β Cephei star κ Sco and for the slowly pulsating B star HD 140873.

4.4.1 12 Boo

12 Boo is a double-lined spectroscopic binary whose orbit has been resolved by interferometry: this has allowed determination of the masses of both components ($M_{\rm A} = 1.416\ {\rm M}_{\odot}$ and $M_{\rm B} = 1.374\ {\rm M}_{\odot}$) with a relative precision of about 0.3% (Boden et al. 2005b; Tomkin and Fekel 2006). Even though the masses of the components are very similar, their different luminosities, when compared with theoretical predictions, suggest that the secondary component is still in the central-hydrogen burning phase, while the primary is more evolved and burning hydrogen in a shell. As presented by Boden et al. (2005b), however, this conclusion is highly dependent on the model details and needs further investigation. A detailed modelling of the system (Miglio et al. 2007b) shows that several models of 12 Boo, based on different theoretical predictions of extra-mixing processes in the core (e.g. overshooting), are able to reproduce the available observational constraints.

In order to discriminate among these scenarios, additional and independent observational constraints are needed. These could be provided by solar-like oscillations, as these are expected to be excited in both components of the system. A precise knowledge of the frequencies of high-order p modes in the primary component would help determining the evolutionary state of the system and would give information on the chemical composition gradient built by the combined action of nuclear burning and mixing in the central regions of the star.

4.4.2 λ Sco

Tango et al. (2006) observed the triple system λ Sco, composed of two early-B stars and a pre-main-sequence star (Uytterhoeven et al. 2004a), interferometrically with the Sydney University Stellar Interferometer. This allowed them to determine the elements of the wide orbit with much higher precision than the previous estimates from spectroscopy alone (Uytterhoeven et al. 2004a). The wide orbit turns out to have a low eccentricity, suggesting that the three stars were formed at the same time, only a few million years ago.

From the brightness ratio and the colour index of the two B stars, Tango et al. (2006) confirmed the previous classification of λ Sco A as B1.5IV and λ Sco B as B2IV. They used the mass–luminosity relation for main-sequence stars to determine the mass ratio of the two B stars and found $M_{\rm B}/M_{\rm A} = 0.76 \pm 0.04$. The individual masses were subsequently derived from this mass ratio, the mass function, spectrum

synthesis and the requirement that the age of both components must be the same. This led to $M_{\rm A} = 10.4 \pm 1.3\,{\rm M}_{\odot}$ and $M_{\rm B} = 8.1 \pm 1.0\,{\rm M}_{\odot}$.

Uytterhoeven et al. (2004b) found λ Sco A to be a relatively fast rotator with a $v \sin i$ of $125\,{\rm km\,s^{-1}}$ and to have clear line–profile variations due to a dominant prograde dipole oscillation mode. Additional low-amplitude modes were also found and these seem to originate from modes with degree $l > 2$. Ground-based photometry does not reveal these higher degree modes seen in the line–profile variations. Progress could be achieved from high-precision space photometry, however. Such data have meanwhile been gathered with the WIRE satellite (Bruntt et al., in preparation). Hopefully this will lead to accurate modelling results for this massive B star in the near future.

4.4.3 β Cen

Ausseloos et al. (2006) have presented dedicated methodology to derive high-precision estimates of the fundamental parameters of the double-lined spectroscopic binary β Cen which contains a pulsating β Cephei component in its 357 day orbit with an eccentricity of 0.81. Their method is based on high-resolution spectral time series and interferometric data with a good phase distribution along the orbit. Such data allowed them to derive the component masses and dynamical parallax with a relative precision of 6 and 4%, respectively, where the two B stars have almost the same masses and stellar properties. The equatorial rotation velocity of the primary is, however, about twice the one of the secondary, which is quite remarkable and forms a challenge to current formation scenarios and tidal theories of massive binaries.

Two oscillation frequencies with values expected in the range of β Cephei stars were derived from the line–profile variations of the broad-lined primary. Spectroscopic mode identification pointed out that their degree is definitely higher than 2, but secure values for l could not be deduced. Ground-based photometry will not help to resolve this ambiguity, because the binary is photometrically constant. The high-degree modes will probably be well visible from space photometry, but such data have not yet been assembled so far (the star is outside the viewing zone of MOST). No evidence of oscillations in the narrow-lined secondary was found from the high-resolution spectroscopy. It would definitely be worthwhile to measure this binary from space with high-precision photometry.

4.4.4 κ Sco

Future interferometric observations of the β Cephei star κ Sco were approved by the AMBER Science Group in the framework of the Guaranteed Time Observations in a proposal that included also the slowly pulsating B star HD 140873.

The β Cephei star κ Sco has a quite large rotational velocity of $120\,{\rm km\,s^{-1}}$. This target thus provides an opportunity, just as λ Sco and β Cen, to estimate the influence of rotation on pulsation, once masses and tidal parameters are determined. The main pulsation period has been identified as an ($l = 1$ or $2, m = -1$) mode. Five other frequencies are present, but in addition to pulsation, rotational modulation is also

invoked to interpret the complex spectral line profile variations (Uytterhoeven et al. 2005). The orbital period of the star is $P = 195$ days, and the eccentricity is close to 0.5 (Uytterhoeven et al. 2001). The mass ratio of this SB2 system is 1.11. An estimation of the mass of the main component led to an orbital inclination close to 80°, and a maximal visual separation of the order of 10 mas. The system can thus be easily resolved with the Auxiliary (ATs) or Unit Telescopes (UTs) at ESO.

4.4.5 α Vir

The bright β Cephei star α Vir (Spica) has been measured interferometrically with the CHARA Array and the FLUOR instrument by Aufdenberg et al. (2007). Spica is a massive, non-eclipsing, double-lined spectroscopic binary with a 4-day orbital period and two relatively rapid rotators. The projected rotational velocity $v \sin i$ is again of order 120 km s^{-1}, just as for κ and λ Sco and β Cen. Previous interferometric data with the Sydney University Stellar Interferometer are also available. Modelling of the new and archival interferometric and spectroscopic data is in progress.

On the other hand, Spica was the main target of a 23-day MOST run from 26 March to 18 April 2007. This, together with a simultaneous but longer high-resolution spectroscopic campaign with the CORALIE spectrograph, attached to the 1.2-m Euler telescope at La Silla and with the spectrograph attached to the 1.22-m telescope at the Dominian Astrophysical Observatory, should offer a very detailed picture of Spica's oscillations. This β Cephei star has not been revisited since the pioneering work of Smith (1985a, b) who suggested tidally affected modes for this star and a tentative mode identification of $l = 2$ and 8.

The combination of these state-or-the-art interferometric, spectroscopic and space photometric data should allow detailed modelling of this β Cephei binary in the near future.

4.4.6 HD 140873

The slowly pulsating B star HD 140873 is member of a B8 III + A7V binary system. This double-lined binary has an orbital period of $P = 39$ day and a quite high eccentricity of 0.73 (De Cat et al. 2000). Only one pulsation frequency has been definitively identified as an $(l = 1, m = +1)$ mode (De Cat et al. 2005) but other frequencies seem to be present. The mass ratio of the system amounts to 2. The estimate of the mass of the primary leads to an inclination angle of about 50°, implying a maximum separation of 6 mas and a minimum separation of 1 mas. In the latter case, the fringe signal will be poorly sampled with the UTs. Among the four known binary slowly pulsating B stars, HD 140873 is the one with the longest orbital period, hence allowing the best observational set-up.

In principle, two interferometric points on the orbit should be enough to derive the inclination angle if one of these points is on the line of the nodes. However, due to the uncertainties on the ephemeris, 10 points seem necessary to derive a proper interferometric orbit, in order to get a precision of a few percent on the stellar mass.

5 A look into the future

As has been the case for observations of the 5-min oscillations in the Sun, the most obvious way to overcome the fundamental observational limitations to the study of solar-like pulsators, namely observing length and daily aliases, is to establish networks of telescopes and/or observe from the poles.

Several projects are now in preparation or underway to explore these possibilities and include the creation of facilities at DOME-C in Antarctica and global networks of telescopes at different longitudes and latitudes. At the time of writing we are not aware of any networks which are funded. A short but incomplete list of ongoing studies includes: *SIAMOIS* (Mosser 2006) which aims at using a small telescope with a Fourier transform spectrometer at Dome C, and the Stellar Oscillations Network Group (SONG) aiming at a network of several telescopes with spectrographs for high-precision radial velocities (Grundahl et al. 2007).

It is to be expected that such efforts as *SIAMOIS* or SONG will lead to significant progress in the field of asteroseismology. Prior to that it would seem fruitful to try to explore the use of existing facilities for short, 1–2 weeks, dedicated campaigns of carefully selected solar-type targets. For equatorial objects the current location of the existing facilities allows for good possibilities of obtaining a high duty-cycle if such campaigns can be organized. An example is the major campaign on Procyon which was organized in January 2007.

The Concordia station at Dome C also opens important new opportunities for asteroseismic studies of classical pulsators. This station began as a Franco-Italian scientific base, but has recently expanded under FP6 funding for the ARENA European Network,[26] which includes seven countries (Belgium, France, Germany, Italy, Portugal, Spain, and UK), and also Australia. Site testing has been underway for some time, and the first winter-over and night-time tests were made in 2005.

Dome C is at latitude $-75°$ high on the Antarctic plateau (3,200 m elevation). During the day the median seeing is $0.5''$; it is smaller than $0.3''$ for 25% of the time, and can at times decrease to only $0.1''$—nearly space values. A recent winter-over has shown that at night there is a layer near the ground that degrades the seeing because of the extreme temperature gradient (night time temperatures are ~ -75 C), but 30 m above the ground the exceedingly low values given above are recovered, so giant telescopes being planned for the site will be mounted on high platforms.

For asteroseismic photometry the most important characteristic is the low wind speeds and scintillation. Because the winds of Antarctica are katabatic, they flow away from Dome C. They are low speed at all altitudes, as tested by balloon flights—significantly lower than at Mauna Kea or Paranal, for example. The result is significantly lower scintillation noise, which is the major noise source in ground-based high-speed photometry for stars that are not photon-noise limited. Since the first winter-over indicates photometric conditions occur 80% of the time, asteroseismic telescopes at Dome C will be able to obtain data sets with 80% duty cycles for over 20 weeks during the long polar night, and with higher precision than for any other ground-based site.

[26] see http://arena.unice.fr/.

Just as the South Pole observations dominated helioseismology for many years in the 1980s (Grec et al. 1980), Dome C asteroseismic observations will do so for stars that cannot be observed with the satellite missions.

Improvements in interferometric facilities, with potential impact to asteroseismology, are also expected over the next decade, as discussed in some detail in Sect. 3.5. In particular, the Magdalena Ridge Observatory interferometer, which is currently under construction, will have six 1.4-m telescopes with baselines up to 340 m, and will operate in the red-near infrared range (Buscher et al. 2006). Being driven by interferometric imaging, this facility will have a superior (u, v) plane coverage to the CHARA array and similar sensitivity. Simultaneously, upgrades of existing facilities are expected, with particular emphasis on: combinations of larger numbers of telescopes; extension to shorter wavelengths, in particular pushing facilities currently operating in the near-infrared to visible wavelengths; pushing the limiting magnitude of the interferometers which are still far from the nominal limiting magnitude; and, when the site allows, extension to longer baselines.

Just as in the case of ground-based projects, a number of space projects including a significant asteroseismology programme may be expected in the future. In North America, the Canadian nanosatellite project BRight Target Explorer (BRITE) will observe the oscillations of a few bright stars; the NASA Kepler mission, essentially aimed at detecting planetary transits, will also include an asteroseismology programme (Basri 2005); the long-term Stellar Imager project (Carpenter 2005), presently under study at NASA, will in principle provide a sufficient resolution at the surface of nearby stars to study high degree modes up to $l = 10$. On the European side, a new call for missions was issued by ESA in the Spring of 2007. A European consortium has prepared and submitted an answer to this call for an asteroseismology and exoplanet search mission named PLAnetary Transits and Oscillations of Stars (PLATO) (Catala et al. 2005). The novelty of the proposed approach will be to search for planetary transits and analyse stellar oscillations on the same targets, thus providing strong observational constraints on star and planet evolution, e.g. by measuring the ages of stars that are hosting planets, and studying the distribution of planet sizes and orbits as a function of age. A significant number of these targets will be bright and sufficiently nearby to envisage high-precision interferometric measurements of their diameters and surface structures.

More ambitious space projects are being discussed for the longer term future. One of them, tentatively named AIM (for AsteroInterferometric Mission), couples interferometric techniques and ultra-high precision photometry or Doppler velocimetry to resolve stellar disks and measure high-degree modes at the surface of stars. A free flying fleet of 10–100 telescope units of 1-m diameter each, on baselines of 10–40 km, would constitute a powerful interferometer capable of resolving high-degree oscillation modes, up to $l = 200$ for a solar-type star at 10 pc, or $l = 10$ for a typical cool star in the Pleiades.

On the interferometry side, it is possible that within a time frame of a decade or so, a small interferometric mission like PEGASE (Ollivier et al. 2006) will be launched. It will combine two 40-cm siderostats in baselines up to 500 m and operate primarily in the 1.5-6 μm range. However an extension to the 0.8–1.5 μm range would complement existing ground facilities for stellar diameter measurements. PEGASE would further

allow the following of diameter variations in rapid (few hours to few days) pulsators that will be uncovered by MOST and CoRoT.

The future of asteroseismology, interferometry and their synergy looks very bright, indeed.

Acknowledgments The authors are very grateful to Hans Kjeldsen and Günter Houdek for providing important input to parts of this review. Thanks go also to Michael Bazot, Kara Burke, Cristina Fernandes, João Fernandes, Michael Gruberbauer, João P. Marques, Fernando Pinheiro, Jonathan Riley, Marta Santos, Nuno Santos and Sérgio Sousa, for useful discussions during the CAUP/OPTICON workshop on Interferometry and Asteroseismology. JC-D thanks Michael Knölker for hospitality at the High Altitude Observatory where much of his contribution was written. This work was supported by the OPTICON through funds from the European Commission. MC is supported by the EC's FP6, FCT and FEDER (POCI2010) through the HELAS international collaboration and through the project POCI /CTE-AST /57610 /2004. CA is supported by the Research Council of Leuven University under grant GOA/2003/04. GP acknowledges support from PHASE, the space and ground-based high angular resolution partnership between ONERA, Observatoire de Paris, CNRS and University Denis Diderot Paris 7. PJVG was supported in part by the Fundação para a Ciência e a Tecnologia through projects POCI/CTE-AST/55691/2004 and PTDC/CTE-AST/65971/2006 from POCI, with funds from the European program FEDER.

References

Adorf HM (1995) Interpolation of irregularly sampled data series—a survey. In: Shaw RA, Payne HE, Hayes JJE (eds) Astronomical Data Analysis Software and Systems IV, ASP Conference Series vol 77, p 460

Aerts C (1996) Mode identification of pulsating stars from line–profile variations with the moment method: a more accurate discriminant. Astron Astrophys 314:115–122

Aerts C, De Cat P (2003) β Cep stars from a spectroscopic point of view. Space Sci Rev 105:453–492

Aerts C, De Pauw M, Waelkens C (1992) Mode identification of pulsating stars from line profile variations with the moment method. an example—The Beta Cephei star Delta Ceti. Astron Astrophys 266:294–306

Aerts C, De Cat P, Peeters E, Decin L, De Ridder J, Kolenberg K, Meeus G, Van Winckel H, Cuypers J, Waelkens C (1999) Selection of a sample of bright southern Slowly Pulsating B Stars for long-term photometric and spectroscopic monitoring. Astron Astrophys 343:872–882

Aerts C, Thoul A, Daszyńska J, Scuflaire R, Waelkens C, Dupret MA, Niemczura E, Noels A (2003) Asteroseismology of HD 129929: core overshooting and nonrigid rotation. Science 300:1926–1928

Aerts C, Cuypers J, De Cat P, Dupret MA, De Ridder J, Eyer L, Scuflaire R, Waelkens C (2004) Long-term multicolour photometry and high-resolution spectroscopy of the two γ Doradus stars HD 12901 and HD 48501. Astron Astrophys 415:1079–1088

Aerts C, Marchenko SV, Matthews JM, Kuschnig R, Guenther DB, Moffat AFJ, Rucinski SM, Sasselov D, Walker GAH, Weiss WW (2006a) δ Ceti is not monoperiodic: seismic modeling of a β Cephei star from *MOST* space-based photometry. Astrophys J 642:470–477

Aerts C, De Cat P, Kuschnig R, Matthews JM, Guenther DB, Moffat AFJ, Rucinski SM, Sasselov D, Walker GAH, Weiss WW (2006b) Discovery of the new slowly pulsating B star HD 163830 (B5 II/III) from *MOST* space-based photometry. Astrophys J 642:L165–L168

Aime C, Martin F, Petrov R, Ricort G, Kadiri S (1984) Measurement of submilliarcsecond speckle displacements using a cross spectrum analysis technique—test on atmospheric dispersion. Astron Astrophys 134:354–359

Aizenman M, Smeyers P, Weigert A (1977) Avoided crossing of modes of non-radial stellar oscillations. Astron Astrophys 58:41–46

Andersen J (1991) Accurate masses and radii of normal stars. Astron Astrophys Rev 3:91–126

Antia HM, Basu S (2005) The discrepancy between solar abundances and helioseismology. Astrophys J 620:L129–L132

Antoci V, Breger M, Rodler F, Bischof K, Garrido R (2007) Is 44 Tauri an exceptional case among the δ Scuti stars?. Astron Astrophys 463:225–232

Appourchaux T, Berthomieu G, Michel E, Ballot J, Barban C, Baudin F, Boumier P, De Ridder J, Floquet M, García RA, Garrido R, Goupil MJ, Lambert P, Lochard J, Mazumdar A, Neiner C, Poretti E, Provost J, Roxburgh I, Samadi R, Toutain T (2006) Evaluation of the scientific performances for the seismology programme. In: Friedlund M, Baglin A, Lochard J, Conroy L (eds) The CoRoT mission pre-launch status. stellar seismology and planet finding. ESA SP-1306, ESA Publications, Noordwijk, pp 429–441

Armstrong JT, Hummel CA, Quirrenbach A, Buscher DF, Mozurkewich D, Vivekanand M, Simon RS, Denison CS, Johnston KJ, Pan XP, Shao M, Colavita MM (1992a) The orbit of ϕ Cygni measured with long-baseline optical interferometry: component masses and absolute magnitudes. Astron J 104:2217–2223

Armstrong JT, Mozurkewich D, Vivekanand M, Simon RS, Denison CS, johnston KJ, Pan XP, Shao M, Colavita MM (1992b) The orbit of Alpha Equulei measured with long-baseline optical interferometry - Component masses, spectral types, and evolutionary state. Astron J 104:241–252

Armstrong JT, Mozurkewich D, Rickard LJ, Hutter DJ, Benson JA, Bowers PF, Elias NM II, Hummel CA, Johnston KJ, Buscher DF, Clark JH III, Ha L, Ling LC, White NM, Simon RS (1998) The navy prototype optical interferometer. Astrophys J 496:550–571

Armstrong JT, Nordgren TE, Germain ME, Hajian AR, Hindsley RB, Hummel CA, Mozurkewich D, Thessin RN (2001) Diameters of δ Cephei and η Aquilae measured with the navy prototype optical interferometer. Astron J 121:476–481

Armstrong JT, Mozurkewich D, Hajian AR, Johnston KJ, Thessin RN, Peterson DM, Hummel CA, Gilbreath GC (2006) The Hyades binary θ^2 Tauri: Confronting evolutionary models with optical interferometry. Astron J 131:2643–2651

Arnold L, Lagrange A, Mourard D, Riaud P, Ferrari M, Gillet S, Kern P, Koechlin L, Labeyrie A, Lardière O, Malbet F, Perrin G, Rousset G, Tallon M (2002) High angular resolution in 2010–2020: a comparison between possible post-VLT/VLTI instruments. In: Traub WA (ed) Interferometry for optical astronomy II., Proc. SPIE vol. 4838, pp 134–143

Asplund M (2005) New light on stellar abundance analysis: departures from LTE and homogeneity. Annu Rev Astron Astrophys 43:481–540

Asplund M, Nordlund Å, Trampedach R, Allende Prieto C, Stein RF (2000) Line formation in solar granulation. I. Fe line shapes, shifts and asymmetries. Astron Astrophys 359:729–742

Asplund M, Grevesse N, Sauval AJ, Allende Prieto C, Blomme R (2005) Line formation in solar granulation. VI. C I, C I, CH and C2 lines and the photospheric C abundance. Astron Astrophys 431:693–705

Aufdenberg JP, Ludwig HG, Kervella P (2005) On the limb darkening, spectral energy distribution, and temperature structure of Procyon. Astrophys J 633:424–439

Aufdenberg JP, Mérand A, Coudédu Foresto V, Absil O, Di Folco E, Kervella P, Ridgway ST, Berger DH, Brummelaar TA ten, McAlister HA, Sturmann J, Sturmann L, Turner NH (2006) First results from the CHARA Array. VII. Long-baseline interferometric measurements of Vega consistent with a pole-on, rapidly rotating star. Astrophys J 645:664–675

Aufdenberg JP, Ireland MJ, Mérand A, CoudéDu Foresto V, Absil O, Folco E Di, Kervella P, Bagnuolo WG, Gies DR, Ridgway ST, Berger DH, Ten Brummelaar TA, McAlister HA, Sturmann J, Sturmann L, Turner NH, Jacob AP (2007) Interferometric constraints on gravity darkening with application to the modeling of spica A & B. In: Hartkopf WI, Guinan EF, Harmanec P (eds) Binary stars as critical tools & tests in contemporary astrophysics, IAUS 240. Cambridge University Press, UK, pp 271–280

Ausseloos M (2005) Seismic Studies of selected Beta Cephei stars: Beta Centauri, Nu Eridani and 12 Lacertae. PhD Thesis, Katholieke Universiteit Leuven, Belgium

Ausseloos M, Scuflaire R, Thoul A, Aerts C (2004) Asteroseismology of the β Cephei star ν Eridani: massive exploration of standard and non-standard stellar models to fit the oscillation data. Mon Not R Astr Soc 355:352–358

Ausseloos M, Aerts C, Lefever K, Davis J, Harmanec P (2006) High-precision elements of double-lined spectroscopic binaries from combined interferometry and spectroscopy. Application to the β Cephei star β Centauri. Astron Astrophys 455:259–269

Backus G, Gilbert F (1968) The resolving power of gross Earth data. Geophys J R Astr Soc 16:169–205

Backus G, Gilbert F (1970) Uniqueness in the inversion of inaccurate gross Earth data. Phil Trans R Soc London, Ser A 266:123–192

Baglin A (2003) COROT: A minisat for pionnier science, asteroseismology and planets finding. Adv Space Res 31(2):345–349

Bagnuolo WG Jr, Hartkopf WI (1989) Binary star orbits from speckle interferometry. III - The evolution of the Capella stars. Astron J 98:2275–2279

Bagnuolo WG, Taylor SF, McAlister HA, ten Brummelaar T, Gies DR, Ridgway ST, Sturmann J, Sturmann L, Turner NH, Berger DH, Gudehus D (2006) First results from the CHARA Array. V. Binary star astrometry: the case of 12 Persei. Astrophys J 131:2695–2699

Bahcall JN, Serenelli AM, Basu S (2006) 10,000 standard solar models: a Monte Carlo simulation. Astrophys J Suppl 165:400–431

Baker NH (1987) Time dependent convection in stars—a review of the theories. In: Hillebrandt W, Meyer-Hofmeister E, Thomas HC (eds) Physical processes in comets, stars and active galaxies. Springer, Berlin, pp 105–124

Baker NH, Gough DO (1979) Pulsations of model RR Lyrae stars. Astrophys J 234:232–244

Baker N, Kippenhahn R (1962) The pulsations of models of δ Cephei stars. Z Astrophys 54:115–151

Baker N, Kippenhahn R (1965) The pulsations of models of delta Cephei stars. II. Astrophys J 142:868–889

Baldwin JE, Haniff CA (2002) The application of interferometry to optical astronomical imaging. Phil Trans A 360:969–986

Baldwin JE, Beckett MG, Boysen RC, Burns D, Buscher DF (1996) The first images from an optical aperture synthesis array: mapping of Capella with COAST at two epochs. Astron Astrophys 306:L13–L16

Ballot J, García RA, Lambert P (2006) Rotation speed and stellar axis inclination from modes: how *CoRoT* would see other suns. Mon Not R Astr Soc 369:1281–1286

Balmforth NJ (1992) Solar pulsational stability. I: Pulsation-mode thermodynamics. Mon Not R Astr Soc 255:603–631

Balmforth NJ, Cunha MS, Dolez N, Gough DO, Vauclair S (2001) On the excitation mechanism in roAp stars. Mon Not R Astr Soc 323:362–372

Balona LA (1986a) Mode identification from line profile variations. Mon Not R Astr Soc 219:111–129

Balona LA (1986b) Mode identification from line profile variations. II—A quantitative least-squares algorithm. Mon Not R Astr Soc 220:647–656

Balona LA (1987) Mode identification from line profile variations. III—Temperature variation and toroidal modes. Mon Not R astr Soc 224:41–52

Balona LA, Aerts C, Stefl S (1999) Simultaneous photometry and spectroscopy of the Be star 28 (omega) CMa—II. Line profile modelling. Mon Not R ast Soc 305:519–526

Balona LA, Evers EA (1999) Mode identification and asteroseismology of δ Scuti stars. Mon Not R Astr Soc 302:349–361

Balona LA, Stobie RS (1979) The effect of radial and non-radial stellar oscillations on the light, colour and velocity variations. Mon Not R Astr Soc 189:649–658

Bedding TR, Butler RP, Kjeldsen H, Baldry IK, O'Toole SJ, Tinney CG, Marcy GW, Kienzle F, Carrier F (2001) Evidence for solar-like oscillations in hydri. Astrophys J 549:L105–L108

Bedding TR, Kjeldsen H, Butler RP, McCarthy C, Marcy GW, O'Toole SJ, Tinney CG, Wright JT (2004) Oscillation frequencies and mode lifetimes in α Centauri A. Astrophys J 614:380–385

Bedding TR, Butler RP, Carrier F, Bouchy F, Brewer BJ, Eggenberger P, Grundahl F, Kjeldsen H, McCarthy C, Nielsen TB, Retter A, Tinney CG (2006) Solar-like oscillations in the metal-poor subgiant ν Indi: constraining the mass and age using asteroseismology. Astrophys J 647:558–563

Bedding TR, Kjeldsen H, Arentoft T, Bouchy F, Brandbyge J, Brewer BJ, Butler P, Christensen-Dalsgaard J, Dall T, Frandsen S, Karoff C, Kiss LL, Monteiro MJPFG, Pijpers FP, Teixeira TC, Tinney CG, Baldry IK, Carrier F, O'Toole SJ (2007) Solar-like oscillations in the G2 subgiant beta Hydri from dual-site observations. Astrophys J 663:1315–1324

Basri G, Borucki WJ, Koch D (2005) The Kepler Mission: A wide-field transit search for terrestrial planets. NewAR 49:478–485

Basu S, Chaplin WJ, Christensen-Dalsgaard J, Elsworth Y, Isaak GR, New R, Schou J, Thompson MJ, Tomczyk S (1997) Solar internal sound speed as inferred from combined BiSON and LOWL oscillation frequencies. Mon Not R Astr Soc 292:243–251

Basu S, Christensen-Dalsgaard J, Thompson MJ (2002) SOLA inversions for the core structure of solar-type stars. In: Favata F, Roxburgh IW, Galadí-Enríquez D (eds) Proc. 1st Eddington workshop, 'stellar structure and habitable planet finding', ESA SP-485.. ESA Publications Division, Noordwijk, pp 249–252

Basu S., Mazumdar A, Antia HM, Demarque P (2004) Asteroseismic determination of helium abundance in stellar envelopes. Mon Not R Astr Soc 350:277–286

Basu S, Chaplin WJ, Elsworth Y, New R, Serenelli AM, Verner GA (2007) Solar abundances and helioseismology: fine-structure spacings and separation ratios of low-degree p-modes. Astrophys J 655:660–671

Batchelor GK (1953) The theory of homogeneous turbulence. Cambridge University Press, UK

Beckers JM (1982) Differential speckle interferometry. J Modern Optics 29:361–362

Bedding TR, Kjeldsen H (2006) Observations of solar-like oscillations. In: Fletcher K, Thompson M (eds)Proc. of SOHO 18/GONG 2006/HELAS I, Beyond the spherical Sun, ESA SP-624, pp 25.1–25.5

Bedding TR, Kjeldsen H (2007) Asteroseismology from solar-like oscillations. In: Proc. of the 14th Cambridge Workshop on Cool Stars, Stellar Systems, and the Sun, ASP conference Series (in press)

Bennett PD, Harper GM, Brown A, Hummel CA (1996) The masses and radii of the eclipsing binary ζ Aurigae. Astrophys J 471:454–479

Benson JA, Hutter DJ, Elias NM, Bowers PF, Johnston KJ, Hajian AR, Armstrong JT, Mozurkewich D, Pauls TA, Rickard LJ, Hummel CA, White NM, Black D, Denison CS (1997) Multichannel optical aperture synthesis imaging of ζ^1 Ursae Maioris with the navy prototype optical interferometer. Astron J 114:1221–1226

Berdyugina SV, Telting JH, Korhonen H (2003a) Surface imaging of stellar non-radial pulsations. I. Inversions of simulated data. Astron Astrophys 406:273–280

Berdyugina SV, Telting JH, Korhonen H, Schrijvers C (2003b) Surface imaging of stellar non-radial pulsations. II. The β Cepheii star ω^1 Sco. Astron Astrophys 406:281–285

Berger DH, Gies DR, McAlister HA, ten Brummelaar TA, Henry TJ, Sturmann J, Sturmann L, Turner NH, Ridgway ST, Aufdenberg JP, Mérand A (2006) First results from the CHARA Array. IV. The interferometric radii of low-mass stars. Astrophys J 644:475–483

Bergeron J, Monnet G (2002) Scientific drivers for ESO future VLT/VLTI instrumentation. ESO astrophysics symposia, Springer, Hidelberg, ISBN: 3-540-43755-X

Bevington PR, Robinson DK (2003) Data reduction and error analysis for the physical sciences, 3rd ed. McGraw-Hill, New York

Bigot L, Dziembowski WA (2002) The oblique pulsator model revisited. Astron Astrophys 391:235–245

Bigot L, Provost J, Berthomieu G, Dziembowski WA, Goode PR (2000) Non-axisymmetric oscillations of roAp stars. Astron Astrophys 356:218–233

Bigot L, Kervella P, Thévenin F, Ségransan D (2006) The limb darkening of α Centauri B. Matching 3(hydrodynamical models with interferometric measurements. Astron Astrophys 446):635–641

Blackwell DE, Shallis MJ (1977) Stellar angular diameters from infrared photometry. Application to Arcturus and other stars with effective temperatures. Mon Not Roy Astr Soc 180:177–191

Bloomfield P (1976) Fourier analysis of time series: an introduction. Wiley, New York

Boden AF, Lane BF (2001) A preliminary visual orbit of BY Draconis. Astrophys J 547:1071–1076

Boden AF, Koresko CD, van Belle GT, Colavita MM, Dumont PJ, Gubler J, Kulkarni SR, Lane BF, Mobley D, Shao M, Wallace JK, The PTI Collaboration, Henry GW (1999a) The visual orbit of ι Pegasi. Astrophys J 515:356–364

Boden AF, Lane BF, Creech-Eakman MJ, Colavita MM, Dumont PJ, Gubler J, Koresko CD, Kuchner MJ, Kulkarni SR, Mobley DW, Pan XP, Shao M, van Belle GT, Wallace JK, Oppenheimer BR (1999b) The visual orbit of 64 Piscium. Astropys J 527:360–368

Boden AF, Creech-Eakman MJ, Queloz D (2000) The visual orbit and evolutionary state of 12 Bootis. Astrophys J 536:880–890

Boden AF, Sargent AI, Akeson RL, Carpenter JM, Torres G, Latham DW, Soderblom DR, Nelan E, Franz OG, Wasserman LH (2005a) Dynamical masses for low-mass pre-main-sequence stars: a preliminary physical orbit for HD 98800 B. Astrophys J 635:442–451

Boden AF, Torres G, Hummel CA (2005b) Testing stellar models with an improved physical orbit for 12 bootis. Astrophys J 627:464–476

Boden AF, Torres G, Latham DW (2006) A physical orbit for the high proper motion binary HD 9939. Astrophys J 644:1193–1201

Boden AF, Torres G, Sargent AI, Akeson RL, Carpenter JM, Boboltz DA, Massi M, Ghez AM, Latham DW, Johnston KJ, Menten KM, Ros E (2007) Dynamical masses for pre-main sequence stars: a preliminary physical orbit for V773 Tau A. Astrophys J, astro-ph/0706.2376 (in press)

Böhm-Vitense E (1958) Über die Wasserstoffkonvektionszone in Sternen verschiedener Effektivtemperaturen und Leuchtkräfte. Z Astrophys 46:108–143

Bordé P, Coudé du Foresto V, Chagnon G, Perrin G (2002) A catalogue of calibrator stars for long baseline stellar interferometry. Astron Astrophys 393:183–193
Bouchy F, Carrier F (2002) The acoustic spectrum of α Cen A. Astron Astrophys 390:205–212
Bradley PA, Winget DE (1994) An asteroseismological determination of the structure of the DBV white dwarf GD 358. Astrophys J 430:850–857
Bradley PA, Winget DE, Wood MA (1993) The potential for asteroseismology of DB white dwarfs. Astrophys J 406:661–673
Brassard P, Fontaine G (2004) Asteroseismology of the Crystallized ZZ Ceti Star BPM 37093: a Different View (part I). In: Danesy D (ed) SOHO 14 / GONG 2004 workshop: helio- and asteroseismology: towards a golden future, ESA SP-559, pp 333–336
Brassard P, Fontaine G, Wesemael F (1995) The modeling of energy distributions and light curves of ZZ Ceti stars. 1: Basic theory and semianalytic expressions for the emergent flux. Astrophys J Suppl 96:545–580
Breger M (2000) The multiperiodic δ Scuti star 4 Canum Venaticorum: amplitude variability. Mon Not R Astr Soc 313:129–135
Breger M, Pamyatnykh AA (2006) Amplitude variability or close frequencies in pulsating stars—the δ Scuti star FG Vir. Mon Not R Astr Soc 368:571–578
Breger M, Pamyatnykh AA, Zima W, Garrido R, Handler G, Reegen P (2002) Pulsation of the δ Scuti star θ^2 Tau: new multisite photometry and modelling of instability. Mon Not R Astr Soc 336:249–258
Breger M, Lenz P, Antoci V, Guggenberger E, Shobbrook RR, Handler G, Ngwato B, Rodler F, Rodriguez E, López de Coca P, Costa V (2005) Detection of 75+ pulsation frequencies in the δ Scuti star FG Virginis. Astron Astrophys 435:955–965
Briquet M, Aerts C (2003) A new version of the moment method, optimized for mode identification in multiperiodic stars. Astron Astrophys 398:687–696
Brewer BJ, Bedding TR, Kjeldsen H, Stello D (2007) Baysian inference from observations of solar-like oscillations. Astrophys J 654:551–557
Brickhill AJ (1983) The pulsations of ZZ Ceti stars. Mon Not R Astr Soc 204:537–556
Brickhill AJ (1991) The pulsations of ZZ Ceti stars—III. The driving mechanism. Mon Not R ast Soc 251:673–680
Brookes JR, Isaak GR, van der Raay HB (1978) The observation of a rotating body using high-resolution spectroscopy. Mon Not R Astr Soc 185:19–22
Brown TM, Gilliland RL, Noyes RW, Ramsey LW (1991) Detection of possible p-mode oscillations on Procyon. Astrophys J 368:599–609
Brown TM, Christensen-Dalsgaard J, Mihalas B, Gilliland RL (1994) The effectiveness of oscillation frequencies in constraining stellar model parameters. Astrophys J 427:1013–1034
Buscher DF, Bakker EJ, Coleman TA, Creech-Eakman MJ, Haniff CA, Jurgenson CA, Klinglesmith DA, Parameswariah CB, Young JS (2006) The Magdalena Ridge Observatory Interferometer: a high-sensitivity imaging array. In: Gamiz VL, Idell PS, Strojnik MS (eds) Unconventional imaging II, Proc. of the SPIE 6307, pp 63070B
Bruntt H, Kjeldsen H, Buzasi DL, Bedding TR (2005) Evidence for granulation and oscillations in Procyon from photometry with the *WIRE* satellite. Astrophys J 633:440–446
Butler RP, Bedding TR, Kjeldsen H, McCarthy C, O'Toole SJ, Tinney CG, Marcy GW, Wright JT (2004) Ultra-high-precision velocity measurements of oscillations in α Centauri A. Astrophys J 600:L75–L78
Buzasi DL, Bruntt H, Bedding TR, Retter A, Kjeldsen H, Preston HL, Mandeville WJ, Suarez JC, Catanzarite J, Conrow T, Laher R (2005) Altair: The Brightest δ Scuti Star. Astrophys J 619:1072–1076
Canuto VM, Mazzitelli I (1991) Stellar turbulent convection: a new model and applications. Astrophys J 370:295–311
Canuto VM, Mazzitelli I (1992) Further improvements of a new model for turbulent convection in stars. Astrophys J 389:724–730
Canuto VM, Goldman I, Mazzitelli I (1996) Stellar turbulent convection: a self-consistent model. Astrophys J 473:550–559
Carpenter KG, Schrijver CJ, Karovska M (2005) SI—The Stellar imager: results from the vision mission study. In: American Astronomical Society Meeting 207, 23.07, Bulletin of the American Astronomical Society, vol 37, p. 1196
Carrier F., Bourban G. (2003) Solar-like oscillations in the K1 dwarf star α Cen B. Astron Astrophys 406:L23–L26

Carrier F, Bouchy F, Kienzle F, Bedding TR, Kjeldsen H, Butler RP, Baldry IK, O'Toole SJ, Tinney CG, Marcy GW (2001) Solar-like oscillations in vec Hydri: Confirmation of a stellar origin for the excess power. Astron Astrophys 378:142–145

Carrier F, Eggenberger P, Bouchy F (2005) New seismological results on the G0IV η Bootis. Astron Astrophys 434:1085–1095

Carrier F, Kjeldsen H, Bedding TR, Brewer BJ, Butler RP, Eggenberger P, Grundahl F, McCarthy C, Retter A, Tinney CG (2007) Solar-like oscillations in the metal-poor subgiant ν Indi. II. Acoustic spectrum and mode lifetime. Astron Astrophys 470:1059–1063

Castanheira BG, Nitta A, Kepler SO, Winget DE, Koester D (2005) HST observations of the pulsating white dwarf GD 358. Astron Astrophys 432:175–179

Catala C, Aerts C, Aigrain S, Antonello E, Appourchaux T, Auvergne M, Baglin A, Barge P, Barstow MA, Baudin F, Boumier P, Cameron AC, Christensen-Dalsgaard J, Cutispoto G, Deeg H, Deleuil M, Desidera S, Donati JF, Favata F, Foing BH, Gameiro JF, Garcia R, Garrido F, Horne K, Lanza AF, Lanzafame AC, Lecavelier des Etangs A, Léger A, Mas-Hesse M, Messina S, Micela G, Michel E, Monteiro MJPFG, Mosser B, Noels A, Pagano I, Piotto G, Poretti E, Rauer H, Roca-Cortes T, Rodono M, Rouan D, Roxburgh I, Schneider J, Strassmeier K, Turck-Chièze S, Vauclair S, Vidal-Madjar A, Weiss WW, Wheatley P (2005) The Life of Stars and Their Planets. In: Favata F, Sanz-Forcada J, Giménez A (eds) Proc. 39th ESLAB symposium on trends in space science and cosmic vision 2020, ESA SP-588, Noordwijk, The Netherlands, pp 99–104

Chandrasekhar S (1964) A general variational principle governing the radial and the non-radial oscillations of gaseous masses. Astrophys J 139:664–674

Chaplin WJ, Elsworth Y, Isaak GR, Marchenkov KI, Miller BA, New R, Pinter B, Appourchaux T (2002a) Peak finding at low signal-to-noise: low-ℓ solar acoustic eigenmodes at $n \leq 9$ from the analysis of BiSON data. Mon Not R Astr Soc 336:979–991

Chaplin WJ, Elsworth Y, Isaak GR, Miller BA, New R (2002b) On the measurement precision of solar p-mode eigenfrequencies. Mon Not R Astr Soc 330:731–736

Chaplin WJ, Houdek G, Elsworth Y, Gough DO, Isaak GR, New R (2005) On model predictions of the power spectral density of radial solar p modes. Mon Not R Astr Soc 360:859–868

Chaplin WJ, Appourchaux T, Baudin F, Boumier P, Elsworth Y, Fletcher ST, Fossat E, García RA, Isaak GR, Jiménez A, Jiménez-Reyes SJ, Lazrek M, Leibacher JW, Lochard J, New R, Pallé P, Régulo C, Salabert D, Seghouani N, Toutain T, Wachter R (2006) Solar FLAG hare and hounds: on the extraction of rotational p-mode splittings from seismic, Sun-as-a-star data. Mon Not R Astr Soc 369:985–996

Chaplin WJ, Elsworth Y, Miller BA, Verner GA (2007) Solar p-mode frequencies over three solar cycles. Astrophys J 659:1749–1760

Chelli A, Petrov RG (1995) Model fitting and error analysis for differential interferometry. II. Application to rotating stars and binary systems. Astron Astophys Suppl Ser 109:401–415

Chlebowski T (1978) Nonradial oscillations of slowly rotating white dwarfs. Acta Astron 28:441–463

Christensen-Dalsgaard J (1980) On adiabatic non-radial oscillations with moderate or large l. Mon Not R Astr Soc 190:765–791

Christensen-Dalsgaard J (1982) On solar models and their periods of oscillation. Mon Not R Astr Soc 199:735–761

Christensen-Dalsgaard J (1984) What will asteroseismology teach us? In: Mangeney A, Praderie F (eds) Space research prospects in stellar activity and variability. Paris Observatory Press, Paris, pp 11–45

Christensen-Dalsgaard J (1988) A Hertzsprung-Russell diagram for stellar oscillations. In: Christensen-Dalsgaard J, Frandsen S (eds) Proc. IAU symposium No 123, advances in helio- and asteroseismology. Reidel, Dordrecht, pp 295–298

Christensen-Dalsgaard J (1989) The effect of rotation on whole-disc Doppler observations of solar oscillations. Mon Not R Astr Soc 239:977–994

Christensen-Dalsgaard J (1991) Some aspects of the theory of solar oscillations. Geophys Astrophys Fluid Dyn 62:123–152

Christensen-Dalsgaard J (2002) Helioseismology. Rev Mod Phys 74:1073–1129

Christensen-Dalsgaard J (2004) Physics of solar-like oscillations. Solar Phys 220:137–168

Christensen-Dalsgaard J (2007) ASTEC – the Aarhus STellar evolution code. Astrophys Space Sci (in press)

Christensen-Dalsgaard J, Berthomieu G (1991) Theory of solar oscillations. In: Cox AN, Livingston WC, Matthews M (eds) Solar interior and atmosphere, Space science series. University of Arizona Press, Arizona, pp 401–478

Christensen-Dalsgaard J, Frandsen S (1983) Stellar 5 min oscillations. Solar Phys 82:469–486

Christensen-Dalsgaard J, Gough DO (1980) Is the Sun helium-deficient? Nature 288:544–547
Christensen-Dalsgaard J, Gough DO (1982) On the interpretation of five-minute oscillations in solar spectrum line shifts. Mon Not R Astr Soc 198:141–171
Christensen-Dalsgaard J, Thompson MJ (1997) On solar p-mode frequency shifts caused by near-surface model changes. Mon Not R Astr Soc 284:527–540
Christensen-Dalsgaard J, Duvall TL Jr, Gough DO, Harvey JW, Rhodes EJ Jr (1980) Speed of sound in the solar interior. Nature 315:378–382
Christensen-Dalsgaard J, Gough DO, Libbrecht KG (1989) Seismology of solar oscillation line widths. Astrophys J 341:L103–L106
Christensen-Dalsgaard J, Bedding TR, Kjeldsen H (1995) Modelling solar-like oscillations in η Bootis. Astrophys J 443:L29–L32
Christensen-Dalsgaard J, Däppen W, Ajukov SV, Anderson ER, Antia HM, Basu S, Baturin VA, Berthomieu G, Chaboyer B, Chitre SM, Cox AN, Demarque P, Donatowicz J, Dziembowski WA, Gabriel M, Gough DO, Guenther DB, Guzik JA, Harvey JW, Hill F, Houdek G, Iglesias CA, Kosovichev AG, Leibacher JW, Morel P, Proffitt CR, Provost J, Reiter J, Rhodes EJ Jr, Rogers FJ, Roxburgh IW, Thompson MJ, Ulrich RK (1996) The current state of solar modeling. Science 272:1286–1292
Christensen-Dalsgaard J, Arentoft T, Brown TM, Gilliland RL, Kjeldsen H, Borucki WJ, Koch D (2007) Asteroseismology with the *Kepler mission*. In: Handler G, Houdek G (eds) Proc. Vienna workshop on the future of asteroseismology, Comm. in asteroseismology vol 150, pp 350–356
Christy RF (1966) A study of pulsation in RR Lyrae models. Astrophys J 144:108–179
Claret A (2000) A new non-linear limb-darkening law for LTE stellar atmosphere models. Calculations for $-5.0 \leq \log$ M/H $\leq +1$,2000 K $\leq$ Teff $\leq$ 50000 K at several surface gravities. Astron Astrophys 363:1081–1190
Colavita MM, Wallace JK, Hines BE, Gursel Y, Malbet F, Palmer DL, Pan XP, Shao M, Yu JW, Boden AF, Dumont PJ, Gubler J, Koresko CD, Kulkarni SR, Lane BF, Mobley DW, van Belle GT (1999) The palomar testbed interferometer. Astrophys J 510:505–521
Colavita MM, Wizinowich PL, Akeson RL (2004) Keck interferometer status and plans. In: Traub WA (ed) New frontiers in stellar interferometry, Proc. of the SPIE, vol 5491, pp 454–463
Cox JP (1974) Pulsating stars. Rep Prog Phys 37:563–698
Cox JP, Giuli RT (1968) Principles of stellar structure. Gordon and Breach, New York
Cox JP, Whitney C (1958) Stellar pulsation. IV. A semitheoretical period-luminosity relation for classical Cepheids. Astrophys J 127:561–572
Creevey OL, Monteiro MJPFG, Metcalfe TM, Brown TM, Jiménez-Reyes SJ, Belmonte JA (2007) The complementary roles of interferometry and asteroseismology in determining the mass of solar-type stars. Astrophys J 659:616–625
Cunha MS (2001) The sixth frequency of roAp star HR 1217. Mon Not R Astr Soc 325:373–378
Cunha MS (2002) A theoretical instability strip for rapidly oscillating Ap stars. Mon Not R Astr Soc 333:47–54
Cunha MS (2005) Asteroseismic theory of rapidly oscillating Ap Stars. J Astrophys Astron 26:213
Cunha MS (2006) Improved pulsating models of magnetic Ap stars—I. Exploring different magnetic field configurations. Mon Not R Astr Soc 365:153–164
Cunha MS (2007) Theory of rapidly oscillating Ap stars. In: Handler G, Houdek G (eds) Proc. Vienna workshop on the future of asteroseismology, Comm. in Asteroseismology, vol. 150, pp 48–54
Cunha MS, Gough D (2000) Magnetic perturbations to the acoustic modes of roAp stars. Mon Not R Astr Soc 319:1020–1038
Cunha MS, Metcalfe TS (2007) Asteroseismic signatures of small convective cores: theoretical analysis. Astrophys J 666:413–422
Cunha MS, Fernandes JMMB, Monteiro MJPFG (2003) Seismic tests of the structure of rapidly oscillating Ap stars: HR 1217. Mon Not R Astr Soc 343:831–838
Cunha MS, Theádo S, Vauclair S (2004) Excitation of the oscillations in roAp stars: Magnetic fields, diffusion, and winds In: IAU symp. No. 224,The A-Star Puzzle:Cambridge University Press, UK, pp 359–365
Cutri RM, Skrutskie MF, Van Dyk S, Beichman CA, Carpenter JM, Chester T, Cambresy L, Evans T, Fowler J, Gizis J, Howard E, Huchra J, Jarrett T, Kopan EL, Kirkpatrick JD, Light RM, Marsh KA, McCallon H, Schneider S, Stiening R, Sykes M, Weinberg M, Wheaton WA, Wheelock S, Zacarias N (2003) 2MASS all sky catalog of point sources. University of Massachusetts and IPAC, http://www.ipac.caltech.edu/2mass.

Danchi WC, Bester M, Degiacomi CG, Greenhill LJ, Townes C (1994) Characteristics of dust shells around 13 late-type stars. Astron J 107:1469–1513

Daszyńska-Daszkiewicz J, Dziembowski WA, Pamyatnykh AA, Goupil MJ (2002) Photometric amplitudes and phases of nonradial oscillation in rotating stars. Astron Astrophys 392:151–159

Daszyńska-Daszkiewicz J, Dziembowski WA, Pamyatnykh AA, Breger M, Zima W, Houdek G (2005) Inferences from pulsational amplitudes and phases for multimode δ Scuti star FG Vir. Astron Astrophys 438:653–660

Daszyńska-Daszkiewicz J, Dziembowski WA, Pamyatnykh AA (2006) On the nature of small amplitude peaks in δ Scuti oscillation spectra. Mem Soc Astron Ital 77:113–116

Davis J, Tango WJ, Booth AJ, ten Brummelaar TA, Minard RA, Owens SM (1999) The Sydney University Stellar Interferometer—I. The instrument. Mon Not Ry Astr Soc 303:773–782

Davis J, Mendez A, Seneta EB, Tango WJ, Booth AJ, O'Byrne JW, Thorvaldson ED, Ausseloos M, Aerts C, Uytterhoeven K (2005) Orbital parameters, masses and distance to β Centauri determined with the Sydney University Stellar Interferometer and high-resolution spectroscopy. Mon Not Roy Astr Soc 356:1362–1370

De Cat P, Aerts C (2002) A study of bright southern slowly pulsating B stars. II. The intrinsic frequencies. Astron Astrophys 393:965–981

De Cat P, Aerts C, De Ridder J, Kolenberg K, Meeus G, Decin L (2000) A study of bright southern slowly pulsating B stars. I. Determination of the orbital parameters and of the main frequency of the spectroscopic binaries. Astron Astrophys 355:1015–1030

De Cat P, Briquet M, Daszyńska-Daszkiewicz J, Dupret MA, De Ridder J, Scuflaire R, Aerts C (2005) A study of bright southern slowly pulsating B stars. III. Mode identification for singly-periodic targets in spectroscopy. Astron Astrophys 432:1013–1024

De Cat P, Eyer L, Cuypers J, Aerts C, Vandenbussche B, Uytterhoeven K, Reyniers K, Kolenberg K, Groenewegen M, Raskin G, Maas T, Jankov S (2006) A spectroscopic study of southern (candidate) γ Doradus stars. I. Time series analysis. Astron Astrophys 449:281–292

De Cat P, Briquet M, Aerts C, Goossens K, Saesen S, Cuypers J, Yakut K, Scuflaire R, Dupret MA, Uytterhoeven K, van Winckel H, Raskin G, Davignon G, Le Guillou L, van Malderen R, Reyniers M, Acke B, de Meester W, Vanautgaerden J, Vandenbussche B, Verhoelst T, Waelkens C, Deroo P, Reyniers K, Ausseloos M, Broeders E, Daszy ska-Daszkiewicz J, Debosscher J, de Ruyter S, Lefever K, Decin G, Kolenberg K, Mazumdar A, van Kerckhoven C, de Ridder J, Drummond R, Barban C, Vanhollebeke E, Maas T, Decin L (2007) Astron Astrophys 463:243–249

De Ridder J, Dupret MA, Neuforge C, Aerts C (2002) Influence of non-adiabatic temperature variations on line profile variations of slowly rotating β Cep stars and SPBs. II. Simulations of line profile time series. Astron Astrophys 385:572–584

De Ridder J, Telting JH, Balona LA, Handler G, Briquet M, Daszyńska-Daszkiewicz J, Lefever K, Korn AJ, Heiter U, Aerts C (2004) Asteroseismology of the β Cephei star ν Eridani—III. Extended frequency analysis and mode identification. Mon Not R ast Soc 351:324–332

Delplancke F, Derie F, Lévêque S, Ménardi S, Abuter R, Andolfato L, Ballester P, de Jong J, Di Lieto N, Duhoux Ph, Frahm R, Gitton Ph, Glindemann A, Palsa R, Puech F, Sahlmann J, Schuhler N, Duc Th Ph, Valat B, Wallander A (2006) PRIMA for the VLTI: a status report. In: Monnier JD, Schöller M, Danchi WC (eds) Advances in stellar interferometry: Proc. of the SPIE, vol 6268, p 62680U

Deubner FL, Gough DO (1984) Helioseismology: oscillations as a diagnostic of the solar interior. Annu Rev Astron Astrophys 22:593–619

Di Folco E, Thévenin F, Kervella P, Domiciano de Souza A, Coudé du Foresto V, Ségransan D, Morel P (2004) VLTI near-IR interferometric observations of Vega-like stars. Radius and age of α PsA, β Leo, β Pic, ϵ Eri and τ Cet. Astron Astrophys 426:601–617

Di Mauro MP, Christensen-Dalsgaard J, Paternò L (2003) A Study of the Solar-Like Properties of Hydri. Astrophys Space Sci 284:229–232

Di Mauro MP, Christensen-Dalsgaard J, Paternó L, D'Antona F (2004) Interpretation of the solar-like pulsational behaviour of η Bootis. Solar Phys 220:185–198

Domiciano de Souza A, Vakili F, Jankov S, Janot-Pacheco E, Abe L (2002) Modelling rapid rotators for stellar interferometry. Astron Astrophys 393:345–357

Domiciano de Souza A, Kervella P, Jankov S, Abe L, Vakili F, di Folco E, Paresce F (2003) The spinning-top Be star Achernar from VLTI-VINCI. Astron Astrophys 407:L47–L50

Domiciano de Souza A, Zorec J, Jankov S, Vakili F, Abe L, Janot-Pacheco E (2004) Stellar differential rotation and inclination angle from spectro-interferometry. Astron Astrophys 418:781–794

Domiciano de Souza A, Kervella P, Jankov S, Vakili F, Ohishi N, Nordgren TE, Abe L (2005) Gravitational-darkening of Altair from interferometry. Astron Astrophys 442:567–578
Dravins D, Nordlund A (1990a) Stellar Granulation—Part Four—Line Formation in Inhomogeneous Stellar Photospheres. Astron Astrophys 228:184–202
Dravins D, Nordlund A (1990b) Stellar Granulation—Part Five—Synthetic Spectral Lines in Disk Integrated Starlight. Astron Astrophys 228:203–217
Dupret MA, De Ridder J, De Cat P, Aerts C, Scuflaire R, Noels A, Thoul A (2003) A photometric mode identification method, including an improved non-adiabatic treatment of the atmosphere. Astron Astrophys 398:677–685
Dupret MA, Grigahcène A, Garrido R, Gabriel M, Scuflaire R (2004) Theoretical instability strips for δ Scuti and γ Doradus stars. Astron Astrophys 414:L17–L20
Dupret MA, Grigahcène A, Garrido R, Gabriel M, Scuflaire R (2005a) Convection-pulsation coupling. II. Excitation and stabilization mechanisms in δ Scuti and γ Doradus stars. Astron Astrophys 435:927–939
Dupret MA, Grigahcène A, Garrido R, De Ridder J, Scuflaire R, Gabriel M (2005b) Time-dependent convection seismic study of five γ Doradus stars. Mon Not R Astr Soc 360:1143–1152
Dupret MA, Grigahcène A, Garrido R, De Ridder J, Scuflaire R, Gabriel M (2005c) Time-dependent convection seismic study of δ Sct stars. Mon Not R Astr Soc 361:476–486
Duvall TL Jr (1982) A dispersion law for solar oscillations. Nature 300:242–243
Duvall TL Jr, Dziembowski WA, Goode PR, Gough DO, Harvey JW, Leibacher JW (1982) Internal rotation of the sun. Nature 310:22–25
Dyck HM (2000) Interferometry with Two Telescopes. In: Lawson PR (ed) Principles of long baseline stellar interferometry. Published by NASA, JPL, CIT, Pasadena, pp 185–202
Dziembowski WA (1977) Light and radial velocity variations in a nonradially oscillating star. Acta Astron 27:203–211
Dziembowski WA, Goode PR (1992) Effects of differential rotation on stellar oscillations: a second-order theory. Astrophys J 394:670–687
Dziembowski WA, Goode PR (1996) Magnetic effects on oscillations in roAp stars. Astrophys J 458:338–346
Dziembowski W, Królikowska M (1985) Nonlinear mode coupling in oscillating stars. II. Limiting amplitude effect of the parametric resonance in main sequence stars. Acta Astron 35:5–28
Dziembowski WA, Gough DO, Houdek G, Sienkiewicz R (2001) Oscillations of α UMa and other red giants. Mon Not R Astr Soc 328:601–610
Eddington AS (1926) The internal constitution of the stars. Cambridge University Press, Cambridge
Edmonds PD, Cram LE (1995) A search for global acoustic oscillations on α^1 Cen and β Hyi. Mon Not R Astr Soc 276:1295–1302
Eggenberger P, Charbonnel C, Talon S, Meynet G, Maeder A, Carrier F, Bourban G (2004) Analysis of α Centauri AB including seismic constraints. Astron Astrophys 417:235–246
Eisner JA, Graham JR, Akeson RL, Ligon ER, Colavita MM, Basri G, Summers K, Ragland S, Booth A (2007) Stellar and molecular radii of a Mira star: first observations with the Keck interferometer grism. Astrophys J 654:L77–L80
Ellis AN (1984) The base of the solar convection zone. In: Theoretical problems in stellar stability and oscillations, Institute d'Astrophysique, Liège, pp 298–301
Ellis AN (1986) An improved asymptotic formula for solar gravity-mode periods. In: Gough DO (ed) Seismology of the Sun and the distant stars. Reidel, Dordrecht, pp 173–175
Fernandes J, Monteiro MJPFG (2003) HR diagram and asteroseismic analysis of models for beta Hydri. Astron Astrophys 399:243–251
Feuchtinger MU (1999) A nonlinear convective model for radial stellar pulsations. I. The physical description. Astron Astrophys Suppl 136:217–226
Fletcher ST, Chaplin WJ, Elsworth Y, Schou J, Buzasi D (2006) Frequency, splitting, linewidth and amplitude estimates of low-ℓ p modes of α Cen A: analysis of wide-field infrared explorer photometry. Mon Not R Astr Soc 371:935–944
Fontaine G, Brassard P (2005) Asteroseismology of the crystallized ZZ ceti Star BPM 37093: a different view (Part II). In: Koester D, Moehler S (eds) 14th European Workshop on White Dwarfs. ASP Conference Series, vol 334, p 565
Fontaine G, Brassard P, Charpinet S, Green EM, Chayer P, Billères M, Randall SK (2003) A driving mechanism for the newly discovered long-period pulsating subdwarf B stars. Astrophys J 597:518–534

Frandsen S (1987) An upper limit on p-mode amplitudes in β Hyi. Astron Astrophys 181:289–292
Frandsen S, Carrier F, Aerts C, Stello D, Maas T, Burnet M, Bruntt H, Teixeira TC, de Medeiros JR, Bouchy F, Kjeldsen H, Pijpers F, Christensen-Dalsgaard J (2002) Detection of solar-like oscillations in the G7 giant star ξ Hya. Astron Astrophys 394:L5–L8
Frazier EN (1968) A spatio-temporal analysis of velocity fields in the solar photosphere. Zeitschrift fr Astrophysik 68:345–356
Gabriel M (1996) Solar oscillations: theory. Bull Astr Soc India 24:233–243
Gabriel M (2000) Linear interaction between pulsations and convection, scattering and line profiles of solar p-modes. Astron Astrophys 353:399–408
Gabriel M, Scuflaire R, Noels A, Boury A (1974) Influence de la convection sur la stabilité des oscillations non radiales des étoiles. Bull Acad R Belg Classe des Sc, 5^{e} Série 60:866–887
Gabriel M, Scuflaire R, Noels A, Boury A (1975) Influence of convection on the vibrational stability of stars towards non-radial oscillations. Astron Astrophys 40:33–39
García RA, Régulo C, Turck-Chièze S, Bertello L, Kosovichev AG, Brun AS, Couvidat S, Henney CJ, Lazrek M, Ulrich RK, Varadi F (2001) Low-degree low-order solar p modes as seen by GOLF on board SOHO. Solar Phys 200:361–379
Garrido R (2000) Photometric modal discrimination in δ Scuti and γ Doradus stars. In: Breger M, Montgomery MH (eds) Delta Scuti and related stars, ASP Conference Series, vol 210, San Francisco, pp 67–98
Gehmeyr M (1993) On nonlinear radial oscillations in convective RR Lyrae stars. III. A full-amplitude investigation of the red edge. Astrophys J 412:341–350
Gehmeyr M, Winkler KHA (1992) On a new one-dimensional, time-dependent model for turbulence and convection. I. A basic discussion of the mathematical model. Astron Astrophys 253:92–100
Gies DR, Kullavanijaya A (1988) The line profile variations of Epsilon Persei. I - Evidence for multimode nonradial pulsations. Astrophys J 326:813–831
Gillessen S, Perrin G, Brandner W, Straubmeier C, Eisenhauer F, Rabien S, Eckart A, Lena P, Genzel R, Paumard T, Hippler S (2006) GRAVITY: the adaptive-optics-assisted two-object beam combiner instrument for the VLTI. In: Monnier JD, Schöller M, Danchi WC (eds) Advances in stellar interferometry, Proc. SPIE vol 6268, p 626811
Gilliland RL, Brown TM, Kjeldsen H, McCarthy JK, Peri ML, Belmonte JA, Vidal I, Cram LE, Palmer J, Frandsen S, Parthasarathy M, Petro L, Schneider H, Stetson PB, Weiss WW (1993) A search for solar-like oscillations in the stars of M67 with CCD ensemble photometry on a network of 4 m telescopes. Astron J 106:2441–2476
Gizon L, Solanki S (2003) Determining the inclination of the rotation axis of a Sun-like star. Astrophys J 589:1009–1019
Gizon L, Solanki S (2004) Measuring stellar differential rotation with asteroseismology. Solar Phys 220:169–184
Glindemann A, Abuter R, Carbognani F, Delplancke F, Derie F, Gennai A, Gitton PB, Kervella P, Koehler B, Leveque SA, Menardi S, Michel A, Paresce F, Duc, Th. P., Richichi A, Schoeller M, Tarenghi M, Wallander A, Wilhelm R (2000) The VLT interferometer: a unique instrument for high-resolution astronomy. In: Léna PJ, Quirrenbach A (eds) Interferometry in optical astronomy, Proc. SPIE, 4006, pp 2–12
Glindemann A, Albertsen M, Avila G, Ballester P, Bauvir B, Delplancke F, Derie F, et al. (2004) VLTI technical advances: present and future. In: Traub WA (ed) New frontiers in stellar interferometry, Proc. SPIE, 5491, p 447
Goldreich P, Keeley DA (1977) Solar seismology. II. The stochastic excitation of the solar p-modes by turbulent convection. Astrophys J 212:243–251
Goldreich P, Wu Y (1999) Gravity modes in ZZ Ceti stars. I. Quasi-adiabatic analysis of overstability. Astrophys J 511:904–915
Gonczi G (1981) On local theories of time dependent convection in the stellar pulsation problem. Astron Astrophys 96:138–141
Goodman JW (1985) Statistical Optics. Wiley, New York
Gough DO (1977a) Random remarks on solar hydrodynamics. In: Bonnet RM, Delache Ph (eds) The energy balance and hydrodynamics of the solar chromosphere and corona. G.de Bussac, Clermont-Ferrand, pp 3–36
Gough DO (1977b) Mixing-length theory for pulsating stars. Astrophys J 214:196–213

Gough DO (1977c) The current state of stellar mixing-length theory. In: Spiegel EA, Zahn JP (eds) Problems of stellar convection, IAU Colloq. No. 38, Lecture notes in physics vol 71. Springer, Berlin, pp 15–56
Gough DO (1978) The significance of solar oscillations. In: Pleins feux sur la physique solaire. Proc. 2me Assemblée Européenne de Physique Solaire. CNRS, Paris, pp 81–103
Gough DO (1981) A new measure of the solar rotation. Mon Not R Astr Soc 196:731–745
Gough DO (1985a) Theory of solar oscillations. In: Rolfe E, Battrick B (eds) Future missions in solar, heliospheric and space plasma physics, ESA SP-235, ESTEC, Noordwijk, pp 183–197
Gough DO (1985b) Inverting helioseismic data. Solar Phys 100:65–99
Gough DO (1986) EBK quantization of stellar waves. In: Osaki Y (ed) Hydrodynamic and magnetohydrodynamic problems in the Sun and stars, Department of Astronomy, University of Tokyo, Tokyo, pp 117–143
Gough DO (1987) Seismological measurement of stellar ages. Nature 326:257–259
Gough DO (1993) Course 7. In: Linear adiabatics tellar pulsation. Zahn JP, Zinn-Justin J (eds) Astrophysical fluid dynamics, Les Houches Session XLVII. Elsevier, Amsterdam, pp 399–560
Gough DO, Kosovichev AG (1990) Using helioseismic data to probe the hydrogen abundance in the solar core. In: Berthomieu G, Cribier M (eds) Proc. IAU Colloquium No 121, Inside the Sun. Kluwer, Dordrecht, pp 327–340
Gough DO, Thompson MJ (1990) The effect of rotation and a buried magnetic field on stellar oscillations. Mon Not R Astr Soc 242:25–55
Gough DO, Kosovichev AG, Toomre J, Anderson ER, Antia HM, Basu S, Chaboyer B, Chitre SM, Christensen-Dalsgaard J, Dziembowski WA, Eff-Darwich A, Elliott JR, Giles PM, Goode PR, Guzik JA, Harvey JW, Hill F, Leibacher JW, Monteiro MJPFG, Richard O, Sekii T, Shibahashi H, Takata M, Thompson MJ, Vauclair S, Vorontsov SV (1996) The seismic structure of the Sun. Science 272:1296–1300
Goupil MJ, Samadi R, Lochard J, Dziembowski WA, Pamyatnykh A (2004) Inferring information about rotation from stellar oscillations. In: Favata F, Aigrain S (eds) Proc. 2nd Eddington workshop, stellar structure and habitable planet finding, ESA SP-538. ESA Publications Division, Noordwijk, The Netherlands, pp 133–140
Gray DF (1977) A quest for differential stellar rotation in A stars. Astrophys J 211:198–206
Grec G, Fossat E, Pomerantz M (1980) Solar oscillations: full disk observations from the geographic South Pole. Nature 288:541–544
Grigahcène A, Dupret MA, Gabriel M, Garrido R, Scuflaire R (2005) Convection-pulsation coupling. I. A mixing-length perturbative theory. Astron Astrophys 434:1055–1062
Grundahl F, Kjeldsen H, Christensen-Dalsgaard J, Arentoft T, Frandsen S (2007) Stellar oscillations network group. In: Handler G, Houdek G (eds) Proc. Vienna workshop on the future of Asteroseismology, Comm. in asteroseismology, vol 150, pp 300–306
Guenther DB (2004) Quantitative analysis of the oscillation spectrum of η Bootis. Astrophys J 612:454–462
Guenther DB, Brown KIT (2004) Matching stellar models to oscillation data. Astrophys J 600:419–434
Guenther DB, Demarque P (1996) Seismology of η Bootis. Astrophys J 456:798–810
Guzik JA (2006) Reconciling the revised solar abundances with helioseismic constraints. In: Fletcher K (ed)Proc. SOHO 18 / GONG 2006 / HELAS I Conf. beyond the spherical Sun, ESA SP-624, ESA Publications Division, Noordwijk, The Netherlands, pp 17.1–17.11
Guzik JA, Kaye AB, Bradley PA, Cox AN, Neuforge C (2000) Driving the gravity-mode pulsations in γ Doradus variables. Astrophys J 542:L57–L60
Hajian AR, Armstrong JT, Hummel CA, Benson JA, Mozurkewich D, Pauls TA, Hutter DJ, Elias NM, Johnston KJ, Rickard LJ, White NM (1998) Direct confirmation of stellar limb darkening with the Navy Prototype Optical Interferometer. Astrophys J 496:484–489
Hale DDS, Weiner J, Townes CH (2004) ISI: recent technology and science. In: Traub WA (ed) New frontiers in stellar interferometry, Proc. SPIE 5491, pp 490–498
Hanbury Brown R, Davis J, Allen R (1974a) The angular diameters of 32 stars. Mon Not R Astr Soc 167:121–136
Hanbury Brown R, Davis J, Lake RJW, Thompson RJ (1974b) The effects of limb darkening on measurements of angular size with an intensity interferometer. Mon Not R Astr Soc 167:475–484
Handler G, Arentoft T, Shobbrook RR, Wood MA, Crause LA, Crake P, Podmore F, Habanyama A, Oswalt T, Birch PV, Lowe G, Sterken C, Meintjes P, Brink J, Claver CF, Medupe R, Guzik JA, Beach TE, Martinez P, Leibowitz EM, Ibbetson PA, Smith T, Ashoka BN, Raj NE, Kurtz DW, Balona LA, O'Donoghue D, Costa JES, Breger M (2000) Delta Scuti Network observations of XX Pyx: detection

of 22 pulsation modes and of short-term amplitude and frequency variations. Mon Not R Astr Soc 318:511–525

Handler G, Shobbrook RR, Vuthela FF, Balona LA, Rodler F, Tshenye T (2003) Asteroseismological studies of three ? Cephei stars: IL Vel, V433 Car and KZ Mus. Mon Not R Astr Soc 341:1005–1019

Handler G, Shobbrook RR, Jerzykiewicz M, Krisciunas K, Tshenye T, Rodríguez E, Costa V, Zhou AY, Medupe R, Phorah WM, Garrido R, Paparó M, Zsuffa D, Ramokgali L, Crowe R, Purves N, Avila R, Knight R, Brassfield E, Kilmartin PM, Cottrell PL (2004) Asteroseismology of the β Cephei star ν Eridani—I. Photometric observations and pulsational frequency analysis. Mon Not R Astr Soc 347:454–462

Handler G, Shobbrook RR, Mokgwetsi T (2005) An asteroseismic study of the β Cepehi star θ Ophiuchi: photometric results. Mon Not R Astr Soc 362:612–618

Handler G, Jerzykiewicz M, Rodríguez E, Uytterhoeven K, Amado PJ, Dorokhova TN, Dorokhov NI, Poretti E, Sareyan JP, Parrao L, Lorenz D, Zsuffa D, Drummond R, Daszyńska-Daszkiewicz J, Verhoelst T, De Ridder J, Acke B, Bourge PO, Movchan AI, Garrido R, Paparó M, Sahin T, Antoci V, Udovichenko SN, Csorba K, Crowe R, Berkey B, Stewart S, Terry D, Mkrtichian DE, Aerts C (2006) Asteroseismology of the β Cephei star 12 (DD) Lacertae: photometric observations, pulsational frequency analysis and mode identification. Mon Not R Astr Soc 365:327–338

Hansen CJ, Cox JP, van Horn HM (1977) The effects of differential rotation on the splitting of nonradial modes of stellar oscillation. Astrophys J 217:151–159

Hao J (1998) Line profile analysis of nonradial pulsation modes based on Doppler imaging. Astrophys J 500:440–448

Hauschildt PH, Allard F, Ferguson J, Baron E, Alexander DR (1999) The NEXTGEN model atmosphere grid. II. Spherically symmetric model atmospheres for giant stars with effective temperatures between 3000 and 6800 K. Astrophys J 525:871–880

Hekker S, Caerts C, De Ridder J, Carrier F (2006) Pulsations detected in the line profile variations of red giants. Modelling of line moments, line bisector and line shape. Astron Astrophys 458:931–940

Henyey LG, Vardya MS, Bodenheimer P (1965) Studies in stellar evolution. III. The calculation of model envelopes. Astrophys J 142:841–854

Herbison-Evans D, Hanbury Brown R, Davis J, Allen LR (1971) A study of α Virginis with an intensity interferometer. Mon Not Roy Astr Soc 151:161–176

Heynderickx D, Waelkens C, Smeyers P (1994) A photometric study of β Cephei stars. II. Determination of the degrees L of pulsation modes. Astron Astrophys Suppl 105:447–480

Hoffleit D (1997) History of the discovery of Mira stars. JAVSO 25:115–136

Houdek G (2000) Convective effects on p-mode stability in Delta Scuti stars. In: Breger M, Montgomery MH (eds) Delta Scuti and related stars, ASP Conference Series, vol 210, San Francisco, pp 454–463

Houdek G (2002) Stochastic excitation in solar-type stars. In: Aerts C, Bedding TR, Christensen-Dalsgaard J (eds) Proc. IAU Colloq. 185: Radial and nonradial pulsations as probes of stellar physics, ASP Conference Series, vol 259, pp 447–455

Houdek G (2004) Asteroseismic helium abundance determination. In: Čelebonović V, Däppen W, Gough D (eds) Equation-of-state and phase-transition issues in models of ordinary astrophysical matter, AIP Conference Proceedings vol 731, AIP, Melville, New York, pp 193–207

Houdek G (2006) Stochastic excitation and damping of solar-type oscillations. In: Fletcher K (ed) Proc. SOHO 18 / GONG 2006 / HELAS I Conf. Beyond the spherical Sun, ESA SP-624, ESA Publications Division, Noordwijk, pp 28.1–28.12

Houdek G, Gough DO (2002) Modelling pulsation amplitudes of ξ Hydrae. Mon Not R Astr Soc 336:L65–L69

Houdek G, Gough DO (2006) On seismic signatures of rapid variation. In: Fletcher K (ed) Proc. SOHO 18 / GONG 2006 / HELAS I Conference Beyond the spherical Sun, ESA SP-624, ESA Publications Division, Noordwijk pp 88.1–88.6

Houdek G, Gough DO (2007) An asteroseismic signature of helium ionization. Mon Not R Astr Soc 375:861–880

Houdek G, Balmforth NJ, Christensen-Dalsgaard J, Gough DO (1999) Amplitudes of stochastically excited oscillations in main-sequence stars. Astron Astrophys 351:582–596

Hummel CA, Armstrong JT, Quirrenbach A, Buscher DF, Mozurkewich D, Simon RS, Johnston KJ (1993) The spectroscopic binary η Andromedae: determination of the orbit by optical interferometry. Astron J 106:2486–2492

Hummel CA, Armstrong JT, Quirrenbach A, Buscher DF, Mozurkewich D, Elias NM, Wilson RE (1994) Very high precision orbit of Capella by long baseline interferometry. Astron J 107:1859–1867

Hummel CA, Armstrong JT, Buscher DF, Mozurkewich D, Quirrenbach A, Vivekanand M (1995) Orbits of small angular scale binaries resolved with the Mark III interferometer. Astron J 110:376–390

Hummel CA, Mozurkewich D, Armstrong JT, Hajian AR, Elias NM, Hutter DJ (1998) Navy Prototype Optical Interferometer Observations of the Double Stars Mizar A and Matar. Astron J 116:2536–2548

Hummel CA, Carquillat JM, Ginestet N, Griffin RF, Boden AF, Hajian AR, Mozurkewich D, Nordgren TE (2001) Orbital and stellar parameters of Omicron Leonis from spectroscopy and interferometry. Astron J 121:1623–1635

Hummel CA, Benson JA, Hutter DJ, Johnston KJ, Mozurkewich D, Armstrong JT, Hindsley RB, Gilbreath GC, Rickard LJ, White NM (2003) First observations with a co-phased six-station optical long-baseline array: application to the triple star η Virginis. Astron J 125:2630–2644

Jackson S, MacGregor KB, Skumanich A (2005) On the use of the self-consistent-field method in the construction of models for rapidly rotating main-sequence stars. Astrophys J Suppl 156:245–264

Jankov S, Vakili F, Domicianode Souza A Jr, Janot-Pacheco E (2001a) Interferometric-Doppler imaging of stellar surface structure. Astron Astrophys 377:721–734

Jankov S, Vakili F, Domiciano de Souza A Jr, Janot-Pacheco E (2001b) Interferometric-Doppler Imaging of Nonradial Stellar Pulsations. In: Aerts C, Bedding TR, Christensen-Dalsgaard J (eds) Radial and nonradial pulsations as probes of stellar physics, ASP Conference Series, vol 259, pp 172–175

Jankov S, Mathias P, Domiciano de Souza A Jr, Uytterhoeven K, Aerts C (2004) Latitude distribution of nonradial pulsations in rapidly rotating B stars. In: Variable Stars in the Local Group, ASP Conference Series, vol 310, pp 204–207

Jeffery CS, Aerts C, Dhillon VS, Marsh TR, Gänsicke BT (2005) Multicolour high-speed photometry of the subdwarf B star PG 0014+067 with ULTRACAM. Mon Not R Astr Soc 362:66–78

Jeffery CS, Dhillon VS, Marsh TR, Ramachandran B (2004) Multicolour high-speed photometry of pulsating subdwarf B stars with ULTRACAM. Mon Not R Astr Soc 352:699–707

Kanaan A, Nitta A, Winget DE, Kepler SO, Montgomery MH, Metcalfe TS, Oliveira H, Fraga L, da Costa AFM, Costa JES, Castanheira BG, Giovannini O, Nather RE, Mukadam A, Kawaler SD, O'Brien MS, Reed MD, Kleinman SJ, Provencal JL, Watson TK, Kilkenny D, Sullivan DJ, Sullivan T, Shobbrook B, Jiang XJ, Ashoka BN, Seetha S, Leibowitz E, Ibbetson P, Mendelson H, Meištas EG, Kalytis R, Ališauskas D, O'Donoghue D, Buckley D, Martinez P, van Wyk F, Stobie R, Marang F, van Zyl L, Ogloza W, Krzesinski J, Zola S, Moskalik P, Breger M, Stankov A, Silvotti R, Piccioni A, Vauclair G, Dolez N, Chevreton M, Deetjen J, Dreizler S, Schuh S, Gonzalez Perez JM, Østensen R, Ulla A, Manteiga M, Suarez O, Burleigh MR, Barstow MA (2005) Whole Earth Telescope observations of BPM 37093: A seismological test of crystallization theory in white dwarfs. Astron Astrophys 432:219–224

Kaye AB, Handler G, Krisciunas K, Poretti E, Zerbi FM (1999) Gamma doradus stars: defining a new class of pulsating variables. Publ Astron Soc Pacific 111:840–844

Kennelly EJ, Walker GAH (1996a) Publ Astron Soc Pacific 108:327–331

Kennelly EJ, Walker GAH, Catala C, Foing BH, Huang L, Jiang S, Hao J, Zhai D, Zhao F, Neff JE, Houdebine ER, Ghosh KK, Charbonneau P (1996b) The oscillation modes of θ2 Tauri. Results from the 1992 MUSICOS campaign. Astron Astrophys 313:571–580

Kepler SO (2007) Observational white dwarf seismology. *CoAst* 150:221–226

Kervella P, Domicianode Souza A (2006) The polar wind of the fast rotating Be star Achernar. VINCI/VLTI interferometric observations of an elongated polar envelope. Astron Astrophys 453:1059–1066

Kervella P, Gitton Ph, Ségransan D, di Folco E, Kern PY, Kiekebusch M, Duc TP, Longinotti A, Coude du Foresto V, Ballester P, Sabet C, Cotton, William D., Schoeller M, Wilhelm R (2003a) VINCI, the VLTI commissioning instrument: status after one year of operations at Paranal. In: Traub WA (ed) Interferometry for optical astronomy II, Proc. SPIE 4838, pp 858–869

Kervella P, Thévenin F, Ségransan D, Berthomieu G, Lopez B, Morel P, Provost J (2003b) The diameters of α Centauri A and B. A comparison of the asteroseismic and VINCI/VLTI views. Astron Astrophys 404:1087–1097

Kervella P, Nardetto N, Bersier D, Mourard D, Coudédu Foresto V (2004a) Cepheid distances from infrared long-baseline interferometry. I. VINCI/VLTI observations of seven galactic cepheids. Astron Astroph 416:941–953

Kervella P, Thévenin F, Di Folco E, Ségransan D (2004b) The angular sizes of dwarf stars and subgiants. Surface brightness relations calibrated by interferometry. Astron Astrophys 426:297–307

Kervella P, Thévenin F, Morel P, Berthomieu G, Bordé P, Provost J (2004c) The diameter and evolutionary state of Procyon A. Multi-technique modeling using asteroseismic and interferometric constraints. Astron Astrophys 413:251–256

Kilkenny D, Reed MD, O'Donoghue D, Kawaler SD, Mukadam A, Kleinman SJ, Nitta A, Metcalfe TS, Provencal JL, Watson TK, Sullivan DJ, Sullivan T, Shobbrook R, Jiang XJ, Joshi S, Ashoka BN, Seetha S, Leibowitz E, Ibbetson P, Mendelson H, Meištas E, Kalytis R, Ališauskas D, Martinez P, van Wyk F, Stobie RS, Marang F, Zola S, Krzesinski J, Ogloza W, Moskalik P, Silvotti R, Piccioni A, Vauclair G, Dolez N, Chevreton M, Dreizler S, Schuh SL, Deetjen JL, Solheim JE, Gonzalez Perez JM, Ulla A, Østensen R, Manteiga M, Suarez O, Burleigh M, Kepler SO, Kanaan A, Giovannini O (2003) A Whole Earth Telescope campaign on the pulsating subdwarf B binary system PG 1336–018 (NY Vir). Mon Not R Astr Soc 345:834–846

Kjeldsen H, Bedding TR (1995) Amplitudes of stellar oscillations: the implications for asteroseismology. Astron Astrophys 293:87–106

Kjeldsen H, Bedding TR, Viskum M, Frandsen S (1995) Solarlike oscillations in η Boo. Astron J 109:1313–1319

Kjeldsen H, Bedding TR, Baldry IK, Bruntt H, Butler RP, Fischer DA, Frandsen S, Gates EL, Grundahl F, Lang K, Marcy GW, Misch A, Vogt SS (2003) Confirmation of solar-like oscillations in η Bootis. Astron J 126:1483–1488

Kjeldsen H, Bedding TR, Butler RP, Christensen-Dalsgaard J, Kiss LL, McCarthy C, Marcy GW, Tinney CG, Wright JT (2005) Solar-like oscillations in α Centauri B. Astrophys J. 635:1281–1290

Kochukhov O (2004) Indirect imaging of nonradial pulsations in a rapidly oscillating Ap Star. Astrophys J 615:L149–L152

Kochukhov O, Drake NA, Piskunov N, de la Reza R (2004) Multi-element abundance Doppler imaging of the rapidly oscillating Ap star HR 3831. Astron Astrophys 424:935–950

Koen C (1999) The analysis of indexed astronomical time series - V. Fitting sinusoids to high-speed photometry. Mon Not R Astr Soc 309:769–802

Koen C, Lombard F (1995) The analysis of indexed astronomical time series - III. Intrinsic period scatter. Mon Not R Astr Soc 274:821–831

Konacki M, Lane BF (2004) The visual orbits of the spectroscopic binaries HD 6118 and HD 27483 from the Palomar Testbed Interferometer. Astrophys J 610:443–455

Kosovichev AG (1995) The upper convective boundary layer. In: Hoeksema JT, Domingo V, Fleck B, Battrick B (eds) Proc. Fourth SOHO Workshop: Helioseismology. ESA SP-376, vol 1, ESTEC, Noordwijk, pp 165–176

Kosovichev AG, Schou J, Scherrer PH, Bogart RS, Bush RI, Hoeksema JT, Aloise J, Bacon L, Burnette A, de Forest C, Giles PM, Leibrand K, Nigam R, Rubin M, Scott K, Williams SD, Basu S, Christensen-Dalsgaard J, Däppen W, Rhodes EJ Jr, Duvall TL Jr, Howe R, Thompson MJ, Gough DO, Sekii T, Toomre J, Tarbell TD, Title AM, Mathur D, Morrison M, Saba JLR, Wolfson CJ, Zayer I, Milford PN (1997) Structure and rotation of the solar interior: initial results from the MDI medium-l program. Solar Phys 170:43–61

Kraus S, Balega YY, Berger JP, Hofmann KH, Millan-Gabet R, Monnier JD, Ohnaka K, Pedretti E, Preibisch Th, Schertl D, Schloerb FP, Traub WA, Weigelt G (2007) Visual/infrared interferometry of Orion Trapezium stars: preliminary dynamical orbit and aperture synthesis imaging of the θ^1 Orionis C system. Astron Astrophys 466:649–659

Kuhfuß R (1986) A model of time-dependent turbulent convection. Astron Astrophys 160:116–120

Kurtz DW (2002) Meeting summary and outlook for the future. In: Aerts C, Bedding TR, Christensen-Dalsgaard J (eds) Radial and nonradial pulsations as probes of stellar physics. ASP Conference Series, vol 259, 639–667

Kurtz DW, Kawaler SD, Riddle RL, Reed MD, Cunha MS, Wood M, Silvestri N, Watson TK, Dolez N, Moskalik P, Zola S, Pallier E, Guzik JA, Metcalfe TS, Mukadam AS, Nather RE, Winget DE, Sullivan DJ, Sullivan T, Sekiguchi K, Jiang X, Shobbrook R, Ashoka BN, Seetha S, Joshi S, O'Donoghue D, Handler G, Mueller M, Gonzalez Perez JM, Solheim JE, Johannessen F, Ulla A, Kepler SO, Kanaan A, da Costa A, Fraga L, Giovannini O, Matthews JM (2002) Discovery of the 'missing' mode in HR1217 by the Whole Earth Telescope. Mon Not R Astr Soc 330:L57–L61

Kurtz DW, Elkin VG, Mathys G, Riley J, Cunha MS, Shibahashi H, Kambe E (2004) Some recent discoveries in roAp stars. In: Zverko J, Ziznovsky J, Adelman SJ, Weiss WW (eds) The A-Star puzzle, IAU symposium, No 224. Cambridge University Press, Cambridge, pp 343–352

Kurtz DW, Cameron C, Cunha MS, Dolez N, Vauclair G, Pallier E, Ulla A, Kepler SO, da Costa A, Kanaan A, Fraga L, Giovannini O, Wood MA, Silvestri N, Kawaler SD, Riddle RL, Reed MD, Watson TK, Metcalfe TS, Mukadam A, Nather RE, Winget DE, Nitta A, Kleinman SJ, Guzik JA, Bradley PA, Matthews JM, Sekiguchi K, Sullivan DJ, Sullivan T, Shobbrook R, Jiang X, Birch PV, Ashoka BN, Seetha S, Girish V, Joshi S, Moskalik P, Zola S, O'Donoghue D, Handler G, Mueller M, Gonzalez Perez JM, Solheim JE, Johannessen F, Bigot L (2005) Pushing the ground-based limit: 14-μmag photometric precision with the definitive Whole Earth Telescope asteroseismic data set for the rapidly oscillating Ap star HR 1217. Mon Not R Astr Soc 358:651–664

Kurucz RL (1992) Model atmospheres for population synthesis. In: Barbuy B, Renzini A (eds) Proc. IAU symposium No 149: the stellar populations of galaxies. Kluwer, Dordrecht, pp 225–232

Lamb H (1909) On the theory of waves propagated vertically in the atmosphere. Proc London Math Soc 7:122–141

Lane BF, Kuchner MJ, Boden AF, Creech-Eakman M, Kulkarni SR (2000) Direct detection of pulsations of the Cepheid star ζ Gem and an independent calibration of the period-luminosity relation. Nature 407:485–487

Lane BF, Boden AF, Kulkarni SR (2001) Interferometric measurement of the angular sizes of dwarf stars in the spectral range K3-M4. Astrophys J 551:L81–L83

Lardière O, Martinache F, Patru F (2007) Direct imaging with highly diluted apertures - I. Field-of-view limitations. Mon Not R Astr Soc 375:977–988

Lawson, Peter R (2000) Principles of long baseline stellar interferometry. In: Lawson PR (ed) Course notes from the 1999 Michelson Summer School, held August 15–19, 1999, National Aeronautics and Space Administration, Jet Propulsion Laboratory, Passadena

Leavitt HS (1908) 1777 Variables in the magellanic clouds. Ann Harvard College Observ 60:87–108

Leccia S, Kjeldsen H, Bonanno A, Claudi RU, Ventura R, Paternó L (2007) Seismology of Procyon A: determination of mode frequencies, amplitudes, and granulation noise. Astron Astrophys 464:1059–1067

Leckrone DS (1973) Ultraviolet photometry from the orbiting astronomical observatory. VIII. The blue AP stars. Astrophys J 185:577–596

Ledoux P (1951) The nonradial oscillations of gaseous stars and the problem of beta Canis Majoris. Astrophys J 114:373–384

Lefèvre L, Marchenko SV, Moffat AFJ, Chené AN, Smith SR, St-Louis N, Matthews JM, Kuschnig R, Guenther DB, Poteet CA, Rucinski SM, Sasselov D, Walker GAH, Weiss WW (2005) Oscillations in the Massive Wolf-Rayet Star WR 123 with the MOST Satellite. Astrophys J 634:L109–L112

Leighton RB, Noyes RW, Simon GW (1962) Velocity Fields in the Solar Atmosphere. I. Preliminary Report. Astrophys J 135:477–499

Leinert C, Graser U, Waters LBFM, Perrin GS, Jaffe W, Lopez B, Przygodda F, Chesneau O, Schuller PA, Glazenborg-Kluttig AW, Laun W, Ligori S, Meisner JA, Wagner K, Bakker EJ, Cotton B, de Jong J, Mathar R, Neumann U, Storz C (2003) Ten-micron instrument MIDI: getting ready for observations on the VLTI. In: Traub WA (ed) Interferometry for optical astronomy II, Proc. SPIE 4838, pp 893–904

Léna PJ, Quirrenbach A (eds) (2000) Interferometry in optical astronomy. Proc. SPIE 4006, 2 parts, 1152 pages. ISBN 0-8194-3631-3

Libbrecht KG (1992) On the ultimate accuracy of solar oscillation frequency measurements. Astrophys J 387:712–714

Lighthill MJ (1952) On sound generated aerodynamically I. General theory. Proc Ry Soc London A211:564–587

Lignières F, Rieutord M, Reese D (2006) Acoustic oscillations in rapidly rotating polytropic stars. I. Effects of the centrifugal distortion. Astron Astrophys 455:607–620

Lochard J, Samadi R, Goupil MJ (2005) Rotation profile inversion in solar-like stars. Astron Astrophys 438:939–948

Lopez B, Wolf S, Lagarde S, Abraham P, Antonelli P, Augereau JC, Beckman U, Behrend J, Berruyer N, Bresson Y, Chesneau O, Clausse JM, Connot C, Demyk K, Danchi WC, Dugué M, Flament S, Glazenborg A, Graser U, Henning T, Hofmann KH, Heininger M, Hugues Y, Jaffe W, Jankov S, Kraus S, Laun W, Leinert, Ch., Linz H, Mathias, Ph., Meisenheimer K, Matter A, Menut JL, Millour F, Neumann U, Nussbaum E, Niedzielski A, Mosonic L, Petrov R, Ratzka T, Robbe-Dubois S, Roussel A, Schertl D, Schmider FX, Stecklum B, Thiebaut E, Vakili F, Wagner K, Waters LBFM, Weigelt G (2006) MATISSE: perspective of imaging in the mid-infrared at the VLTI. In: Monnier JD, Schöller M, Danchi WC (eds) Advances in stellar interferometry, Proc. SPIE vol 6268, p 62680Z

MacGregor KB, Jackson S, Skumanich A, Metcalfe TS (2007) On the structure and properties of differentially rotating, main-sequence stars in the $1 - 2M_{\odot}$ range. Astrophys J 663:560–572
Malbet F, Kern PY, Berger JP, Jocou L, Garcia P, Buscher D, Rousselet-Perraut K, Weigelt G, Gai M, Surdej J, Hron J, Neuhäuser R, Le Coarer E, Labeye PR, Le Bouquin J, Benisty M, Herwats E (2006) VSI: a milli-arcsec spectro-imager for the VLTI. In: Monnier JD, Schöller M, Danchi WC (eds) Advances in stellar interferometry, Proc. SPIE, vol 6268, p 62680Y
Malbet F, Petrov R, Weigelt G, Chesneau O, Domicianode Souza A, Meilland A, Millour F, Tatulli E, The Amber Consortium (2007) First AMBER/VLTI science. Messenger 127:37–40
Mantegazza L (2000) Mode detection from line–profile variations. In: Breger M, Montgomery M (eds) Delta Scuti and related stars, ASP Conference Series, vol. 210, pp 138–169
Marengo M, Sasselov D, Karovska M, Papaliolios C, Armstrong JT (2002) Theoretical limb darkening for pulsating Cepheids. Astrophys J 567:1131–1139
Mariotti JM, Ridgway ST (1988) Double Fourier spatio-spectral interferometry – combining high spectral and high spatial resolution in the near infrared. Astron Astrophys 195:350–363
Martić M, Lebrun JC, Appourchaux T, Korzennik SG (2004) p-mode frequencies in solar-like stars: I. Procyon A. Astron Astrophys 418:295–303
Matthews J (2005) A suitcase full of astrophysics: The MOST microsat and opportunities for low-cost space astronomy. In: Kenneth Seidelmann P, Monet AKB (eds) Astrometry in the age of the next generation of large telescopes, ASP Conference Series, vol 338, p 297
Matthews JM, Kurtz DW, Martinez P (1999) Parallaxes versus p-modes: Comparing HIPPARCOS and asteroseismic results for pulsating AP stars. Astrophys J 511:422–428
Mazumdar A (2005) Asteroseismic diagrams for solar-type stars. Astron Astrophys 441:1079–1086
Mazumdar A, Briquet M, Desmet M, Aerts C (2006) An asteroseismic study of the β Cephei star β Canis Majoris. Astron Astrophys 459:589–596
McAlister HA (1976) Spectroscopic binaries as a source for astrometric and speckle interferometric studies. Publ Astron Soc Pacific 88:317–322
McAlister HA (2000) Why Build Stellar Interferometers?. In: Lawson PR (ed) Principles of long baseline stellar interferometry. NASA, JPL, CIT, Pasadena, pp 3–8
McAlister HA, ten Brummelaar TA, Gies DR, Huang W, Bagnuolo WG, Shure MA, Sturmann J, Sturmann L, Turner NH, Taylor SF, Berger DH, Baines EK, Grundstrom E, Ogden C, Ridgway ST, van Belle G (2005) First results from the CHARA Array. I. An interferometric and spectroscopic study of the fast rotator α Leonis (Regulus). Astrophys J 628:439–452
Mékarnia D, Gay J (1990) Infrared multispectral interferometry. Astron Astrophys 238:469–474
Mérand A, Kervella P, Coudé Du Foresto V, Ridgway ST, Aufdenberg JP, ten Brummelaar TA, Berger DH, Sturmann J, Sturmann L, Turner NH, McAlister HA (2005) The projection factor of δ Cephei. A calibration of the Baade-Wesselink method using the CHARA Array. Astron Astrophys 438:L9–L12
Metcalfe TS (2005) Lessons for asteroseismology from white dwarf stars. J Astrophys Astr 26:273–281
Metcalfe TS, Charbonneau P (2003) Stellar structure modeling using a parallel genetic algorithm for objective global optimization. J Comp Phys 185:176–193
Metcalfe TS, Nather RE, Winget DE (2000) Genetic-algorithm-based asteroseismological analysis of the DBV white dwarf GD 358. Astrophys J 545:974–981
Michel E (2006) Theoretical aspects of asteroseismology. Comm Asteroseismol 147:40–47
Michelson AA, Pease FG (1921) Measurement of the diameter of alpha Orionis with the interferometer. Astrophys J 53:249–259
Mieremet AL, Braat J, Bokhove H, Ravel K (2000) Achromatic phase shifting using adjustable dispersive elements. In: Léna PJ, Quirrenbach A (eds) Interferometry in optical astronomy, Proc. SPIE, vol 4006, pp 1035–1041
Miglio A., Montalbán J (2005) Constraining fundamental stellar parameters using seismology. Application to α Centauri AB. Astron Astrophys 441:615–629
Miglio A, Christensen-Dalsgaard J, Di Mauro MP, Monteiro MJPFG, Thompson MJ (2003) Seismic analysis of the helium ionization zones in low- and moderate-mass stars. In: Thompson MJ, Cunha MS, Monteiro MJPFG (eds) Asteroseismology across the HR diagram. Kluwer, Dordrecht, pp 537–540
Miglio A, Montalbán J, Dupret MA (2007a) Instability strips of slowly pulsating B stars and β Cephei stars: the effect of the updated OP opacities and of the metal mixture. Mon Not R Astr Soc 375:L21–L25
Miglio A, Montalbán J, Maceroni C (2007b) 12 Bootis: a test bed for extra-mixing processes in stars. Mon Not R Astr Soc 377:373–382
Monnier JD (2003) Optical interferometry in astronomy. Rep Prog Phys 66:789–857

Monnier JD, Schöller M, Danchi WC (2006) Advances in stellar interferometry. Proc. SPIE, vol 6268, ISBN 9780819463333

Monnier JD, Zhao M, Pedretti E, Thureau N, Ireland M, Muirhead P, Berger JP, Millan-Gabet R, Van Belle G, ten Brummelaar T, McAlister H, Ridgway S, Turner N, Sturmann L, Sturmann J, Berger D (2007) Imaging the Surface of Altair. Science 317:342–345

Monteiro MJPFG, Thompson MJ (1998) On the seismic signature of the HeII ionization zone in stellar envelopes. In: Deubner FL, Christensen-Dalsgaard J, Kurtz DW (eds) Proc. IAU Symp. 185: New eyes to see inside the Sun and stars. Kluwer, Dordrecht, pp 317–318

Monteiro MJPFG, Thompson MJ (2005) Seismic analysis of the second ionization region of helium in the Sun—I. Sensitivity study and methodology. Mon Not R Astr Soc 361:1187–1196

Monteiro MJPFG, Christensen-Dalsgaard J, Thompson MJ (1996) Seismic properties of the Sun's superadiabatic layer I. Theoretical modelling and parametrisation of the uncertainties. Astron Astrophys 306:624–634

Monteiro MJPFG, Christensen-Dalsgaard J, Thompson MJ (2000) Seismic study of stellar convective regions: the base of the convective envelope in low-mass stars. Mon Not R Astr Soc 316:165–172

Monteiro MJPFG, Christensen-Dalsgaard J, Thompson MJ (2002) Asteroseismic Inference for Solar-Type Stars. In: Favata F, Roxburgh IW, Galadí-Enríquez D (eds) Proc. 1st Eddington workshop, 'stellar structure and habitable planet finding', ESA SP-485, ESA Publications Division, Noordwijk, pp 291–298

Montgomery MH (2005) A new technique for probing convection in pulsating white dwarf stars. Astrophys J 633:1142–1149

Montgomery MH, O'Donoghue DO (1999) A derivation of the errors for least squares fitting to time series data. Delta Scuti Newslett 13:28

Montgomery MH, Metcalfe TS, Winget DE (2003) The core/envelope symmetry in pulsating stars. Mon Not R Astr Soc 344:657–664

Mozurkewich D, Johnston KJ, Simon RS, Bowers PF, Gaume R, Hutter DJ, Colavita MM, Shao M, Pan XP (1991) Angular diameter measurements of stars. Astron J 101:2207–2219

Mozurkewich D, Armstrong JT, Hindsley RB, Quirrenbach A, Hummel CA, Hutter DJ, Johnston KJ, Elias NM, Hajian AR, Buscher DF, Simon RS (2003) Angular diameters of stars from the Mark III optical interferometer. Astron J 126:2502–2520

Mosser B (2006) SIAMOIS: an asteroseismic network with 1 site. in Antarctica. In: Fletcher K (ed) Proc. SOHO 18 / GONG 2006 HELAS I Conference beyond the spherical Sun, ESA SP-624, ESA Publications Division, Noordwijk

Mourard D, Abe L, Domiciano A, Bonneau D, Blazit A, Vakili F, Stee P (2003) Status report on the GI2T interferometer. In: Traub WA (eds) Interferometry for optical astronomy II, Proc. SPIE, vol 4838, pp 9–18

Moya A, Suárez JC, Amado PJ, Martin-Ruíz S, Garrido R (2005) Frequency ratio method for seismic modeling of γ Doradus stars. Astron Astrophys 432:189–198

Munteanu A, Bono G, José J, García-Berro E, Stellingwerf RF (2005) Limit-cycle behaviour in one-zone convective models. Astrophys J 627:454–463

Muterspaugh MW, Lane BF, Konacki M, Burke BF, Colavita MM, Kulkarni SR, Shao M (2005) PHASES high-precision differential astrometry of δ Equulei. Astron J 130:2866–2875

Muterspaugh MW, Lane BF, Konacki M, Wiktorowicz S, Burke BF, Colavita MM, Kulkarni SR, Shao M (2006) PHASES differential astrometry and iodine cell radial velocities of the κ Pegasi triple star system. Astrophys J 636:1020–1032

Nordlund Å (1982) Numerical simulations of the solar granulation. I - Basic equations and methods. Astron Astrophys 107:1–10

Nordlund Å, Stein RF (1991) Granulation: non-adiabatic patterns and shocks. In: Gough DO, Toomre J (eds) Challenges to theories of the structure of moderate-mass stars, Lecture notes in physics, vol 388. Springer, Heidelberg, pp 141–146

North JR, Davis J, Bedding TR, Ireland MJ, Jacob AP, O'Byrne J, Owens SM, Robertson JG, Tango WJ, Tuthill PG (2007a) The radius and mass of the subgiant star β Hyi from interferometry and asteroseismology. Mon Not R Astr Soc 380:L80–L83

North JR, Davis J, Tuthill PG, Tango WJ, Robertson JG (2007b) Orbital solution & fundamental parameters of σ Scorpii. Mon Not Ry Astr Soc 380:1276–1284

North JR, Tuthill PG, Tango WJ, Davis J (2007c) γ^2 Velorum: orbital solution and fundamental parameter determination with SUSI. Mon Not Ry Astr Soc 377:415–424

Nowakowski RM (2005) Multimode resonant coupling in pulsating stars. Acta Astron 55:1–41
Ohishi N, Nordgren TE, Hutter DJ (2004) Asymmetric surface brightness distribution of Altair observed with the navy prototype optical interferometer. Astrophys J 612:463–471
Ohnaka K, Bergeat J, Driebe T, Graser U, Hofmann KH, Köhler R, Leinert C, Lopez B, Malbet F, Morel S, Paresce F, Perrin G, Preibisch T, Richichi A, Schertl D, Schöller M, Sol H, Weigelt G, Wittkowski M (2005) Mid-infrared interferometry of the Mira variable RR Sco with the VLTI MIDI instrument. Astron Astrophys 429:1057–1067
Olivier EA, Wood PR (2005) Non-linear pulsation models of red giants. Mon Not R Astr Soc 362:1396–1412
Ollivier Met al. (2006) PEGASE: a DARWIN/TPF pathfinder. In: Aime C, Vakili F (eds) Direct imaging of exoplanets: science and techniques, IAU Colloquium 200. Cambridge University Press, Cambridge, p 241
Osaki Y (1975) Nonradial oscillations of a 10 solar mass star in the main-sequence stage. Publ Astron Soc Japan 27:237–258
Otí Floranes H, Christensen-Dalsgaard J, Thompson MJ (2005) The use of frequency-separation ratios for asteroseismology. Mon Not R Astr Soc 356:671–679
Pamyatnykh AA (1999) Pulsational instability domains in the upper main sequence. Acta Astron 49:119–148
Pamyatnykh AA, Handler G, Dziembowski WA (2004) Asteroseismology of the β Cephei star ν Eridani: interpretation and applications of the oscillation spectrum. Mon Not R Astr Soc 350:1022–1028
Pan XP, Shao M, Colavita MM, Mozurkewich D, Simon RS, Johnston KJ (1990) Apparent orbit of the spectroscopic binary *beta* Arietis with the Mark III stellar interferometer. Astrophys J 356:641–645
Pan XP, Shao M, Colavita MM, Armstrong JT, Mozurkewich D, Vivekanand M, Denison CS, Simon RS, Johnston KJ (1992) Determination of the visual orbit of the spectroscopic binary α Andromedae with submilliarcsecond precision. Astrophys J 384:624–633
Paresce F (1997) Science with the VLT Interferometer. Springer-verlag, series: ESO astrophysics symposia, ISBN 3540632646
Pasquini L, Alonso J, Avila G, Barriga P, Biereichel P, Buzzoni B, Cavadore C, Cumani C, Dekker H, Delabre B, Kaufer A, Kotzlowski H, Hill V, Lizon JL, Nees W, Santin P, Schmutzer R, Kesteren AV, Zoccali M (2003) Installation and first results of FLAMES, the VLT multifibre facility. In: Iye M, Moorwood AFM (eds) Instrument design and performance for optical/infrared groundbased telescopes, Proc. SPIE, vol 4841, pp 1682–1693
Paternò L, Ventura R, Canuto VM, Mazzitelli I (1993) Helioseismological test of a new model for stellar convection. Astrophys J 402:733–740
Pérez Hernández F, Christensen-Dalsgaard J (1998) The phase function for stellar acoustic oscillations - IV. Solar-like stars. Mon Not R Ast Soc 295:344–352
Perrin G (2003) The calibration of interferometric visibilities obtained with single-mode optical interferometers. Computation of error bars and correlations. Astron Astrophys 400:1173–1181
Perrin G, Ridgway ST (2005) Squared Visibility Estimators: Calibrating Biases to Reach Very High Dynamic Range. Astrophys J 626:1138–1148
Perrin G, Ridgway ST, Coudédu Foresto V, Mennesson B, Traub WA, Lacasse MG (2004) Interferometric observations of the supergiant stars α Orionis and α Herculis with FLUOR at IOTA. Astron Astrophys 418:675–685
Perrin G, Woillez J, Lai O, Guérin J, Kotani T, Wizinowich PL, Le Mignant D, Hrynevych M, Gathright J, Léna P, Chaffee F, Vergnole S, Delage L, Reynaud F, Adamson AJ, Berthod C, Brient B, Collin C, Crétenet J, Dauny F, Deléglise C, Fédou P, Goeltzenlichter T, Guyon O, Hulin R, Marlot C, Marteaud M, Melse BT, Nishikawa J, Reess JM, Ridgway ST, Rigaut F, Roth K, Tokunaga AT, Ziegler D (2006) Interferometric coupling of the Keck telescopes with single-mode fibers. Science 311:194
Perryman MAC, Lindegren L, Kovalevsky J, Hoeg E, Bastian U, Bernacca PL, Crézé M, Donati F, Grenon M, van Leeuwen F, van der Marel H, Mignard F, Murray CA, Le Poole RS, Schrijver H, Turon C, Arenou F, Froeschlé M, Petersen CS (1997) The Hipparcos Catalogue. Astron Astrophys 323:L49–L52
Pesnell WD (1987) A new driving mechanism for stellar pulsations. Astrophys J 314:598–604
Peterson DM, Hummel CA, Pauls TA, Armstrong JT, Benson JA, Gilbreath GC, Hindsley RB, Hutter DJ, Johnston KJ, Mozurkewich D, Schmitt HR (2006c) Vega is a rapidly rotating star. Nature 440:896–899

Peterson DM, Hummel CA, Pauls TA, Armstrong JT, Benson JA, Gilbreath GC, Hindsley RB, Hutter DJ, Johnston KJ, Mozurkewich D, Schmitt H (2006b) Resolving the effects of rotation in Altair with long-baseline interferometry. Astrophys J 636:1087–1097

Petrov RG (1989) Differential interferometry. In: Alloin DM, Mariotti JM (eds) Diffraction-limited imaging with very large telescopes, NATO ASI vol **274**, pp 249–271

Petrov RG & Amber Consortium, The (2003) The near infrared VLTI instrument AMBER. In: Perrin G, Malbet F (eds) Observing with the VLTI, EAS Publications Series vol **6**, pp 111–126

Petrov RG, Malbet F, Weigelt G, Antonelli P, Beckmann U, Bresson Y, Chelli A, Dugué M, Duvert G, Gennari S, Glück L, Kern P, Lagarde S, Le Coarer E, Lisi F, Millour F, Perraut K, Puget P, Rantakyrö F, Robbe-Dubois S, Roussel A, Salinari P, Tatulli E, Zins G, Accardo M, Acke B, Agabi K, Altariba E, Arezki B, Aristidi E, Baffa C, Behrend J, Blöcker T, Bonhomme S, Busoni S, Cassaing F, Clausse JM, Colin J, Connot C, Delboulbé A, Domicianode Souza A, Driebe T, Feautrier P, Ferruzzi D, Forveille T, Fossat E, Foy R, Fraix-Burnet D, Gallardo A, Giani E, Gil C, Glentzlin A, Heiden M, Heininger M, Hernandez Utrera O, Hofmann KH, Kamm D, Kiekebusch M, Kraus S, Le Contel D, Le Contel JM, Lesourd T, Lopez B, Lopez M, Magnard Y, Marconi A, Mars G, Martinot-Lagarde G, Mathias P, Mège P, Monin JL, Mouillet D, Mourard D, Nussbaum E, Ohnaka K, Pacheco J, Perrier C, Rabbia Y, Rebattu S, Reynaud F, Richichi A, Robini A, Sacchettini M, Schertl D, Schöller M Solscheid M Spang M Stee M Stefanini M Tallon M Tallon-Bosc M Tasso M Testi M Vakili M von der Lühe M Valtier M Vannier M Ventura M (2007) AMBER, the near-infrared spectro-interferometric three-telescope VLTI instrument. Astron Astrophys 464:1–12

Pickering EC (1912) Periods of 25 variable stars in the small magellanic cloud. Harvard College Observatory, circular 173, Harvard

Pigulski A (2006) Intrinsic variability in multiple systems and clusters: an overview. In: Sterken C Aerts C (eds) Astrophysics of variable stars, ASP Conference Series, vol 349, p 137

Pijpers FP (2006) Methods in helio- and asteroseismology. Imperial College Press

Pijpers FP, Thompson MJ (1992) Faster formulations of the optimally localized averages method for helioseismic inversion. Astron Astrophys 262:L33–L36

Pijpers FP, Thompson MJ (1994) The SOLA method for helioseismic inversion. Astron Astrophys 281: 231–240

Pijpers FP, Teixeira TC, Garcia PJ, Cunha MS, Monteiro MJPFG, Christensen-Dalsgaard J (2003) Interferometry and asteroseismology: The radius of τ Cet. Astron Astrophys 406:L15–L18

Poretti E, Buzasi D, Laher R, Catanzarite J, Conrow T (2002) Asteroseismology from space: The delta Scuti star theta 2 Tauri monitored by the WIRE satellite. Astron Astrophys 382:157–163

Pourbaix D, Nidever D, McCarthy C, Butler RP, Tinney CG, Marcy GW, Jones HRA, Penny AJ, Carter BD, Bouchy F, Pepe F, Hearnshaw JB, Skuljan J, Ramm D, Kent D (2002) Constraining the difference in convective blueshift between the components of α Centauri with precise radial velocities. Astron Astrophys 386:280–285

Pourbaix D, Tokovinin AA, Batten AH, Fekel FC, Hartkopf WI, Levato H, Morrell NI, Torres G, Udry S (2004) SB9: the ninth catalogue of spectroscopic binary orbits. Astron Astrophys 424:727–732

Press WH, Flannery BP, Teukolsky SA, Vetterling WT (1986) Numerical Recipes, Cambridge, Sect 14.5

Provost J, Berthomieu G (1986) Asymptotic properties of low degree solar gravity modes. Astron Astrophys 165:218–226

Quirrenbach A (2000) Principles of long baseline stellar interferometry. In: Lawson PR (ed) Course notes from the 1999 Michelson Summer School, held August 15–19, 1999, National Aeronautics and Space Administration, Jet Propulsion Laboratory, Passadena, p 71

Quirrenbach A (2001a) Optical Interferometry. Annu Rev Astron Astrophys 39:353–401

Quirrenbach A (2001b) Optical and infrared long-baseline interferometry: application to binary star science. In: Zinnecker H, Mathieu RD (eds) Proc. IAU Symposium 200, the formation of binary stars, pp 539–546

Quirrenbach A (2004a) Interferometric high-resolution spectroscopy. In: Traub WA (ed) New frontiers in stellar interferometry, Proc. SPIE, vol 5491, pp 146–153

Quirrenbach A (2004b) Design considerations for an Extremely Large Synthesis Array. In: Traub WA (ed) New frontiers in stellar interferometry, Proc. SPIE, vol 5491, pp 1563–1573

Quirrenbach A, Aufdenberg J (2004) Wavelength-dependent diameters of cool giant stars. In: Piskunov N, Weiss WW, Gray DF (eds) Modelling of stellar atmospheres, IAU Symposium 210, E68

Quirrenbach A, Mozurkewich D, Armstrong JT, Johnston KJ, Colavita MM, Shao M (1992) Interferometric observations of Mira (o Ceti). Astron Astrophys 259:L19–L22

Quirrenbach A, Mozurkewich D, Armstrong JT, Buscher DF, Hummel CA (1993) Angular diameter measurements of cool giant stars in strong TiO bands and in the continuum. Astrophys J 406:215–219
Quirrenbach A, Mozurkewich D, Buscher DF, Hummel CA, Armstrong JT (1996) Angular diameter and limb darkening of Arcturus. Astron Astrophys 312:160–166
Quirrenbach A, Bjorkman KS, Bjorkman JE, Hummel CA, Buscher DF, Armstrong JT, Mozurkewich D, Elias NM, Babler BL (1997) Constraints on the geometry of circumstellar envelopes: Optical interferometric and spectropolarimetric observations of seven Be stars. Astroph J 479:477–496
Quirrenbach A, Coudé du Foresto V, Daigne G, Hofmann KH, Hofmann R, Lattanzi M, Osterbart R, le Poole R, Queloz D, Vakili F (1998) PRIMA—study for a dual-beam instrument for the VLT Interferometer. In: Reasenberg RD (ed) Astronomical interferometry, Proc. of the SPIE 3350, pp 807–817
Quirrenbach A, Henning T, Queloz D, Albrecht S, Bakker E, Baumeister H, Bizenberger P, Bleuler H, Dändliker R, de Jong J, Fleury M, Frink S, Gillet D, Jaffe W, Hanenburg SH, Hekker S, Launhardt R, le Poole R, Maire C, Mathar R, Mullhaupt P, Murakawa K, Pepe F, Pragt J, Sache L, Scherler O, Ségransan D, Setiawan J, Sosnowska D, Tubbs R, Venema L, Wagner K, Weber L, Wüthrich R (2004) The PRIMA astrometric planet search project. In: Traub WA (ed) New frontiers in stellar interferometry, Proc. SPIE, vol 5491, pp 424–432
Rabello-Soares MC, Basu S, Christensen-Dalsgaard J (1999) On the choice of parameters in solar structure inversion. Mon Not R Astr Soc 309:35–47
Ragland S, Traub WA, Berger JP, Danchi WC, Monnier JD, Willson LA, Carleton NP, Lacasse MG, Millan-Gabet R, Pedretti E, Schloerb FP, Cotton WD, Townes CH, Brewer M, Haguenauer P, Kern P, Labeye P, Malbet F, Malin D, Pearlman M, Perraut K, Souccar K, Wallace G (2006) First surface-resolved results with the infrared optical telescope array imaging interferometer: detection of asymmetries in asymptotic giant branch stars. Astrophys J 652:650–660
Randall SK, Matthews JM, Fontaine G, Rowe J, Kuschnig R, Green EM, Brassard P, Chayer P, Guenther DB, Moffat AFJ, Rucinski S, Sasselov D, Walker GAH, Weiss WW (2005a) Detection of long-period variations in the subdwarf B star PG 0101+039 on the basis of photometry from the MOST 443. satellite. Astrophys J 633:460–464
Randall SK, Fontaine G, Brassard P, Bergeron P (2005b) The potential of multicolor photometry for pulsating subdwarf B stars. Astrophys J Suppl 161:456–479
Rantakyro FT, Galliano E, Hummel CA, Kaufer A, Kervella P, Morel S, Schöller M, Vannier M, Wittkowski M. (2004) VLTI science operations at Paranal. In: Traub WA (ed) New frontiers in stellar interferometry, Proc. SPIE, vol 5491, p 1690
Reese D, Lignières F, Rieutord M (2006a) Oscillations of rapidly rotating stars. Comm Asteroseismol 147:65–68
Reese D, Lignières F, Rieutord M (2006b) Acoustic oscillations of rapidly rotating polytropic stars. II. Effects of the Coriolis and centrifugal accelerations. Astron Astrophys 455:621–637
Rice JB (2002) Doppler imaging of stellar surfaces—techniques and issues. Astron Nachrichten 323: 220–235
Ridgway ST, Roddier FJ (2000) Infrared very large array for the 21st century. In: Léna PJ, Quirrenbach A (eds) Interferometry in optical astronomy, Proc. SPIE, vol 4006, pp 940–950
Rieutord M (2006a) The dynamics of the radiative envelope of rapidly rotating stars. I. A spherical Boussinesq model. Astron Astrophys 451:1025–1036
Rieutord M (2006b) Modeling rapidly rotating stars. In: Barret D, Casoli F, Lagache G, Lecavelier A, Pagani L (eds) Proceedings of the annual meeting of the French Society of Astronomy and Astrophysics, p 501
Rivinius TH, Baade D, Stefl S (2003) Non-radially pulsating Be stars. Astron Astrophys 411:229–247
Robe H (1968) Les oscillations non radiales des polytropes. Ann d'Astrophys 31:475–482
Robinson FJ, Demarque P, Li LH, Kim YC, Chan KL, Guenther DB (2003) Three-dimensional convection simulations of the outer layers of the Sun using realistic physics. Mon Not R Astr Soc 340:923–936
Roca Cortés T, Montañés P, Pallé PL, Pérez Hernández F, Jiménez A, Régulo C, and the GOLF Team (1999) Low ℓ solar p-mode oscillation parameters and convection. In: Giménez A, Guinan EF, Montesinos B (eds) Theory and tests of convection in stellar structure, ASP Conference Series, vol 173, pp 305–308
Rodríguez E, Breger M (2001) δ Scuti and related stars: analysis of the R00 Catalogue. Astron Astrophys 366:178–196
Rosenthal CS, Christensen-Dalsgaard J, Nordlund Å, Stein RF, Trampedach R (1999) Convective contributions to the frequencies of solar oscillations. Astron Astrophys 351:689–700

Roxburgh IW (2004) 2-Dimensional models of rapidly rotating stars. I. Uniformly rotating zero age main sequence stars. Astron Astrophys 428:171–179
Roxburgh IW (2005) The ratio of small to large separations of stellar p-modes. Astron Astrophys 434:665–669
Roxburgh IW (2006) 2-Dimensional models of rapidly rotating stars. II. Hydrostatic and acoustic models with $\Omega = \Omega(r, \theta)$. Astron Astrophys 454:883–888
Roxburgh IW, Vorontsov SV (1994) The seismology of stellar cores: a simple theoretical description of the 'small frequency separations'. Mon Not R Astr Soc 267:297–302
Roxburgh IW, Vorontsov SV (2000) Semiclassical approximation for low-degree stellar p modes – II. Classical ray tracing. Mon Not R ast Soc 317:151–157
Roxburgh IW, Vorontsov SV (2001) Semiclassical approximation for low-degree stellar p modes – III. Acoustic resonances and diagnostic properties of the oscillation frequencies. Mon Not R ast Soc 322:85–96
Roxburgh IW, Vorontsov SV (2003) The ratio of small to large separations of acoustic oscillations as a diagnostic of the interior of solar-like stars. Astron Astrophys 411:215–220
Roxburgh IW, Vorontsov SV (2006) The autocorrelation function of stellar p-mode measurements and its diagnostic properties. Mon Not R Astr Soc 369:1491–1496
Ryabchikova TA, Landstreet JD, Gelbmann MJ, Bolgova GT, Tsymbal VV, Weiss WW (1997) Abundance analysis of roAp stars. IV. HD24712. Astron Astrophys 327:1137–1146
Sabbey CN, Sasselov DD, Fieldus MS, Lester JB, Venn KA, Butler RP (1995) On spectral line formation and measurement in Cepheids: implications to distance determination. Astrophys J 446:250–260
Saio H (1981) Rotational and tidal perturbations of nonradial oscillations in a polytropic star. Astrophys J 244:299–315
Saio H (2005) A non-adiabatic analysis for axisymmetric pulsations of magnetic stars. Mon Not R Astr Soc 360:1022–1032
Saio H, Gautschy A (2004) Axisymmetric p-mode pulsations of stars with dipole magnetic fields. Mon Not R Astr Soc 350:485–505
Saio H, Kuschnig R, Gautschy A, Cameron C, Walker GAH, Matthews JM, Guenther DB, Moffat AFJ, Rucinski SM, Sasselov D, Weiss WW (2006) MOST Detects g- and p-modes in the B supergiant HD 163899 (B2 Ib/II). Astrophys J 650:1111–1118
Saio H, Cameron C, Kuschnig R, Walker GAH, Matthews JM, Rowe JF, Lee U, Huber D, Weiss WW, Guenther DB, Moffat AFJ, Rucinski SM, Sasselov D (2007) MOST Detects g-Modes in the Late-Type Be Star β Canis Minoris (B8 Ve). Astrophys J 654:544–550
Samadi R, Nordlund Å, Stein RF, Goupil MJ, Roxburgh I (2003a) Numerical 3D constraints on convective eddy time-correlations: consequences for stochastic excitation of solar p modes. Astron Astrophys 404:1129–1137
Samadi R, Nordlund Å, Stein RF, Goupil MJ, Roxburgh I (2003b) Numerical constraints on the model of stochastic excitation of solar-type stars. Astron Astrophys 403:303–312
Samadi R, Goupil MJ, Alecian E, Baudin F, Georgobiani D, Trampedach R, Stein R, Nordlund Å (2005) Excitation of solar-like oscillations: from PMS to MS stellar models. J Astrophys Astr 26:171–184
Samadi R, Kupka F, Goupil MJ, Lebreton Y, van't Veer-Menneret C (2006) Influence of local treatments of convection upon solar p mode excitation rates. Astron Astrophys 445:233–242
Scargle JD (1982) Studies in astronomical time series analysis. II—Statistical aspects of spectral analysis of unevenly spaced data. Astrophys J 263:835–853
Scherrer PH, Wilcox JM, Christensen-Dalsgaard J, Gough DO (1983) Detection of solar five-minute oscillations of low degree. Solar Phys 82:75–87
Schmitz F, Fleck B (1998) On wave equations and cut-off frequencies of plane atmospheres. Astron Astrophys 337:487–494
Schou J, Buzasi DL (2001) Observations of p-modes in α Cen. In: Wilson A (ed) SOHO 10/GONG 2000 workshop: helio- and asteroseismology at the dawn of the millennium. ESA SP-464, pp 391–394
Schou J, Antia HM, Basu S, Bogart RS, Bush RI, Chitre SM, Christensen-Dalsgaard J, Di Mauro MP, Dziembowski WA, Eff-Darwich A, Gough DO, Haber DA, Hoeksema JT, Howe R, Korzennik SG, Kosovichev AG, Larsen RM, Pijpers FP, Scherrer PH, Sekii T, Tarbell TD, Title AM, Thompson MJ, Toomre J (1998) Helioseismic studies of differential rotation in the solar envelope by the Solar Oscillations Investigation using the Michelson Doppler Imager. Astrophys J 505:390–417

Schrijvers C, Telting JH, Aerts C, Ruymaekers E, Henrichs HF (1997) Line-profile variations due to adiabatic non-radial pulsations in rotating stars. I. Observable characteristics of spheroidal modes. Astron Astrophys Suppl 121:343–368
Schwarzenberg-Czerny A (1997) The Correct Probability Distribution for the Phase Dispersion Minimization Periodogram. Astrophys J 489:941–945
Scuflaire R (1974) The non radial oscillations of condensed polytropes. Astron Astrophys 36:107–111
Seaton MJ (2005) Opacity Project data on CD for mean opacities and radiative accelerations. Mon Not R Astr Soc 362:L1–L3
Ségransan D, Kervella P, Forveille T, Queloz D (2003) First radius measurements of very low mass stars with the VLTI. Astron Astrophys 397:L5–L8
Shao M, (ed) (2003) Interferometry in Space. Proc. SPIE, vol 4852, ISBN 9780819446312
Shao M, Colavita MM (1992) Long-baseline optical and infrared stellar interferometry. Annu Rev Astron Astrophys 30:457–498
Shapley H (1914) On the Nature and Cause of Cepheid Variation. Astrophys J 40:448–465
Shobbrook RR, Handler G, Lorenz D, Mogorosi D (2006) Photometric studies of three multiperiodic β Cephei stars: β CMa, 15 CMa and KZ Mus. Mon Not R Astr Soc 369:171–181
Smeyers P (1968) Sur la forme asymptotique des modes non radiaux dans les étoiles massives. Ann d'Astrophys 31:159–165
Smith MA (1985a) The nonradial oscillations of Spica. I - Two commensurable modes. II - A 'quasi-toroidal' mode. Astrophys J 297:206–232
Smith MA (1985b) The nonradial oscillations of SPICA—part two—a Quasi-toroidal mode. Astrophys J 297:224–232
Smolec R, Moskalik P (2007) Amplitude saturation in β Cephei models. Mon Not R Astr Soc 377:645–656
Soufi F, Goupil MJ, Dziembowski WA (1998) Effects of moderate rotation on stellar pulsation. I. Third order perturbation formalism. Astron Astrophys 334:911–924
Stamford PA, Watson RD (1981) Baade-Wesselink and related techniques for mode discrimination in non-radial stellar pulsations. Astrophys Space Sci 77:131–158
Stankov A, Handler G (2005) Catalog of galactic β cephei stars. Astrophys J Suppl 158:193–216
Stein RF (1968) Waves in the solar atmosphere. I. The acoustic energy flux. Astrophys J 154:297–306
Stein RF, Nordlund Å (1989) Topology of convection beneath the solar surface. Astrophys J 342:L95–L98
Stein RF, Nordlund Å (1998) Simulations of solar granulation. I. General properties. Astrophys J 499:914–933
Stein RF, Nordlund Å (2001) Solar oscillations and convection: II. Excitation of radial oscillations. Astrophys J 546:585–603
Stein R, Georgobiani D, Trampedach R, Ludwig HG, Nordlund Å (2004) Excitation of radial p-modes in the Sun and stars. Solar Phys 220:229–242
Stein RF, Benson D, Georgobiani D, Nordlund Å (2006) Supergranule scale convection simulations. In: Fletcher K (ed) Proceedings SOHO 18 / GONG 2006 / HELAS I Conference Beyond the spherical Sun, ESA SP-624, ESA Publications Division, Noordwijk, pp 79.1–79.4
Stellingwerf RF (1982) Convection in pulsating stars. I. Nonlinear hydrodynamics. Astrophys J 262:330–338
Stellingwerf RF (1984) Convection in pulsating stars. III. The RR Lyrae instability strip. Astrophys J 277:322–326
Stello D, Kjeldsen H, Bedding TR, Buzasi D (2006) Oscillation mode lifetimes in ξ Hydrae: will strong mode damping limit asteroseismology of red giant stars. Astron Astrophys 448:709–715
Suárez JC, Bruntt H, Buzasi D (2005) Modelling of the fast rotating δ Scuti star Altair. Astron Astrophys 438:633–641
Surdej J, Caro D, Detal A, eds (2005) Science cases for next generation optical/infrared interferometric facilities. In: Proceedings of the 37th Liège international astrophysical colloquium. Liège University, Liège
Surdej J, Caro D, Detal A (eds) (2006) Technology roadmap for future inteferometric facilities. Liège University
Svensson F, Ludwig HG (2005) Hydrodynamical simulations of convection-related stellar micro-variability. In: Favata F, Hussain G, Battrick B (eds) Proc 13th Cool Stars Workshop, Hamburg, 5–9 July 2004, ESA SP-560, ESA Publication Division, Noordwijk, pp 979–984
Söderhjelm S. (1999) Visual binary orbits and masses post Hipparcos. Astron Astrophys 341:121–140

Takata M (2005) Momentum conservation and model classification of the dipolar oscillations in stars. Publ Astron Soc Jpn 57:375–389

Tango WJ, Davis J, Ireland MJ, Aerts C, Uytterhoeven K, Jacob AP, Mendez A, North JR, Seneta EB, Tuthill PG (2006) Orbital elements, masses and distance of λ Scorpii A and B determined with the Sydney University Stellar Interferometer and high-resolution spectroscopy. Mon Not R Astr Soc 370:884–890

Tassoul M (1980) Asymptotic approximations for stellar nonradial pulsations. Astrophys J Suppl 43:469–490

Tassoul M (1990) Second-order asymptotic approximations for stellar nonradial acoustic modes. Astrophys J 358:313–327

Telting JH, Aerts C, Mathias P (1997) A period analysis of the optical line variability of β Cephei: evidence for multi-mode pulsation and rotational modulation. Astron Astrophys 322:493–506

Telting JH, Schrijvers C (1997) Line-profile variations of non-radial adiabatic pulsations of rotating stars. II. The diagnostic value of amplitude and phase diagrams derived from time series of spectra. Astron Astrophys 317:723–741

Telting JH, Schrijvers C (1998) A new bright beta Cephei star: line–profile variability in omega[1] SCO. Astron Astrophys 339:150–158

Teixeira TC, Emerson JP, Palumbo ME (1998) Ice CO-cktails in molecular cloud cores. Astron Astrophys 330:711–725

ten Brummelaar TA, McAlister HA, Ridgway ST, Bagnuolo WG, Turner NH, Sturmann L, Sturmann J, Berger DH, Ogden CE, Cadman R, Hartkopf WI, Hopper CH, Shure MA (2005) First Results from the CHARA Array. II. A Description of the Instrument. Astrophys J 628:453–465

ten Brummelaar TA, McAlister HA, Ridgway ST, Turner NH, Sturmann L, Sturmann J, Bagnuolo WG, Jr., Shure MA (2003) An Update of the CHARA Array. In: Traub WA (ed) nterferometry for optical astronomy II, Proc. SPIE, vol 4838, p 69

Théado S, Vauclair S, Castro M, Charpinet S, Dolez N (2005a) Asteroseismic tests of element diffusion in solar type stars. Astron Astrophys 437:553–560

Théado S, Vauclair S, Cunha MS (2005b) Helium settling and mass loss in magnetic Ap stars. I. The chemical stratification. Astron Astrophys 443:627–641

Thévenin F, Idiart T (1999) Stellar Iron abundances: non-LTE effects. Astrophys J 521:753–763

Thévenin F, Provost J, Morel P, Berthomieu G, Bouchy F, Carrier F (2002) Asteroseismology and calibration of alpha Cen binary system. Astron Astrophys 392:L9–L12

Thévenin F, Kervalla P, Pichon B, Morel P, Di Folco E, Lebreton Y (2005) VLTI/VINCI diameter constraints on the evolutionary status of δ Eri, ξ Hya, η Boo. Astron Astrophys 436:253–262

Thompson MJ, Christensen-Dalsgaard J (2002) On inverting asteroseismic data. In: Favata F, Roxburgh IW, Galadí-Enríquez D (eds) Proc. 1st Eddington workshop, 'stellar structure and habitable planet finding', ESA SP-485, ESA Publications Division, Noordwijk, pp 95–101

Thompson MJ, Christensen-Dalsgaard J, Miesch MS, Toomre J (2003) The internal rotation of the Sun. Annu Rev Astron Astrophys 41:599–643

Thoul A, Scuflaire R, Noels A, Vatovez B, Briquet M, Dupret MA, Montalbán J (2003) A new seismic analysis of Alpha Centauri. Astron Astrophys 402:293–297

Thoul A, Ausseloos M, Barban C, Briquet M, Bourge PO, Cuypers J, Daszynska K, De Cat P, De Ridder J, Dupret MA, Montalban J, Noels A, Scuflaire R, Uytterhoeven K, Aerts C (2003) A hare and hound in a BAG. Asteroseismology of β Cephei stars. Comm Asteroseismol 143:25–28

Tikhonov AN, Arsenin VA (1977) Solution of ill-posed problems. Winston, Washington

Tomkin J, Fekel FC (2006) New precision orbits of bright double-lined spectroscopic binaries. I. RR Lyncis, 12 Bootis, and HR 6169. Astron J 131:2652–2663

Tomkin J, Pan X, McCarthy JK (1995) Spectroscopic detection of the secondaries of the Hyades interferometric spectroscopic binary theta2 Tauri and of the interferometric spectroscopic binary alpha Andromedae. Astrophys J 109:780–790

Torres G, Boden AF, Latham DW, Pan M, Stefanik RP (2002) Testing models of stellar evolution for metal-poor stars: an interferometric–spectroscopic orbit for the binary HD 195987. Astron J 124:1716–1737

Townsend RHD (1997) Spectroscopic modelling of non-radial pulsation in rotating early-type stars. Mon Not R Astr Soc 284:839–858

Trampedach R, Christensen-Dalsgaard J, Nordlund, Å, Stein RF (1998) Stellar background power spectra from hydrodynamical simulations of stellar atmospheres. In: Kjeldsen H, Bedding TR (eds) Proc. Workshop on science with a small space telescope, Aarhus Universitet, Aarhus, pp 59–67

Traub WA (ed) (2003) Interferometry for optical astronomy II. Proc SPIE vol 4838, ISBN 9780819446176

Traub WA (ed) (2004) Interferometry for optical astronomy II. Proc SPIE 5491, ISBN 9780819454232
Tremblay PE, Fontaine G, Brassard P, Bergeron P, Randall SK (2006) A quantitative analysis of the available multicolor photometry for rapidly pulsating hot B subdwarfs. Astrophys J Suppl 165:551–567
Turck-Chièze S, Couvidat S, Piau L, Ferguson J, Lambert P, Ballot J, García RA, Nghiem P (2004) Surprising Sun: a new step towards a complete picture? Phys Rev Lett 93:211102–(1–4)
Ulrich RK (1970) The Five-Minute Oscillations on the Solar Surface. Astrophys J 162:993–1002
Ulrich RK (1986) Determination of stellar ages from asteroseismology. Astrophys J 306:L37–L40
Ulrich RK (1986) Determination of stellar ages from asteroseismology. Mon Not R Astr Soc 330:731–736
Unno W (1967) The stellar radial pulsation coupled with the convection. Publ Astron Soc Jpn 19:140–153
Unno W, Osaki Y, Ando H, Saio H, Shibahashi H (1989) Nonradial oscillations of stars, 2nd edn. University of Tokyo Press, Tokyo
Uytterhoeven K, Aerts C, De Cat P, De Mey K, Telting JH, Schrijvers C, De Ridder J, Daems K, Meeus G, Waelkens C (2001) Line–profile variations of the double-lined spectroscopic binary kappa Scorpii. Astron Astrophys 371:1035–1047
Uytterhoeven K, Willems B, LefeverK Aerts C, Telting JH, Kolb U (2004a) Interpretation of the variability of the β Cephei star λ Scorpii. I. The multiple character. Astron Astrophys 427:581–592
Uytterhoeven K, Telting JH, Aerts C, Willems B (2004b) Interpretation of the variability of the β Cephei star λ Scorpii. II. The line–profile diagnostics. Astron Astrophys 427:593–605
Uytterhoeven K, Briquet M, Aerts C, Telting JH, Harmanec P, Lefever K, Cuypers J (2005) Disentangling component spectra of λ Scorpii, a spectroscopic binary with a pulsating primary. II. Interpretation of the line–profile variability. Astron Astrophys 432:955–967
Vakili F, Percheron I (1991) On the Possibility to Detect NRP's by Optical Interferometry. In: Baade D (ed) Rapid variability of OB-stars: nature and diagnostic value, ESO, p 77
van Belle GT, Lane BF, Thompson RR, Boden AF, Colavita MM, Dumont PJ, Mobley DW, Palmer D, Shao M, Vasisht GX, Wallace JK, Creech-Eakman MJ, Koresko CD, Kulkarni SR, Pan XP, Gubler J (1999) Radii and effective temperatures for G, K, and M giants and supergiants. Astron J 117:521–533
van Belle G, Ciardi DR, Thompson RR, Akeson RL, Lada EA (2001) Altair's oblateness and rotation velocity from long-baseline interferometry. Astrophys J 559:1155–1164
van Belle GT, Ciardi DR, ten Brummelaar T, McAlister HA, Ridgway ST, Berger DH, Goldfinger PJ, Sturmann J, Sturmann L, Turner N, Boden AF, Thompson RR, Coyne J (2006) First results from the CHARA Array. III. Oblateness, rotational velocity, and gravity darkening of Alderamin. Astrophys J 637:494–505
van Boekel R, Kervella P, Schöller M, Herbst T, Brandner W, de Koter A, Waters LBFM, Hillier DJ, Paresce F, Lenzen R, Lagrange AM (2003) Direct measurement of the size and shape of the present-day stellar wind of η Carinae. Astron Astrophys 410:L37–L40
van Boekel R, Min M, Leinert C, Waters LBFM, Richichi A, Chesneau O, Dominik C, Jaffe W, Dutrey A, Graser U, Henning Th, de Jong J, Köhler R, de Koter A, Lopez B, Malbet F, Morel S, Paresce F, Perrin G, Preibisch Th, Przygodda F, Schöller M, Wittkowski M (2004) The building blocks of planets within the 'terrestrial' region of protoplanetary disks. Nature 432:479–482
Vandakurov Yu V (1967) The frequency distribution of stellar oscillations. Astron Zh 44:786–797 (English translation: Soviet Astronomy AJ 11:630–638)
Vauclair S, Théado S (2004) Asteroseismic signatures of helium gradients in main-sequence A stars, application to the roAp star HD 60435. Astron Astrophys 425:179–185
Vio R, Strohmer T, Wamsteker W (2000) On the Reconstruction of Irregularly Sampled Time Series. Publ Astron Soc Pacific 112:74–90
Viskum M, Kjeldsen H, Bedding TR, Dall TH, Baldry IK, Bruntt H, Frandsen S (1998) Oscillation mode identifications and models for the δ Scuti star FG Virginis. Astron Astrophys 335:549–560
von Neuman J, Wigner E (1929) Über merkwürdige diskrete Eigenwerte. Über das Verhalten von Eigenwerten bei adiabatischen Prozessen. Phys Z 30:467–470
von Zeipel H (1924) The radiative equilibrium of a rotating system of gaseous masses. Mon Not R Astr Soc 84:665–683
Waelkens C (1991) Slowly pulsating B stars. Astron Astrophys 246:453–468
Walker G, Matthews J, Kuschnig R, Johnson R, Rucinski S, Pazder J, Burley G, Walker A, Skaret K, Zee R, Grocott S, Carroll K, Sinclair P, Sturgeon D, Harron J (2003) The *MOST* asteroseismology mission: Ultraprecise photometry from space. Publ Astron Soc Pacific 115:1023–1035

Walker GAH, Kuschnig R, Matthews JM, Reegen P, Kallinger T, Kambe E, Saio H, Harmanec P, Guenther DB, Moffat AFJ, Rucinski SM, Sasselov D, Weiss WW, Bohlender DA, Božić H, Hashimoto O, Koubský P, Mann R, Ruždjak D, Škoda P, Šlechta M, Sudar D, Wolf M, Yang S (2005a) Pulsations of the Oe Star ζ Ophiuchi from MOST satellite photometry and ground-based Spectroscopy. Astrophys J 623:L145–L148

Walker GAH, Kuschnig R, Matthews JM, Cameron C, Saio H, Lee U, Kambe E, Masuda S, Guenther DB, Moffat AFJ, Rucinski SM, Sasselov D, Weiss WW (2005b) MOST Detects g-Modes in the Be Star HD 163868. Astrophys J 635:L77–L80

Warner PB, Kaye AB, Guzik JA (2003) A theoretical γ Doradus instability strip. Astrophys J 593:1049–1055

Watson RD (1988) Contributing factors to flux changes in nonradial stellar pulsations. Astrophys Space Sci 140:255–290

Winget DE, Nather RE, Clemens JC, Provencal J, Kleinman SJ, Bradley PA, Wood MA, Claver CF, Frueh ML, Grauer AD, Hine BP, Hansen CJ, Fontaine G, Achilleos N, Wickramasinghe DD, Marar TMK, Seetha S, Ashoka BN, O'Donoghue D, Warner B, Kurtz DW, Buckley DA, Brickhill J, Vauclair G, Dolez N, Chevreton M, Barstow MA, Solheim JE, Kanaan A, Kepler SO, Henry GW, Kawaler SD (1991) Asteroseismology of the DOV star PG 1159–035 with the whole earth telescope. Astrophys J 378:326–346

Winget DE, Nather RE, Clemens JC, Provencal JL, Kleinman SJ, Bradley PA, Claver CF, Dixson JS, Montgomery MH, Hansen CJ, Hine BP, Birch P, Candy M, Marar TMK, Seetha S, Ashoka BN, Leibowitz EM, O'Donoghue D, Warner B, Buckley DAH, Tripe P, Vauclair G, Dolez N, Chevreton M, Serre T, Garrido R, Kepler SO, Kanaan A, Augusteijn T, Wood MA, Bergeron P, Grauer AD (1994) Whole Earth telescope observations of the DBV white dwarf GD 358. Astrophys J 430:839–849

Wittkowski M, Hummel CA, Johnston KJ, Mozurkewich D, Hajian AR, White NM (2001) Direct multiwavelength limb-darkening measurements of three late-type giants with the Navy Prototype Optical Interferometer. Astron Astrophys 377:981–993

Wittkowski M, Aufdenberg JP, Kervella P (2004) Tests of stellar model atmospheres by optical interferometry. VLTI/VINCI limb-darkening measurements of the M4 giant ψ Phe. Astron Astrophys 413:711–723

Wittkowski M, Hummel CA, Aufdenberg JP, Roccatagliata V (2006) Tests of stellar model atmospheres by optical interferometry. III. NPOI and VINCI interferometry of the M0 giant γ Sagittae covering 0.5-2.2 μm. Astron Astrophys 460:843–853

Wittkowski M, Boboltz DA, Ohnaka K, Driebe T, Scholz M (2007) The Mira variable S Orionis: relationships between the photosphere, molecular layer, dust shell, and SiO maser shell at 4 epochs. Astron Astrophys 470:191–210

Wolff CL (1974) Distinctive patterns on the surface of slowly rotating stars whose oscillations are nonlinearly coupled. Astrophys J 193:721–727

Wu Y (2001) Combination frequencies in the Fourier spectra of white dwarfs. Mon Not R Astr Soc 323:248–256

Xiong DR, Deng L (2001) Turbulent convection and pulsational stability of variable stars. – IV. The red edge of the δ Scuti instability strip. Mon Not R astr Soc 324:243–248

Xiong DR, Chen QL, Deng L (1997) Nonlocal time-dependent convection theory. Astrophys J Suppl 108:529–544

Xiong DR, Deng L, Cheng QL (1998) Turbulent convection and pulsational stability of variable stars. I. Oscillations of long-period variables. Astrophys J 499:355–366

Yildiz M (2007) Models of α Centauri A and B with and without seismic constraints: time dependence of the mixing-length parameter. Mon Not R Astr Soc 374:1264–1270

Zahn JP (1991) Convective penetration in stellar interiors. Astron Astrophys 252:179–188

Zhao M, Monnier JD, Torres G, Boden AF, Claret A, Millan-Gabet R, Pedretti E, Berger JP, Traub WA, Schloerb FP, Carleton NP, Kern P, Lacasse MG, Malbet F, Perraut K (2007) Physical orbit for λ Virginis and a test of stellar evolution models. Astrophys J 659:626–641

Zhevakin SA (1953) K Teorii Cefeid. I (On the theory of Cepheids I) (in Russian). Astron Zh 30:161–179

Zhevakin SA (1963) Physical basis of the pulsation theory of variable stars. Annu Rev Astron Astrophys 1:367–400

Zima W (2006) A new method for the spectroscopic identification of stellar non-radial pulsation modes. I. The method and numerical tests. Astron Astrophys 455:227–234

Zima W, Wright D, Bentley J, Cottrell PL, Heiter U, Mathias P, Poretti E, Lehmann H, Montemayor TJ, Breger M (2006) A new method for the spectroscopic identification of stellar non-radial pulsation modes. II. Mode identification of the δ Scuti star FG Virginis. Astron Astrophys 455:235–246

Zwahlen N, North P, Debernardi Y, Eyer L Galland F, Groenewegen MAT, Hummel CA (2004) A purely geometric distance to the binary star Atlas, a member of the Pleiades. Astron Astrophys 425:L45–L48

Zwintz K, Weiss WW, Kuschnig R, Gruber R, Frandsen S, Gray R, Jenkner H (2000) Variable HST guide stars (I). Astron Astrophys Suppl 145:481–490